# Proteomic identification of posttranslational modifications: cAMP-induced changes of phosphorylation and investigation of novel approaches detecting posttranslational modifications at lysine and arginine residues

Dissertation

zur

Erlangung des Doktorgrades (Dr. rer. nat.)

der

Mathematisch-Naturwissenschaftlichen Fakultät

der

Rheinischen Friedrich-Wilhelms-Universität Bonn

vorgelegt von

**Peter Christian Schein**

aus

Bad Neuenahr-Ahrweiler

Bonn, 2020

Angefertigt mit Genehmigung der Mathematisch-Naturwissenschaftlichen Fakultät der Rheinischen Friedrich-Wilhelms-Universität Bonn

1. Gutachter: Prof. Dr. V. Gieselmann

2. Gutachter: Prof. Dr. D. Fürst

Tag der mündlichen Prüfung: 19.03.2020

Erscheinungsjahr: 2020

# Table of contents

# List of Figures

# List of Tables

# Abbreviations

| | |
|---|---|
| °C | degree Celsius |
| µg | microgram |
| µl | microliter |
| µU | microunit (enzyme activity) |
| 2D | two dimensional |
| A.U. | arbitrary units |
| ABTS | 2,2'-azino-bis(3-ethylbenzothiazoline-6-sulfonic acid) |
| AC | adenylyl cyclases |
| adj. | adjusted |
| AGC | automatic gain control |
| AKAPs | A-kinase anchoring proteins |
| AMP | adenosine monophosphate |
| ANOVA | analysis of variance |
| approx. | approximately |
| APS | ammonium persulfate |
| ASA | arylsulfatase A |
| ATP | adenosine triphosphate |
| BCA | bicinchoninic acid |
| BLOC-1 | biogenesis of lysosome-related organelles complex 1 |
| BLOC1S6 | biogenesis of lysosome-related organelles complex 1 subunit 6 |
| BORC | BLOC-1 related complex |
| BSA | bovine serum albumin |
| CaMK | calcium/calmodulin-dependent protein kinase |
| CaMKK1 | calcium/calmodulin dependent protein kinase kinase |
| cAMP | cyclic adenosine monophosphate |
| Cas9 | CRISPR associated protein 9 |
| CDK | cyclin-dependent kinase |
| CHAPS | 3-((3-cholamidopropyl) dimethylammonio)-1-propanesulfonate |
| CID | collision induced dissociation |
| Co-IP | co-immunoprecipitation |
| Cr | crotonylation |
| cRAP | contaminant repository for affinity purification |
| CREB | cAMP responsive element binding protein 1 |
| CRISPR | clustered regularly interspaced short palindromic repeats |
| crRNA | CRISPR RNA |
| CRTC | CREB-regulated transcription coactivator |
| C-terminal | carboxy-terminal |
| ctrl. | Control |
| CTSD | cathepsin D |
| CV | coefficient of variation |
| d | layer thickness |
| Da | dalton |
| db-cAMP | dibutyryl-cAMP |
| DC | detergent compatible |

| | |
|---|---|
| di-Me | di-methylation |
| DMSO | dimethyl sulfoxide |
| DNA | deoxyribonucleic acid |
| DPBS | Dulbecco's phosphate-buffered saline |
| DTT | dithiothreitol |
| *E. coli* | *Escherichia coli* |
| ECL | enhanced chemiluminescence |
| EDTA | ethylenediaminetetraacetic acid |
| EGFR | epidermal growth factor receptor |
| ELISA | Enzyme Linked Immunosorbent Assay |
| EPAC | exchange factor directly activated by cAMP |
| ER | endoplasmic reticulum |
| ESI | electrospray ionization |
| FA | formic acid |
| FCS | fetal calf serum |
| FDR | false discovery rate |
| FSK | forskolin |
| g | gram |
| GDP | guanosine diphosphate |
| GO | gene ontology |
| GPCR | G-protein coupled receptor |
| $G_s$PCR | stimulatory G-protein coupled receptors |
| GTP | guanosine triphosphate |
| h | hours |
| HCD | higher-energy collisional dissociation |
| HEK | human embryonic kidney |
| HeLa | Henrietta Lacks |
| HEPES | 4-(2-hydroxyethyl)-1-piperazineethanesulfonic acid |
| HPS | Hermansky-Pudlak syndrome |
| HRP | horseradish peroxidase |
| HSD | Tukey honest significant difference |
| ICC | immunocytochemistry |
| IEF | isoelectric focusing |
| IgG (H+L) | immunoglobulin G (heavy + light chains) |
| IMAC | immobilized metal affinity chromatography |
| indel | Insertion or deletion mutation |
| ITMS | ion-trap mass analyzer |
| K | lysine |
| kb | kilobases |
| kDa | kilodalton |
| KO | knock-out |
| l | liter |
| L99K | substitution of leucin at amino acid position 133 with lysine |
| LAMP | lysosome-associated membrane glycoprotein |
| LC | liquid chromatography |
| LC-MS2 | liquid chromatography coupled tandem MS |
| LDH | lactate dehydrogenase |

| | |
|---|---|
| LE | late endosomes |
| $log_{10}$ | logarithm with base 10 |
| $log_2$ | binary logarithm |
| LTQ | linear trap quadrupole |
| LysArg | LysArginase |
| M | molar (mol/l) |
| m/z | mass-to-charge |
| M6P | mannose-6-phosphate |
| MALDI | matrix-assisted laser desorption/ionization |
| MAPK p38 | mitogen-activated protein kinase p38 |
| MCS | missed cleavage sites |
| MEF | mouse embryonic fibroblasts |
| meth. | methylated |
| mg | milligram |
| min | minutes |
| ml | milliliter |
| mM | millimolar (mmol/l) |
| mmu | milli mass units |
| MPR | mannose-6-phosphate receptor |
| MPR300 | cation-independent mannose-6-phosphate receptor |
| MPR46 | cation-dependent mannose-6-phosphate receptor |
| mRNA | messenger ribonucleic acid |
| MS | mass spectrometry |
| MS1 | precursor ion analysis |
| MS2 | fragment ion analysis |
| MSA | multistage activation |
| mTOR | mechanistic target of rapamycin |
| mTORC1 | mechanistic target of rapamycin complex 1 |
| mU | milliunit (enzyme activity) |
| n.s. | not significant |
| NANOS1 | Nanos homolog 1 |
| ng | nanogram |
| NGS | next generation sequencing |
| NHEJ | non-homologous end joining |
| NHS | N-hydroxysuccinimide |
| NHS-LC | N-hydroxysuccinimide-long chain |
| nm | nanometer |
| N-phosphorylation | phosphorylation at nitrogen of HLR |
| N-terminal | amino-terminal |
| $N^{\alpha}$ | amino-terminal primary amine group |
| o.n. | over night |
| $OD_{405}$ | optical density at 405 nm |
| O-GlcNAc | N-acetyl-glucosamine at hydroxyl group of STY |
| O-phosphorylation | phosphorylation at hydroxyl group of STY |
| PAM | protospacer adjacent motif |
| PBS | phosphate-buffered saline |
| PCR | polymerase chain reaction |

| | |
|---|---|
| pCREB | cAMP responsive element binding protein 1 phosphorylated at S133 |
| PD | Proteome Discoverer |
| Pen/Strep | penicillin/streptomycin |
| PEP | posterior error probability |
| pep. | peptide |
| PFKFB2 | 6-phosphofructo-2-kinase/fructose-2,6-bisphosphatase 2 |
| phospho | phosphorylation |
| PI | isoelectric point |
| $PI(3,5)P_2$ | phosphatidylinositol 3,5-bisphosphate |
| PIKFYVE | phosphatidylinositol 3-phosphate 5-kinase |
| PKA | protein kinase A |
| PKB | protein kinase B |
| PNK | T4-polynucleotide kinase |
| ppm | parts per million |
| PSM | peptide spectrum matches |
| PTM | posttranslational modification |
| Pumilio2 | Pumilio homolog 2 |
| R | arginine |
| RE | recycling endosomes |
| red. | reductive |
| rel. | relative |
| Rep | replicate |
| RT | room temperature |
| s | seconds |
| S133 | serine at amino acid position 133 |
| S133A | substitution of serine at amino acid position 133 with alanine |
| S133E | substitution of serine at amino acid position 133 with glutamate |
| S6 | 40S ribosomal protein S6 |
| S6K | p70S6 kinase |
| sAC | soluble adenylyl cyclases |
| Sc | succinylation |
| SCX | strong cation exchange |
| SDC | sodium deoxycholate |
| SDM | site directed mutagenesis |
| SDS | sodium dodecyl sulfate |
| SDS-PAGE | sodium dodecyl sulfate polyacrylamide gel electrophoresis |
| sec. AB. Ctrl | Secondary antibody control |
| SIK | salt-inducible kinase |
| SILAC | stable isotope labeling by amino acids in cell culture |
| SNAP-23 | synaptosomal-associated protein 23 |
| SNAP-25 | synaptosomal-associated protein 25 |
| SNAPIN | SNARE-associated protein |
| SNARE | soluble N-ethylmaleimide-sensitive-factor attachment receptor |
| S-phosphorylation | phosphorylation at thiol group of C |
| Strep | streptavidin |
| SV | synaptic vesicles |
| t | time |

| | |
|---|---|
| TBS | Tris-buffered saline |
| TEAB | triethylammonium bicarbonate |
| TEMED | N,N,N',N'-Tetramethyl ethylenediamine |
| term | terminal |
| TFA | trifluoroacetic acid |
| TFEB | transcription factor EB |
| TGN | trans-Golgi network |
| $TiO_2$ | titanium dioxide |
| Tip47 | Perilipin-3 |
| TLS | T-loading solution |
| TOF | time of flight |
| TORC | transducers of regulated CREB |
| tr | technical replicate |
| tracrRNA | trans-activating crRNA |
| Tricine | N-(2-Hydroxy-1,1-bis(hydroxymethyl)ethyl)glycine |
| Tris | tris(hydroxymethyl)aminomethane |
| U | unit |
| UK | United Kingdom |
| USA | United States of America |
| UV | ultraviolet |
| v/v | volume per volume |
| VAMP7 | Vesicle-associated membrane protein 7 |
| $V_{sample}$ | sample volume |
| v-SNARE | vesicular soluble N-ethylmaleimide-sensitive-factor attachment receptor |
| $V_{total}$ | total volume of mixture |
| w/o | without |
| w/v | weight per volume |
| WB | Western Blot |
| wt | wildtype |
| X | derivatization position |
| β-Hex | β-hexosaminidase |
| $\varepsilon_{405}$ | molar extinction coefficient |

# 1. Summary

Cyclic adenosine monophosphate (cAMP) is an important second messenger which can be generated in response to signals binding to stimulatory G-protein coupled receptors. Inside the cell, protein kinase A is a well-known cAMP sensor. Within the present study, cAMP-dependent changes in the phosphorylation (phospho) pattern of lysosomal membrane and lysosome-associated proteins were investigated. The serine phospho-site at position 133 (S133) of the lysosome-associated SNARE-associated protein (SNAPIN) was found to be significantly downregulated in the phosphoproteomic data set of the lysosomal membrane fraction after elevating the intracellular cAMP level by a Forskolin/dibutyryl-cAMP (FSK/db-cAMP) treatment. In addition to that, a tendency of SNAPIN to dissociate from the lysosomes upon elevated cAMP levels was observed. Therefore, the cAMP-dependent downregulation of the S133 phospho-site detected in the MS-based approach could have also been caused by a translocation of SNAPIN after FSK/db-cAMP treatment. Nevertheless, a dephosphorylation of SNAPIN was observed in 2D-gelelectrophoresis of whole cell protein lysate after elevating the intracellular cAMP level. This observation confirmed the findings of the phosphoproteomic study although the dephosphorylation site could not be mapped to a specific amino acid position by 2D-gelelectrophoresis. Pull-down assays with a phosphomimetic proteoform of the S133 phospho-site (S133E) indicate an interaction of the biogenesis of lysosome-related organelles complex-1 subunit 6 (BLOC1S6) with the S133E but not the S133A SNAPIN isoform (serine to alanine substitution mimics unphosphorylated SNAPIN at position 133). Furthermore, SNAPIN knock-out (KO) was associated with decreased endocytosis and increased exocytosis of lysosomal hydrolases compared to wildtype cells. Elevation of intracellular cAMP levels neither influenced these processes in wildtype nor in SNAPIN KO cells. This indicates that the dephosphorylation of SNAPIN detected after FSK/db-cAMP treatment might not be involved in regulating these secretion or uptake events.

Posttranslational modifications (PTMs) of lysine and arginine residues are important regulators in different cellular processes. In bottom-up mass spectrometry-based approaches, these PTMs are most commonly enriched with pan-specific antibodies. Here, the investigations are limited to one specific PTM and depend on the quality and availability of proper antibodies in order to obtain an efficient enrichment of modified peptides. In addition to that, huge amounts of samples are usually required in these immunoprecipitation approaches which might be problematic when dealing with limited amounts of starting material. The present study aimed at developing and testing of two novel antibody-free techniques for improving the detection of

specific PTMs from small quantities of starting sample. For example, such techniques would facilitate PTM analysis of enriched lysosomes or other purified subcellular compartments. The first technique, called the serial digestion workflow, was assumed to enhance the identification of lysine modifications. Compared to that, the second method, called the $N^{\alpha}$-selective derivatization workflow (derivatization of primary amine group at amino-terminus), was hypothesized to improve the detection of PTMs occurring on both, lysine and arginine residues. Applying the two workflows to proteins from human embryonic kidney (HEK 293) cell lysate was not associated with an increased identification of lysine modifications. In contrast, sample treatment according to the $N^{\alpha}$-selective derivatization method yielded an increase in the detection rate of arginine methylation. However, a similar rise was observed in both workflows after strong cation exchange chromatography which was originally performed as a sample clean-up procedure. Here, depending on the sample type, either the identification of arginine or of lysine and arginine methylation was increased. Comparison of the methylated peptides detected in the different samples showed only a partial overlap. This indicates the necessity of analyzing different samples coming from both workflows in order to get the most comprehensive protein methylation data set. Based on these findings, a new hybrid workflow is suggested.

# 2. Introduction

## 2.1. Proteins

Proteins are macromolecules consisting of sequentially arranged amino acids covalently linked by an amide bond. Within the cell, amino acid sequence information is stored in protein coding regions of the deoxyribonucleic acid (DNA). After DNA transcription, the messenger ribonucleic acid (mRNA) is processed and translated into an amino acid sequence. The interaction among amino acid residues within the newly formed polypeptide chain determines the formation of secondary structures such as α-helices and β-sheets, thus being crucial for protein folding (tertiary structure) and function.

In 2004, the complete human euchromatic DNA sequence was published by the International Human Genome Sequencing Consortium. Within this article, the authors predicted the human genome to comprise a total number of 20,000 to 25,000 protein coding genes (International Human Genome Sequencing Consortium 2004). Today, the latest assembly of the human genome by the Genome Reference Consortium suggests a total number of 23,376 (primary assembly + alternative sequences) open reading frame containing genes (ensembl.org, retrieved 11.02.2019, GRCh38.p12). Although the quantity of protein coding genes has been refined within the last couple of years, processes such as alternative mRNA splicing and posttranslational chemical modification (PTM) of amino acids increase proteome complexity, thus hampering estimations on the total number of proteins and proteoforms present within the human body based on the genomic data.

### 2.1.1. Mass spectrometry-based proteomic studies

The proteome is the highly dynamic set of proteins present inside a cell under specific conditions. Its composition varies depending on the cell type, differentiation, drug treatment as well as on other internal and external stimuli (Ribet et al. 2010; Walther et al. 2015; Doll et al. 2017; Ebhardt et al. 2018; Hurrell et al. 2019). Mass spectrometry (MS) is a frequently used method for protein identification in proteomic studies. In this technique, peptides or proteins are ionized followed by the analysis of their mass to charge ratio (reviewed by Aebersold and Mann 2003).

In bottom-up MS approaches, protein identifications are based on the detection and sequencing of unique peptides during mass spectrometric analysis. Therefore, this method requires the

enzymatic digestion of the proteins prior to the MS run. The protease trypsin is commonly used for cleaving the protein backbone in proteomic studies. Based on its specificity towards lysine and arginine, tryptic digestion offers the advantage of generating peptides with lengths compatible with common detector capabilities (reviewed by Vandermarliere et al. 2013). In order to be detectable by mass spectrometry, peptides must be ionized. Two of the most commonly used ionization techniques are the electrospray ionization (ESI) and the matrix-assisted laser desorption/ionization (MALDI) (Tanaka et al. 1988; Fenn et al. 1989). Once the peptide has been ionized and entered the spectrometer, its mass to charge ratio is determined by a mass analyzer (MS1 scan). In low complex peptide samples, the mass to charge ratios obtained in the MS1 scan might be enough to uniquely assign the measured ions to certain peptides and proteins (Henzel et al. 1993; Pappin et al. 1993). When investigating complex samples, several peptide ions with different sequences might feature the same mass to charge ratio on MS1 level. Therefore, the peptide identification usually involves an additional step. In data dependent MS analysis, usually the most abundant ions (precursor ions) detected in the MS1 scan are selected and isolated before their fragmentation (Stahl et al. 1996). In the latter step, the peptide backbone is fragmented by collision with an inert gas followed by the mass to charge ratio measurement of the fragment ions in the mass analyzer (MS2 scan) (Hunt et al. 1986; Stahl et al. 1996). As a result of the dissociation, the MS2 spectra contain information about the amino acid sequence of the fragmented peptide ion (Hunt et al. 1986). During data processing, the precursor MS1 mass to charge ratio and the ions detected in the MS2 scan are compared to sequence information provided in a database in order to assign the spectra to a certain peptide (Eng et al. 1994).

In proteomic approaches, the mass spectrometers are often coupled to liquid chromatography (LC) systems (LC-MS), thus allowing peptide separation prior to the MS analysis (Huang and Henion 1990). During peptide elution, changes in the intensities of each precursor ion can be traced over time. As the chromatographic peak area is proportional to the peptide abundance, this information can be used for relative precursor ion-based quantification (reviewed by Ong and Mann 2005). However, comparison of the abundances determined with these MS approaches are only possible among peptides with the same sequence. This is caused by the fact that differences in the amino acid composition might influence the ionization behavior and therefore the chromatographic peak area of the precursor ion (reviewed by Ong and Mann 2005; reviewed by Gillet et al. 2016).

## 2.2. Posttranslational modifications

Posttranslational modifications of proteins have been known for many decades. Their functional impacts range from modulation of enzyme function, signal transduction and polypeptide degradation to changes in protein localization, interaction and the regulation of other cellular processes (Ciechanover et al. 1980; Sette and Conti 1996; Holz et al. 2005; Martina et al. 2012; Napolitano et al. 2018; Borodinova et al. 2019).

Besides the addition of small functional groups (e.g. methyl- and phosphoryl-groups) and more complex chemical compounds such as carbohydrates, peptides or lipids to amino acid side chains or termini of proteins, the group of PTMs also comprises the proteolytic cleavage of precursor proteins. (Burnett and Kennedy 1954; Kim and Paik 1965; Carlson 1966; Ciechanover et al. 1980; Erickson et al. 1981; Magee and Courtneidge 1985). The processing of zymogens is an example for such a modification of the primary protein structure (Sanny et al. 1975). However, whereas these proteolytic modulations are static and irreversible, other PTMs are highly dynamic and reversible (reviewed by Neurath and Walsh 1976; reviewed by Deribe et al. 2010). Especially these dynamic PTMs enable a quick cellular response to certain stimuli thus facilitating adaptations to changing conditions inside and outside of the cell (reviewed by Deribe et al. 2010).

Crosstalk describes the functional interplay between two or more modifications, caused by the competition of PTM for the same amino acid residue or their occurrence at adjacent sites within the protein (Kamemura et al. 2002; Yang et al. 2006). This phenomenon has been well studied among modifications reactive towards the same functional group such as O-GlcNAcylation and O-phosphorylation (reviewed by Hart et al. 2007). Nevertheless, PTM occurring at different side chains might also be able to influence each other. A prominent example for such an interplay is the crosstalk between phosphorylation and lysine acetylation. In 2015, Bryson and White described a site-specific acetylation and deacetylation of lysine residues upon stimulation of receptor tyrosine kinases. *Vice versa*, inhibition of the class I/II histone deacetylase was associated with significant alterations in the phosphorylation of four different tyrosine residues, thus further supporting the interplay between these two PTM (Bryson and White 2015).

### 2.2.1. Mass spectrometry-based identification of posttranslational modifications

Within the past decades, bottom-up mass spectrometry (MS) has evolved as the method of choice for PTM analysis. Based on the mass shift caused by the PTM, modified peptides can be identified, and modifications can be assigned to specific amino acids within the sequence after

tandem MS measurement. However, one major challenge during these analyses is the low abundance of the PTM containing peptides within the sample. Hence, reduction of sample complexity is required prior to MS measurements as most peptides present within proteolytic peptide mixture are unmodified and might be preferably selected for fragmentation (reviewed by Zhang et al. 2015).

### 2.2.2. Phosphorylation

Protein phosphorylation is a well-studied PTM and a key regulator in processes such as enzyme activation, protein localization and gene expression (Acosta-Jaquez et al. 2009; Settembre et al. 2012). Recently, data mining of high- and low-throughput phosphoproteomic studies estimated a total number of 13,000 phosphoproteins and 230,000 phosphorylation sites in humans (Vlastaridis et al. 2017). Although the percentage of false predictions is unknown, the high number of potential phospho-sites emphasizes the importance of investigating this PTM under different cellular conditions.

According to the functional group to which the phosphoryl-group is attached, phosphorylation events can be classified as O-phosphorylation (serine, threonine, tyrosine), S-phosphorylation (cysteine), N-phosphorylation (lysine, arginine, histidine) and acyl-phosphorylation (glutamate and aspartate) (Olsen et al. 2006; Hardman et al. 2019). Among those, O-phosphorylation is the most frequently investigated PTM as these modifications are stable during acidic conditions used in the process of sample preparation and for peptide separation during LC (reviewed by Zhang et al. 2015).

In bottom-up MS based phosphorylation studies, phosphopeptides are first enriched and subsequently investigated by liquid chromatography coupled tandem MS (LC-MS2) analysis. Most prominently, positively charged metal ions with high affinity towards the negatively charged phosphate groups are used for the enrichment (Neville et al. 1997; Nühse et al. 2003). Another popular method is based on the binding of phosphopeptides to $TiO_2$ columns (Pinkse et al. 2004; Larsen et al. 2005). However, these methods enrich all phosphopeptides present within a sample and do not distinguish between the different amino acids which are phosphorylated. Therefore, antibodies have been developed to selectively enrich for phosphopeptides comprising the phosphorylation at a specific amino acid residue (reviewed by Mann et al. 2002; Sathe et al. 2018).

### 2.2.3. Lysine modification

Within the past decades, many different types of lysine modifications have been reported. Among those, acetylation, methylation and ubiquitination are the most prominent ones. Whereas ubiquitination is known to play an important role in proteasome based protein degradation, the functional impact of lysine acetylation and methylation ranges from regulating gene expression and protein interactions to the stimulation of signaling pathways and other cellular processes (Ciechanover et al. 1980; Hershko et al. 1980; Hebbes et al. 1988; Gu and Roeder 1997; Strahl et al. 1999; Chen et al. 2001; Huang et al. 2006; Wang et al. 2008; Elkouris et al. 2016; Kaimori et al. 2016; Fischer et al. 2017).

Lysine modification containing peptides are often enriched by using PTM-specific antibody-based pull-down assays followed by their analysis via LC-MS2 (Kim et al. 2006; Xu et al. 2010; Guo et al. 2014). However, the specificity of the antibody towards one single modification makes investigations of the plethora of different lysine modifications expensive and laborious. Additionally, antibodies against rare modifications might not be easily accessible, thus highlighting the importance of developing non-antibody-based techniques for the enrichment of lysine-modified peptides.

### 2.2.4. Arginine modification

Different types of arginine modifications have been identified within the past years with methylation probably being the best characterized PTM occurring at this amino acid. Primarily considered as a histone modification involved in the regulation of gene expression, arginine methylation has also been observed at non-histone proteins playing key roles in other cellular processes such as signal transduction, pre-mRNA splicing and protein-protein interactions (Bedford et al. 2000; Mowen et al. 2001; Boisvert et al. 2002; Zhao et al. 2009; Geoghegan et al. 2015) .

Arginine methylated peptides are often enriched by pan-specific antibodies (Guo et al. 2014). After the enrichment, peptides are analyzed by LC-MS2 in order to map the modification site to a specific amino acid position.

## 2.3. Lysosomes

Lysosomes are eukaryotic, membrane coated organelles predominantly responsible for macromolecule breakdown by the action of acidic hydrolases (de Duve et al. 1955; Coffey and

de Duve 1968). Up to now, more than 50 different lysosomal hydrolases are known (reviewed by Perera and Zoncu 2016). Their common characteristic is the requirement of an acidic pH in order to fulfill their molecular function (Coffey and de Duve 1968; Aronson and de Duve 1968; Fowler and de Duve 1969). Therefore, protons are pumped into the lysosomal lumen by membranous, adenosine triphosphate (ATP)-dependent v-ATPases (vacuolar-ATPase), thus generating and maintaining an acidic inner lysosomal pH which is optimal for the activity of these hydrolases (Ohkuma et al. 1982).

The molecules degraded by the lysosomes originate from different pathways such as endocytosis and autophagy, an intracellular catabolic process (reviewed by Perera and Zoncu 2016). Here, cargo delivery depends on the tethering of endosomes or autophagosomes to the lysosomes, followed by the assembly of soluble *N*-ethylmaleimide-sensitive factor-attachment protein receptor (SNARE) complexes and the fusion of the membrane bound compartments (Ward et al. 2000; Itakura et al. 2012; Pols et al. 2013; Jiang et al. 2014). Recently, a study by Bright et al. (2016) suggest that the hydrolytic activity primarily occurs in these intermediate endolysosomes whereas hydrolases are inactive in terminal lysosomes.

### 2.3.1. Biogenesis of soluble, lysosomal enzymes

During their translation, soluble lysosomal proteins are translocated into the endoplasmic reticulum (ER) mediated by an amino-terminal (N-terminal) signaling sequence (Erickson and Blobel 1979; Erickson et al. 1981). In the ER lumen, proteins are modified by processes such as N-glycosylation. Here, complex glycans are added to selected asparagine residues of the polypeptides before the glycosylated proteins are further transported to the Golgi apparatus (Erickson and Blobel 1979; Erickson et al. 1981; reviewed by Braulke and Bonifacino 2009). Once reaching the Golgi, glycan chains are further modified. In a two-step process, mannose residues are phosphorylated thus leading to the formation of mannose-6-phosphate (M6P) and allowing the binding of the protein to transmembrane M6P receptors (MPR) (Kaplan et al. 1977; Hasilik et al. 1980; Tabas and Kornfeld 1980; Varki and Kornfeld 1980; Waheed et al. 1981). Inside the cell, one can distinguish between 46 kDa cation-dependent (MPR46) and the 300 kDa cation-independent MPR (MPR300) (Sahagian et al. 1981; Hoflack and Kornfeld 1985). Subsequent to the MPR binding, M6P containing enzymes exit the trans-Golgi network (TGN) by formation of vesicles and are transported to endosomes (reviewed by van Meel and Klumperman 2008). After dissociation of the M6P containing ligand from the MPR in the acidic lumen of the endosomes, the receptor cycles back to the Golgi where it can be reused for the transport of newly synthesized lysosomal enzymes (Duncan and Kornfeld 1988).

In addition to the pathway described above, acidic hydrolases can also be transported to the lysosomes by M6P independent pathways (Dittmer et al. 1999). For example, such a mechanism has been identified for the LIMP-2 mediated lysosomal transport of β-glucocerebrosidase (Reczek et al. 2007).

Besides the TGN and endosomal vesicles, the MPR are also localized at the plasma membrane (Kaplan et al. 1977). Here, the MPR300 has been described in mediating endocytosis of M6P containing enzymes as well as in binding non-glycosylated proteins such as the insulin-like growth factor II (Kaplan et al. 1977; MacDonald et al. 1988).

### 2.3.2. Biogenesis of lysosomal membrane proteins

Lysosomal membrane proteins are targeted to the lysosomes through cytosolic peptide signal sequences and require the interaction with vesicle coat components such as the adaptor protein-1 complex (Williams and Fukuda 1990; Höning and Hunziker 1995; Höning et al. 1996). In contrast to the luminal lysosomal enzymes, this sorting is independent of M6P modifications of the membrane proteins (Barriocanal et al. 1986; Waheed et al. 1988).

Two different pathways have been described in order to transport lysosomal membrane proteins from the TGN to the lysosomes (reviewed by Braulke and Bonifacino 2009). In the indirect pathway, the lysosomal membrane proteins are first translocated to the plasma membrane before they are re-internalized and delivered to the endosomal system (Braun et al. 1989). In contrast, the direct pathway is based on the immediate transport of lysosomal membrane proteins from the TGN to the endosomes or lysosomes (Harter and Mellman 1992).

### 2.3.3. Lysosomal secretion

Originally found in *Tetrahymena pyriformis*, the $Ca^{2+}$ dependent secretion of lysosomal hydrolases has been described for different mammalian cell types (Müller 1972; Rodríguez et al. 1997). The involvement of SNARE complexes in such exocytotic processes has been suggested by studies focusing on the secretion of lysosome related secretory granules in mast cells (Paumet et al. 2000). In 2004, Rao et al. identified synaptotagmin VII as well as a SNARE complex consisting of the synaptosomal-associated protein 23 (SNAP-23), Syntaxin-4 and the v-SNARE (vesicular SNARE) vesicle-associated membrane protein 7 (VAMP7) as components being involved in $Ca^{2+}$ dependent lysosome secretion. It has been proposed that the exocytosis of lysosomes plays important roles in processes such as plasma membrane repair upon cell disruption (Reddy et al. 2001). Besides conventional lysosomes, some cell types comprise

lysosome related organelles (LRO) specialized for secretion (reviewed by Luzio et al. 2014). Among others, such LRO can be found as lytic granules in cytotoxic T-lymphocytes involved in the targeted apoptosis of infected or tumorigenic cells (Yannelli et al. 1986; Stinchcombe et al. 2001).

### 2.3.4. Lysosomes as an important intracellular signaling hub

Besides their importance in macromolecule degradation, lysosomes are an important hub in processes such as cellular signaling and nutrition sensing (Sancak et al. 2008; Kim et al. 2008). For example, an increasing body of evidence indicates the sensitivity of the lysosome-associated mechanistic target of rapamycin complex 1 (mTORC1) towards the availability of amino acids (Sancak et al. 2008; Kim et al. 2008). If amino acids are present, Ras-related GTPases (Rag) promote the translocation of mTORC1 to the lysosomes where its kinase function is activated by the Rheb protein (Long et al. 2005; Sancak et al. 2008; Kim et al. 2008; Sancak et al. 2010). As a result of its activation, mTORC1 phosphorylates different target proteins such as the transcription factor EB (TFEB) thus inhibiting catabolic pathways. After its phosphorylation, TFEB binds to 14-3-3 proteins leading to its cytosolic localization (Martina et al. 2012; Settembre et al. 2012). However, upon starvation, mTORC1 is inactive and dissociates from the lysosomes. Therefore, the phosphorylation status of TFEB changes which facilitates its dissociation from the 14-3-3 proteins and enables its translocation into the nucleus (Martina et al. 2012; Settembre et al. 2012). Here, TFEB induces the transcription of lysosome- and autophagy-related genes thus promoting cellular catabolic processes (Martina et al. 2012; Settembre et al. 2012).

## 2.4. cAMP-based signal transduction

Since its discovery in 1957/58, cyclic adenosine monophosphate (cAMP) has been described as an important cellular second messenger (Berthet et al. 1957; Rall and Sutherland 1958; Sutherland and Rall 1958). Inside the cell, cAMP is produced in response to various signals sensed by stimulatory G-protein coupled receptors ($G_S$PCRs). For example, glucagon, a hormone secreted by pancreatic cells in response to hypoglycemia, is a well-known activator of the cAMP pathway after complexing with $G_S$PCRs (Jelinek et al. 1993; reviewed by Habegger et al. 2010). Upon ligand binding, guanosine diphosphate (GDP) bound to the stimulatory G-protein is exchanged by guanosine triphosphate (GTP) (reviewed by Freissmuth et al. 1989). This activates intracellular adenylyl cyclases (AC) thus leading to an increase of the cytoplasmic cAMP level

(Rodbell et al. 1971; Northup et al. 1980; reviewed by Freissmuth et al. 1989). The exchange proteins directly activated by cAMP (EPAC) and the protein kinase A (PKA) are two main intracellular cAMP sensors (Walsh et al. 1968; Tao et al. 1970; Kawasaki et al. 1998; Rooij et al. 1998). Degradation of cAMP is achieved by the conversion of cAMP to AMP catalyzed by cyclic 3',5'-cyclic nucleotide phosphodiesterase (Butcher and Sutherland 1962).

### 2.4.1. Protein kinase A (PKA)

PKA is a cAMP dependent, tetrameric serine/threonine kinase consisting of two regulatory and two monomeric catalytic subunits ($R_2C_2$-complex) (Walsh et al. 1968; Tao et al. 1970; Ramseyer et al. 1974). According to the isoform of the regulatory subunit, the holoenzymes are either classified as PKA-I or PKA-II (Corbin et al. 1975; Zoller et al. 1979). The spatial localization of the tetramer is regulated by the interaction of the regulatory subunits with A-kinase anchoring proteins (AKAPs) (Theurkauf and Vallee 1982; Lohmann et al. 1984; reviewed by Welch et al. 2010). PKA phosphorylates its substrates at the R-R/K-X-S/T consensus sequence (reviewed by Kennelly and Krebs 1991).

PKA is activated upon binding of cAMP to the regulatory subunit of the holoenzyme (Walsh et al. 1968; Tao et al. 1970). It has been shown that cAMP binding to the regulatory subunit can result in dissociation of the $R_2C_2$-complex (Tao et al. 1970; Ramseyer et al. 1974). Here, the release of the catalytic subunit is believed to be crucial for fulfilling its kinase activity. However, there is strong evidence that cAMP induced activation of PKA-II is also possible while the holoenzyme stays intact (Yang et al. 1995; Smith et al. 2017). In this case, PKA-IIs sphere of action is limited to the proximity to its anchorage site, thus maybe affecting the functional role of the holoenzyme compared to its dissociated form (Smith et al. 2017).

The regulatory role of PKA in retrograde and anterograde vesicle transport has been described intensively within the past years (Muñiz et al. 1996; Muñiz et al. 1997; Birkeli et al. 2003). However, PKA also influences organelle-specific processes. In 2008, Vergarajauregui et al. identified the serine residues at the positions 557 and 559 of the lysosomal cation channel Mucolipin 1 as PKA targets. Additionally, the authors demonstrated that PKA inhibition increases the activity of Mucolipin 1. When mutating S557 and S559 to alanine, no difference in the channel activity between the control and the PKA inhibited samples was observed (Vergarajauregui et al. 2008).

### 2.4.2. Exchange protein directly activated by cAMP (EPAC)

In contrast to PKA, the two EPAC family members are monomeric proteins consisting of an N-terminal regulatory domain and a catalytic region located at the C-terminus of the polypeptide chain (Kawasaki et al. 1998). cAMP binding to the regulatory domain activates EPAC's carboxy-terminal (C-terminal) guanine exchange factor function (Kawasaki et al. 1998; Rooij et al. 1998). Once active, the EPACs are able to mediate the activation of the small GTPases such as Rap1A which belongs to the Ras superfamily (Kawasaki et al. 1998; Rooij et al. 1998).

EPACs have been demonstrated to play important roles in different cellular processes such as in cell adhesion and exocytosis (Ozaki et al. 2000; Rangarajan et al. 2003). Although EPAC can act independent from PKA activation, both cAMP sensors might affect downstream effects in a synergistic fashion (Shibasaki et al. 2007). For example, such a converging action has been described for secretion of neurotensin in endocrine cells (Li et al. 2007). Besides that, PKA and EPAC were also described in having opposing effects. Here, the phosphorylation/activation of protein kinase B (PKB) is an example for such an antithetic function of these cAMP sensors (Mei et al. 2002). The synergistic and antagonistic functions of PKA and EPAC indicate the complexity of the cAMP-based signaling machinery.

## 2.5. SNAPIN

In the course of this thesis, a phospho-site of the SNARE-associated protein (SNAPIN) was identified to be downregulated in the lysosomal membrane fraction upon FSK/db-cAMP treatment (see section 5.1.2.2). Based on this finding, this protein has been further investigated in different biochemical approaches.

SNAPIN was first described in neurons as being potentially involved in docking and the release of synaptic vesicles to the plasma membrane via its interaction with the SNARE complex protein SNAP-25 (synaptosomal-associated protein 25) (Ilardi et al. 1999). Starting from this initial observation, the function of SNAPIN in tethering vesicles to the outer membrane has also been suggested for non-neuronal cells (Somanath et al. 2016). In 2016, Somanath et al. demonstrated that SNAPIN is involved in insulin secretion of pancreatic beta-cells by docking the secretory granules to the membrane after binding to SNAP-25. Besides its vesicle tethering function, SNAPIN has been shown to be crucial for dynein-driven retrograde vesicle transport, such as cargo delivery from the presynaptic terminals to the endolysosomal system and the transfer of the beta-site amyloid precursor protein cleaving enzyme 1 to the lysosomes for its degradation (Cai et al. 2010; Ye and Cai 2014; Di Giovanni and Sheng 2015).

SNAPIN is phosphorylated by PKA at its serine 50 position (S50) (Chheda et al. 2001). Studies with PKA stimulated cells and expression systems comprising the phosphomimetic SNAPIN S50D proteoform revealed an increased SNAPIN/SNAP-25 interaction in cells derived from rat hippocampal slices and pancreatic beta-cells thus suggesting the importance of this PTM in exocytosis (Chheda et al. 2001; Song et al. 2011). This altered interaction behavior might be attributed to changes in SNAPINs secondary structure, as the phosphomimetic S50D isoform comprises less alpha helical structures compared to is non-phosphorylatable S50A counterpart (Navarro et al. 2012).

Homozygous SNAPIN knock-out has been shown to be perinatal lethal, likely caused by developmental defects of the brain which might be associated with the previously mentioned role of SNAPIN in vesicle tethering but also with alterations in the autophagy-lysosomal pathway (Tian et al. 2005; Zhou et al. 2011). The effect of SNAPIN on lysosomal function has been investigated in detail within the past years. Within these studies, the importance of SNAPIN in lysosome maturation and retrograde cargo delivery by late endocytic trafficking as well as its interaction with the late endosomal SNARE complex has been demonstrated (Lu et al. 2009; Cai et al. 2010).

SNAPIN has been identified as a subunit of two complexes, the biogenesis of lysosome related organelles complex-1 (BLOC-1) and the BLOC-1 related complex (BORC) (Starcevic and Dell'Angelica 2004; Pu et al. 2015). Besides SNAPIN, both complexes share two additional subunits, namely BLOC subunit-1 (BLOS1) and BLOC subunit-2 (BLOS2) (Pu et al. 2015).

BLOC-1 consists of eight subunits and plays an important role in the biogenesis of lysosome related organelles (Falcón-Pérez et al. 2002; Ciciotte et al. 2003; Li et al. 2003; Starcevic and Dell'Angelica 2004; reviewed by Bowman et al. 2019). Several mutations in genes encoding for BLOC-1 subunits have been reported to cause the hereditary Hermansky-Pudlak syndrome (HPS) (Li et al. 2003; Morgan et al. 2006; Cullinane et al. 2012). Hypopigmentation and extended bleeding caused by an impaired function of melanosomes and platelet dense granules are common characteristics in HPS (reviewed by Di Pietro and Dell'Angelica 2005). In melanocytes, BLOC-1 has been demonstrated to play a key role in cargo delivery from sorting endosomes to melanosomes probability by coordinating the formation of tubular recycling endosomes (Setty et al. 2007; Delevoye et al. 2016). Downregulation of BLOC-1 subunits reduces the cellular melanin content thus indicating the importance of this complex in the biogenesis of melanosomes (Delevoye et al. 2016). Although the mechanism is poorly understood, a similar role of BLOC-1 has also been proposed during biogenesis of platelet dense granules (reviewed by Ambrosio and Di Pietro 2016; reviewed by Chen et al. 2018).

BORC is a protein complex consisting of eight subunits with crucial roles in lysosome positioning and lysosome-autophagosome fusion (Pu et al. 2015; Guardia et al. 2016; Jia et al. 2017; Filipek et al. 2017). Recently, Yordanov et al. (2019) demonstrated a decrease in late endosomal/lysosomal size and elevated phosphatidylinositol 3,5-bisphosphate ($PI(3,5)P_2$) upon knock out of the two BORC subunits Diaskedin and Myrlysin. The authors suggested that the increase in $PI(3,5)P_2$ was caused by a dysregulation of phosphatidylinositol 3-phosphate 5-kinase (PIKFYVE) activity in the KO cells thus indicating that BORC subunits might also participate in enzyme regulation (Yordanov et al. 2019).

## 2.6. Aim of this study

Glucagon, a peptide hormone secreted by pancreatic cells upon hypoglycemia, is a known activator of the cAMP-dependent protein kinase A pathway (Jelinek et al. 1993; reviewed by Habegger et al. 2010). After its activation, PKA mediates the break-down of glycogen thus directly counteracting the glucose starvation signal (reviewed by Unger 1985). Another process known to be upregulated upon nutrient deprivation is the expression of genes encoding for lysosomal proteins which correlates with an increase lysosome-dependent macromolecule catabolism (Sardiello et al. 2009; Settembre et al. 2011). As PKA and lysosomes play an important role in the degradation of complex molecules upon starvation, one could hypothesize an involvement of PKA in rapid regulation of lysosomal processes. In order to investigate this hypothesis, the first goal of the thesis is the identification of regulated phosphorylation sites at lysosomal membrane or lysosome-associated proteins upon elevation of the intracellular cAMP levels.

The low abundance of posttranslationally modified peptides in complex protein digests hinders their detection in classical bottom-up MS approaches. Therefore, PTM containing peptides are usually enriched prior to the LC-MS analysis. Immuno-affinity purification is the most common enrichment procedure used when investigating lysine and arginine PTMs (Guo et al. 2014). However, the standard protocol of this antibody-based method requires huge amount of starting material. Especially when dealing with limited sample amounts such as enriched organelles, this technique cannot be easily applied thus making such investigations laborious. In addition to that, the specificity of the antibody restricts the analysis to one specific lysine/arginine PTM. Hence, investigations of multiple different modifications in a sample require the utilization of several antibodies which not only increase the workload but also the experimental costs. As a result of these limitations, the second part of the thesis aims at developing an antibody-free technique which allows the MS-based detection of lysine and/or arginine PTM from small quantities of starting material. For this purpose, two different strategies are tested. These techniques are assumed to be not restricted to a specific lysine/arginine PTM, thus potentially allowing the detection of several modifications in a single MS experiment. Additionally, these methods are expected to be applicable to enriched lysosome factions as they are hypothesized to be compatible with low amounts of starting samples.

# 3. Material

## 3.1 Chemicals

As far as not otherwise stated, chemicals were purchased from Sigma-Aldrich (St. Louis, USA), Carl Roth (Karlsruhe, Germany), Merck (Darmstadt, Germany), Alfa Aesar (Haverhill, USA) or Thermo Fisher Scientific (Waltham, USA). Substances were either of analytical grade or had a purity ≥95 %. Organic solvents (HPLC/LC-MS grade) used for MS experiments were bought from VWR (Radnor, USA), Merck, Honeywell (Charlotte, USA), AppliChem (Darmstadt, Germany) or Biosolve (Valkenswaard, Netherlands).

## 3.2 Consumables

Consumables were bought from Sarstedt (Nümbrecht, Germany), Corning (Falcon®) (Corning, USA), Greiner Bio-One (Kremsmünster, Austria) or Beckman Coulter (Brea, USA) as far as not otherwise mentioned. For mass spectrometry experiments, plastic materials were purchased from Corning (Axygen®), Sarstedt or STARLAB (Hamburg, Germany).

## 3.3 Enzymes

| Enzyme | Manufacturer |
|---|---|
| Arylsulfatase A | Rentschler Biopharma (Laupheim, Germany) |
| BamHI (Fast Digest) | Thermo Fisher Scientific (Waltham, USA) |
| Calf Intestine Alkaline Phosphatase | Invitrogen (Carlsbad, USA) |
| DpnI | Thermo Fisher Scientific (Waltham, USA) |
| LysArginase | Structural Biology Unit CSIC (Barcelona, Spain) |
| LysN | Thermo Fisher Scientific (Waltham, USA) |
| Pfu DNA Polymerase | Thermo Fisher Scientific (Waltham, USA) |
| Phusion DNA Polymerase | Thermo Fisher Scientific (Waltham, USA) |
| Proteinase K | Carl Roth (Karlsruhe, Germany) |
| RnaseA | Thermo Fisher Scientific (Waltham, USA) |
| T4-Polynucleotide Kinase | Thermo Fisher Scientific (Waltham, USA) |
| Trypsin (MS-Experiments) | Promega (Fitchburg, USA) |
| Trypsin-EDTA solution (cell culture) | life technologies™ (Carlsbad, USA) |

## 3.4 Antibodies

### 3.4.1 Primary antibodies

| Antigen | Host | Dilution | Application | Manufacturer |
|---|---|---|---|---|
| Cathepsin D | rabbit | 1:1000 | WB | Abcam (Cambridge, UK); Order Number: ab97499 |
| CREB | rabbit | 1:1,000 | WB | Cell Signaling Technology (Danvers, USA); Order Number: 9197S |
| human ASA (Antiserum) | rabbit | 1:2000 | ELISA | self-made by AG Matzner |
| human MPR300 Dom9 N1+N2 del* | rabbit | 1:1000 | WB | self-made by Tilman Schuster |
| LAMP-2 | mouse | 1:50 | ICC | Hybridoma Bank (Iowa City, USA); Order Number: H4B4 |
| p-CREB | rabbit | 1:1,000 | WB | Cell Signaling Technology (Danvers, USA) ; Order Number: 9198S |
| SNAPIN | rabbit | 1:500 | WB | Proteintrech (Manchester, UK); Order Number: 10055-1-AP |
| α-Tubulin | mouse | 1:10,000-1:20,000 | WB | Sigma-Aldrich (St. Louis, USA); Order Number: T5168 |

* Dom9 N1+N2 Del: domain 9 with deletion of two glycosylation sites

### 3.4.2 Secondary antibodies

| Antigen | Tag | Host | Dilution | Application | Manufacturer |
|---|---|---|---|---|---|
| mouse IgG (H+L) | HRP | goat | 1:5,000 | WB | Jackson ImmunoResearch (Pennsylvania, USA); Order Number: 115-035-044 |
| rabbit IgG (H+L) | HRP | goat | 1:5,000 | WB | Jackson ImmunoResearch (Pennsylvania, USA); Order Number: 111-035-003 |
| rabbit IgG (H+L) | HRP | goat | 1:2,000 | ELISA | Jackson ImmunoResearch (Pennsylvania, USA); Order Number: 111-035-003 |
| mouse IgG (H+L) | Cy3 | goat | 1:250 | ICC | Jackson ImmunoResearch (Pennsylvania, USA); Order Number: 115-165-003 |

## 3.5 Cells

| Bacterial Strain | Genotype |
|---|---|
| *E. coli* XL1-Blue | *recA1 endA1 gyrA96 thi-1 hsdR17 supE44 relA1 lac* [F′ *proAB lacI*$^{q}$Z*ΔM15* Tn*10* (Tet$^{r}$)] |

| Mammalian Cell Lines | Supplier |
|---|---|
| HEK 293 | DSMZ-German Collection of Microorganisms and Cell Culture (Braunschweig, Germany) |
| HeLa | DSMZ-German Collection of Microorganisms and Cell Culture (Braunschweig, Germany) |

## 3.6 Peptides

| Sequence | Supplier |
|---|---|
| FSEEKHLEDLER | Dr. D. Winter (IBMB) |
| MHTGHANAKHIAGLSR | JPT, Berlin, Germany |

## 3.7 Primers

All primers were synthesized by Biomers (Ulm, Germany).

| Name | Sequence | Application |
|---|---|---|
| SNAPIN S133A fwd | GGAATTTACCCCCCTGGCGCTCCAGGCAAAAGCGGACCG | SDM SNAPIN S133A |
| SNAPIN S133A rev | CGGTCCGCTTTTGCCTGGAGCGCCAGGGGGGTAAATTCC | SDM SNAPIN S133A |
| SNAPIN S133E fwd | GGAATTTACCCCCCTGGCGAGCCAGGCAAAAGCGGACCG | SDM SNAPIN S133E |
| SNAPIN S133E rev | CGGTCCGCTTTTGCCTGGCTCGCCAGGGGGGTAAATTCC | SDM SNAPIN S133E |
| pCMV fwd | CCGTTGACGCAAATGGG | Sequencing pCMV-vector |
| SNAPIN fwd CRISPR-Cas9 1st PCR | ACACTCTTTCCCTACACGACGCTCTTCCGATCTGTTGGCAAAAACCTAAGGTCCTG | 1st PCR gene KO valid. |
| SNAPIN rev CRISPR-Cas9 1st PCR | TGACTGGAGTTCAGACGTGTGCTCTTCCGATCTAAACTGATTCGAGGCGGGGAGGA | 1st PCR gene KO valid. |
| D501_long Primer A | AATGATACGGCGACCACCGAGATCTACACTATAGCCTACACTCTTTCCCTACACGACGCT | 2nd PCR gene KO valid. |
| D502_long Primer A | AATGATACGGCGACCACCGAGATCTACACATAGAGGCACACTCTTTCCCTACACGACGCT | 2nd PCR gene KO valid. |
| D503_long Primer A | AATGATACGGCGACCACCGAGATCTACACCCTATCCTACACTCTTTCCCTACACGACGCT | 2nd PCR gene KO valid. |
| D701_long Primer B | CAAGCAGAAGACGGCATACGAGATCGAGTAATGTGACTGGAGTTCAGACGTGTGCT | 2nd PCR gene KO valid. |
| D702_long Primer B | CAAGCAGAAGACGGCATACGAGATTCTCCGGAGTGACTGGAGTTCAGACGTGTGCT | 2nd PCR gene KO valid. |
| D703_long Primer B | CAAGCAGAAGACGGCATACGAGATAATGAGCGGTGACTGGAGTTCAGACGTGTGCT | 2nd PCR gene KO valid. |
| D704_long Primer B | CAAGCAGAAGACGGCATACGAGATGGAATCTCGTGACTGGAGTTCAGACGTGTGCT | 2nd PCR gene KO valid. |
| D705_long Primer B | CAAGCAGAAGACGGCATACGAGATTTCTGAATGTGACTGGAGTTCAGACGTGTGCT | 2nd PCR gene KO valid. |
| D706_long Primer B | CAAGCAGAAGACGGCATACGAGATACGAATTCGTGACTGGAGTTCAGACGTGTGCT | 2nd PCR gene KO valid. |
| D707_long Primer B | CAAGCAGAAGACGGCATACGAGATAGCTTCAGGTGACTGGAGTTCAGACGTGTGCT | 2nd PCR gene KO valid. |
| D708_long Primer B | CAAGCAGAAGACGGCATACGAGATGCGCATTAGTGACTGGAGTTCAGACGTGTGCT | 2nd PCR gene KO valid. |
| D709_long Primer B | CAAGCAGAAGACGGCATACGAGATCATAGCCGGTGACTGGAGTTCAGACGTGTGCT | 2nd PCR gene KO valid. |
| D710_long Primer B | CAAGCAGAAGACGGCATACGAGATTTCGCGGAGTGACTGGAGTTCAGACGTGTGCT | 2nd PCR gene KO valid. |
| D711_long Primer B | CAAGCAGAAGACGGCATACGAGATGCGCGAGAGTGACTGGAGTTCAGACGTGTGCT | 2nd PCR gene KO valid. |
| D712_long Primer B | CAAGCAGAAGACGGCATACGAGATCTATCGCTGTGACTGGAGTTCAGACGTGTGCT | 2nd PCR gene KO valid. |

## 3.8 Vectors

| Name | Construct | Supplier |
|---|---|---|
| pCMV6_SNAPIN | SNAPIN Myc-DDK | Origene (Rockville, USA) |
| pCMV6_SNAPIN_S133A | SNAPIN S133A Myc-DDK | self-made SDM (Template: pCMV6_SNAPIN) |
| pCMV6_SNAPIN_S133E | SNAPIN S133E Myc-DDK | self-made SDM (Template: pCMV6_SNAPIN) |
| Edit-R Cas9 nuclease expression plasmid (Puro$^{R}$) | Cas9 | Dharmacon/Horizon (Cambridge, UK), |

## 3.9 Instruments

| Instrument | Model | Manufacturer |
|---|---|---|
| Centrifuge (max. 2 ml) | Z 216 MK | Hermle(Wehingen, Germany) |
| Centrifuge benchtop | Allegra X-15R | Beckman Coulter (Brea, USA) |
| Centrifuge cell culture | Labofuge 400e | Heraeus (Hanau, Germany) |
| Counting Camber | Fuchs-Rosenthal | Brand (Wertheim, Germany) |
| Cryopreservation system | MVE TS; Tank 800 series-190 | CHART (Luxembourg, Luxembourg) |
| Detection system agarose gels | BioDoc Analyze | Biometra/Analytik Jena (Jena, Germany) |
| Detection system HRP-based immune detection | Fusion Solo | Vilbert Lourmat (Collégien, France) |
| Dounce homogenizer | 7 ml, small clearance pestle | Kimble Chase (Rockwood, USA) |
| Electrotransfer system | Trans-Blot® Cell | Bio-Rad (Hercules, USA) |
| Electrotransfer system | PerfectBlue™ Semi-Dry Electro Blotter | peqlab (Erlangen, Germany) |
| Electrotransfer system | Trans-Blot® Turbo | Bio-Rad (Hercules, USA) |
| Equipment agarose gel electrophoresis | PerfectBlue™ Gel System | peqlab (Erlangen, Germany) |
| Equipment isoelectic focusing | PROTEAN® IEF cell | Bio-Rad (Hercules, USA) |
| Equipment SDS-PAGE electrophoresis (self-made gels) | Mini-PROTEON® Tetra Cell | Bio-Rad (Hercules, USA) |
| Equipment SDS-PAGE electrophoresis (precast gels) | Mini Gel Tank | life technologies™ (Carlsbad, USA) |
| Fluorescence microscope | LSM 980 Airyscan 2 detector, inverse AxioObserver 7 | Zeiss (Oberkochen, Germany) |
| Freeze dryer | Lyovac GT2 | Finn-Aqua (Hürth, Germany) |
| Heating block | MHR23, BM15 | Ditabis (Pforzheim, Germany) |
| Ice machine | | Ziegra (Isernhagen, Germany) |
| Incubator bacteria | Function Line B12 | Heraeus (Hanau, Germany) |
| Incubator bacteria (shaking) | Innova™ 43 | New Brunswick Scientific (Edison, USA) |
| Incubator cell culture | HERAcell® 240 | Heraeus (Hanau, Germany) |
| Laboratory rocker | Rotamax 120 | Heidolph (Schwabach, Germany) |
| Laminar flow cabinet | Clean-Air | Bio-Flow (Meckenheim, Germany) |
| Liquid chromatography system | Ultimate 3000 RSLC nano HPLC system | Dionex (Idstein, Germany) |
| Magnetic stand lysosome enrichment | Quadro MACS Separator | Miltenyi Biotec (Bergisch Gladbach, Germany) |
| Magnetic stirrer | WiseStir® MSH-20D | Witeg (Wertheim, Germany) |
| Mass spectrometer | LTQ Orbitrap Velos | Thermo Fisher Scientific (Bremen, Germany) |
| Mass spectrometer | Orbitrap Fusion Lumos | Thermo Fisher Scientific (Bremen, Germany) |
| Mass spectrometer | MALDI-TOF/TOF Autoflex III | Bruker Daltonik (Bremen, Germany) |
| Micro scale | CP1245-DCE | Sartorius (Göttingen, Germany) |
| Micropipettes | | Gilson (Middleton, USA) |
| Microplate reader | GENios | Tecan (Männedorf, Switzerland) |
| Microplate reader | Infinite Pro 2000 | Tecan (Männedorf, Switzerland) |
| Microplate washer | HydroFlex™ | Tecan (Männedorf, Switzerland) |
| Microscope cell culture | Axio Vert.A1 | Zeiss (Oberkochen, Germany) |

| Instrument | Model | Manufacturer |
|---|---|---|
| Multi-channel micropipette | Transferpette S-12 | Brand (Wertheim, Germany) |
| Orbital shaker | PTR-35 | Grant-bio (Cambridge, UK) |
| pH electrode | WTW SenTix 50 | Xylem (Weilheim, Germany) |
| pH meter | pH-Meter 761 calimatic | Knick (Berlin, Germany) |
| Power supply | PowerPac 300 | Bio-Rad (Hercules, USA) |
| Spectrophotometer | NanoDrop 2000 | Thermo Fisher Scientific (Waltham, USA) |
| Thermal cycler | T3 Thermalcycler | Biometra/Analytik Jena (Jena, Germany) |
| Tip sonicator | Sonifier 250 | Branson (Danbury, USA) |
| Tip sonicator | UP50H | Hielscher (Teltow, Germany) |
| Tube Rotator | LD79 | Labinco (Breda, Netherlands) |
| Ultracentrifuge | Optima TLX | Beckman Coulter (Brea, USA) |
| Ultrasonic bath | 2510 | Branson (Danbury, USA) |
| Vacuum centrifuge | ScanSpeed 40; Rotor GRV-m2.0-200 | ScanVac/Labogene (Lynge, Denmark) |
| Vortex | ZX3 | UniEquip (Planegg, Germany) |
| Water bath cell culture | 1083 | GFL (Burgwedel, Germany) |
| Water purification system | arium® Pro | Sartorius, Göttingen, Germany |

## 3.10 Software

| Software | Application | Supplier |
|---|---|---|
| Capt Advance Solo 4 | Software Fusion Solo HRP-based immune detection system; Signal quantification | Vilbert Lourmat (Collégien, France) |
| Chromeleon | Controlling Dionex LC-system | Thermo Fisher Scientific(Waltham, USA) |
| CorelDRAW | Home & Student 2019 | Corel Corporation (Ottawa, Canada) |
| Excel 2016 | Data analysis and visualization | Microsoft (Redmond, USA) |
| flexAnalysis | MALDI TOF data analysis | Bruker Daltonik (Bremen, Germany) |
| flexControl | MALDI TOF data acquisition | Bruker Daltonik (Bremen, Germany) |
| Genome Compiler | Primer design and Sanger sequencing analysis | Genome Compiler Corporation (Los Altos, USA); www.genomecompiler.com |
| i-control™ | Software Infinite Pro 200 Microplate Reader | Tecan (Männedorf, Switzerland) |
| ImageJ | Maximum intensity projection LSM Z-stacks | Schneider et al. 2012 |
| MaxQuant | Orbitrap data analysis | Cox and Mann 2008; Cox et al. 2011 |
| NetPhos | Kinase consensus sequence analysis | Blom et al. 1999; Blom et al. 2004; www.cbs.dtu.dk/services/NetPhos |
| OutKnocker | NGS data analysis | Schmid-Burgk et al. 2014; www.outknocker.org |
| PEAKs | Orbitrap data analysis | Bioinformatics Solutions Inc. (Waterloo, Canada) |
| Proteome Discoverer | Orbitrap data analysis | Thermo Fisher Scientific (Waltham, USA) |
| R-studio | Data analysis and visualization; statistics | R Core Team 2019 |
| UCSC Genome Browser | Determination of SNAPIN reference sequence (NGS data analysis) | Kent et al. 2002; www.genome.ucsc.edu |
| Word 2016 | Text processing program | Microsoft (Redmond, USA) |
| Xcalibur | Orbitrap data I | Thermo Fisher Scientific (Waltham, USA) |
| Xfluor4 | Software GENios Microplate Reader | Tecan (Männedorf, Switzerland) |
| Zen | Image Acquisition LSM 980 Airyscan 2 | Zeiss (Oberkochen, Germany) |

# 4. Methods

## 4.1 Protein-biochemistry techniques

### 4.1.1 Determination of protein level in solution

Colorimetric determination of protein concentrations was either performed with the detergent compatible (DC) protein assay (Bio-Rad, Hercules, USA) or the Pierce™ bicinchoninic acid (BCA) assay (Thermo Fisher Scientific, Waltham, USA).

For the DC protein assay, solution A´ was prepared by adding 20 µl of solution S to 1 mL of solution A. Afterwards, 5 µl of sample was pipetted into one well of a 96-well plate and mixed with 25 µL of solution A´. After adding 200 µl of solution B, the mixture was incubated for 15 min at room temperature (RT) before measuring the absorption at a wavelength of 750 nm (GENios, Tecan). Bovine serum albumin (BSA) solutions served as standards and were used for calculating the protein amount of the samples (linear regression).

In case of the BCA assay, the working solution was prepared by mixing one part of solution B with 50 parts of solution A. 25 µl sample or BSA standard solution were added to one well of a 96-well plate and mixed with 200 µl working solution. The assay was incubated for 30 min at 37°C. Absorbance was measured at a wavelength of 595 nm (GENios, Tecan). Based on the BSA standard curve (polynomial regression), the protein amounts of the samples were calculated.

### 4.1.2 Cell lysis

As far as not otherwise stated, cells were lysed according to the following procedure.

After removing the cultivation medium, cells were washed twice with ice cold PBS. Subsequent to this, cells were scraped in 500 µl ice cold lysis buffer (supplemented with 1x Halt™ Phosphatase Inhibitor Cocktail (Thermo Fisher Scientific, Waltham, USA) if needed). The cell lysate was transferred to a fresh reaction tube and either stored at -20°C or directly treated with a tip sonicator (Hielscher, UP50H) in order to shear high molecular DNA. In the next step, the lysate was centrifuged for 5 min at 10,000 x g at 4°C. The supernatant was transferred to a fresh reaction tube. Protein concentrations were measured by the BCA or DC assay.

| Solution | Concentration | Component |
|---|---|---|
| NP-40 Lysis Buffer | 1 % (w/v) | NP-40 |
| | 25 mM | Tris-HCl (pH 7.4) |
| | 1 mM | EDTA |
| | 150 mM | NaCl |
| | 1x | Halt™ Protease Inhibitor Cocktail* |
| SDC Lysis Buffer | 5 % (w/v) | SDC |
| | 20 mM | TEAB |
| | 1x | Halt™ Protease Inhibitor Cocktail* |
| Calf Intestine Alkaline Phosphatase (CIAP) Lysis Buffer | 0.02 % (w/v) | Triton X-100 |
| | 50 mM | Tris-HCl (pH 7.9) |
| | 100 mM | NaCl |
| | 10 mM | $MgCl_2$ |
| | 1 mM | DTT |
| | 1x | Halt™ Protease Inhibitor Cocktail* |
| 1x PBS | 10 mM | $Na_2HPO_4$ x $2H_2O$ |
| | 1.77 mM | $KH_2PO_4$ |
| | 137 mM | NaCl |
| | 2.7 mM | KCl |

* Thermo Fisher Scientific, Waltham, USA

### 4.1.3 Sodium dodecyl sulfate polyacrylamide gel electrophoresis (SDS-PAGE)

Sodium dodecyl sulfate polyacrylamide gel electrophoresis (SDS-PAGE) enables separation of proteins according to their molecular mass (Laemmli 1970).

The solutions and recipes used for preparation of a discontinuous SDS polyacrylamide gel are listed below.

| Component | Stacking gel (5 %) | Separating gel (10 %) | Separating gel (12.5 %) | Separating gel (15 %) |
|---|---|---|---|---|
| **Acrylamide (40 %)** | 5 % (v/v) | 10 % (v/v) | 12.5 % (v/v) | 15 % (v/v) |
| **Tris-HCl, pH 6.8** | 0.125 M | - | - | - |
| **Tris- HCl, pH 8.8** | - | 0.375 M | 0.375 M | 0.375 M |
| **SDS** | 0.1 % (w/v) | 0.1 % (w/v) | 0.1 % (w/v) | 0.1 % (w/v) |
| **APS** | 0.04 % (w/v) | 0.06 % (w/v) | 0.06 % (w/v) | 0.06 % (w/v) |
| **TEMED** | 0.075 % (v/v) | 0.075 % (v/v) | 0.075 % (v/v) | 0.075 % (v/v) |

Prior to the SDS-PAGE, samples were mixed with 4x Laemmli-buffer and incubated for 5 min at 95°C. In addition to the samples, 3-5 µl PageRuler™ Prestained Protein Ladder (Thermo Fisher Scientific, Waltham, USA) were loaded onto the gels. Gel electrophoresis was performed at 80-140 V by using the vertical Mini-PROTEAN tetra cell system (Bio-Rad).

In order to investigate the MPR300 level in wt and SNAPIN KO cells, protein samples were mixed with 4 x NuPAGE™ LDS sample buffer (life technologies™, Carlsbad, USA) and incubated for 5 min at 95°C. Afterwards, the samples and 10 µl Multicolor High Range Protein Ladder (Thermo

Fisher Scientific, Waltham, USA) were loaded onto a precast NuPAGE™ 3-8 % Tris-Acetate gel (life technologies™, Carlsbad, USA). For gel electrophoresis, the Mini Gel Tank system (life technologies™) was used (60-90 V).

| Solution | Concentration | Component |
|---|---|---|
| SDS-running buffer (for self-made gels) | 25 mM | Tris |
| | 192 mM | Glycine |
| | 3.5 mM | SDS |
| NuPAGE running buffer (for precast NuPAGE™ Tris-Acetate gels) | 50 mM | Tricine |
| | 50 mM | Tris |
| | 3.5 mM | SDS |
| 4x Laemmli-buffer | 0.25 mM | Tris-HCl (pH 6.8) |
| | 8 % (w/v) | SDS |
| | 40 % (v/v) | Glycerol |
| | 0.004 % (w/v) | Bromphenol blue |
| | 100 mM | DTT |

### 4.1.4 Coomassie staining of SDS polyacrylamide gels

After SDS-PAGE, gels were washed three times for 5 min with $H_2O$ before incubating with PageBlue™ protein staining solution (Thermo Fisher Scientific, Waltham, USA) (1 h – overnight (o.n.)). Subsequent to this, gels were washed several times with water in order to reduce background staining.

### 4.1.5 2D gelelectrophoresis

2-dimensional (2D) gelelectrophoresis is a combination of isoelectric focusing (IEF) and SDS-PAGE which enhances protein and protein-isoform separation in cell lysates and other complex mixtures (O'Farrell 1975; Klose 1975).

Prior to the IEF, proteins were precipitated according to the method described by Wessel and Flügge (1984). In brief, 300 µg protein sample (in 100 µl aqueous solution) were mixed with 400 µl methanol and centrifuged for 10 s at 9,000 x g. Afterwards, 100 µl chloroform were added before the mixture was vortexed and centrifuged again (10 s, 9,000 x g). This step was followed by the addition of 300 µl $H_2O$, vigorous mixing and centrifugation for 1 min at 9,000 x g. The upper phase was discarded before 300 µl methanol were added to the reaction tube. After an additional centrifugation step (2 min, 9,000 x g), the supernatant was discarded and the protein pellet was air dried.

Dephosphorylation of proteins prior to IEF was performed by incubating 300 µg protein lysate with 300 units (U) calf intestine alkaline phosphatase (CIAP) in a total volume of 100 µl lysis puffer (see section 4.1.2). The reaction was incubated for 1 h at 37°C before the proteins were precipitated by the Wessel-Flügge method.

For IEF, protein pellets were dissolved in 125 µl rehydration solution. Prior to isoelectric focusing, active rehydration of the IEF strip (7 cm, pH range 6-11 (linear), GE Healthcare, Chicago, USA) with the protein solution was performed for 12 h at 50 V. The different steps of IEF are listed below. The IEF was performed with the PROTEAN IEF cell (Bio-Rad).

| Step | Voltage | Duration |
|---|---|---|
| **Conditioning step** | 250 V | 15 min |
| **Voltage ramping** | 4000 V (linear ramp) | 2 h |
| **Final focusing** | 4000 V (rapid ramp) | 20,000 Vh |
| **Hold step** | 500 V | ∞ |

After IEF, the gel stripes were stored at -80°C until gel electrophoresis was performed. For SDS-PAGE, 15 % separating gels (1.5 mm thickness) without stacking gels were prepared. The IEF strip and a small piece of Whatman paper soaked with PageRuler™ prestaind protein ladder (Thermo Fisher Scientific, Waltham, USA) were placed on top of the polyacrylamide gel. Subsequently, 0.5 % Agarose (w/v), dissolved in SDS-PAGE-running buffer, was added. Gel electrophoresis was performed at 110 V in the Mini-PROTEAN gel system (Bio-Rad).

| Solution | Concentration | Component |
|---|---|---|
| Rehydration solution | 8 M | Urea |
| | 2 % (w/v) | CHAPS |
| | 0.005 % (w/v) | Bromphenol blue |
| | 20 mM | DTT |
| | 0.2 % | IEF buffer for pH range 6-11* |

* GE Healthcare, Chicago, USA

### 4.1.6 Western Blot and immune detection of proteins

The western blot method aims at transferring proteins from polyacrylamide gels onto membranes. Subsequently, the immobilized protein of interest can be detected via antibodies. For signal visualization, these antibodies are often linked to a fluorophore or a horseradish peroxidase (HRP). Whereas fluorophores are emitting electromagnetic radiation after excitation with a certain wavelength, the HRP catalyzes a chemical reaction which is associated with the emission of light (chemoluminescence) (Towbin et al. 1979).

Prior to western blotting, the nitrocellulose membrane was activated in water. Afterwards, the gel and the nitrocellulose membrane were dipped in blotting buffer before placing them between two stacks of presoaked Whatman paper. Electrotransfer was either performed by semi-dry (for self-made gels) or wet blot (for NuPAGE™ Tris-Acetate gels) condition. The currents used for protein transfer are listed below.

| **Method** | **Current [mA · (cm² membrane)$^{-1}$ · min$^{-1}$]** |
|---|---|
| Semi-dry protein transfer | 0.02 or 0.1 |
| Wet protein transfer | 0.08 |

After electrotransfer, proteins bound to the nitrocellulose membrane were stained for 10 min with Ponceau staining solution at RT. Subsequent to this, the membrane was blocked with 5 % BSA (w/v) or 5 % powdered milk (w/v) in TBST (1x TBS, 0.1 % Tween-20 (v/v)) for 1 h followed by the incubation with the primary antibody overnight at 4°C. Afterwards, the membrane was washed three times for 5 min with TBST and then incubated with the horseradish peroxidase conjugated secondary antibody for 1 h at RT. Three additional washing steps (three times for 5 min with TBST) were performed before detecting the target proteins by enhanced chemoluminescence (ECL).

| **Solution** | **Concentration** | **Component** |
|---|---|---|
| Blotting buffer (for self-made gels) | 25 mM | Tris |
| | 0.2 M | Glycine |
| | 20 % (v/v) | Methanol |
| Blotting buffer (for precast NuPAGE™ Tris-Acetate gels*) | 25 mM | Bis-Tris |
| | 25 mM | Bicine |
| | 1 mM | EDTA |
| | 20 % (v/v) | Methanol |
| 10x TBS (pH 7.6) | 0.2 M | Tris |
| | 1.5 M | NaCl |
| Ponceau staining solution | 0.2 % (w/v) | Ponceau-S |
| | 5 % (v/v) | Acetic acid |

* life technologies™, Carlsbad, USA

### 4.1.7 Quantification of Western Blot signals

ECL signals below saturation were quantified using the FusionCapt Advanced camera software version 16.15 (Vilber Lourmat). For normalization, signal intensities derived from the protein of interest were divided lane-wise by a corresponding intensity value measured for a "housekeeping" protein, such as α-Tubulin.

If Western Blot signals were statistically analyzed, R-studio was used to test the homogeneity of variances by a Levene's test. Within the present study, all significance value of the Levene's test

were higher than 0.05. Therefore, homoscedasticity was assumed and a normal two sample t-test was performed by using R-studio (Null-hypothesis = difference in means is 0, two-sided, unpaired, confidence interval 0.95) (version 1.2.5019) (R Core Team 2019).
For calculating the standard deviation, the denominator n-1 was used.

## 4.2 Molecular biology techniques

### 4.2.1 Agarose gel electrophoresis

Agarose gel electrophoresis is a method used to separate DNA fragments according to their length. By adding intercalating substances such as ethidium bromide to the agarose gel, DNA fragments can be visualized via ultraviolet (UV)-light.

For gel preparation, agarose was dissolved in hot 1x TAE-buffer. Ethidium bromide (final concentration 0.5 µg/ml) was added to the agarose solution before polymerization. Once the gel was polymerized, DNA samples were mixed with 6x DNA gel loading dye (Thermo Fisher Scientific, Waltham, USA) and loaded onto the gel. The GeneRuler 1 kb DNA Ladder (Thermo Fisher Scientific, Waltham, USA) was loaded for size determination of DNA fragments. Electrophoresis was performed at 120 V and DNA fragments were visualized by UV-light.

| Solution | Concentration | Component |
|---|---|---|
| 1x TAE | 40 mM | Tris |
| | 5.7 % (v/v) | Acetic acid |
| | 2 mM | EDTA |

### 4.2.2 Transformation

In molecular biology, transformation is a process which aims at introducing foreign DNA constructs into bacteria. Inside the cells, the DNA vector is replicated and the genes encoded on the plasmid are expressed (Cohen et al. 1972).

For transformation, competent *Escherichia coli* (*E. coli*) XL1-Blue were thawed on ice before 10 ng of plasmid DNA were added. The mixture was incubated on ice for 20 min. Heat shock was performed for 45 s at 42°C. Subsequently, the cells were placed on ice for 2 min. After adding 1 ml prewarmed LB-medium, the cell suspension was transferred to a 15 ml reaction tube and incubated for 1 h at 37°C and 200 rpm. 50 µl and 100 µl of the bacteria suspension were plated

on two antibiotic containing LB agar plates, respectively. The agar plates were incubated at 37°C overnight.

| LB-medium (pH 7.2) |
|---|
| 10 g/l tryptone/peptone |
| 5 g/l Bacto™ yeast extract* |
| 10 g/l NaCl |

* Thermo Fisher Scientific, Waltham, USA

### 4.2.3 Plasmid extraction and purification

After transformation, single bacteria colonies were picked and cultivated for 8-10 h at 37°C in 5 ml LB-medium containing 25 µg/ml kanamycin. Subsequently, the entire pre-culture was added to 100 ml LB-medium (25 µg/ml kanamycin). This main culture was incubated at 37°C overnight. On the next day, bacteria were harvested and used for plasmid DNA purification. For this purpose, either the QIAprep® Spin Miniprep Kit (Qiagen, Hilden, Germany) or the Pure Link® HiPure plasmid filter midiprep kit (Invitrogen, Carlsbad, USA) was used according to the instruction given in the manual.

### 4.2.4 Site directed mutagenesis

Site directed mutagenesis (SDM) is a technique aiming at generating point mutations at a specific position within the plasmid DNA sequence, thus leading to an amino acid exchange in the gene product. In this method, the mutation is introduced by polymerase chain reaction (PCR)-based amplification of the template vector with specific primers carrying the modified DNA pattern within their sequence (Agilent Technologies SDM Manual). The technique is often used in phosphomimetic studies in order to investigate the functional impact of a certain phosphorylation site. Here, the substitution of an amino acid residue at a potential phospho-site with an acidic amino acid mimics a permanent phosphorylation. In contrast, the replacement by non-charged amino acid such as alanine imitates a non-phosphorylatable isoform.

Prior to PCR, SDM-primers were phosphorylated by using a T4-polynucleotide kinase (PNK) according to the recipe given below. The reaction was incubated for 1 h at 37 °C.

| Component | |
|---|---|
| Primer | 500 pmol |
| 10 x T4-PNK buffer | 5 µl |
| 100 mM ATP | 1 µl |
| T4-PNK | 0.5 units |
| $H_2O$ | ad 50 µl |

The pCMV6_SNAPIN plasmid used as a template (purchased from Origene) in SDM was amplified in *E. coli* XL1-Blue stain and purified by the Pure Link™ HiPure plasmid filter midiprep kit (Invitrogen, Carlsbad, USA). SDM was performed via PCR. The master mix components and program used for PCR are listed below. For SDM, the master mix was preheated to 95°C before 1 µl of Pfu DNA polymerase was added.

| Master mix component | |
|---|---|
| Template | 20 ng |
| 10x Pfu buffer | 5 µl |
| 2 mm dNTP mix | 5 µl |
| Phospho. forward primer | 10 pmol |
| Phospho. reverse primer | 10 pmol |
| DMSO | 5 µl |
| 25 mm $MgCl_2$ | 3 µl |
| $H_2O$ | ad 49 µl |

| Step | Temperature | Time | |
|---|---|---|---|
| **Initial denaturation** | 95°C | 30 sec | |
| **Denaturation** | 95°C | 30 sec | |
| **Annealing** | 55°C | 60 sec | x 16 cycles |
| **Elongation** | 68°C | 300 sec | |
| **Final elongation** | 72°C | 5 min | |
| **Storage** | 4 C | ∞ | |

In order to digest the methylated template vector, the PCR mixture was incubated with 1 µl DpnI at 37°C overnight. On the next day, the oligonucleotides were purified by using a silica column and the buffers of the QIAprep® Spin Miniprep Kit (Qiagen, Hilden, Germany). For this purpose, the oligonucleotide mixture after PCR and DpnI digestion was mixed with 150 µl QIAprep® PB-buffer and added to a QIAprep® silica column. The column was centrifuged for 30 s at 12,000 x g and the flow through was loaded again. After another centrifugation step at 12,000 x g for 30 sec, the column was washed twice with 750 µl QIAprep® PE-buffer (30 sec, 12,000 x g). In order to remove residual washing buffer, the column was centrifuged for 1 min at 12,000 x g. Oligonucleotides were eluted by adding 30 µl $H_2O$ to the column. After incubation for 1 min at RT, the column was centrifuged at 12,000 x g for 1 min and the whole flow through was used for transformation into *E. coli* XL1-Blue. The plasmids were purified by the QIAprep® Spin Miniprep

Kit followed by a control digestion with BamHI (see section 4.2.5). Digestions with the expected fragment pattern were sent for Sanger Sequencing.

### 4.2.5 Restriction digestion

Restriction endonucleases are frequently used tools in molecular biology for DNA cleavage at specific sequence pattern (Meselson and Yuan 1968; Smith and Wilcox 1970).

For control digestion after SDM, plasmid DNA was digested with fast-digest (FD) restriction BamHI according to the recipe below. The mixture was incubated for 45 min at 37°C. Afterwards, DNA fragments were separated according to their length by agarose gel electrophoresis.

| **Component** | |
|---|---|
| Plasmid DNA | 600-900 ng |
| 10 x FD green buffer | 1.5 µl |
| FD BamHI | 1 µl |
| $H_2O$ | ad 15 µl |

### 4.2.6 Sanger sequencing

After cloning, vector assembly was validated by Sanger sequencing (Sanger et al. 1977).

Sequencing samples were prepared by mixing 500 ng plasmid with 25 pmol sequencing primer and adjusting the volume to 10 µl with $H_2O$. For LightRun Sanger sequencing, the samples were sent to Eurofins Genomics (Ebersberg, Germany).

## 4.3 Cell culture

### 4.3.1 Cell cultivation

Human embryonic kidney (HEK 293) and Henrietta Lacks (HeLa) cells were cultivated in DMEM GlutaMAX™ medium supplemented with 9 % (v/v) fetal calf serum (FCS) and 0.9 % (v/v) penicillin/streptomycin (Pen/Strep). The single medium components were purchased from life technologies™ (Carlsbad, USA).

For subcultivation, cells were washed twice with Dulbecco's phosphate-buffered saline (DPBS) (life technologies™, Carlsbad, USA) and detached from the surface by adding 0.5 ml 0.05 %

trypsin-EDTA (life technologies™, Carlsbad, USA) solution per 10 cm petri dish. Once the cells were in suspension, a minimum of 2.5 ml cultivation medium were added in order to inactivate the trypsin. According to the split ratio, cells were transferred to a centrifugation tube and centrifuged for 3 min at 328-1,000 x g. Afterwards, the cell pellet was resuspended in fresh medium and the cells were cultivated at 37 °C and 5 % (HEK cells) or 5-10 % (HeLa cells) $CO_2$ respectively.

### 4.3.2 Cell counting

Cells were counted with a Fuchs-Rosenthal counting camber. For this purpose, the cell pellet after trypsinization and centrifugation was resuspended in cultivation medium and, if necessary, further diluted before 10 µl of the suspension were mixed with 10 µl 0.4 % trypan blue stain solution (life technologies™, Carlsbad, USA). Afterwards, the mixture was pipetted into a Fuchs-Rosenthal counting camber with 16 one square millimeter areas (16 b-fields) and a depth of 0.2 mm. The number of cells present within four b-fields was counted and the cell concentration of the suspension was calculated with the following formula:

$$\text{cell concentration [cells/ml]} = \text{number of cells in 4 b-fields x dilution factor} \cdot 1250$$

### 4.3.3 Cryopreservation and thawing of cells

For cryopreservation, cells were trypsinized according to the procedure mentioned for cell subcultivation. After centrifugation, cells were resuspended in cultivation medium containing 10 % DMSO (v/v). The cell suspension was transferred to cryovials and frozen at -80 °C for at least 24 h in a polystyrene rack. For long term storage, cryovials were transferred to a liquid nitrogen cryopreservation container.

Frozen cells were thawed by incubating the cryovial at 37 °C in a water bath until approx. 90 % of the suspension was defrosted. Afterwards, cells were transferred to 9 ml of prewarmed medium and centrifuged for 3 min at 328-1000 x g. Subsequent to this, the cells were resuspended in fresh medium and cultivated at 37 °C and 5 % (HEK cells) or 5-10 % (HeLa cells) $CO_2$ respectively.

### 4.3.4 Stable isotope labeling with amino acids in cell culture (SILAC)

In order to label proteins on cell culture level, the cultivation media can be supplemented with three different isotopically labeled arginine and lysine variants. These amino acids are incorporated into the protein sequence during translation thus leading to light, medium and heavy labeled cell populations which originated from the same cell-starting material. After their generation, these cells in which the proteins were isotopically labeled according to the SILAC procedure can be used for investigating stimulus-induced quantitative changes in the proteome. For example, a specific cell treatment can be applied to cells grown in cultivation medium containing heavy arginines and lysines (mass shifts compared to light variants R +10 Da and K +8 Da). In contrast, cells used as a stimulation control could be cultivated in medium supplemented with light variants of these two amino acids. After cell lysis, the lysates of the treated and non-treated samples are combined. Tryptic peptides generated during mass spectrometry sample preparation contain at least one isotopically labeled arginine or lysine (except peptide derived from protein C-terminus). Therefore, a mass shift can be observed for peptides with the same sequence derived from the different sample groups. Based on this, differences in the peptide abundances can be relatively quantified by MS analysis (Ong et al. 2002; Ong et al. 2003; Ong and Mann 2006).

The media used for SILAC and cultivation of isotopically labeled cells are listed below.

| **SILAC light cultivation medium** | **SILAC medium cultivation medium** | **SILAC heavy cultivation medium** |
|---|---|---|
| DMEM for SILAC | DMEM for SILAC* | DMEM for SILAC* |
| + 9 % FCS (v/v)* | + 9 % FCS (v/v)* | + 9 % FCS (v/v)* |
| + 0.9 % Pen/Strep (v/v)* | + 0.9 % Pen/Strep (v/v)* | + 0.9 % Pen/Strep (v/v)* |
| + 0.8 mM Lysine light** | + 0.8 mM Lysine medium (+4)$ | + 0.8 mM Lysine heavy (+8)$ |
| + 0.4 mM Arginine light** | + 0.4 mM Arginine medium (+6)$ | + 0.4 mM Arginine heavy (+10)$ |

* Thermo Fisher Scientific, Waltham, USA
** Sigma Aldrich, St. Louis, USA
$ Cambridge Isotopes Laboratories, Tewksbury, USA

In order to start isotopic labeling of proteins, cells were detached from the cultivation dish like mentioned before. The cell suspension after inactivation of trypsin was split into three centrifugation tubes. After centrifugation for 3 min at 328-1000 x g, the cell pellets were either resuspended in SILAC light, medium or heavy medium. Cells were cultivated at 37 °C and 5 % (HEK cells) or 5-10 % (HeLa cells) $CO_2$ respectively. Protein labeling was performed by subcultivating the cells in the particular medium for at least seven cell cycles.

### 4.3.5 Cell treatment

For cell stimulation, the cultivation media was aspirated and replaced by the corresponding stimulation medium (cultivation medium plus additives). Adding FSK and Torin1 (both dissolved in DMSO) to the media resulted in a final DMSO concentration of 0.1 % (v/v). Therefore, DMSO was added to the control media in order to yield the same final DMSO concentration. The different stimulation media used in this study are listed below.

| Condition | db-cAMP* concentration | Forskolin$ concentration | Torin1**$ concentration | DMSO concentration | Duration |
|---|---|---|---|---|---|
| **PKA/EPAC stimulation medium** | 100 µM | 10 µM | - | 0.1 % (v/v) | 30 min |
| **PKA/EPAC Stimulation control** | - | - | - | 0.1 % (v/v) | 30 min |
| **mTOR inhibition medium** | - | - | 125 nM | 0.1 % (v/v) | 50 min |
| **mTOR inhibition control** | - | - | - | 0.1 % (v/v) | 30 min |

* dibutyryl-cyclic adenosine monophosphate
** Tocris Bioscience (Bristol, UK)
$ dissolved in DMSO

### 4.3.6 Transfection

TurboFect™ (Thermo Fisher Scientific, Waltham, USA) is a cationic polymer designed to complex DNA and facilitate the introduction of nucleic acids into eukaryotic cells by a process called transfection.

Cells were transfected by using the TurboFect™ reagent according to the manufacturer's instructions. In brief, cells were grown in a 6-well plate to a confluency of 50-90 %. For preparation of the transfection mixture, 1 µg of plasmid DNA was mixed with 300 µl DMEM GlutaMAX™ (life technologies™, Carlsbad, USA) and 6 µl TurboFect™. The mixture was incubated for 15-20 min at room temperature before it was added drop-wise to the cells. After incubation at 37 °C in a $CO_2$ incubator for 5 h, the transfection medium was aspirated and replaced by fresh cultivation medium.

### 4.3.7 Stable transfection

For generating cell lines stably expressing the transgene of interest, cells were transfected with TurboFect™ (Thermo Fisher Scientific, Waltham, USA) according to the procedure mentioned in section 4.3.6. 24 h after transfection, 1 mg/ml G418 (life technologies™, Carlsbad, USA) was added to the culture in order to select for cells expressing the neomycin resistance gene located on the plasmid encoding for the transgene. Every two to three days, the medium was changed until stable colonies were formed. Single colonies were picked, transferred to a new cultivation plate and further incubated at 37°C and 5 % $CO_2$. After reaching a confluency of min. 50%, the cells were prepared for cryopreservation as mentioned before. For Co-immunoprecipitation (Co-IP) experiments, cells were labeled according to the SILAC procedure.

### 4.3.8 Gene knock-out via CRISPR-Cas9

Clustered regularly interspaced short palindromic repeats (CRISPR)-CRISPR associated protein 9 (Cas9) is a technique which allows genome editing of living organisms. Cells are co-transfected with a CRISPR (cr)- and a transactivating cr (tracr)-RNA as well as a plasmid encoding for the Cas9 endonuclease. After partial binding of the crRNA to the DNA target sequence, the tracrRNA hybridized with the free end of the crRNA thus building the recognition site for Cas9 and promoting DNA cleavage at this position (Jinek et al. 2012; Le Cong et al. 2013; Mali et al. 2013). DNA double strand breaks can be repaired by the host cell DNA repair machinery via processes such as non-homologous end joining (NHEJ). However, as NHEJ is an error prone procedure, nucleotide insertion or deletion might occur at these positions thus resulting in truncated or non-sense gene products and generating a functional gene knock-out (reviewed by Chiruvella et al. 2013).

In order to knock-out the SNAPIN gene with the CRISPR-Cas9 technique, HEK 293 (150,000 cells per well) and HeLa cells (80,000 cells per well) were seeded in a 24-well plate and cultivated for 24 h at 37 °C and 5 % or 10 % $CO_2$, respectively. Prior to co-transfection, the dried nucleotide constructs (all obtained from Dharmacon/Horizon (Cambridge, UK)) were dissolved in 10 mM Tris-HCl pH 7.5. The CRISPR-Cas9 nucleotide solution was prepared by mixing 35 µl DMEM GlutaMAX™ (life technologies™, Carlsbad, USA) with 2.5 µl 10 µM Edit-R tracrRNA, 2.5 µl 10 µM SNAPIN Edit-R crRNA (target sequence: TTTGTTCCCGGAGCTCTACC; protospacer adjacent motif (PAM): TGG; Exon 2) and 10 µl 100 ng/µl Edit-R Cas9-Plasmid solution. For preparation of the transfection solutions, DharmaFECT (Dharmacon/Horizon (Cambridge, UK)) (1 mg/ml) was diluted in DMEM GlutaMAX™ (life technologies™, Carlsbad, USA) in order to generate solutions

containing either 20-30 µg/ml (HeLa cells) or 60 µg/ml (HEK 293 cells) of the transfection reagent. The dilutions were incubated for 5 min at RT. Subsequently, 50 µl of the transfection solutions were mixed with the equal volume of the CRISPR-Cas9 nucleotide solution. After incubating for 20 min at RT, the transfection medium was prepared by adding the DharmaFECT-nucleotide-mixture to 400 µl DMEM GlutaMAX™ supplemented with 9 % FCS (life technologies™, Carlsbad, USA). For cell transfection, the cultivation medium was replaced by 500 µl transfection medium and cells were cultivated for 48 h at 37°C and 5 % or 10 % $CO_2$, respectively.

As the Cas9 Plasmid contains a puromycin resistance cassette, this antibiotic can serve as a selection marker for validating the transfection of cells with the Cas9 plasmid.
48 h after transfection, cells were washed three times with PBS and detached from the cultivation surface by adding 200 µl 0.05 % Trypsin-EDTA (life technologies™, Carlsbad, USA) to the wells. After the addition of 1 ml cultivation medium, cells were centrifuged for 5 min at 300 x g. The cell pellet was resuspended in 500 µl medium before 100 µl of the cell suspension were added to one well of a 24-well plate. Subsequent to this, 400 µl puromycin (life technologies™, Carlsbad, USA) containing media were added in order to obtain a final volume of 500 µl and a puromycin concentration of 2.5 µg/ml. Cells were cultivated at 37 °C and selection medium was replaced every two days. For HeLa cells, the transfection as well as the initial cultivation after transfecting the nucleotides were performed by Pawel Mozolewski (laboratory trainee).
After reaching a confluency of 80 %, cells were detached from the cultivation surface like mentioned before and counted with a Fuchs-Rosenthal counting camber. In order to prepare a monoclonal cell population, the suspension was diluted to achieve a theoretical cell concentration of 0.7 cells per 200 µl. Afterwards, the wells of two 96 well plates were inoculated with 200 µl of this suspension before the cells were cultivated at 37°C and 5 % or 10 % $CO_2$, respectively. Cell growth was monitored by light microscopy. When observing three-dimensional cell growth, each monoclonal colony was splitted to one well of three microtiter plates. Cells were cultivated at 37°C and 5% or 10 % $CO_2$ until a minimum confluency of 60 % was reached.
For cryopreservation, the cells grown in two 96-well plates were washed twice with 100 µl DPBS (life technologies™, Carlsbad, USA) before 25 µl 0.05 % Trypsin-EDTA were added. Once they were detached, cells were mixed with 50 µl DMEM GlutaMAX™ containing 20 % FCS, 1 % Pen/Strep (life technologies™, Carlsbad, USA) and 10 % DMSO. The cell suspension was transferred to a fresh microtiter plate and stored at -80 °C.

Monoclonal colonies were further investigated for successful generation of a SNAPIN gene knock-out by next generation sequencing (NGS). For this purpose, cells grown on the third multitier plate were washed twice with 100 µl DPBS and lysed with 30 µl cold lysis buffer. The lysates were transferred to a MicroAmp™ optical 96 well reaction plate (Thermo Fisher Scientific, Waltham, USA), sealed with a foil and heated for 10 min at 65 °C and 15 min at 95 °C. After a short centrifugation, the cell lysates were stored at -20°C.

| Solution | Concentration | Component |
|---|---|---|
| Lysis buffer | 1 % (w/v) | Triton X-100 |
| | 10 mM | Tris-HCl (pH 7.5) |
| | 1 mM | CaCl2 |
| | 3 mM | MgCl2 |
| | 1 mM | EDTA |
| | 0.2 mg/ml | Proteinase K |

Functional gene knock out via CRISPR-Cas9 was validated by NGS. For this purpose, the DNA region comprising the Cas9 target site was amplified via two PCRs. Besides amplification, the first PCR aims in fusing nucleotide adapters to the target site containing DNA sequence. These adapter sequences are important for the binding of the barcode primers used in the second PCR. The second PCR is performed with a unique set of barcode primers for each monoclone grown in a multitier plate after gene knock out via CRISPR-Cas9 (e.g. clone A1: D501_long Primer A + D701_long Primer B; see section 3.7 for primer sequences). Together with the gene sequence, the barcode primer combinations are used for deducing successful gene knock out among the monoclones within the NGS data set.

The cell lysates of the monoclones were used as a template for the first PCR. Below, the components and the program used for PCR are listed.

| Components 1st PCR | |
|---|---|
| Template | 1 µl |
| 5x Phusion HF buffer | 4 µl |
| 2 mM dNTP mix | 2 µl |
| Forward primer | 10 pmol |
| Reverse primer | 10 pmol |
| Phusion DNA polymerase | 0.4 units |
| $H_2O$ | ad 20 µl |

| Step | Temperature | Time | |
|---|---|---|---|
| **Initial denaturation** | 98 °C | 2 min | |
| **Denaturation** | 98 °C | 10 sec | |
| **Annealing** | 60 °C | 20 sec | x 19 cycles |
| **Elongation** | 72 °C | 30 sec | |
| **Final elongation** | 72 °C | 5 min | |
| **Storage** | 4 °C | ∞ | |

For the second PCR, 2 µl of the different forward and reverse barcode primer mixes were added to the wells of a MicroAmp™ optical 96 well reaction plate. After adding 3 µl PCR products of the first PCR, 15 µl master mix were added. The composition of the master mix is listed below. For PCR, the same program was used as in the first PCR.

| **Components Master Mix 2nd PCR** | |
|---|---|
| 5x Phusion HF buffer | 4 µl |
| 2 mM dNTP mix | 2 µl |
| Phusion DNA polymerase | 0.4 units |
| $H_2O$ | ad 15 µl |

For NGS, 3-5 µl of all PCR products of the second amplification reaction were combined in a 1.5 ml reaction tube and send to the NGS Core Facility of the Medical Faculty of the University of Bonn for MiSeq sequencing (Illumina, San Diego, USA).
Data analysis was performed by using the "OutKnocker" web tool (version 1.31; Indel Threshold 2%, Phred Score Threshold 27 %) as well as the SNAPIN reference gene sequence obtained from the UCSC Genome Browser (retrieved 26.07.2017) by uploading the human genome build (38 release 2) and the primer sequences used for the first CRISPR-Cas PCR (Kent et al. 2002; Schmid-Burgk et al. 2014).

## 4.4 Lysosome enrichment

Superparamagnetic particles can be used for lysosome isolation *in vitro*. This technique is based on the endocytosis of these dextran coated iron oxide beads and their accumulation in the lysosomal compartment after a 24 h chase (Walker and Lloyd-Evans 2015; Thelen et al. 2017).

Prior to HEK 293 cell seeding for lysosome isolation, the 10 cm cultivation dishes were coated with 0.1 mg/ml poly-L-lysine (in DPBS) for 10 min at room temperature. Afterwards, the dishes were washed three times with DPBS (life technologies™, Carlsbad, USA) before 5 x $10^6$ HEK 293 cells were seeded in cultivation medium supplemented with 1 mg/ml EndoMAG superparamagnetic iron oxide particles (Liquids Research, Bangor, UK). The cells were incubated with the magnetite medium for 24 h at 37°C and 5 % $CO_2$. Subsequent to this, the pulse medium was removed, and cells were washed three times with DPBS. For the 24 h chase, cells were cultivated in normal cultivation medium at 37°C and 5 % $CO_2$.

Before starting with the lysosome enrichment, cells were stimulated according to the procedure described in section 4.3.5. For each condition, two 10 cm dishes were used. Afterwards, cells

were washed three times with pre-chilled PBS (recipe see section 4.1.2) and cells were scraped in 0.5-1 ml ice-cold isolation buffer per 10 cm dish. Isotopically labeled cells (SILAC) treated with the different stimulation media were merged at this point and transferred to a tight-fitting Dounce homogenizer. Unlabeled cells were kept separately for homogenization. Cell lysis was performed with 25 strokes on ice. Subsequently, the cell lysate was centrifuged at 1,000 x g for 10 min at 4°C. The supernatant was poured to a fresh 15 ml tube and the pellet was resuspended in 4 ml isolation buffer. After transferring the suspension to the homogenizer, the homogenization and centrifugation procedure was repeated, and the supernatants of both lysis steps were combined.

For lysosome isolation, a ferromagnetic matrix containing LS column (Miltenyi Biotec, Bergisch Gladbach, Germany) was inserted into a magnetic stand (Quadro MACS Separator) and equilibrated with 1 ml 0.5 % BSA in PBS. The combined supernatant was mixed with 4 ml isolation buffer and afterwards applied to the column. Subsequent to this, 1 ml of 1 µg/ml RNAse solution (in isolation buffer) was added and incubated for 10 min at RT. After washing with 5 ml isolation buffer, the column was removed from the magnetic stand. Lysosomes were eluted by pressing two times 500 µl isolation buffer through the column. The eluate was centrifuged for 20 min at 20,000 x g and 4°C. Pelletized lysosomes were resuspended in 500 µl isolation buffer. From each fraction of the isolation process, a sample was removed and investigated by a β-hexosaminidase activity assay (see section 4.5.3).

Lysosomes used for phosphopeptide enrichment were separated into a soluble and membrane fraction. For this purpose, lysosomal membranes were disrupted by treating the eluate of the magnetic column with a tip sonicator (Branson Sonifier 250; 5 mm Tip; 8 x 45 pulses Duty Cycle 50 %, Output 3; 1 x 30 s Duty Cycle constant, Output 3). The disruption of the lysosomal membrane was validated by performing a β-hexosaminidase activity assay. Here, differences in the activity of the same sample incubated with or without detergent could be used as a direct measure of lysosome integrity. Lysosomal membranes were pelletized by centrifuging the sample for 1 h at 4°C and 100,000 x g. The supernatant was removed (soluble fraction) and the membrane pellet was dissolved in 100 µl DB02 containing 1x Halt™ Phosphatase Inhibitor Cocktail (membrane fraction). After performing a BCA protein assay, 120 µg protein of the soluble and membrane fractions were used for tryptic digestion prior to phosphopeptide enrichment. 15 µg of each fraction were prepared for in-gel digestion.

| Solution | Concentration | Component |
|---|---|---|
| Isolation buffer | 10 mM | HEPES (pH 7.4) |
| | 250 mM | Sucrose |
| | 1 mM | $CaCl_2$ |
| | 1 mM | $MgCl_2$ |
| | 1.5 mM | $Mg(CH_3COO)_2$ |
| | 15 mM | KCl |
| | 1 mM | DTT |
| | 5 mM | EDTA[$] |
| | 1x | Halt™ Protease Inhibitor Cocktail* |
| | 1x | Halt™ Phosphatase Inhibitor Cocktail* |
| DB02 | 0.5 % (w/v) | SDC |
| | 20 mM | TEAB |

* HaltTM Protease Inhibitor Cocktail (Thermo Fisher Scientific, Waltham, USA)
[$] Lysosome enrichment from non-isotopically labeled cells was performed without EDTA in the isolation buffer

## 4.5 Biochemical assay

### 4.5.1 Arylsulfatase A (ASA) biotinylation, endocytosis and quantification via ELISA

The Enzyme Linked Immunosorbent Assays (ELISA) is an antibody-based technique to detect and quantify proteins of interest in a liquid sample. This method is based on the immobilization of a specific protein to a microtiter plate surface and its detection via specific antibodies. In presence of an appropriate substrate solution, a colorimetric reaction is catalyzed by an enzyme linked to the antibody used for detection. Here, the strength of the colorimetric reaction correlates with the concentration of the bait protein. Thus, absorbance measurements at a particular wavelength can be used for determination of the abundance of the protein of interest within the sample (Engvall and Perlmann 1972; Wolters et al. 1976).

In order to distinguish endogenous and fed arylsulfatase A (ASA), the supplemented ASA was biotinylated prior to the endocytosis experiments. For this purpose, a 10 kDa cut off spin filter (low protein biding centrifugal filter, VWR, Radnor, USA) was equilibrated with 300 µl 150 mM mannitol in PBS (for recipe see section 4.1.2) by centrifugation for 2 min at 10,000 x g. After adding human ASA solution to the filter, the volume was adjusted to 300 µl and the mixture was centrifuged again (5 min, 10,000 x g). 300 µl 150 mM mannitol in PBS were loaded to the filter device before another centrifugation step (5 min at 10,000 x g) was performed. This step was repeated twice. EZ-Link™ sulfo-NHS-biotin (Thermo Fisher Scientific, Waltham, USA) was dissolved in 150 mM mannitol (in PBS). Compared to ASA, a 100-fold molar excess of sulfo-NHS biotin was added to the protein solution. The mixture was incubated for 30 min at RT. Remaining active NHS sites were blocked by adding a 100-fold molar excess of glycine (compared to sulfo-NHS biotin) to the reaction. After incubating for 15 min at RT, the filter was centrifuged for 5 min

at 10,000 x g. Two times 300 µl ASA buffer (150 mM D-mannitol, 27 mM glycine in PBS) were sequentially added to the filter device with centrifugation steps of 5 min at 10,000 x g in between. Afterwards, the filter supernatant was transferred to a new reaction vial. The concentration of biotinylated ASA within the supernatant was determined by DC protein assay.

For the ASA endocytosis assay, HEK 293 and HEK SNAPIN knock-out (KO) cells were seeded in a 24-well plate (60,000 cells per well) and cultivated for 72 h at 37°C and 5 % $CO_2$. Prior to the assay, stimulation media were prepared in fresh DMEM GlutaMAX™ + 9 % FCS + 0.9 % Pen/Strep (all obtained from life technologies™, Carlsbad, USA) according to the concentrations listed below. Adding FSK (dissolved in DMSO) to the stimulation media resulted in a final DMSO concentration of 0.1 % (v/v). Therefore, DMSO was added to the stimulation control media in order to yield the same final DMSO concentration. Before applying to the cells, media were pre-chilled on ice for at least 45 min. Cells were incubated with the respective stimulation medium for 35 min at 37°C and 5 % $CO_2$. Compared to the FSK/db-cAMP stimulation condition mentioned in section 4.3.5, the duration of the treatment was prolonged for 5 min as the pre-chilled media need to warm up to 37°C first. After stimulation, cells were washed twice with cold PBS. ASA bound to the extracellular side of the plasma membrane was removed by incubating the cells for 2 min with 1 ml of pre-chilled ASA washing buffer (150 mM NaCl, 50 mM glycine pH 3.0). Subsequent to this, cells were washed three times with cold PBS before scraping the cells in 250 µl pre-chilled lysis buffer (0.5 % Triton X-100 in TBS, pH 7.5). The cell lysates were transferred to a reaction tube and stored at -20°C.

| **Condition** | **db-cAMP concentration** | **Forskolin[$] concentration** | **DMSO concentration** | **Biotinylated ASA concentration** |
|---|---|---|---|---|
| Stimulation + ASA | 100 µM | 10 µM | 0.1 % (v/v) | 7.5 µg/ml |
| Stimulation - ASA | 100 µM | 10 µM | 0.1 % (v/v) | - |
| Stimulation control + ASA | - | - | 0.1 % (v/v) | 7.5 µg/ml |
| Stimulation control - ASA | - | - | 0.1 % (v/v) | - |

[$] dissolved in DMSO

Cell lysates were first treated with a tip sonicator (Hielscher, UP50H; 12 pulses, Amplitude 90, Cycle 0.9) and then centrifuged for 5 min at 10,000 x g and 4°C. The supernatant was transferred to a fresh reaction tube and used for BCA assay and ELISA.

For the ELISA, Nunc Immobilizer streptavidin coated 96-well plate (Thermo Fisher Scientific, Waltham, USA) was washed three times with 300 µl PBST (0.05% Tween-20 (v/v) in PBS).

Afterwards, 100 µl 5 % BSA (w/v) in PBST were added to the wells and mixed with 100 µl sample. Solutions with known concentrations of biotinylated ASA served as standards. After incubation for 1 h at RT, the wells were washed three times with 300 µl PBST. Subsequently, 50 µl anti-human-ASA rabbit antiserum (1:2000 diluted with 5% BSA in PBST) were added to the wells and incubated for 1 h at 37°C. The wells were washed three times with 300 µl PBST before 50 µl of HRP-conjugated goat anti-rabbit antibody (1:2000 diluted with 5% BSA in PBST) were added. The secondary antibody was incubated for 1 h at 37°C followed by three washing steps with 300 µl PBST. ABTS substrate was dissolved in ABTS substrate buffer (both obtained from Roche, Basel, Switzerland) at a final concentration of 1 mg/ml. 50 µl ABTS solution were added to each well and incubated at RT until a slight color change was observed. Absorbance was measured at a wavelength of 405 nm (reference wavelength 505 nm) at several times (every 60-90 s; six time points in total). Based on a polynomial regression curve, the concentrations of biotinylated ASA within the particular samples were calculated. Subsequently, these concentrations were normalized to the protein concentrations of the corresponding lysates.

Prior to the analysis of variance (ANOVA), the homogeneity of the group variances was tested in R-studio by using the Brown-Forsythe test (R-package: “car” (version 3.0-6)) (Fox and Weisberg 2019). After demonstrating the homoscedasticity (p-value = 0.5633), R-studio was used to perform the one-way ANOVA and the Tukey honest significant difference (HCD) post hoc test (ordered = false, confidence interval 0.95).

The standard deviation was calculated by using n-1 as the denominator.

### 4.5.2 Exocytosis Assay

The secretion of the lysosomal hydrolase β-hexosaminidase (β-Hex) was induced according to the procedure described by Rodríguez et al. (1997). For this purpose, HeLa wildtype (wt) and SNAPIN KO cells were grown as monolayers in a 6-well plate. Once reaching a confluency of 100%, cells were incubated for 20 min at 37°C and 5 % $CO_2$ with DMEM cultivation medium containing either FSK/db-cAMP or DMSO (see section 4.3.5). Subsequently, secretion was induced by replacing the stimulation- with exocytosis-medium comprising 1 mM $CaCl_2$, 10 µM ionomycin. Media either without one or both additives served as controls. According to the stimulation condition, the exocytosis/control media were also supplemented with FSK/db-cAMP or DMSO. After incubation for 10 min at 37°C and 5 % $CO_2$, the cell supernatant was removed, centrifuged for 5 min at 11,000 x g at 4°C and mixed with BSA solution (end concentration BSA 0.1 mg/ml). The amount of β-Hex secreted during the 10 min exocytosis stimulus was investigated by determining the activity of this enzyme in the supernatant. Additionally, the cells

were washed two times with ice-cold PBS (for recipe see section 4.1.2) and scraped in 250 µl lysis buffer (1 % NP-40 in PBS). The lysates were treated with a tip sonicator (Hielscher, UP50H; 20 pulses, amplitude 90, cycle 0.9) and centrifuged for 5 min at 10,000 x g at 4°C. Afterwards, the β-Hex activity in the lysates was investigated and the protein concentrations were estimated by a BCA assay. For data comparison, the β-Hex activities were normalized to the protein concentration in the cell lysates.

Prior to the statistical comparison of two sample groups, the homogeneity of variances was tested by a Levene's test (with R-studio). As all significance values of the Levene's test performed in this experiment were higher than 0.05, homoscedasticity was assumed and a normal two sample t-test was performed by using R-studio (t-test between two conditions, null-hypothesis = difference in means is 0, two-sided, unpaired, confidence interval 0.95).

For calculating the standard deviation, the denominator n-1 was used.

### 4.5.3 β-hexosaminidase activity assay

The β-hexosaminidase activity assay is based on the enzymatic conversion of the substrate 4-nitrophenyl-N-acetyl-β-D-glucosaminide to 4-nitrophenol. The quantity of the hydrolysis product directly correlates with the amount of free enzyme and can be determined by measuring the absorbance at 405 nm (Chatterjee et al. 1975; Marciniak et al. 2006).

In the lysosome isolation process, the β-Hex activity can be used for lysosome quantification within the different fractions. By investigating the β-Hex activity of the input, flow through, wash and elution samples in the presence and in the absence of detergents, the proportion of intact and disrupted lysosomes can be quantified. In addition to that, the β-Hex activity assay can be used for monitoring lysosomal secretion upon elevated intracellular $Ca^{2+}$ concentrations.

For the β-hexosaminidase activity assay with samples of the lysosome enrichment procedure, 25 µl of each sample were loaded to four different wells of a microtiter plate. The samples present in two of those wells were mixed with 8 µl 10 % (w/v) Triton-X100 solution. Afterwards, 50 µl β-hexosaminidase substrate solution were added and the assay was incubated for 20 min at 37 °C. The reaction was stopped by adding 200 µl β-hexosaminidase stop solution to the wells before measuring the absorbance at 405 nm.

Similar to the procedure mentioned above, the β-Hex activity in the cell lysates of the exocytosis experiment was investigated by loading 25 µl of each sample to a microtiter plate (double determination). After adding 50 µl β-hexosaminidase substrate solution, the reaction was

incubated for 30 min at 37°C. The assay was stopped by pipetting 200 µl β-hexosaminidase stop solution to each well. The absorbance was measured at 405 nm.

In order to determine the β-Hex activity in the cell supernatant after the exocytosis experiment, 200 µl of each sample was mixed with 200 µl β-hexosaminidase substrate solution in a 1.5 ml reaction tube (double determination). The mixture was incubated in a water bath at 37°C for 5 h before the assay was stopped by the addition of 200 µl β-hexosaminidase stop solution. Afterwards, 200 µl of each sample was loaded onto a microtiter plate. Subsequently, the absorbance was measured at 405 nm.

Formula for calculating β-Hex activity:

$$\frac{\mathrm{mU}}{\mathrm{ml}} = \frac{\mathrm{V_{total}} \cdot 10^6 \cdot \mathrm{OD_{405}}}{\varepsilon_{405} \cdot \mathrm{V_{sample}} \cdot \mathrm{t} \cdot \mathrm{d}}$$

$\varepsilon_{405}$ = 18,500 $M^{-1} \cdot cm^{-1}$; d = 0.75 cm (layer thickness 96-well plate)

| Solution | Concentration | Component |
|---|---|---|
| β-hexosaminidase substrate solution (pH 4.6) | 0.1 M | Citric acid monohydrate |
| | 0.2 % (w/v) | BSA |
| | 10 mM | 4-Nitrophenyl-N-Acetyl-β-D-glucosaminide |
| β-hexosaminidase stop solution | 0.4 M | Glycine (pH 10.4) |

## 4.6 Interaction studies

Co-immunoprecipitation (Co-IP) is a technique used to identify protein-protein interactions *in vitro*. The method is based on an antibody mediated pull down of the protein of interest together with its interaction partners.

Co-Immunoprecipitation was performed by using isotopically labeled HEK SNAPIN KO cells (SILAC) stably transfected with a plasmid containing the SNAPIN S133A or the SNAPIN S133E proteoforms. Non-transfected SNAPIN KO cells served as a control.
Cells grown on a 10 cm petri dish were harvested by scraping them from the surface (in 500 µl PBS (for recipe see section 4.1.2)). The cell suspension was centrifuged for 3 min at 1,000 x g. Afterwards the supernatant was removed and the cell pellet was snap frozen in liquid nitrogen. Cell lysis was performed by suspending the pellet in 500 µl ice-cold lysis buffer followed by a treatment with a tip sonicator (Hielscher, UP50H; 20 pulses, Amp 100%, Cycle 0.9). Subsequent to a centrifugation step at 10,000 x g for 5 min at 4 °C, the supernatant of the lysate was transferred to a fresh 1.5 ml tube. The protein concentration was determined by a BCA assay.

For each Co-IP sample, 45 µl Myc-Trap® beads (ChromoTek, Planegg-Martinsried, Germany) were transferred to a fresh 1.5 ml reaction tube and mixed with 500 µl Co-IP lysis buffer. Afterwards, the bead suspension was centrifuged for 2 min at 4 °C and 2,500 x g. The supernatant was removed and the washing procedure was repeated twice before the beads were incubated with 500 µg protein lysate for 2 h at 4°C on an orbital shaker (total volume 500 µl). Subsequent to this, the beads were centrifuged (2 min, 4°C, 2,500 x g) and the supernatant was removed. The beads were washed three times with 500 µl lysis buffer. During the second washing step, the beads were transferred to a fresh tube. Proteins were eluted by incubating the beads for 5 min at 95 °C in 30 µl 2x SDS sample buffer. Prior to SDS-PAGE and in-gel digestion, 10 µl of the isotopically labeled protein samples, belonging to the same replicate, were combined. SDS-PAGE was performed by using a 5 % stacking and a 10 % separation gel. For in-gel digestion, each lane was cut horizontally into six pieces.

| Solution | Concentration | Component |
|---|---|---|
| Lysis buffer | 1 % (w/v) | Triton X-100 |
| | 40 mM | HEPES (pH 7.4) |
| | 150 mM | NaCl |
| | 2.5 mM | $MgCl_2$ |
| | 1x | Halt™ Protease Inhibitor Cocktail* |

* Thermo Fisher Scientific, Waltham, USA

## 4.7 Immunocytochemistry and image acquisition

High precision cover slips (12 mm) were placed in a 24-well plate and coated with 10 µg/ml fibronectin solution (AppliChem, Darmstadt, Germany) (in DPBS) for 60 min at 37 °C. Subsequent to this, the cover slips were washed once with DPBS (life technologies™, Carlsbad, USA). For immunocytochemistry, 60,000 HeLa wt and SNAPIN KO cells were seeded per cover slip/well. Cells were incubated at 37°C and 5 % $CO_2$. After 24 h, the cells were treated with FSK/db-cAMP or DMSO as mentioned before (see section 4.3.5). Following this treatment, the cells were washed once with PBS (for recipe see section 4.1.2) before 300 µl 4 % PFA (w/v) (in PBS) were added to each well. Fixation was performed for 10 min at 37°C and 5 % $CO_2$. The cells were washed three times with PBS and stored at 4°C covered with this solution until further usage.

Prior to immune staining, cells were permeabilized with 0.2 % Triton X-100 in PBS (v/v) for 5 min at RT. Blocking was performed by incubating the cells for 1h (RT) with 5 % BSA in PBS (w/v). Afterwards, the cover slips were transferred to a wet chamber and incubated with the primary antibody over night at 4°C. On the next day, cells were washed three times with PBS (5 min, RT) on a shaking device before they were incubated with the secondary antibody for 1 h (RT) in a

wet chamber. After two washing steps with PBS, cells were shortly dipped in $H_2O$. ProLong Diamond™ (with DAPI) (Thermo Fisher Scientific, Waltham, USA) was used in order to mount the cover slips to the specimen slides.

Images were obtained together with Angnes von Keller from Zeiss Microscopy by using a LSM 980 equipped with an Airyscan 2 detector (inverse AxioObserver 7 microscope) (Zeiss, Oberkochen, Germany). A Zeiss Apochromat 63x/1.4 objective was used to acquire the images as Z-stacks. The Cy3 fluorophore was excited by a 561 nm laser (laser power 1 %). For excitation of DAPI, a 405 nm laser (laser power 0.99 %) was used. The detection wavelengths were set to 422-477 and 573-627 nm. Images were processed by the Zeiss software with the "FastAiryScanSheppardSum" Airyscan mode. The single Z-stack images were combined by maximum intensity projection using the ImageJ software (version 1.51j8; Java 1.8.0_112) (Schneider et al. 2012).

## 4.8 Mass spectrometry sample preparation

### 4.8.1 Sample preparation for bottom up mass spectrometry analysis

Bottom up mass spectrometry is a valuable tool in proteomic studies. The method is based on the proteolytic cleavage of proteins and the detection and identification of the resulting peptides by a mass spectrometer.

#### 4.8.1.1 Filter aided sample preparation (FASP)

In filter aided sample preparation (FASP), proteins are retained above a molecular mass cut off spin filter thus allowing precise adjustments in the buffer compositions for protein reduction and alkylation prior to the proteolytic cleavage. However, after protein digestion, the peptides pass through the filter and can be collected in small reaction tubes for further purification, fractionation and mass spectrometric analysis (Manza et al. 2005; Wiśniewski et al. 2009).

Protein samples from living cells were obtained by cell lysis in a buffer containing 5 % SDC (w/v), 20 mM TEAB and 1x Halt™ Protease Inhibitor Cocktail (Thermo Fisher Scientific, Waltham, USA). Afterwards, the lysate was treated with a tip sonicator (Hielscher, UP50H; 1-3 x 20-30 pluses, Amp 90-100, Cycle 0.9) and centrifuged for 5 min and 4°C at 10,000 x g. Subsequent to this, the protein concentration in the supernatant was determined by a BCA assay.

LysN and LysArginase digestion of biotinylated protein mixtures (DB03 buffer) was performed according to the FASP protocol. As far as not otherwise stated, the same technique was used for protein digestion with trypsin (DB02 buffer).

A 10 kilodalton (kDa) cut off filter (VWR, Radnor, USA) was equilibrated with 300 µl DB02 or DB03 and centrifuged for 2 min at 10,000 x g. Afterwards, the protein solution was applied to the filter device. In case the buffer of the protein solution had to be exchanged, two times 300 µl DB02 were sequentially added to the filter (centrifugation at 10,000 x g for 5 min in between). Proteins were reduced by adding dithiothreitol (DTT) to a final concentration of 20 mM to the filter supernatant followed by an incubation for 30-45 min at 30-55°C. Subsequently, the DTT solution was removed by centrifuging two to three times 300 µl DB02 or DB03 through the filter (5 min, 10,000 x g). For protein alkylation, the sample was incubated for 30 min at RT in DB02 or DB03 containing 40 mM acrylamide. Afterwards, 300 µl digestion buffer was added and the filter device was centrifuged for 5 min at 10,000 x g. This step was repeated twice before the volume of the filter supernatant was adjusted to 100 µl and proteases were added to a mass ratio of 1:25 or 1:100 (e.g. 1 µg protease for 100 µg proteins) to the sample. Protein digestion was performed at 37°C overnight. On the next day, peptides were collected by centrifuging the filter device for 5 min at 10,000 x g. Subsequent to this, the filter was washed with 200-300 µl DB02 or DB03 and centrifuged again (5-10 min, 10,000 x g). Whereas urea containing peptide solutions were acidified with 25 % formic acid (FA) (v/v) and directly desalted via reversed phase chromatography, tryptic peptides in DB02 were transferred to a fresh 1.5 ml reaction tube and mixed with trifluoroacetic acid (TFA) in order to adjust the TFA concentration to approx. 2.5 % (v/v). Acidification of the tryptic peptide solution led to precipitation of SDC which was then pelletized by centrifugation at 14,000 x g for 10 min. The supernatant was transferred to a fresh reaction tube and the pellet was suspended in 250 µl 0.1 % TFA (v/v). After an additional centrifugation step (10 min, 14,000 x g), the supernatants were combined and residual SDC was removed by mixing the peptide solution three times with 500 µl ethyl acetate (2 min, 10,000 x g centrifugation steps in between). In the end, the peptide solution in the aqueous phase was dried in a vacuum centrifuge (1,000 rpm, 40-60 °C).

| Solution | Concentration | Component |
|---|---|---|
| DB02/trypsin digestion buffer | 0.5 % (w/v) | SDC |
| | 20 mM | TEAB |
| DB03 | 8 M | Urea |
| | 20 mM | TEAB |
| LysN digestion buffer | 6 M | Urea |
| | 20 mM | TEAB |
| | 0.1 mM | $MgCl_2$ |
| LysArginase digestion buffer | 0.8 M | Urea |
| | 20 mM | TEAB |
| | 10 mM | $CaCl_2$ |

#### 4.8.1.2 Single vial standard digestion

Protein mixtures in an aqueous environment can be digested by a single vial standard digestion. Compared to FASP, buffers cannot be exchanged during the sample preparation procedure because all reactions are taking place in a single vial without any kind of protein collection step (e.g. without cut off filter) prior to the digestion.

In solution digestions of biotinylated and non-biotinylated peptides were performed by adding LysN or LysArginase to a mass ratio of 1:25 to 1:100 to the peptides (in TEAB). In case of the digestion optimization experiment, the reaction buffer was supplemented with $ZnCl_2$, $MnCl_2$ or $MgCl_2$ to achieve final concentrations of 0.1 mM or 1 mM, respectively. Digestion was performed at 37°C overnight before the samples were acidified and desalted by reversed phase chromatography.

The cells used for phosphopeptide enrichment from whole cell lysate were lysed in a buffer containing 9 M urea, 20 mM HEPES, 1x Halt™ Protease Inhibitor Cocktail (Thermo Fisher Scientific, Waltham, USA) and 1x Halt™ Phosphatase Inhibitor Cocktail (Thermo Fisher Scientific, Waltham, USA). Afterwards, the lysates were treated with a tip sonicator (Hielscher, UP50H) to shear high molecular DNA and centrifuged for 15 min at RT and 18,514 x g. Protein concentration of the lysates were measured by a DC protein assay. 2 mg protein were used for in solution digestion. First, disulfide bonds were reduced by adding DTT to a final concentration of 10 mM to the sample. The mixture was incubated in a water bath at 55°C for 30 min. Afterwards, samples were alkylated with 20 mM acrylamide for 30 min at RT. The samples were diluted with 20 mM HEPES (pH 8.0) to adjust the urea concentration to 2 M before the proteins were digested over night with trypsin at 37°C (protein-trypsin-mass ratio of 200:1). On the next day, the samples were acidified by adding TFA to a final concentration of 1 % (v/v) to the mixture. The samples were incubated on ice for 15 min and subsequently centrifuged at 1,780 x g for 15 min at RT. The peptide mixtures were desalted by reversed phase chromatography.

#### 4.8.1.3 In gel digestion

In gel digestion is a technique aiming at proteolytic cleavage of proteins separated via SDS-PAGE. This method is often used to reduce sample complexity or to remove polyethylene glycol-based detergents prior to MS measurements (Shevchenko et al. 1996).

After SDS-PAGE and protein staining with colloidal Coomassie, the gels were destained with water and protein bands were excised. In order to further destain the protein bands, the gel pieces were incubated with 50 % acetonitrile (ACN) (v/v) for 5 min. This step was repeated until

the supernatant was not blue anymore. Subsequently, the gel pieces were dehydrated with ACN for 5 min and dried in a vacuum centrifuge (1,000 rpm, 40-60 °C). For protein reduction, 100 µl 20 mM DTT (in 50 mM $NH_4HCO_3$) was added to the dried gel pieces and incubated for 30 min at 55 °C. Afterwards, the gel pieces were washed with 100 µl 50 mM $NH_4HCO_3$ before proteins were alkylated by adding 100 µl 40 mM acrylamide solution (in 50 mM $NH_4HCO_3$). After protein alkylation for 30 min at RT, the gel pieces were washed with water, dehydrated by incubation with 50 % (v/v) and ACN and dried in a vacuum centrifuge like mentioned before. For protein digestion, the gel pieces were rehydrated in 50 mM $NH_4HCO_3$ containing 10 % ACN (v/v) and 250 ng trypsin and incubated at 37 °C overnight. On the next day, the supernatant was transferred to a fresh 1.5 ml reaction vial and the gel pieces were washed with water for 5 min. The water was combined with the supernatant after digestion and peptides were extracted by sequentially incubating the gel pieces with 50 % ACN (v/v) and ACN for 5 min at RT. Finally, the peptide extracts were added to the mixture of water and digestion solution and dried in a vacuum centrifuge (1,000 rpm, 40-60 °C).

### 4.8.2 Biotinylation via NHS-esters

The reactivity of NHS-esters towards primary amine groups was used in order to biotinylate peptides and proteins *in vitro*.

#### 4.8.2.1 Sulfo-NHS-biotin

Biotinylation of peptides and proteins via EZ-Link™ sulfo-NHS-biotin (Thermo Fisher Scientific, Waltham, USA) was performed by incubating the sample with a 100-150 fold molar excess of sulfo-NHS-biotin in 20-60 mM TEAB (pH 8.5) or 1x PBS (pH 7.4) (for recipe see section 4.1.2) for 30 min at RT. Remaining sulfo-NHS-biotin was quenched by incubating the reaction mixture for 15 min with a 10-100 fold molar excess of hydroxylamine compared to the biotinylation reagent. Subsequent to this, samples were acidified and desalted by reversed phase chromatography

#### 4.8.2.2 Sulfo-NHS-LC-biotin

Peptides were biotinylated with a 100-fold molar excess of EZ-Link™ sulfo-NHS-LC-biotin (Thermo Fisher Scientific, Waltham, USA). For this purpose, 10 mM sulfo-NHS-LC-biotin solution (in $H_2O$) was mixed with 0.5 µg peptides, dissolved in PBS. After incubation for 30 min at RT, samples were acidified with TFA and desalted by reversed phase chromatography.

#### 4.8.2.3 NHS-biotin

NHS-biotin (Sigma-Aldrich, St. Louis, USA) was dissolved in DMSO to achieve a final concentration of 0.1 M. Biotinylation of peptides was performed in 20 mM TEAB and 30 % DMSO with a 20-fold molar excess of NHS-biotin. After incubation for 30 min at RT, remaining NHS-biotin was quenched by adding a 100-fold molar excess of hydroxylamine (compared to biotinylation reagent) to the mixture. Subsequently, the samples were acidified with TFA and directly used for strong cation exchange (SCX)-based sample clean up.

### 4.8.3 Streptavidin incubation

The high affinity between streptavidin and biotin was used to sequester biotinylated peptides.

210 µl streptavidin sepharose® (GE Healthcare, Chicago, USA) was transferred to a fresh reaction tube and washed twice with 500 µl binding buffer (1 min, 500 x g). Afterwards, peptides dissolved in binding buffer were mixed with the streptavidin beads. The volume was adjusted to 200 µl (with binding buffer) before the mixture was incubated for 1 h at RT on an orbital shaker (device parameters: orbital: 70 rpm, 5 s; Reciprocal: 45 deg., 5 s; Vibro/pause: 5°, 5 s). Subsequent to this, the samples were centrifuged for 1 min at 500 x g. The supernatant was transferred to a fresh reaction tube and the beads were washed once with 100 µl binding buffer. After centrifugation (1 min, 500 x g), the supernatant was combined with the previous one and desalted by reversed phase chromatography (“StageTip” procedure).

| Solution | Volume | Component |
|---|---|---|
| Binding buffer (pH 7.5) | 1.6 ml | 0.4 M $NaH_2PO_4$ |
| | 8.4 ml | 0.4 M $Na_2HPO_4$ |
| | 3.33 ml | 3 M NaCl |
| | 6.67 ml | $H_2O$ |

### 4.8.4 Phosphopeptide-enrichment

Phosphopeptides were enriched by Titanium dioxide ($TiO_2$) beads. Here, phosphopeptides were bound to the beads in an acidic environment and were eluted by raising the pH to an alkaline level (Pinkse et al. 2004; Larsen et al. 2005).

#### 4.8.4.1 Phosphopeptide-enrichment from tryptic whole cell protein digest followed by SCX-based peptide fractionation

20 mg $TiO_2$ beads (GL Sciences, Torrance, USA) were suspended in 1 ml T-loading solution (TLS) and subsequently added to 2 mg dried, tryptic peptides from whole cell protein digest (1 mg $TiO_2$ per 100 µg peptide). The mixture was incubated on an orbital shaker for 15 min (device parameters: orbital: 11 rpm, 1 s; Reciprocal: 45 deg., 6 s; Vibro/pause: 1°, 3 s). After centrifuging the samples for 30 s at 8,000 x g (RT), the supernatant was removed before the beads were washed with 500 µl TLS. The mixture was centrifuged again (30 s at 8,000 x g) and two additional washing steps with 1 ml 80 % ACN (v/v), 1 % TFA (v/v) were performed. Subsequent to this, the $TiO_2$ beads were dried in a SpeedVac (40°C, 1000 rpm). Peptides were eluted by incubating the $TiO_2$ beads with 200 µl freshly prepared 0.5 % $NH_4OH$ (v/v) solution (pH > 11) for 10 min at RT. The beads were pelletized by centrifugation at 8,000 x g for 30 s before the supernatant was removed and acidified with 5 µl FA. After acidification, peptides were desalted by reversed phase chromatography ("StageTip" procedure).

The SCX columns were prepared by stamping out small pieces of Empore™ Supelco® SCX material (3M, Saint Paul, USA) and placing them into a 200 µl pipette tip. Each column, comprising eight of these small SCX discs, were washed sequentially with 100 µl methanol, SCX elution buffer 5, water, SCX equilibration buffer, water and SCX loading buffer with centrifugation steps for 3 min at 3,000 x g in between. Phosphopeptides were re-dissolved in 300 µl SCX loading buffer, sonicated for 2 min and loaded to the column. After centrifugation for 3 min at 3,000 x g, the flow through was kept as fraction 1. Five different SCX elution buffers with increasing KCl concentrations were sequentially added to the column (3 min at 3,000 x g in between) and the flow throughs were collected (factions 2-6). In the end, all fractions were desalted by reversed phase chromatography ("StageTip" procedure).

| Solution | Concentration | Component |
|---|---|---|
| T-loading solution | 1 M | glycolic acid |
| | 80 % (v/v) | ACN |
| | 5 % (v/v) | TFA |
| SCX equilibration buffer (pH 7.5) | 50 mM | $KH_2PO_4$ |
| | 500 mM | NaCl |
| SCX loading buffer (pH 2.65) | 7 mM | $KH_2PO_4$ |
| | 30 % (v/v) | ACN |
| SCX elution buffer 1 (pH 2.65) | 7 mM | $KH_2PO_4$ |
| | 30 % (v/v) | ACN |
| | 30 mM | KCl |
| SCX elution buffer 2 (pH 2.65) | 7 mM | $KH_2PO_4$ |
| | 30 % (v/v) | ACN |
| | 60 mM | KCl |

| Solution | Concentration | Component |
|---|---|---|
| SCX elution buffer 3 (pH 2.65) | 7 mM | $KH_2PO_4$ |
| | 30 % (v/v) | ACN |
| | 90 mM | KCl |
| SCX elution buffer 4 (pH 2.65) | 7 mM | $KH_2PO_4$ |
| | 30 % (v/v) | ACN |
| | 120 mM | KCl |
| SCX elution buffer 5 (pH 2.65) | 7 mM | $KH_2PO_4$ |
| | 30 % (v/v) | ACN |
| | 350 mM | KCl |

#### 4.8.4.2 Phosphopeptide-enrichment from protein digests of the lysosomal fractions

Dried, tryptic peptides were re-dissolved in 50 µl TLS (for recipe see section 4.8.4.1) containing 1 mg $TiO_2$ beads (GL Sciences, Torrance, USA). The mixture was incubated for 15 min on an orbital shaker (device parameters: orbital: 11 rpm, 1 s; Reciprocal: 45 deg., 6 s; Vibro/pause: 1°, 3 s). A column, consisting of a small piece of Empore™ Supelco® C18 material (3M, Saint Paul, USA) plugged to a gel loading tip, was prepared. The column was equilibrated with 20 µl ACN before the peptide-$TiO_2$ suspension was added. A syringe was used to force liquid through the column. The beads retained on top of the column were washed with 100 µl TLS and 35 µl 80 % ACN (v/v), 1 % TFA (v/v). Phosphopeptides were eluted by adding 30 µl 0.5 % $NH_4OH$ (v/v) to the beads/column. Afterwards, 5 µl 30 % ACN (v/v) were added in order to elute peptides bound to the C18 membrane. The eluate was acidified with 20 µl 25% FA (v/v) and dried in a vacuum centrifuge.

### 4.8.5 Selective derivatization of peptide's N-terminal amino group

#### 4.8.5.1 Reductive alkylation

Reductive alkylation was performed according to the procedure described by Chen et al. (2017). In brief, 100 or 300 µg dried peptides were dissolved in 9.6 or 10 µl 25 mM citrate buffer pH 6.0 (5 min, ultrasonic bath), respectively. Afterwards, the peptide solution was transferred to a glass vial and mixed with a fivefold molar excess of sodium cyanoborohydrate (dissolved in 25 mM citrate buffer, pH 6.0) and a twofold molar excess of benzaldehyde (diluted in DMSO). In case of the 300 µg peptide sample, 30.7 µl 25 mM citrate buffer (pH 6.0) were added. The mixtures were incubated for 5-6 h on a magnetic stirrer (500 rpm) before the samples were diluted with 74.1 or 284 µl $H_2O$, respectively. Subsequent to this, the peptide solution was desalted by reversed phase chromatography.

| Solution | Volume | Component |
|---|---|---|
| 25 mM citrate buffer (pH 6.0) | 1.15 ml | 25 mM Cirtric acid monohydrate |
| | 8.85 ml | 25 mM trisodium citrate dihydrate |

#### 4.8.5.2 Acetylation and Propionylation

Acetylation was performed according to the procedure described Mikami et al. (2012). The same principle was used for peptide propionylation. Prior to their derivatization, 0.5-20 µg dried peptides were dissolved in 12 µl 0.1 % (v/v) acetic acid (5 min, ultrasonic bath) and placed on ice for 1 min. Afterwards, 5 µl 0.5 M acetic acid anhydride or 0.5 M propionic acid anhydride (both diluted in ACN) were added to the peptide solution. The mixture was incubated in ice water for at least 5 min, snap-frozen in liquid nitrogen and dried by lyophilization.

#### 4.8.5.3 Transamination

Transamination was performed according to the procedure mentioned by Sonomura et al. (2011). 0.5 µg dried peptides were dissolved in 4 µl $H_2O$ (5 min, ultrasonic bath). Derivatization was performed by adding 4 µl transamination solution containing 20 % pyridine (v/v), 100 mM glyoxylic acid, 12 mM $NiSO_4$ and 500 mM acetic acid to the peptide mixture. After incubation for 30 min at RT, peptides were desalted by reversed phase chromatography.

### 4.8.6 Peptide sample clean-up via SCX chromatography

In order to generate the SCX chromatography columns, small portions of Empore™ Supelco® SCX material (3M, Saint Paul, USA) were stamped out and placed in a 200 µl tip. 20 of these SCX-discs were used to prepare one column. Afterwards, the column was placed in a benchtop centrifuge. The SCX chromatography column was rinsed successively with 100 µl methanol, 100 µl elution buffer (5 % $NH_4OH$ (v/v), 30 % methanol (v/v)) and 3 x 100 µl binding buffer (0.1% TFA (v/v), 30 % methanol (v/v)) (3 min, 3000 x g centrifugation in between). After loading the acidified sample, the column was centrifuged for 3 min at 3000 x g. The flow through was loaded again and the column was washed three times with 100 µl binding buffer. Peptides were eluted by adding two times 100 µl elution buffer to the column. Eluted peptides were dried in a vacuum centrifuge.

### 4.8.7 Peptide desalting via reversed phase chromatography

Reversed phase chromatography is a common tool in MS sample preparation for peptide desalting prior to MS measurements. In an aqueous and acidic environment, peptides bind to the nonpolar stationary phase of the reversed phase chromatography column material and can be eluted by increasing the concentration of an organic solvent that has a lower polarity than water (Rappsilber et al. 2007).

#### 4.8.7.1 Gravity flow reversed phase chromatography columns

For peptide desalting, the gravity flow reversed phase chromatography Oasis® columns (Waters, Milford, USA) were first equilibrated two times with 1 ml ACN. Afterwards, the column was washed three to four times with 1 ml 0.1 % FA (v/v). Columns used for peptide desalting after reductive amination were additionally rinsed with 1 ml 25 mM citrate buffer (pH 6). Subsequently, the peptide solutions were added and the column flow through was loaded again. Columns used for desalting after reductive amination were washed with 1 ml 25 mM citrate buffer (pH 6). Prior to peptide elution, the columns were rinsed three to four times with 1 ml 0.1 % FA (v/v). Peptides were eluted either by adding two times 0.5 ml 80 % ACN (v/v), 0.1 % FA (v/v) or 70 % ACN (v/v) to the column. The eluates were dried in a vacuum centrifuged at 40-60°C and 1,000 rpm.

After single vial standard digestion of proteins in urea containing buffer, peptides were desalted by gravity flow reversed phase chromatography column Oasis® columns (Waters, Milford, USA). First, columns were equilibrated with 5 ml I. Subsequent to this, the columns were sequentially washed with 1 ml, 3 ml and 6 ml 0.1 % TFA (v/v) before the peptide mixtures were loaded. Afterwards, the columns were rinsed with 1 ml, 3 ml and 6 ml 0.1 % TFA (v/v) as well as with 2 ml 0.1 % TFA (v/v) containing 5 % ACN (v/v). Peptides were eluted by adding three times 2 ml 0.1 % TFA (v/v), 40 % ACN (v/v) to the column. The eluates were frozen for 5 h at -80 °C and subsequently dried by lyophilization.

#### 4.8.7.2 Millipore® ZipTip based sample purification

C18 Millipore® ZipTips (Merck, Darmstadt, Germany) are pipette tips stuffed with reversed phase chromatography material. These columns were used for peptide desalting in the LysN digestion optimization experiment. Column conditioning was performed by aspirating 10 µl 50 % ACN (v/v), 0.1 % TFA (v/v). Afterwards, the column was equilibrated three times with 10 µl 0.1 % TFA (v/v) before aspirating and releasing the peptide solution for 5-10 times. After

three additional washing steps with 0.1 % TFA (v/v), peptides were eluted with 10 µl 50 % ACN (v/v), 0.1 % TFA (v/v).

#### 4.8.7.3 StageTip-based sample purification

Phosphopeptides from whole cell protein digest after Titanium dioxide-based enrichment, LysN digested synthetic peptides (+/- NHS-biotin) and samples after streptavidin incubation were desalted by using the StageTip protocol published by Rappsilber et al. (2007) with slight adaptations. In brief, the column was prepared by placing 4-10 Empore™ Supelco® C18 discs (3M, Saint Paul, USA) in a 200 µl pipette tip and equilibrated with 20 µl methanol (centrifugation for 1 min at 5,000 x g). Afterwards, the column was washed sequentially with 20 µl 80 % ACN (v/v), 0.5 % acetic acid (AcOH) (v/v) and two times with 20 µl 0.5 % AcOH (v/v) (centrifugation for 1 min at 5,000 x g). The acidified sample was loaded and the column was centrifuged again for 1 min at 5,000 x g. Subsequent to this, the column was washed with 100 µl 0.5 % AcOH (v/v) either by applying pressure with a syringe or by centrifugation for 3 min at 5,000 x g. Peptides were eluted by forcing two times 20 µl 80 % ACN (v/v), 0.5 % AcOH (v/v) through the column. For desalting of the LysN-digested synthetic peptides, 0.5 % AcOH (v/v) was substituted by 0.1 % TFA (v/v). Eluted peptides were dried in a vacuum centrifuge (40 °C at 1,000 rpm).

## 4.9 MS measurements

### 4.9.1 LC-MS measurement with the LTQ Orbitrap Velos mass spectrometer

Dried peptides were re-dissolved in 0.1 % FA (v/v). LC was performed by using a Dionex Ultimate 3000 RSLC nano HPLC system equipped with an analytical C18 column either packed in-house (inner diameter 75 µm, length 15-25 cm, ReproSil-Pur 120 C18-AQ 1.9-3.0 µm (Dr. Maisch, Ammerbuch, Germany)) or purchased from NanoSeparations (Nieuwkoop, Netherlands) (inner diameter 75 µm, length 20 cm, C18 1.9 µm). Commercially acquired columns were used in combination with a PicoTip emitter (New Objective, Woburn, USA). LC was performed either with or without the presence of an upstream C18 pre-column (self-packed, length 2 cm, inner diameter 100 µm, ReproSil-Pur 120 C18-AQ 5.0 µm (Dr. Maisch, Ammerbuch, Germany)). Solvent A (0.1 % FA (v/v)) was used for loading peptides onto the column. The flow rate was set to 0.25-0.3 µl/min and peptide separation was performed by a linear gradient starting from 1-6% and ranging to 35-45 % solvent B (90 % ACN (v/v), 0.1 % FA (v/v)). Gradient lengths between 13 and 120 min were used. After elution, peptides were directed into a linear trap quadrupole

(LTQ) Orbitrap Velos mass spectrometer. The MS1 scan was performed in the Orbitrap detector at a range between 160-1600 or 200-1800 m/z and a resolution of 30,000-60,000 (maximal injection time 300-400 ms; AGC target 1 x $10^6$). The 25 most intense peptide ions were selected for collision induced dissociation (CID) (normalized collision energy 35) and subsequently analyzed by a linear ion trap (maximal injection time 100 ms; AGC target 1 x $10^4$). As phosphopeptide ions tend to loose phosphoric acid or phosphate (neutral losses), multistage activation (MSA) was used in order to analyze phosphoproteomic data sets. In this technique, ions with neutral losses detected in the MS2 scan are selected for further fragmentation, thus enhancing the detection of phosphorylated peptides. Once an MS2 spectrum was acquired, the corresponding precursor ion was excluded from repeated fragmentation for 12-30 seconds.

### 4.9.2 LC-MS measurement via the Orbitrap Fusion Lumos mass spectrometer

Dried peptides were re-dissolved in 0.1 % FA (v/v). LC was performed by using a Dionex system equipped with a self-pulled and packed analytical column (inner diameter 75 µm, length 26 cm, ReproSil-Pur 120 C18-AQ 1.9 µm (Dr. Maisch, Ammerbuch, Germany)). 0.1 % FA (solvent A) (v/v) was used for loading peptides onto the column. Peptides were separated at a flow rate of 0.3 µl/min by using a linear gradient (90 min) ranging from 1-35% solvent B (90 % ACN (v/v), 0.1 % FA (v/v)). The nano-LC was connected online to an Orbitrap Fusion Lumos mass spectrometer. Peptide precursor ions were scanned in the Orbitrap mass analyzer at a range between 330-1600 m/z and a resolution of 60,000 (maximal injection time 50 ms, AGC target 4 x $10^5$, cycle time 3 sec). Precursor ions with a charge state between 2-7 were isolated with an isolation window of 1.2 Da and fragmented by higher-energy collisional dissociation (HCD) (collision energy 30 %) in the top speed mode. MS2 spectra were acquired in the Orbitrap detector at a resolution of 30,000 and an AGC target of 5 x $10^4$ (max injection time 54 ms). Fragmented precursor ions were excluded from repeated MS2 measurement for 30 seconds.

### 4.9.3 MALDI-TOF measurement

For matrix-assisted laser desorption/ionization time of flight (MALDI-TOF) mass spectrometry analysis, peptides were dissolved in 0.1 % FA (v/v) or 0.1 % TFA (v/v). The matrix was prepared by mixing α-cyano-4-hydroxycinnamic acid (HCCA) with 0.1 % TFA (v/v) or 0.1 % FA (v/v) containing 30-40 % ACN (v/v) in order to generate a saturated solution. Afterwards, 1 µl sample was mixed with 1 µl matrix supernatant directly on the ground steel target (Bruker Daltonik, Bremen, Germany). MALDI-TOF measurements of the dried samples were performed with an

Autoflex III TOF-TOF instrument. Prior to the measurement, the spectrometer was calibrated by using the Peptide Calibration Standard (Bruker Daltonik, Bremen, Germany). Data were acquired with a laser repetition rate of 200 Hz, a laser beam focus between 28-80 and a total number of shots between 845-6861. Spectral analysis was performed by using the flexAnalysis software 3.3.

## 4.10 MS data analysis

### 4.10.1 Analysis of mass spectrometric data via Proteome Discoverer

LC-MS data were analyzed with the Proteome Discoverer (PD) software (Version 2.2.0.338 or 2.3.0.523). Database searches were performed by using an in-house Mascot server (2.6.1) (Matrix Science Ltd, London, UK). As far as not otherwise stated, human protein sequences from SwissProt (release 2018_07 or 2019_06) together with the common contaminants enlisted in the contaminant repository for affinity purification (cRAP) (modified) were used as reference databases (Mellacheruvu et al. 2013). MS2 data derived from investigations of synthetic peptides were search against the cRAP database modified with the according peptide sequence. The precursor mass tolerance was set to 9-10 ppm. MS2 spectra acquired with the Orbitrap mass analyzer were searched with a fragment mass tolerance of 20 mmu. In case of MS2 spectra acquisition in the linear ion trap, the mass tolerance was increased to 0.5 Da. The enzymes used in the data processing workflow were chosen according to the experiment and the maximum number of missed cleavages was set to 1-2. Propionamide (at Cysteine) was searched as a static modification. In case of experiments with isotopically labeled cells (SILAC), the “Quan Method” was adjusted accordingly. Oxidation (at methionine) and acetylation (at protein N-terminus) were set as standard dynamic modifications (except for data analysis of synthetic peptides). For data analysis after phospho-peptide enrichment, the list of dynamic modifications searched was extended by phosphorylation at serine, threonine, and tyrosine. The variable modifications set for analysis of raw data acquired during verification of the serial digestion and $N^{\alpha}$-selective derivatization workflow (derivatization of primary amine group at amino-terminus) are listed in the corresponding data post-processing sections. The Percolator algorithm, implemented in Proteome Discoverer, was used by default for evaluating the Mascot results based on the q-value or the posterior error probability (PEP) (strict false discovery rate (FDR) 0.01) (Käll et al. 2007). Peptide spectrum matches (PSMs) derived from MS2 data analysis of the synthetic peptide samples were validated by the target-decoy approach (strict FDR 0.01). The mass tolerance for feature mapping between different raw files processed was either determined

automatically by the software or set to 5 ppm. Precursor quantification was performed based on the chromatographic peak area and the “total peptide amount” was used for normalization.

### 4.10.2 Analysis of mass spectrometric data via MaxQuant

SILAC-derived data searched for dynamic lysine modifications as well as raw files intended for comparison to such samples were analyzed by using the MaxQuant software and the implemented Andromeda search algorithm (Cox and Mann 2008; Cox et al. 2011).
In case of data processing via the MaxQuant software (version 1.5.1.0 or 1.6.5.0), human (release 2018_08) or bovine protein sequences (release 2018_05) from SwissProt and the contaminant list implemented in MaxQuant were used as reference databases. The main MS1 search was performed with a mass tolerance of 4.5 ppm. Fragment ion spectra were searched with an ion trap mass spectrometry (ITMS) MS/MS match tolerance of 0.5 Da. Database searches were performed with the respective enzymes and a maximum number of two missed cleavage sites. Propionamide (at Cysteine) was set as a static modification. If necessary, the labels for peptide quantification were adjusted according to the experiment. Oxidation (at methionine), acetylation (at protein N-terminus) and carbamylation (at lysine and peptide N-terminus) were searched by default as dynamic modifications. In case proteins were treated with NHS-biotin prior to the digestion, the list of variable modifications was extended by biotinylation (at lysine and peptide N-terminus). Together with the standard modifications mentioned above, phosphorylation (at serine, threonine and tyrosine) were allowed as dynamic modification for the analysis of phosphoproteomic samples. For identifications, FDR was set to 0.01. Most of the post-processing data analysis was performed based on the MaxQuant “Evidence” file. In this table, identical PSMs identified in the same raw file are combined into a single entry if they do not differ in their charge states or retention time window.

### 4.10.3 Analysis of mass spectrometric data via PEAKS

PTM searches were performed with the PEAKS software (version 10.0, PeaksPTM module) (Han et al. 2011). Human protein sequences retrieved from SwissProt (release 2018_08) and the cRAP contaminants list were used as reference databases. The enzyme selected for the database search was chosen according to the experimental settings (max. two missed cleavages). The precursor mass tolerance was set to 10 ppm. For MS2 spectra, a fragment ion mass tolerance of 0.5 Da was used. In case of samples derived from the serial digestion workflow, acetylation (at protein N-terminus), oxidation (at methionine), and biotinylation (at lysine and peptide N-

termini) were searched as dynamic modifications (max. three variable modifications per peptide). For the analysis of raw data after $N^{\alpha}$-selective derivatization, the list of variable modifications was extended by single and double reductive alkylation (at lysine and peptide N-termini). The precursor mass correction setting was enabled. PeaksPTM data were filtered for peptides with an FDR smaller than or equal to 1% and an Ascore of 20 or higher for PTM localization. Afterwards, the peptide table was exported and used for calculating the proportions of peptides containing the different PTMs. Here, only peptides with a quantification value were considered for data analysis.

## 4.11 Post-processing of LC-MS2 data after database analysis

### 4.11.1 Optimization of LysN digestion with a synthetic peptide (section 5.2.1.2)

LC-MS2 data were analyzed by the Proteome Discoverer software (version 2.2.0.338) with the settings described in section 4.10.1. Oxidation at methionine was set as a dynamic modification. The chromatographic peak areas of high confident peptide groups were used to calculate the relative cleavage efficiency. Prior to these calculations, the abundances of peptides varying only in their oxidation status were summed up. Afterwards, the relative cleavage efficiency was calculated as the ratio of the abundances of the cleaved and the non-cleaved precursor peptide multiplied by a factor of 1000.

### 4.11.2 LysN and LysArginase digestion of BSA and complex protein mixtures (section 5.2.1.3)

After processing the LC-MS2 data of the BSA samples digested with LysN or LysArginase, the MaxQuant “Evidence” files were filtered for entries with a BSA protein accession and a PEP smaller than 0.01. For each raw file, the filtered entries were copied into a new Excel sheet. Redundant entries were removed based on the “Modified Sequence” column, thus generating the peptide table. Peptides with the same sequence only varying in the carbamylation and/or oxidation status were considered as one single entry. In contrast, peptides differing in their biotinylation- and acetylation-site (protein N-terminus) were kept separately. Subsequently, the modified peptide table was used for determining the number of biotinylated and non-biotinylated peptides as well as the proportion of missed cleavage sites (MCS) in each sample.

For evaluation of the biotinylation position, the information given in the “Modified Sequence” and in the “Biotinylation [K] Probabilities” columns were used.

In case of the complex HEK protein sample, only evidences (retrieved from MaxQuant “Evidence” file) with a quantification value in all three replicates/SILAC channels and a PEP smaller than 0.01 were considered for further data analysis. For each sample group, the filtered entries were copied to a new Excel sheet. Information about carbamylation and oxidation sites were removed in the sequence entries of the “Modified Sequence” column (e.g. KVTNLLM(ox)L was modified to KVTNLLML). In order to generate the peptide table, redundant entries were removed based on this column. Afterwards, this peptide table was used for data analysis similar to the procedure mentioned above. The boxplots depicting the median protein sequence coverage were generated in Excel by using the “Protein Groups” file. For each enzyme, only proteins identified with more than one unique peptide and with a quantification value in all three replicates of the NHS-biotin treated and non-biotinylated samples were used for data visualization.

### 4.11.3 Evaluation of different derivatization methods regarding their reactivity, reproducibility and selectivity (section 5.2.2.2)

Raw data were processes by using the Proteome Discoverer software (version 2.3.0.523) (see section 4.10.1). For each derivatization technique, the list of standard dynamic modifications was extended by single and double propionylation, acetylation or reductive alkylation (at lysine and peptide N-terminus). Peptides with a Percolator q-value smaller than 0.01 were used for further analysis. Post-processing was performed based on the PD “Peptide Isoforms” table by using a self-written R-script (R-Studio, R-packages: “dplyr” (version 0.8.3), “stringr” (version 1.4.0)) (Hadley et al. 2019; Hadley 2019). Peptides featuring an “sp” entry in the “Master Protein Accession” column (contaminants) were removed. Afterwards, information about the derivatization site were fused to the peptide sequence thus yielding the “Modified Sequence” Column. For each replicate, redundant entries of the “Modified Sequence” column were removed. Subsequent to this, the non-redundant peptide lists were used in order to determine the reactivity, reproducibility and selectivity of the different derivatization methods.

### 4.11.4 Evaluation of the serial digestion and the $N^{\alpha}$-selective derivatization workflow (section 5.2.1.4 and 5.2.2.3)

Data processing was performed with the Proteome Discoverer software (version 2.2.0.338) according to the procedure described in section 4.10.1. Raw files belonging to the same step within the workflow were processed together. In addition to the standard settings, methylation at lysine and arginine were set as dynamic modifications. After NHS-biotin treatment, the list of variable modifications searched during data processing was extended by biotinylation (at lysine and peptide N-terminus). For $N^{\alpha}$-selective derivatized samples, single and double alkylation (at lysine and peptide N-terminus) were searched as dynamic modifications.

#### 4.11.4.1 Investigation of the biotinylation efficiency

PSMs (retrieved from PD "PSM" file) featuring a PEP smaller than 0.01 were used for evaluation of biotinylation efficiency. The percentages of biotinylated PSMs and those with at least one unmodified primary amine was determined. In case the samples were derivatized by reductive alkylation prior to the incubation with NHS-biotin, the proportion of alkylated PSMs was also investigated.

#### 4.11.4.2 Investigation of enhanced lysine and arginine PTM detection

Peptide information were retrieved from the PD "Peptide Group" table. Data were filtered for peptides featuring a PEP smaller than 0.01 and information about the methylation sites were fused to the amino acid sequence (modified sequence column) by using a self-written R-script. Peptide species (entries of the modified sequence column) detected in the single samples/replicates were copied to separate Excel sheets. Non-assignable methylation sites were considered as ambiguous modifications. Based on the modified sequence column, redundant peptide entries were removed. Subsequent to this, the non-redundant entries of the modified sequence column were used to analyze the number of arginine and lysine methylation sites in each replicate and sample.

Evaluation of the number of methylated PSMs was performed by using the PD "PSM" table. For this purpose, the position of the methylation site was deleted in the "Modifications" column. The table was filtered for PSMs featuring a PEP smaller than 0.01. Afterwards, the modified entries of the "Modifications" column were used for determining the number of arginine and lysine methylation sites in each raw file.

#### 4.11.4.3 Investigation of the presence of C-terminal methylation sites after tryptic digestion (serial digestion workflow)

The presence of methylation sites at the C-terminus after tryptic digestion was investigated based on the non-redundant peptide list used for determining the number of arginine and lysine methylation sites in samples of the two workflows (see section 4.11.4.2).

#### 4.11.4.4 Investigation of the number of lysine and arginine containing peptides in samples of the $N^{\alpha}$-selective derivatization workflow

The number of arginine and lysine containing peptides was determined by using the non-redundant peptide lists generated for investigating the amount of methylation sites in the different samples/replicates of the two workflows (see section 4.11.4.2).

#### 4.11.4.5 Generation of Venn diagrams for sample comparison

Proportional Venn diagrams were generated with R-studio by using the “eulerr” package (version 6.0.0) (Larsson 2019). The same software was used to create non-proportional Venn diagrams with the “VennDiagram” package (version 1.6.20) (Hanbo 2018).

### 4.11.5 Analysis of phospho-data sets (section 5.1.2)

#### 4.11.5.1 Post-processing of MaxQuant phospho-data

Post-processing of the MaxQuant data was performed with a self-written R-script. Evidences featuring a PEP smaller than 0.01 were retrieved from the MaxQuant “Evidence“ file. For singly phosphorylated evidences, the phosphorylation site with the highest probability (rounded to the first decimal) was fused to the amino acid sequence. In case the evidence was identified to be doubly phosphorylated, the two highest phospho-site probabilities (rounded to the first decimal) were considered. If the same probability was assigned to two or more phospho-sites, the information about all positions were kept. For each replicate, the evidences were split to separate tables. Afterwards, redundant entries were merged based on the phospho-site and probability containing sequence column previously generated. During this procedure, intensity values of redundant entries were summed up. Subsequently, the intensities of each channel were normalized on the median. In the end, the data in the single replicate tables were merged to one file and analyzed by the “qbaR” R-package (see section 4.11.5.3). Highly regulated phosphopeptides were determined by filtering the normalized data for peptides found in at least

two out of three DMSO replicates without any additional identification in the stimulated samples and *vice versa*.

#### 4.11.5.2 Post-processing of Proteome Discoverer phospho-data

Phospho-data processed with PD were analyzed based on the “Peptide Isoform” table (maximum q-value 1%). Peptides featuring an “sp” entry in the “Master Protein Accession” column were removed. A self-written R-script was used in order to fuse the identified phosphorylation site to the amino acid sequence. Peptide entries without abundance value in all conditions/SILAC channels were removed. Afterwards, the data set was analyzed by the “qbaR” R-package (see section 4.11.5.3). Highly regulated phosphopeptides were determined according to the procedure described in section 4.11.5.1 .

#### 4.11.5.3 Statistical analysis of phospho-data

For phosphoproteome comparison, statistical analysis was performed after filtering the data for phosphopeptides found in at least two out of three replicates of the treated samples and the control. In addition to that, the complete data set without further filtering was analyzed (see Appendix section 7.1). Statistics were performed with an R-script provided by Dr. Farhad Shakeri from the Core Unit for Bioinformatics Data Analysis of the University Hospital of Bonn (R-packages: “qbaR” (version 1.2.3), “FactoMineR” (version 1.42), “ggplot2” (version 3.2.1), “data.table” (version 1.12.6), “tidyverse” (version 1.2.1)) (Lê et al. 2008; Wickham 2016, 2017; Dowle and Srinivasan 2019). In this workflow, the limma-package (version 3.40.6.) was used in order to correct p-values for multiple testing (Ritchie et al. 2015).

### 4.11.6 Statistical analysis of proteome comparison data (section 5.1.5)

Raw data from proteome comparison approaches were analyzed with PD (version 2.3.0.523) (see section 4.10.1). Grouped protein abundances were used to calculate protein ratios. Statistical analysis was performed by ANOVA (individual proteins) implemented in the PD workflow. Proteins identified with at least two unique peptides (maximum q-value 1 %) in more than one replicate of the wt and SNAPIN KO samples were used for data visualization. The volcano plot was generated with the R-software (R-packages: ggplot2, data.table). The PCA plot (see Appendix section 7.4) was retrieved from PD.

### 4.11.7 Analysis of Co-IP data (section 5.1.10)

LC-MS2 data from the Co-IP experiment were processed with PD (version 2.3.0.523) according to the procedure mentioned in section 4.10.1. In addition to the standard databases, data were also searched against a protein list containing sequence information about the SNAPIN wt, S133E and S133A isoforms. In this additional database, the SNAPIN isoforms were listed without sequence information of the Myc-Tag and the linking region between the Tag and the protein. Non-normalized abundances of proteins found with at least two peptides (max. q-value 0.01) were used for post-processing data analysis.

For each protein, the mean and standard deviation of the non-normalized abundances was calculated for the three replicates of the SNAPIN KO, SNAPIN S133E and SNAPIN S133A samples. Subsequent to this, the mean values were used to calculate the S133E/KO and S133A/KO ratios. In case the ratio could not be calculated due to missing values in the KO samples, a value of 200 was set. Each protein with a ratio higher than 10 and found in at least two S133A or S133E replicates was assumed to be a potential interaction partner of the particular isoform. Data visualization was performed with the R-software (R-package: ggplot2). Here, the coefficient of variation (CV) (calculated as the standard deviation abundance divided by mean abundance) of each protein identified in more than one S133E or S133A replicate was plotted against its $\log_2$ sample/KO ratio.

In order to compare the abundances of the potential interaction partners shared between both isoforms, the protein levels of each channel and sample group were normalized on the corresponding SNAPIN quantities. Afterwards, the mean protein abundances of the different replicates were calculated and used to determine the S133A/S133E ratio. Data visualization was performed with R-studio (R-package: ggplot2). The ratios of the mean values were depicted as a bar chart. Abundance ratios determined for single replicates were indicated as dots.

# 5. Results

## 5.1. Investigating cAMP mediated phosphorylations of lysosomal and lysosome-associated proteins

cAMP is an important second messenger. Inside the cell, EPACs and the protein kinase A are two major cAMP sensors (Walsh et al. 1968; Tao et al. 1970; Kawasaki et al. 1998; Rooij et al. 1998). The peptide hormone glucagon, secreted as a starvation signal by pancreatic cells, is a well-known trigger of the cAMP signaling machinery (Jelinek et al. 1993; reviewed by Habegger et al. 2010). Once initiated, the cAMP pathway activates PKA which is associated with the degradation of glycogen, thus counteracting the starvation signal (reviewed by Unger 1985). Another process upregulated upon nutrient deprivation is the expression of genes encoding for lysosomal proteins which also results in an increased break-down of complex molecules (Sardiello et al. 2009; Settembre et al. 2011). Based on their involvement in starvation-induced catabolism, one could hypothesize a functional relationship between PKA and lysosomes. For example, lysosomal membrane proteins might be regulated by PKA-dependent phosphorylation. So far, Mucolipin 1 is the only known lysosomal membrane protein phosphorylated by PKA (Vergarajauregui et al. 2008). Besides that, little is known about the functional impact of this kinase on lysosomes. In 2016, Rahman et al. demonstrated an effect of PKA in lysosome re-acidification during investigations of the lysosomal pH upon depletion of soluble Acs (sAC). Here, the sAC knock-out (KO)-induced increase in lysosomal pH was rescued by the addition of cAMP to the media (Rahman et al. 2016). However, a combinatory treatment of the sAC-KO cells with cAMP and an PKA inhibitor was not associated with complete lysosome re-acidification, thus highlighting the role of PKA in re-adjusting the lysosomal pH (Rahman et al. 2016).

The observations mentioned above suggest cAMP-mediated PKA activation as an important regulator for lysosomal function. Therefore, the present study aimed at investigating changes in the phosphorylation pattern of lysosomal and lysosome-associated proteins upon elevated intracellular cAMP levels, followed by the subsequent characterization of the targets.

### 5.1.1. Validating the Forskolin and dibutyryl-cAMP induced stimulation of PKA

In the course of this study, intracellular cAMP levels were raised by cultivating HEK 293 cells in medium containing forskolin (FSK), an AC stimulatory drug (dissolved in DMSO) (Seamon et al. 1981), and dibutyryl-cAMP (db-cAMP), a cAMP analog. As the addition of FSK to the medium

resulted in a final DMSO concentration of 0.1 %, the same DMSO concentration was used in the stimulation control medium.

The PKA activity was investigated in order to validate the treatment induced elevation of intracellular cAMP levels. After cell lysis, proteins were separated by SDS-PAGE and blotted onto a nitrocellulose membrane. Prior to immune detection, the membrane was cut horizontally between the 40 and 55 kDa marker protein. PKA stimulation was validated by antibody-based detection of a PKA targeted phosphorylation site (S133) of the cAMP-responsive element-binding protein 1 (pCREB). In order to evaluate the influence of elevated cAMP levels on the CREB protein level, the same samples were investigated with an anti-CREB antibody. α-Tubulin detection served as a loading control. After densitometric quantification, pCREB and CREB signals were normalized to the α-Tubulin intensities. The experiment was performed in three biological replicates.

By incubating the nitrocellulose membrane with the anti-CREB antibody, signals at approx. 45 kDa were detected (Figure 5.1A, lower panel). As the position of those polypeptides match to the expected mass of cAMP-responsive element-binding protein 1, it is reasonable to assume that the signals obtained at 45 kDa corresponded to CREB. Except for the FSK/db-cAMP treated sample of the third replicate, the CREB signal intensities of the stimulated and non-stimulated samples as well as of the different replicates were comparable. Incubation of the membrane with an antibody directed against α-Tubulin was associated with a signal detection at approx. 55 kDa (Figure 5.1A, upper panel). These signals match to the expected mass of α-Tubulin thus indicating the specificity of this antibody. Therefore, in the further course of this thesis, signals obtained at 55 kDa after immune detection with the anti-α-Tubulin antibody are assumed to derive from successful α-Tubulin detection. However, in this experiment, similar α-Tubulin signal intensities were observed among the different samples of the first two replicates. Compared to that, the signal intensities of the FSK/db-cAMP treated and non-stimulated samples of the third replicate were slightly reduced.

The normalized CREB quantities were calculated as the ratio of the CREB and the α-Tubulin signal intensities determined for the single replicates of both sample groups. These relative CREB quantities are depicted as dots in figure 5.1B. Comparison of both conditions indicate a slightly lower CREB intensity in the FSK/db-cAMP treated samples. This tendency can also be observed when comparing the average relative CREB intensities of both groups shown as bar charts (Figure 5.1B, +/- standard deviation). However, the mean CREB intensity as well as the standard deviation detected in the FSK/db-cAMP stimulated sample was strongly influenced by the quantification value of the third replicate. As already shown in figure 5.1A, the CREB signal in this sample is noticeably lower compared to those observed for the other two replicates of this

group, thus strongly influencing the mean and standard deviation. Nevertheless, comparison of both sample groups by a two sample t-test indicates that the difference in the mean CREB intensities is not significant (homoscedastic, p-value 0.1328, significance threshold 0.05).

Figure 5.1C (lower panel) shows the signals detected after incubating the membrane with an antibody directed against the phosphorylated S133 CREB motif (p-CREB). According to the information given by the antibody supplier, the signals detected at approx. 38 kDa correspond to a phosphorylated isoform of the cAMP-dependent transcription factor 1. However, based on the signals obtained by using the CREB antibody (Figure 5.1A), the polypeptides detected at approx. 45 kDa in figure 5.1C (lower panel) were ascribed to p-CREB. Compared to the controls, higher p-CREB signal intensities were observed in the FSK/db-cAMP treated samples among all three replicates. As the intensities of the α-Tubulin signals were similar between the different samples, it is reasonable to assume that this increase is rather caused by higher p-CREB levels present within the FSK/db-cAMP treated samples than by different protein amount loaded onto the gel.

In order to determine the level of p-CREB within the different samples, p-CREB intensities obtained by immune detection were normalized to the corresponding α-Tubulin signals. Figure 5.1D depicts the average α-Tubulin-normalized p-CREB intensity (+/- standard deviation) detected in the FSK/db-cAMP treated sample group as well as in the non-stimulated control. Additionally, the values of the single replicates are indicated as dots. Within the control group, the average relative p-CREB intensity amounted to 0.57 (standard deviation +/- 0.04). Compared to that, higher relative p-CREB levels were detected within all replicates of the FSK/db-cAMP stimulated samples. Here, an average p-CREB intensity of 0.96 (standard deviation +/- 0.05) was detected. Statistical analysis (two sample t-test) of the relative pCREB intensities revealed a significant difference between both sample groups (homoscedastic, p-value 0.0006, significance threshold 0.05)

In summary, an increase in the pCREB signal intensity was observed when incubating the cells with FSK/db-cAMP whereas the CREB protein level was not significantly affected by this treatment. Therefore, it is reasonable to assume that PKA was successfully activated upon FSK/db-cAMP stimulation.

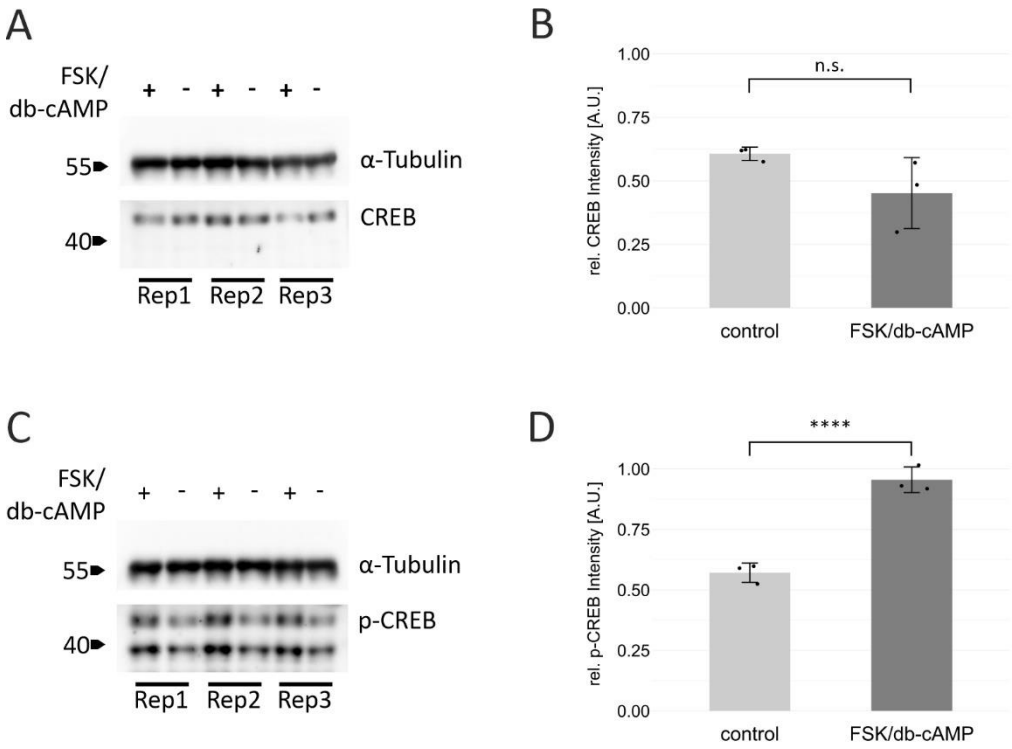


**Figure 5.1: *In vitro* investigation of the Forskolin and dibutyryl-cAMP induced activation of PKA.**
HEK 293 cells were cultivated in media containing either FSK and db-cAMP (PKA stimulation media) or DMSO (control). After cell lysis, proteins were separated by SDS-PAGE and transferred onto a nitrocellulose membrane. The influence of PKA activation on the CREB protein level was investigated by using an anti-CREB antibody (CREB: 30 s exposure; α-Tubulin: 1 s exposure) (A). α-Tubulin-normalized CREB intensities are depicted in B. Here, the average relative CREB intensities (+/- standard deviation) are shown as a bar chart whereas the dots represent the quantification values observed for the single replicates (normalized to the α-Tubulin signals). An antibody directed against a PKA targeted phosphorylation site (S133) of CREB was used to evaluate PKA stimulation (CREB: 30 s exposure; α-Tubulin: 1 s exposure) (C). For both sample groups, the mean values (+/- standard deviation) of the relative p-CREB intensity (normalized to α-Tubulin signals) are shown as a bar chart (D). Additionally, the relative p-CREB intensities detected for the single replicates are indicated as dots. Statistical analysis was performed by a t-test. (A.U. = arbitrary units; n.s.: not significant (p-value >0.05); **** p-value < 0.001).

### 5.1.2. Identification of significantly regulated phosphopeptides upon elevated intracellular cAMP levels

After showing the successful activation of PKA by a combinatory FSK/db-cAMP stimulation, this treatment was used in order to investigate cAMP-dependent regulation of phosphorylation sites on whole cell and lysosomal level. Three biological replicates, using HEK 293 cells (light, medium and heavy labeled) in which the proteins were isotopically labeled according to the SILAC procedure, were analyzed. In each replicate, two of the three SILAC channels contained the FSK/db-cAMP stimulated cells and the corresponding DMSO control. The third SILAC label comprised of proteins from cells incubated with Torin1, a mechanistic target of rapamycin (mTOR) inhibitor (Thoreen et al. 2009). However, as only one significantly regulated phosphopeptide was identified in the mTOR data sets (see Appendix Figure 7.1, figure 7.3, figure 7.5), the results mentioned in this section focus on phospho-sites found in the FSK/db-cAMP treated samples.

#### 5.1.2.1. Phosphopeptide enrichment from whole cell lysate digest

Prior to tryptic protein digestion, the lysates of stimulated, isotopically labeled cells were combined. Afterwards, titanium dioxide ($TiO_2$)-based phosphopeptide-enrichment was performed followed by peptide fractionation via SCX chromatography. Non-phospho-enriched samples of the combined lysates were used for protein quantification in the starting material. The phospho-enriched and the input samples were analyzed by using a Dionex LC-system coupled to an LTQ Orbitrap Velos mass spectrometer. The MaxQuant software was used to search the raw data against a human reference database. Data analysis was performed with the information provided in the evidence table. In case of the enriched samples, the number of phospho-sites as well as the phosphorylation position with the highest probability were fused to the evidence sequence. For each replicate and SILAC channel, the peptide abundances were calculated by summing up all intensities of evidences with the same modified sequence. Subsequently, the peptide abundances were normalized by the median intensity determined for the different replicates and SILAC channels. Phosphopeptides found in at least two out of three replicates per condition were used for statistical analysis. The p-values were corrected for multiple testing by using the limma R-package. The protein quantities in the non-phospho enriched samples were calculated by summing up the evidence intensities belonging to the one UniProt accessions of a given channel and replicate. Subsequent to this, the ratio between the treated sample and the control was determined for each replicate. Finally, the mean and the standard deviation of the ratios of the three replicates were calculated.

Fifty percent of the peptides identified after phospho-enrichment contained at least one phosphorylation site. In figure 5.2, the results of the statistical analysis of the phosphopeptides are visualized in a volcano plot, a special type of scatter plot. The p-value is plotted on the y-axis ($-\log_{10}$) whereas the abscissa contains information about the fold change ($\log_2$) between the FSK/db-cAMP stimulated sample group and the DMSO control. The red horizontal line indicates the adjusted p-value threshold of 0.05. Each point in the volcano plot represents a phosphopeptide identified within the study. The point color assigns each phosphopeptide to a specific data group. Significantly regulated phosphopeptides are colored in red and marked with their UniProt accession number, the peptide sequence, the number of phosphorylation events and the phospho-site position together with the localization probability. Compared to this, phosphopeptides with an adjusted p-value smaller than 0.05 and a $\log_2$ fold-change bigger than 1 or smaller than -1 are colored in orange. The grey points represent the phosphopeptides with $\log_2$ fold-change between 1 and -1 and an adjusted p-value smaller than 0.05. Phosphopeptides found in at least two out of three FSK/db-cAMP-treated replicates but not in any DMSO sample and *vice versa* are considered as being highly regulated. However, as a statistical analysis of

those phosphopeptides is not possible due to the missing values either in the FSK/db-cAMP or DMSO sample group, they are not visualized in the volcano plot but listed in two separate tables (Table 5.2 and table 5.3).

In the present data set, six significantly regulated phosphopeptides were identified (adjusted p-value <0.05 and $\log_2$ fold change <1 or >1; figure 5.2, table 5.1). Additionally, eight phosphopeptides were found in at least two out of three DMSO replicates but not in any FSK/db-cAMP stimulated sample, thus representing the highly downregulated phosphopeptides (Table 5.3). *Vice versa*, the group of highly upregulated phosphopeptides contains 28 peptides. These peptides were detected in at least two FSK/db-cAMP treated replicates but not in the DMSO control (Table 5.2).

As expected, FSK/db-cAMP treatment was associated with the upregulation of peptide phosphorylation. Known PKA target sites of the calcium/calmodulin dependent protein kinase kinase (CaMKK1; S475) (UniProt accession: Q8N5S9), the 6-phosphofructo-2-kinase/fructose-2,6-bisphosphatase 2 (PFKFB2; S466) (O60825) and the CAD protein (CAD) (P27708; S1406) were identified as being upregulated within the present study (Table 5.2) (PhosphoSitePlus online repository; phosphosite.org, retrieved 24.10.2019 (Hornbeck et al. 2015)) (Carrey et al. 1985; Okuno et al. 2001; Pozuelo Rubio et al. 2003). CaMKK1 and PFKFB2 were not detected in the non-phospho enriched starting material of this experiment. The abundance of the CAD protein was not influenced by the FSK/db-cAMP treatment. This indicates that the upregulation of the identified CAD phopsho-site was caused by cAMP mediated phosphorylation and not by an increase in the protein level upon stimulation. However, the detection of highly downregulated phosphopeptides also suggests an association of elevated intracellular cAMP levels with protein dephosphorylation or degradation. For example, such a downregulation was detected for two phospho-sites of the CREB-regulated transcription coactivator 3 (CRTC3) (Q6UUV7) (Table 5.3). The CRTC3 was not identified in the non-phospho enriched samples.

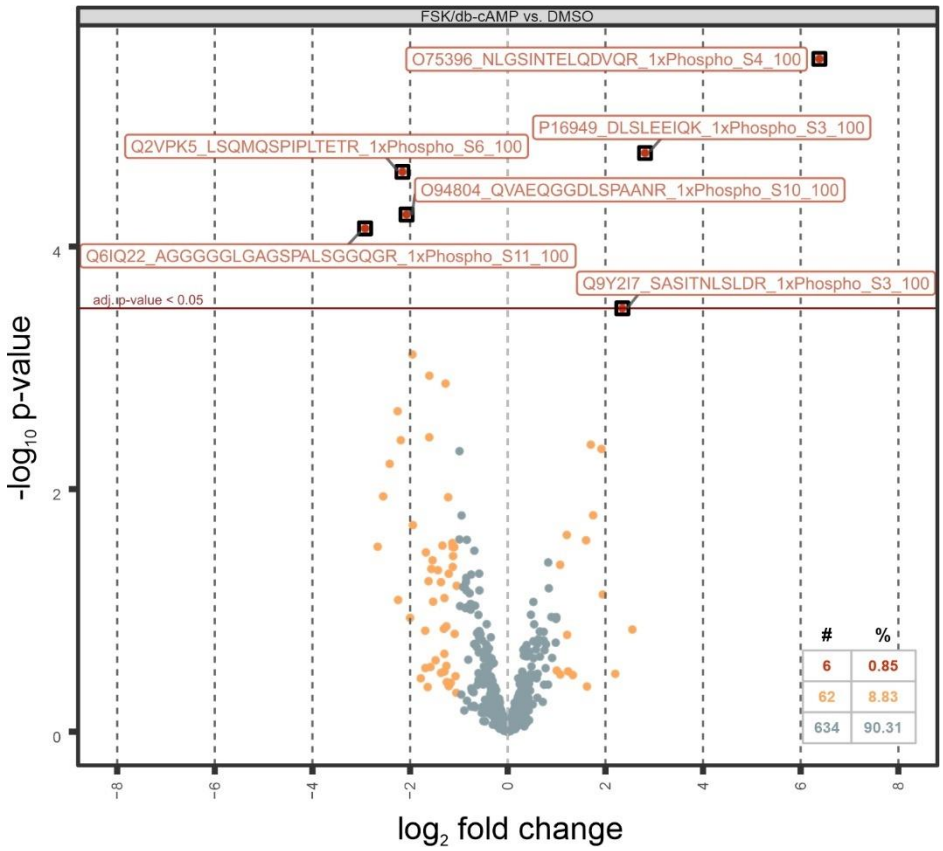


**Figure 5.2: Phosphopeptide enrichment from whole cell lysate digest.**
$TiO_2$-based phosphopeptide enrichment was performed with peptides derived from tryptic digestion of whole cell lysate. Phosphopeptides were fractionated via SCX chromatography prior to LC-MS2 measurements. The experiment was performed in three biological replicates. Raw data were analyzed using the MaxQuant software. Statistical analysis (FSK/db-cAMP vs DMSO) was performed on phosphopeptides found in at least two out of three replicates (adjusted p-value threshold 0.05) by using the limma package implemented in an R-script. Significantly regulated phosphopeptides (adjusted p-value <0.05 and $log_2$ fold change <1 or >1) are highlighted as red points.

**Table 5.1: Significantly regulated phosphopeptides detected in the whole cell lysate digest after FSK/db-cAMP treatment.**
List of proteins corresponding to the six significantly regulated phosphopeptides (red points in figure 5.2) identified after statistical analysis of the phospho-data set derived from the whole cell digest (FSK/db-cAMP vs. DMSO). The mean ratios (+/- standard deviation) of the corresponding protein abundance (FSK/db-cAMP vs. DSMO) determined by MS analysis of the non-phospho-enriched samples are shown.

| Uniprot accession | Protein name | $Log_2$ fold change | Adj. p-value | Mean protein ratio (FSK/db-cAMP vs. DMSO) |
|---|---|---|---|---|
| O75396 | Vesicle-trafficking protein SEC22b | 6.4 | 0.002 | 0.98 (±0.09) |
| P16949 | Stathmin | 2.8 | 0.006 | 0.99 (±0.08) |
| Q2VPK5 | Cytoplasmic tRNA 2-thiolation protein 2 | -2.2 | 0.006 | 1.24 (±0.22) |
| Q6IQ22 | Ras-related protein Rab-12 | -2.9 | 0.010 | Found in less than 2 replicates |
| O94804 | Serine/threonine-protein kinase 10 | -2.1 | 0.010 | Not found |
| Q9Y2I7 | 1-phosphatidylinositol 3-phosphate 5-kinase | 2.3 | 0.038 | Not found |

**Table 5.2: Highly upregulated phosphopeptides detected in the whole cell lysate digest upon elevation of the intracellular cAMP level.**
List of phosphopeptides found to be highly upregulated in the whole cell lysate after FSK/db-cAMP treatment (found in at least two out of three FSK/db-cAMP replicates but not in any DMSO sample). For each phosphopeptide, the mean protein abundance ratios (+/- standard deviation) determined in the non-phospho-enriched samples are listed.

| Uniprot accession | Modified sequence | Protein name | Mean ratio protein abundance (FSK/db-cAMP vs. DMSO) |
|---|---|---|---|
| Q13206 | APSLTNDEVEEFR_1xPhospho_S3_100 | Probable ATP-dependent RNA helicase DDX10 | 1.47 (±0.75) |
| P49792 | KQSLPATSIPTPASFK_1xPhospho_S3_100 | E3 SUMO-protein ligase RanBP2 | 1.03 (±0.07) |
| Q96PK6 | RLSESQLSFR_1xPhospho_S3_100 | RNA-binding protein 14 | 0.94 (±0.11) |
| Q9BXB4 | SFSLASSSNSPISQR_1xPhospho_S3_90 | Oxysterol-binding protein-related protein 11 | 1.30 (±0.06) |
| Q9H3N1 | SLGPSLATDKS_1xPhospho_S1_100 | Thioredoxin-related transmembrane protein 1 | 1.03 (±0.05) |
| P46019 | SLNLVDSPQPLLEK_1xPhospho_S1_100 | Phosphorylase b kinase regulatory subunit alpha, liver isoform | Not found |
| Q8N5S9 | SMSAPGNLLVK_1xPhospho_S3_100 | Calcium/calmodulin-dependent protein kinase kinase 1 | Not found |
| O43353 | SPSLNLLQNK_1xPhospho_S3_100 | Receptor-interacting serine/threonine-protein kinase 2 | Not found |
| Q7Z2W4 | SSLGSLQTPEAVTTR_1xPhospho_S1_S2_50 | Zinc finger CCCH-type antiviral protein 1 | 1.10 (±0.23) |
| Q9Y4F5 | AGSFTGTSDPEAAPAR_1xPhospho_S3_100 | Centrosomal protein of 170 kDa protein B | Not found |
| P10412; P16403 | KASGPPVSELITK_1xPhospho_S3_100 | Histone H1.4; Histone H1.3; Histone H1.2 | 1.00 (±0.21); 0.99 (±0.19) |
| Q9NPD8 | KASQLVGIEK_1xPhospho_S3_100 | Ubiquitin-conjugating enzyme E2 T | 1.23 (±0.05) |
| P35711 | KGSLADVVDTLK_1xPhospho_S3_100 | Transcription factor SOX-5; Transcription factor SOX-6 | Not found |
| P48634 | KQSSSEISLAVER_1xPhospho_S3_100 | Protein PRRC2A | 0.92 (±0.21) |
| Q9Y4H2 | KSSEGGVGVGPGGGDEPPTSPR_1xPhospho_S2_60 | Insulin receptor substrate 2 | 1.20 (±0.38) |
| Q09666 | LPSGSGAASPTGSAVDIR_1xPhospho_S3_100 | Neuroblast differentiation-associated protein AHNAK | 1.00 (±0.15) |
| P52569 | NLSSPFIFHEK_1xPhospho_S3_100 | Cationic amino acid transporter 2 | Not found |
| O60825 | NSFTPLSSSNTIR_1xPhospho_S2_100 | 6-phosphofructo-2-kinase/fructose-2,6-bisphosphatase 2 | Not found |
| Q13610 | NSSISGPFGSR_1xPhospho_S3_100 | Periodic tryptophan protein 1 homolog | 0.95 (±0.11) |
| Q14671 | RDSLTGSSDLYK_1xPhospho_S3_100 | Pumilio homolog 1 | 1.16 (±0.15) |
| P27708 | RLSSFVTK_1xPhospho_S3_100 | CAD protein | 1.00 (±0.09) |
| Q92794 | RLSSQDVLR_1xPhospho_S3_100 | Histone acetyltransferase KAT6A | 0.95 (±0.06) |
| Q9BXB4 | SFSLASSSNSPISQR_1xPhospho_S1_90 | Oxysterol-binding protein-related protein 11 | 1.30 (±0.06) |
| A3KN83 | SIDPDSIQSALLASGLGSK_1xPhospho_S1_100 | Protein strawberry notch homolog 1 | 1.21 (±0.35) |
| Q08AD1 | SISNEGLTLNNSHVSK_1xPhospho_S1_S3_50 | Calmodulin-regulated spectrin-associated protein 2 | Not found |
| Q9UPR0 | SLEVIPEKANDETGE_1xPhospho_S1_100 | Inactive phospholipase C-like protein 2 | Not found |
| Q96RR4 | SLSAPGNLLTK_1xPhospho_S3_100 | Calcium/calmodulin-dependent protein kinase kinase 2 | Found in less than 2 replicates |
| O60343 | SLTSSLENIFSR_1xPhospho_S1_100 | TBC1 domain family member 4 | 0.99 (±0.11) |

**Table 5.3: Highly downregulated phosphopeptides detected in the whole cell lysate digest upon elevation of the intracellular cAMP level.**
List of phosphopeptides found to be highly downregulated in the whole cell lysate after FSK/db-cAMP treatment (found in at least two out of three DMSO replicates but not in any FSK/db-cAMP sample). For each phosphopeptide, the mean protein abundance ratios (+/- standard deviation) determined in the non-phospho-enriched samples are listed.

| Uniprot accession | Modified sequence | Protein name | Mean ratio protein abundance (FSK/db-cAMP vs. DMSO) |
|---|---|---|---|
| Q5SQI0 | LLLAADPGGSPAQR_1xPhospho_S10_100 | Alpha-tubulin N-acetyltransferase 1 | Not found |
| Q12830 | NLSESPVITK_1xPhospho_S5_100 | Nucleosome-remodeling factor subunit BPTF | 1.25 (±0.17) |
| Q7Z417 | NLSSDEATNPISR_1xPhospho_S3_100 | Nuclear fragile X mental retardation-interacting protein 2 | 1.12 (±0.05) |
| Q6UUV7 | SNPSIQATLNK_1xPhospho_S1_100 | CREB-regulated transcription coactivator 3 | Not found |
| Q15758 | GPAGDATVASEKESVM_1xPhospho_S10_100 | Neutral amino acid transporter B(0) | 0.95 (±0.06) |
| Q6UUV7 | LFSLSNPSLSTTNLSGPSR_1xPhospho_S5_80 | CREB-regulated transcription coactivator 3 | Not found |
| Q9BXB4 | SFSLASSSNSPISQR_1xPhospho_S10_100 | Oxysterol-binding protein-related protein 11 | 1.30 (±0.06) |
| Q9UKG1 | VNQSALEAVTPSPSFQQR_1xPhospho_S12_100 | DCC-interacting protein 13-alpha | 1.10 (±0.15) |

#### 5.1.2.2. Phosphopeptide enrichment from lysosomal fractions

Prior to lysosome enrichment, the lysates of stimulated, isotopically labeled cells were combined. Enriched lysosomes were further separated into a soluble and a membrane fraction. After tryptic digestion, phosphopeptides were enriched from the two lysosomal fractions by $TiO_2$. Non-phospho-enriched peptides were used for MS-based protein quantification thus allowing conclusions about treatment-dependent changes of protein levels in the single fractions. The experiment was performed in three biological replicates. Phosphopeptides were analyzed by LC-MS2 either using the LTQ Orbitrap Velos (soluble fraction) or the Orbitrap Fusion Lumos mass spectrometer (membrane fraction). Raw data of the phospho- and non-phospho-enriched samples were searched against a human reference database using the Mascot search engine implemented in the Proteome Discoverer software. The data of the phospho-data set were analyzed based on the peptide isoform table. Here, the number of phospho-sites as well as the position and localization probability of the phosphorylation event was fused to the peptide sequence. Statistical analysis of this data set was performed according to the procedure mentioned in section 5.1.2.1. For the non-phospho-enriched samples, the protein ratios enlisted in the “Protein” PD-output table were used without any further data modification.

Within the soluble lysosomal fraction, 32 % of the peptides featured at least one phosphorylation site. However, no significantly regulated phosphopeptide was found in this sample group (see Appendix figure 7.4). Additionally, only one highly up- and one highly down-regulated phospho-site was detected after FSK/db-cAMP treatment (highly upregulated: found in at least two out of three FSK/db-cAMP replicates but not in any DMSO sample; highly downregulated: found in at least two out of three DMSO replicates but not in any FSK/db-cAMP sample). These two phosphopeptides were derived from the Golgin subfamily B member 1- and the PRRC2A-protein. Nevertheless, 238 proteins found in at least two FSK/db-cAMP and DMSO replicates featured “lysosome” as a gene ontology (GO) annotation in the non-phospho-enriched proteomic data set of the soluble fraction, thus indicating the presence of lysosomal proteins in the samples used for the phospho-enrichment.

Similarly, 261 proteins with a “lysosome” GO annotation were identified in at least two out of three replicates of both, the control and FSK/db-cAMP treated samples of the lysosomal membrane fraction. After phospho-enrichment, 28 % of the peptides identified in the eluate contained at least one phosphorylation site. Figure 5.3 depicts the fold change and the p-value of phosphopeptides found in at least two out of three FSK/db-cAMP and DMSO replicates of the lysosomal membrane fraction. Twelve phosphopeptides were found to be significantly regulated upon elevation of the intracellular cAMP level (adjusted p-value $<0.05$ and $\log_2$ fold change $<1$ or $>1$; red points in figure 5.3). The protein names corresponding to those peptides

are listed in table 5.4. Besides that, 18 phosphopeptides were detected in at least two DMSO treated samples but not in any FSK/db-cAMP replicate, thus belonging to the highly downregulated peptide population (Table 5.6). The highly upregulated phospho-site group comprises peptides found in at least two FSK/db-cAMP replicates but not in any DMSO control. Within the present study, 23 phosphopeptides were found to be highly upregulated upon elevated intracellular cAMP levels (Table 5.5).

Known PKA target sites of the CD44 antigen (S697) and the CAD protein (S1406) were identified as being upregulated in the lysosomal membrane fraction after FSK/db-cAMP treatment (PhosphoSitePlus online repository; phosphosite.org, retrieved 09.05.2019; note that the S697 CD44 phospho-site corresponds to the S316 site described by Tzircotis et al. (2006) (Carrey et al. 1985)). Here, an increase in the protein level was not detected. The upregulated phospho-site of the Vesicle-trafficking protein SEC22b, identified after phosphopeptide enrichment from the whole cell digest (Table 5.1), was also found as being significantly upregulated in the lysosomal membrane fractions (Figure 5.3, table 5.4). This demonstrates the comparability of the stimulus applied to the cells within the different experiments, although the starting material for phosphopeptide enrichment was different. The presence of non-lysosomal proteins among the regulated phosphopeptides in the membrane fraction indicate a certain impurity of the lysosome preparation. Highly or significantly regulated phospho-sites were identified for the lysosomal and lysosome-associated proteins regulatory-associated protein of mTOR (RPTOR), serine/threonine-protein kinase mTOR, run domain Beclin-1-interacting and cysteine-rich domain-containing protein (RUBCN), Mucolipin 1, and the SNARE-associated protein (SNAPIN). The protein levels of RPTOR, mTOR and Mucolipin 1 were not regulated in the lysosomal membrane fraction after FSK/db-cAMP treatment. Compared to that, RUBCN and SNAPIN were not detected in the non-phospho enriched samples thus hindering conclusions about the cAMP-induced changes in protein levels within this lysosomal fraction. The phospho-sites identified for the lysosomal proteins are not assigned as PKA target sites in the PhophoSitePlus online repository (phosphosite.org, retrieved 09.05.2019). Compared to that, phosphorylation of SNAPIN (at S50) and Mucolipin 1 (at S557 and S559) have already been associated with PKA activity (Chheda et al. 2001; Vergarajauregui et al. 2008). Interestingly, the S133 phospho-site of SNAPIN identified within the present study was downregulated after FSK/db-cAMP treatment.

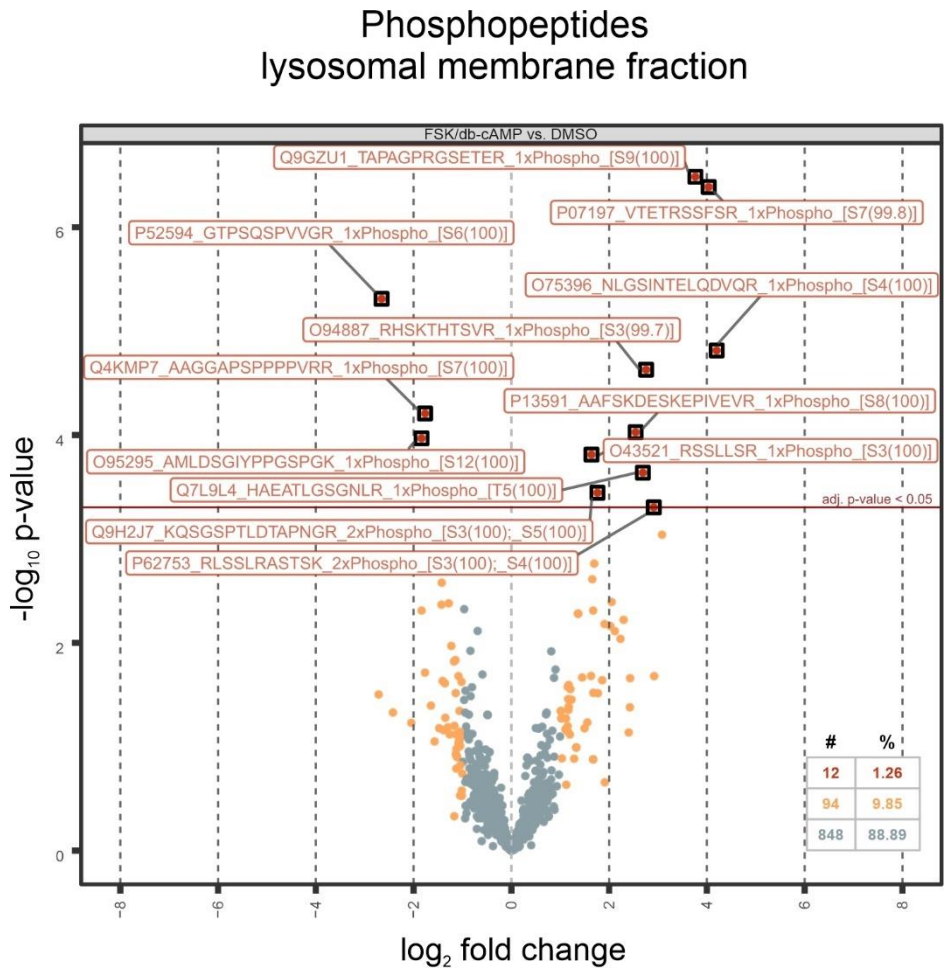


**Figure 5.3: Phosphopeptide enrichment from lysosomal membrane fraction.**
Lysosomes from isotopically labeled cells were enriched and subsequently separated into a water soluble and membrane fraction. After tryptic digestion, phosphopeptide enrichment was performed by $TiO_2$. The experiment was performed in three biological replicates. Phosphopeptides derived from the membrane fractions were analyzed with an Orbitrap Fusion Lumos mass spectrometer. Raw data were searched against a human reference database by using the Mascot search engine. Statistical analysis (FSK/db-cAMP vs DMSO) was performed on phosphopeptides found in at least two out of three replicates (adjusted p-value threshold 0.05) by using the limma package implemented in an R-script. Significantly regulated phosphopeptides (adjusted p-value <0.05 and $log_2$ fold change <1 or >1) are highlighted as red points.

**Table 5.4: Significantly regulated phosphopeptides detected in the lysosomal membrane fraction after FSK/db-cAMP treatment.**
List of proteins corresponding to the twelve significantly regulated phosphopeptides (red points in figure 5.3) identified after statistical analysis of the phospho-data set derived from the lysosomal membrane fraction (FSK/db-cAMP vs. DMSO). The ratios of the corresponding protein abundance (FSK/db-cAMP vs. control) determined by MS analysis of the non-phopho-enriched samples are shown.

| Uniprot accession | Protein name | $Log_2$ fold change | Adj. p-value | Protein ratio (FSK/db-cAMP vs. DMSO) |
|---|---|---|---|---|
| P52594 | Arf-GAP domain and FG repeat-containing protein 1 | -2.7 | 0.0015 | Not found |
| O95295 | SNARE-associated protein SNAPIN | -1.8 | 0.0126 | Not found |
| Q4KMP7 | TBC1 domain family member 10B | -1.8 | 0.0097 | 1.12 |
| O43521 | Bcl-2-like protein 11 | 1.6 | 0.0161 | Not found |
| P13591 | Neural cell adhesion molecule 1 | 2.5 | 0.0126 | 1.04 |
| O94887 | FERM, ARHGEF and pleckstrin domain-containing protein 2 | 2.8 | 0.0044 | 0.47 |
| Q9GZU1 | Mucolipin 1 | 3.8 | 0.0002 | 1.14 |
| P07197 | Neurofilament medium polypeptide | 4.0 | 0.0002 | 0.97 |
| O75396 | Vesicle-trafficking protein SEC22b | 4.2 | 0.0036 | Found in less than 2 replicates |
| Q7L9L4 | MOB kinase activator 1B | 2.7 | 0.0216 | Not found |
| P62753 | 40S ribosomal protein S6 | 2.9 | 0.0389 | 0.81 |
| Q9H2J7 | Sodium-dependent neutral amino acid transporter B(0)AT2 | 1.8 | 0.0307 | 0.93 |

**Table 5.5: Highly upregulated phosphopeptides detected in the lysosomal membrane fraction upon elevation of the intracellular cAMP level.**
List of phosphopeptides found to be highly upregulated in the lysosomal membrane faction after FSK/db-cAMP treatment (found in at least two out of three FSK/db-cAMP replicates but not in any DMSO sample). For each phosphopeptide, protein abundance ratios determined in the non-phospho-enriched samples are listed.

| Uniprot accession | Modified sequence | Protein name | Protein ratio (FSK/db-cAMP vs. DMSO) |
|---|---|---|---|
| Q12846 | AIEPQKEEADENYNSVNTR_1xPhospho_[S15(100)] | Syntaxin-4 | 1.21 |
| P54105 | FEEESKEPVADEEEEDSDDDVEPITEFR_1xPhospho_[S17(100)] | Methylosome subunit pICln | 0.71 |
| Q8N122 | GVHIHQAGGSPPASSTSSSSLTNDVAKQPVSR_1xPhospho_[S10(100)] | Regulatory-associated protein of mTOR | 1.01 |
| P55011 | KESKGPIVPLNVADQK_1xPhospho_[S3(100)] | Solute carrier family 12 member 2 | 0.82 |
| Q9BQG0 | KGVLGKSPLSALAR_1xPhospho_[S7(100)] | Myb-binding protein 1A | 0.82 |
| Q8N7R7 | KYSSCSTIFLDDSTVSQPNLR_1xPhospho_[Y/S/T] | Cyclin-Y-like protein 1 | Not found |
| Q8N7R7 | KYSSCSTIFLDDSTVSQPNLR_1xPhospho_[S/T/Y] | Cyclin-Y-like protein 1 | Not found |
| P16070 | LVINSGNGAVEDRKPSGLNGEASK_1xPhospho_[S16(100)] | CD44 antigen | 1.31 |
| O95297 | SESVVYADIR_1xPhospho_[Y6(100)] | Myelin protein zero-like protein 1 | 1.16 |
| P51610 | ASAVSPANLPAVLLQPR_1xPhospho_[S5(100)] | Host cell factor 1 | Not found |
| Q5VUB5 | DQSTSMSHINLLFSR_1xPhospho_[T/S] | Protein FAM171A1 | Not found |
| Q14789 | KFSDAIQSKEEEIR_1xPhospho_[S3(100)] | Golgin subfamily B member 1 | 1.00 |
| P13746 | KGGSYTQAASSDSAQGSDVSLTACKV_1xPhospho_[S20(99.3)] | HLA class I histocompatibility antigen, A-11 alpha chain | 0.94 |
| Q9C0C9 | KKSIPLSIK_1xPhospho_[S3(100)] | E2 ubiquitin-conjugating enzyme | Not found |
| P49792 | KQSLPATSIPTPASFK_1xPhospho_[S3(100)] | E3 SUMO-protein ligase RanBP2 | 0.90 |
| Q9P2M7 | KVSLVLEK_1xPhospho_[S3(100)] | Cingulin | 1.23 |
| P04920 | NISAGSLGSLLGHHHGQGAESDPHVTEPLMGGVPETR_1xPhospho_[S3(100)] | Anion exchange protein 2 | 1.00 |
| Q9Y2J2 | RASALIDRPAPYFER_1xPhospho_[S3(100)] | Band 4.1-like protein 3 | 0.76 |
| O95613 | RESEVLDLKEQLEK_1xPhospho_[S3(100)] | Pericentrin | 1.17 |
| Q96II8 | RISHEGSPVKPVAIR_1xPhospho_[S3(100)] | Leucine-rich repeat and calponin homology domain-containing protein 3 | 0.81 |
| P27708 | RLSSFVTK_1xPhospho_[S3(100)] | CAD protein | 1.14 |
| Q86W92 | RRPSDENTIAPSEVQK_1xPhospho_[S4(100)] | Liprin-beta-1 | Not found |
| P42345 | TRTDSYSAGQSVEILDGVELGEPAHKK_1xPhospho_[S5(98.4)] | Serine/threonine-protein kinase mTOR | 0.97 |

**Table 5.6: Highly downregulated phosphopeptides detected in the lysosomal membrane fraction upon elevation of the intracellular cAMP level.**
List of phosphopeptides found to be highly downregulated in the lysosomal membrane faction after FSK/db-cAMP treatment (found in at least two out of three DMSO replicates but not in any FSK/db-cAMP sample). For each phosphopeptide, protein abundance ratios determined in the non-phospho-enriched samples are listed.

| Uniprot accession | Modified sequence | Protein name | Protein ratio (FSK/db-cAMP vs. DMSO) |
|---|---|---|---|
| Q9BY89 | AKLDPEPEKAAESPSPR_1xPhospho_[S15(99.5)] | Uncharacterized protein KIAA1671 | Not found |
| P19634 | IPSAVSTVSMQNIHPK_1xPhospho_[S9(100)] | Sodium/hydrogen exchanger 1 | Not found |
| Q9H2J7 | QSGSPTLDTAPNGR_1xPhospho_[S4(100)] | Sodium-dependent neutral amino acid transporter B(0)AT2 | 0.93 |
| O15439 | SGIDFGSLLKKDNEESEQPPVPGTPTLR_1xPhospho_[T24(100)] | Multidrug resistance-associated protein 4 | 0.54 |
| P52594 | SLLGDSAPTLHLNKGTPSQSPVVGR_2xPhospho_[T16(100);_S20(100)] | Arf-GAP domain and FG repeat-containing protein 1 | Not found |
| P52594 | SLLGDSAPTLHLNKGTPSQSPVVGR_2xPhospho_[T/S] | Arf-GAP domain and FG repeat-containing protein 1 | Not found |
| Q09666 | TVIRLPSGSGAASPTGSAVDIR_1xPhospho_[S13(100)] | Neuroblast differentiation-associated protein AHNAK | 1.04 |
| Q12933 | AAASVTPPGSLELLQPGFSK_1xPhospho_[S4(99.2)] | TNF receptor-associated factor 2 | 0.90 |
| O75427 | AAAVAAPLAAGGEEAAATTSVPGSPGLPGRR_1xPhospho_[T/S] | Leucine-rich repeat and calponin homology domain-containing protein 4 | Not found |
| P20042 | SGDEMIFDPTMSKK_1xPhospho_[S1(100)] | Eukaryotic translation initiation factor 2 subunit 2 | Not found |
| Q5T1M5 | DSGSDGHSVSSRDSAAPSPIPGADNLSADPVVSPPTSIPFK_2xPhospho_[S18(100);_S/T] | FK506-binding protein 15 | 0.87 |
| Q9BXB5 | HLSVGAPGVVTITHHKSPAAAR_1xPhospho_[S17(100)] | Oxysterol-binding protein-related protein 10 | Not found |
| Q9H1B7 | KASPEPPDSAEGALK_1xPhospho_[S3(100)] | Probable E3 ubiquitin-protein ligase IRF2BPL | Not found |
| Q92622 | KHESPLLVTK_1xPhospho_[S4(100)] | Run domain Beclin-1-interacting and cysteine-rich domain-containing protein | Not found |
| Q2NKX8 | RFPEAEALSPEQAAHYLR_1xPhospho_[S9(100)] | DNA excision repair protein ERCC-6-like | 0.71 |
| Q4KMP7 | RHGAPAAPSPPPR_1xPhospho_[S9(100)] | TBC1 domain family member 10B | 1.13 |
| Q13427 | RSETPPHWR_1xPhospho_[T4(99.6)] | Peptidyl-prolyl cis-trans isomerase G | Not found |
| Q9BXB4 | SFSLASSSNSPISQR_1xPhospho_[S10(99.6)] | Oxysterol-binding protein-related protein 11 | 0.92 |

The current literature suggests important role of SNAPIN in the proper lysosome functionality (see section 2.5). Therefore, the present study aimed at further elucidating the importance of SNAPIN and the identified downregulated phospho-site at S133 in different processes such as the internalization and secretion of acidic hydrolases as well as lysosome positioning.

### 5.1.3. Analyzing the influence of elevated intracellular cAMP concentrations on SNAPIN protein level, lysosomal association and phosphorylation status

There are at least three explanations for the lower amounts of the SNAPIN S133 containing phosphopeptide detected in the lysosomal membrane fraction upon elevation of the intracellular cAMP level compared to the control. First, FSK/db-cAMP treatment could be associated with the activation of phosphatases which leads to the dephosphorylation of SNAPIN at S133. Second, cAMP-induced alterations in the PTM pattern of SNAPIN or an interacting protein could lead to a dissociation of SNAPIN from the lysosome. In this case, SNAPIN would not be co-purified during lysosome enrichment after FSK/db-cAMP treatment. Therefore, less SNAPIN peptides would be identified in the lysosomal fraction during MS analysis even though the phosphorylation status at S133 might be unaltered. Third, FSK/db-cAMP treatment could lead to a downregulation of SNAPIN expression or induce its degradation. Comparable to the second possibility, this would be associated with a reduced number of detectable total SNAPIN peptides in the lysosomal fractions and would not necessarily involve a cAMP-mediated dephosphorylation at S133.

#### 5.1.3.1. Investigating the influence of FSK/db-cAMP treatment on SNAPIN protein level

The influence of FSK/db-cAMP treatment on whole cell SNAPIN protein level was investigated by Western Blot and immune detection. The experiment was performed in three biological replicates. Prior to protein detection, the nitrocellulose membrane was cut horizontally. The upper part of the membrane was incubated with an antibody directed against α-Tubulin whereas the lower half was used for immune detection of SNAPIN. For signal quantification, SNAPIN intensities were normalized to the α-Tubulin signals.

After incubating the nitrocellulose membrane with an antibody directed against SNAPIN, signals at 15 kDa were observed (Figure 5.4A). Considering its expected mass, these signals can be assigned to the SNAPIN protein. Based on this specificity, signals obtained by using this antibody will be considered as a successful SNAPIN detection in the further course of this thesis. α-Tubulin was detected at 55 kDa on the upper part of the membrane. Similar SNAPIN and α-Tubulin signal intensities were observed for the FSK/db-cAMP treated samples and the controls (Figure 5.4A).

This was consistent among all replicates. Figure 5.4B shows the quantitative analysis of the Western Blot signals. For each replicate and condition, the SNAPIN intensity was normalized on the α-Tubulin signal. Afterwards, the means of the relative SNAPIN intensities were calculated and plotted as a bar chart for both conditions. The variability among the replicates is shown by the standard deviation. Additionally, the relative SNAPIN intensities of the single replicates are indicated as dots. By comparing the FSK/db-cAMP treated sample with the control, no difference in the mean relative SNAPIN intensity was observed. A two sample t-test revealed no significant differences in the relative SNAPIN intensities obtained for the PKA-stimulated and the non-stimulated group (homoscedastic, p-value 0.7898, significance threshold 0.05). Therefore, the results indicate that the SNAPIN protein level was not affected by the treatment.

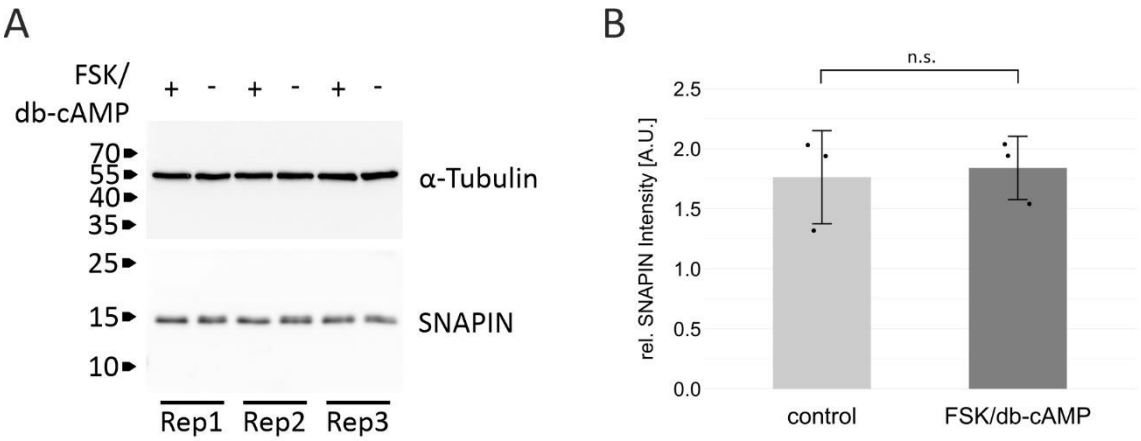


**Figure 5.4: Investigating the influence of FSK/db-cAMP treatment on SNAPIN protein level.**
Cells were either incubated for 30 min with FSK/db-cAMP or DMSO (control). The experiment was performed in triplicates (n=3). Whole cell proteins were separated by SDS-PAGE and transferred onto a nitrocellulose membrane. SNAPIN detection was performed by using an anti-SNAPIN antibody (10 s exposure) (A). α-Tubulin signals were used as a loading control (1 s exposure) (A). For each condition and replicate, SNAPIN intensities were normalized on the corresponding α-Tubulin signals. The relative SNAPIN intensities of the FSK/db-cAMP treated sample group and the control are depicted as bar charts (B). The variability among the replicates is shown by the standard deviation (B). Additionally, the relative SNAPIN intensities of the single replicates are indicated as dots (B). Statistical analysis was performed by a t-test (p-value 0.7898). (A.U.: arbitrary units; n.s.: not significant (p-value > 0.05))

### 5.1.3.2. Investigating SNAPIN's association to the lysosomes upon FSK/db-cAMP treatment

In phosphoproteomic studies, protein levels within the starting material are usually quantified by investigating the non-phospho-enriched fraction of the sample. Especially after organelle enrichment, stimulation dependent changes in the subcellular protein localization might be misinterpreted as phospho-site regulation although the phosphorylation status of the whole protein population remains unaltered. Within the present study, SNAPIN was not detected in the non-phospho enriched proteomic data set of the membrane lysosomal fractions (see table 5.4). In order to investigate cAMP-mediated changes in lysosome association of SNAPIN,

HEK 293 cells were either treated with FSK/db-cAMP or DMSO. Afterwards, the lysosomes were enriched before proteins present in the lysosomal fraction were separated via SDS-PAGE and subsequently transferred onto a nitrocellulose membrane. The experiment was performed in three biological replicates. SNAPIN levels were investigated by immune detection. The signals obtained after incubating the membrane with an antibody directed against the lysosomal protease Cathepsin D (CTSD) were used for normalizing the SNAPIN level to the amounts of lysosomes present within the different samples after the enrichment procedure. For the heavy chain of mature CTSD, a mass of approx. 31-35 kDa was expected (Huang et al. 1979; Hasilik and Neufeld 1980).

SNAPIN was detected at 15 kDa in all samples (Figure 5.5A). After incubating the upper part of the membrane with the anti-CTSD antibody, signals at approx. 35 kDa were observed. These signals were attributed to the heavy chain of CTSD. Figure 5.5B depicts the results of the signal quantification. For each replicate, SNAPIN intensities were normalized to the CTSD signal (indicated as dots). The average SNAPIN intensities identified for the two sample groups are shown as bar charts (+/- standard deviation). By comparing the FSK/db-cAMP treated sample group with the control, the SNAPIN level tends to be reduced in the lysosomal fraction upon elevation of the intracellular cAMP level. However, when applying statistical analysis (two sample t-test), the difference is not significant (homoscedastic, p-value 0.1095, significance threshold 0.05). It is reasonable to assume that the insignificance is predominantly caused by the relative SNAPIN intensity observed in the first replicated of the non-stimulated group (1.1). Compared to the other two replicates of the control, the relative SNAPIN intensity detected in this sample is strongly reduced, thus lowering the mean value and increasing the standard deviation in the non-stimulated group.

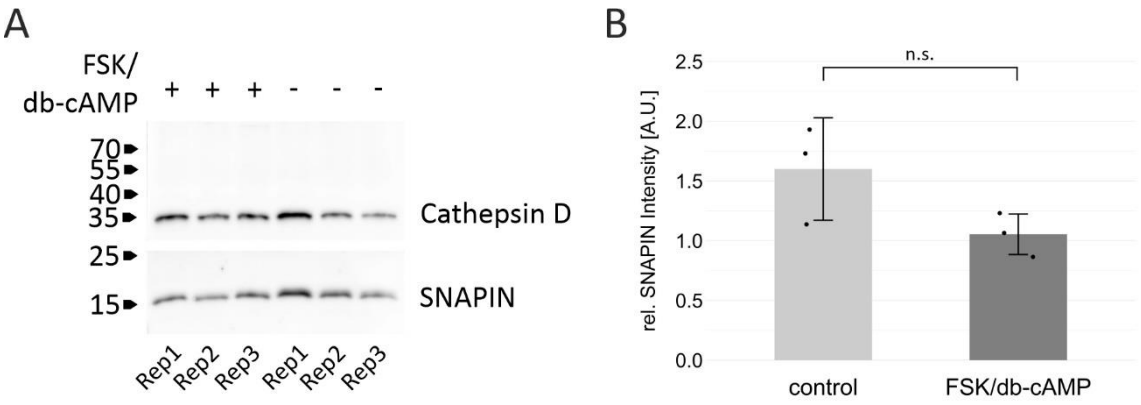


**Figure 5.5: Investigating the influence of elevated intracellular cAMP levels on the lysosome-association of SNAPIN.**
Lysosomes were enriched from HEK 293 cells, treated with FSK/db-cAMP or DMSO (control). Proteins present within the lysosomal fractions were separated by SDS-PAGE and blotted onto a nitrocellulose membrane. Afterwards, SNAPIN (15 s exposure time) and CTSD signals (2 s exposure time) were visualized by immune detection (A). For signal quantification, SNAPIN intensities of each replicate were normalized to the corresponding CTSD signals (B; indicated as dots). The average relative SNAPIN intensity for the stimulated and non-stimulated sample group are depicted as bar charts (B). Statistical analysis was performed by a t-test (p-value 0.1095). (A.U.: arbitrary units; n.s.: not significant (p-value > 0.05))

#### 5.1.3.3. Investigating cAMP-mediated SNAPIN dephosphorylation with 2D-gel electrophoresis

cAMP-mediated changes in the SNAPIN phosphorylation status were investigated by 2D-gel electrophoresis. In the first dimension, proteins were separated according to their isoelectric point (PI). As protein phosphorylation lowers the PI, these proteoforms migrate further to the anode (acidic pH) during IEF compared to their less-phosphorylated counterpart. After IEF, proteins were further separated via SDS-PAGE and subsequently transferred onto a nitrocellulose membrane. A SNAPIN specific antibody was used for the detection of the different proteoforms. In addition to the FSK/db-cAMP treated sample and the DMSO control, a non-stimulated protein lysate was incubated with calf intestine alkaline phosphatase in order to visualize the migration behavior of dephosphorylated SNAPIN isoforms during 2D-gel electrophoresis. The experiment was performed in two biological replicates.

Figure 5.6A depicts the SNAPIN isoforms detected at 15 kDa after incubating the samples of the first replicate with the SNAPIN antibody. The signals corresponding to the highest phosphorylated proteoforms are indicated by the open arrowheads. Five distinct SNAPIN isoforms were observed after FSK/db-cAMP treatment. Compared to that, six proteoforms were detected in the DMSO control. Changes in the relative signal intensities were observed for the first (open arrowheads) and the third (arrow) isoform. In case of the FSK/db-cAMP treated sample, the intensity of the third proteoform is higher compared to the first one. By comparing these two isoforms in the DMSO control, a slightly stronger signal intensity of the first

proteoform was detected. Additionally, the signal pattern of the isoform with the highest PI is less distinct in the DMSO control compared to the FSK/db-cAMP sample. The proteoform pattern observed in the phosphatase treated sample was similar to that obtained upon elevation of the intracellular cAMP levels.

The signals obtained in the second replicate are shown in figure 5.6B. Compared to the first replicate, the background signal is higher thus making the precise detection of the different SNAPIN isoforms more difficult. However, when comparing the first and the third SNAPIN proteoforms in both conditions, the isoform with the highest phosphorylation status seemed to be more abundant in the DMSO control. In case of the phosphatase treated sample, the third isoform was not detected in the second replicate.

The different relative signal intensities of the first and the third SNAPIN proteoform identified in both samples and replicates indicate that SNAPIN is dephosphorylated after FSK/db-cAMP treatment. This finding is further supported by the pattern observed in the phosphatase treated sample of the first replicate in which the third isoform is also highly abundant. Nevertheless, the absence of the third isoform in the phosphatase treated sample of the second replicate indicates that the dephosphorylation in the first replicate was not complete. The detection of at least two proteoforms after phosphatase treatment indicates the existence of two non-phosphorylated SNAPIN isoforms (expected unmodified SNAPIN PI = 9.35; phosphosite.org, retrieved 09.05.2019). In addition to these findings, SNAPIN also seems to be phosphorylated upon FSK/db-cAMP treatment as the signal pattern of the proteoforms with the highest PI appears to be less blurry compared the DMSO control.

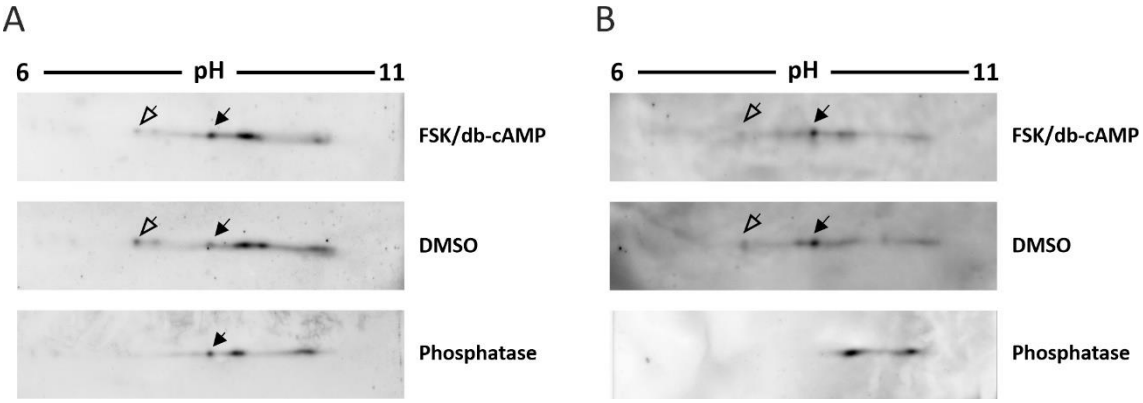


**Figure 5.6: Investigating changes in the abundance of different SNAPIN proteoforms after FSK/db-cAMP treatment by 2D-gel electrophoresis.**

Cells were either incubated in medium containing FSK/db-cAMP or DMSO. Cell lysate treated with calf intestine alkaline phosphatase was used in order to identify the migration behavior of dephosphorylated isoforms. Proteins were first separated according to their PI and subsequently based on their molecular mass. Afterwards, proteins were transferred onto a nitrocellulose membrane followed by immune detection of SNAPIN. The signals shown in this figure were obtained at different exposure times (biological replicate 1 (A): FSK/db-cAMP 3 min; DMSO 5min(for the same exposure time of the FSK/db-cAMP and DMSO sample of the first replicate see Appendix; Phosphatase 1 min) (biological replicate 2 (B): FSK/db-cAMP 3 min; DMSO 3min; Phosphatase 3 min). Furthermore, the contrast (black/white value) between background and signal was adjusted for the signals of the second replicate.

### 5.1.4. SNAPIN gene knock out with the CRISPR-Cas9 method

In order to investigate the cellular function of SNAPIN, HEK 293 and HeLa knock-out cell lines were generated via the CRISPR-Cas9 method. For this purpose, cells were co-transfected with the SNAPIN crRNA, a tracrRNA and a plasmid containing the gene encoding for the Cas9 endonuclease and a puromycin resistance cassette. Cells carrying the Cas9 plasmid were selected by adding puromycin to the medium. Afterwards, monoclonal cell populations were prepared and the SNAPIN gene knock out was validated by next generation sequencing (NGS). The sequencing data were analyzed by the "outknocker" web tool (Schmid-Burgk et al. 2014).

Figure 5.7A shows the output after analyzing the NGS data with "outknocker". Each pie chart represents one monoclonal colony and is labeled according to the well position of the 96-well plate in which the cells were grown. The pie chart size corresponds to the number of sequencing reads whereas the different colors indicate the results of the alignment of the sequenced DNA strand compared to the reference sequence. Here, the shades of red represent different types of detected out of frame insertions or deletions (indels). As the frame shift leads to non-sense mutations or to a premature stop of translation, pie charts completely colored in red might indicate monoclones featuring a functional gene knock out. Detailed information about the alignment can be obtained by clicking on the single pie charts in the web interface (see Appendix Figure 7.8 and figure 7.9).

In case of all HEK 293 monoclones investigated by NGS, some sequencing reads could not be aligned to the uploaded reference sequence (white parts of pie chart). The highest proportion of out-of-frame indels was observed for the HEK 293 clones A2, A3, A4, A7, A12, B1, B2, B10 and B11. Nevertheless, small blue parts, indicating the detection of some in-frame indel mutations, can also be detected in the pie charts of these nine clones. Such a mutation would not be associated with a frame shift and a functional gene knock out. However, as these reads are not displayed in the alignment list, the in-frame mutations were detected in less than 2 % of the reads, thus being considered as false positive identifications (below the 2% indel threshold). Therefore, the NGS data indicate a functional SNAPIN KO for the HEK 293 clones A2, A3, A4, A7, A12, B1, B2, B10 and B11. Except for clone B5, in-frame-mutations above the 2 % indel threshold were not observed in the HeLa NGS data set. Here, five potential HeLa SNAPIN KO clones (A9, A12, B1, B3, B4) have been identified.

In order to verify the functional gene knock-out identified in the NGS data set, the potential HEK 293 and HeLa SNAPIN KO clones were investigated by Western Blot and immune detection of SNAPIN. Wildtype (wt) HEK 293 and HeLa cells served as controls. Detection of α-Tubulin was used to control the amount of protein loaded onto the gel.

SNAPIN was detected at 15 kDa in the HEK 293 and HeLa wt samples when incubating the nitrocellulose membranes with the SNAPIN antibody (Figure 5.7B). At the same height, weak signals were observed in the lanes of the different HEK 293 SNAPIN KO samples. However, as the same signal pattern was detected in the secondary antibody control (sec. AB ctrl), the signals might rather be derived from unspecific binding of the secondary antibody to HEK proteins than from SNAPIN detection in the KO samples. Compared to that, no signals were observed in the lanes containing the HeLa SNAPIN KO samples after incubation with the SNAPIN antibody. The uniformity of the α-Tubulin signals indicates that similar protein amounts were loaded onto the gels. Therefore, the missing SNAPIN signal in the HEK 239 and HeLa KO samples indicates an impaired SNAPIN protein production within these clones, thus supporting the observations made in the NGS data set.

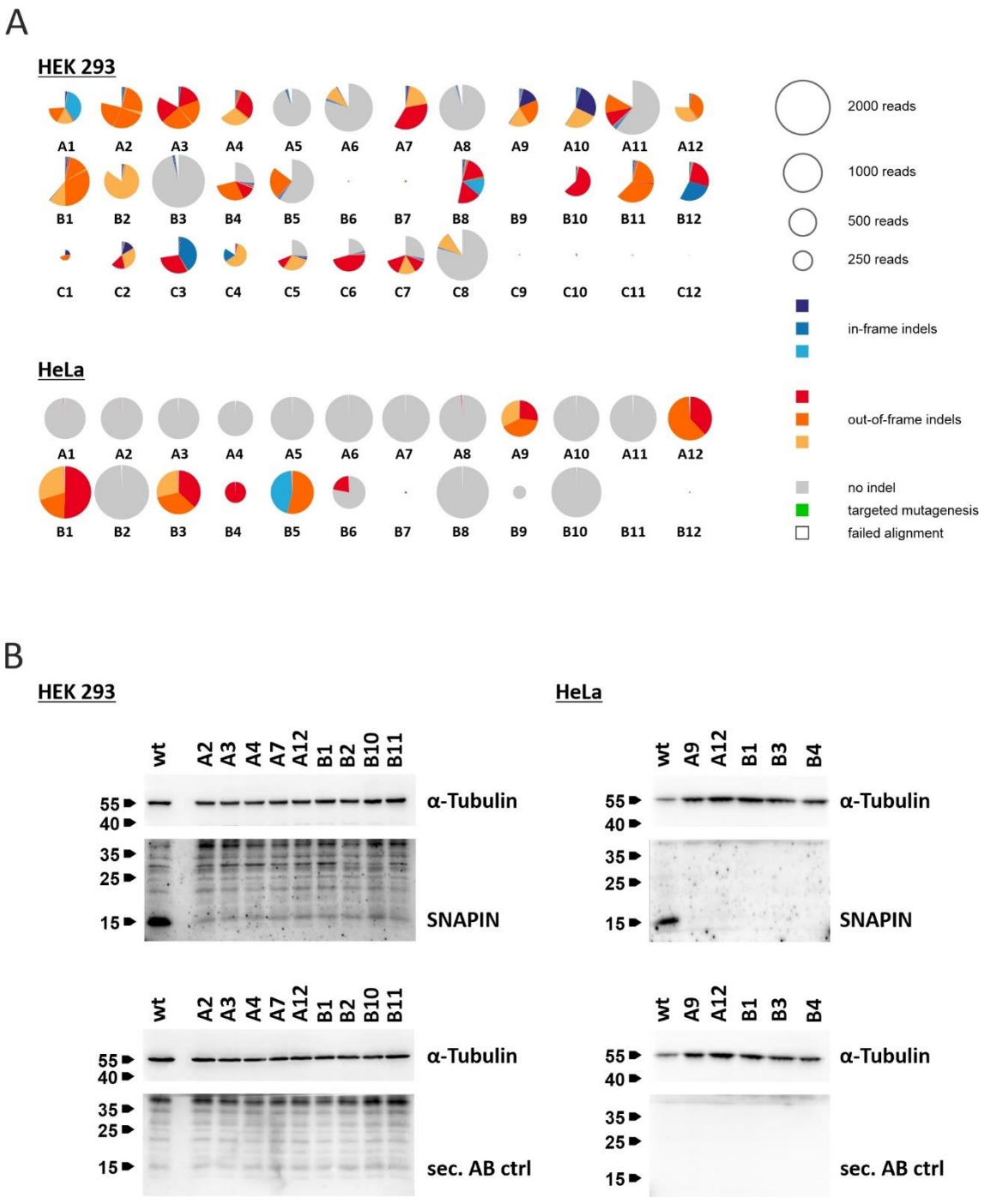


**Figure 5.7: Validation of SNAPIN KO generated with the CRISPR-Cas9 method in HEK 293 and HeLa cells.**
Genetic modifications in the SNAPIN gene of monoclonal cell populations after CRISPR-Cas9 was investigated by NGS. Data analysis was performed by the "outknocker" web tool (Schmid-Burgk et al. 2014). Sequencing results for the different monoclones are depicted as pie charts (A). Nine potential HEK 293 and five HeLa SNAPIN KO monoclonal cell populations were identified. The functional gene knockout was further validated by Western Blot and immune detection of SNAPIN (B) (HEK α-Tubulin: 1 s exposure; HEK SNAPIN + sec. AB ctrl.: 3 min exposure; HeLa α-Tubulin: 3 s exposure; HeLa SNAPIN + sec. AB ctrl.: 4 min exposure).

### 5.1.5. Proteomic comparison of HEK 293 wt and HEK 293 SNAPIN KO cells

SNAPIN KO mediated changes in the proteome were investigated by bottom up mass spectrometry. For this purpose, whole cell lysates of isotopically labeled HEK 293 wt and HEK

293 SNAPIN KO cells were mixed. The third SILAC channel comprised HEK 293 wt cells starved for 50 min but these samples are not further discussed in this thesis. After SDS-PAGE, proteins were digested by in-gel digestion. Tryptic peptides were analyzed by LC-MS2 using a Dionex LC-system coupled to an LTQ Orbitrap Velos mass spectrometer. Data analysis was performed with the Proteome Discoverer software. Based on the protein abundances in the SNAPIN KO and wt group, the protein ratios were calculated. For statistical analysis, the analysis of variance (ANOVA) (individual proteins) setting was used.

The data of the HEK 293 SNAPIN KO and HEK 293 wt proteome comparison are visualized in a volcano plot (Figure 5.8). Here, the $\log_2$ fold change and the p-values of the individual proteins are shown. Proteins with a $\log_2$ fold change higher than 0.75 or lower than -0.75 are depicted as blue points. Out of these, proteins with a p-value smaller than 0.05 ($-\log_{10}$ p-value >1.3) are labeled with their UniProt accession. The protein names corresponding to these accessions are listed in table 5.7. After adjusting the p-value for multiple testing, no significantly regulated protein was detected. The serine/threonine-protein kinase TAO1 (UniProt accession Q7L7X3) was found in two SNAPIN KO but not in any wt sample.

The lysosome annotated cation-independent mannose-6-phosphate receptor (MPR300) was identified as being slightly downregulated in HEK 293 SNAPIN KO cells. Although this downregulation was not ascribed as being significant after p-value correction for the whole data set, detailed analysis of the processing results highlighted the reliability of the MPR300 identification and the consistency of the MPR300 quantification values detected for the different samples among the replicates. In order to validate the MS results, MPR300 quantity in SNAPIN KO and wt cells was investigated by Western Blot and immune detection.

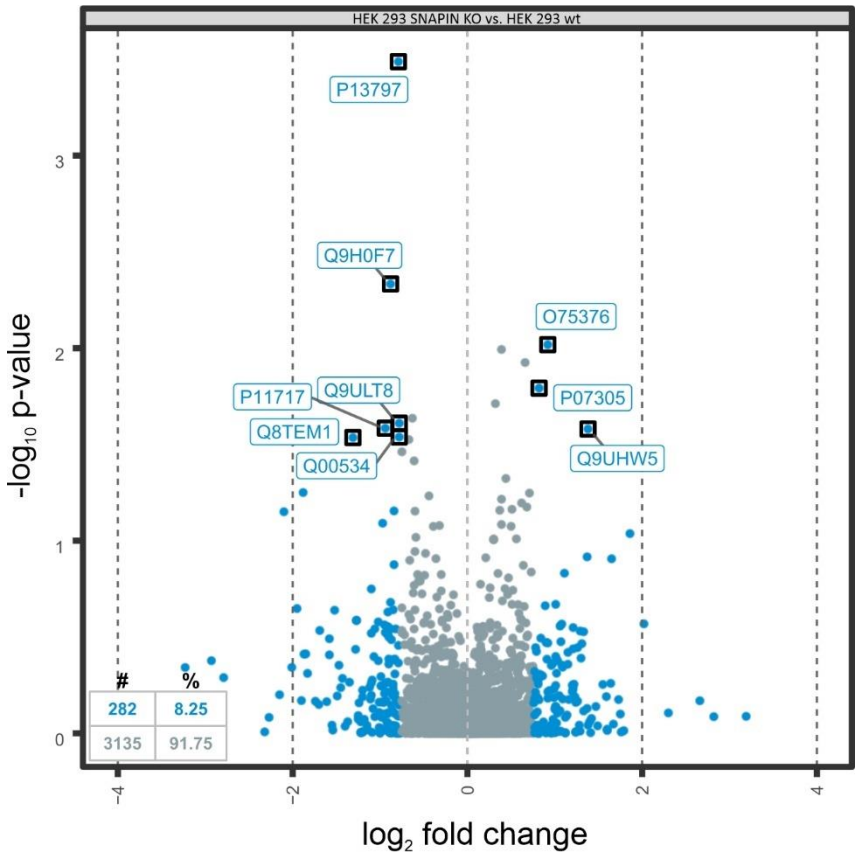


**Figure 5.8: Quantitative proteome comparison of HEK 293 SNAPIN KO and HEK 293 wt cells.**
Proteins of isotopically labeled HEK 293 SNAPIN KO and HEK 293 wt cells were mixed, separated via SDS-PAGE and digested by in-gel digestion. Tryptic peptides were analyzed by LC-MS2. The experiment was performed in three biological replicates. MS spectra were searched against a human reference database. Protein ratios were calculated based on their abundance in the different sample group. Statistical analysis was performed by an ANOVA test (individual proteins). Data are visualized in a volcano plot. Proteins with a $\log_2$ fold change higher than 0.75 or lower than -0.75 are shown as blue points. Among those, proteins with a p-value smaller than 0.05 are labeled with their UniProt accession.

**Table 5.7: Protein names corresponding to the UniProt accessions depicted in figure 5.8.**

| Uniprot accession | Protein name | $Log_2$ fold change | p-value |
|---|---|---|---|
| P13797 | Plastin-3 | -0.79 | 0.0003 |
| Q9H0F7 | ADP-ribosylation factor-like protein 6 | -0.88 | 0.0046 |
| Q9ULT8 | E3 ubiquitin-protein ligase HECTD1 | -0.78 | 0.0245 |
| P11717 | Cation-independent mannose-6-phosphate receptor | -0.94 | 0.0260 |
| Q8TEM1 | Nuclear pore membrane glycoprotein 210 | -1.31 | 0.0291 |
| Q00534 | Cyclin-dependent kinase 6 | -0.78 | 0.0289 |
| O75376 | Nuclear receptor corepressor 1 | 0.92 | 0.0096 |
| P07305 | Histone H1.0 | 0.82 | 0.0161 |
| Q9UHW5 | GPN-loop GTPase 3 | 1.38 | 0.0263 |

### 5.1.6. Investigating the MPR300 level in SNAPIN KO cells

Changes in the MPR300 level after SNAPIN KO were investigated in HeLa and HEK 293 cells by Western blotting and immune detection. MPR300 was detected by using an antiserum directed

against the third domain of the receptor previously made in the laboratory. α-Tubulin detection was used as a loading control. In order to verify the SNAPIN KO, the samples were also probed by the anti-SNAPIN antibody. The experiment was performed in two biological replicates. HEK 293 wt and SNAPIN KO cell lysates of the first replicate were derived from a stimulation experiment. Here, the wt and the KO cells were treated with DMSO for 30 min prior to cell lysis. However, as both samples of the first HEK 293 replicate were treated the same way, the MPR300 intensities obtained for these two lysates were assumed to be comparable. The other samples used in this experiment were not treated with DMSO before cell lysis.

The SNAPIN signals observed for the different cell lines and genotypes are shown in figure 5.9A (lower panel). Here, no SNAPIN signal was detected in any SNAPIN KO sample thus indicating a functional gene knock out in these cell lines. In case of the wt samples, SNAPIN was detected as a 15 kDa signal. Compared to the HeLa cells, stronger SNAPIN signals were observed in the HEK 293 samples. Similar α-Tubulin signal intensities were detected among the different cell lines and genotypes (Figure 5.9A, upper panel). Therefore, the stronger SNAPIN signal observed in the HEK 293 wt cells might be assignable to higher SNAPIN amounts present within this cell type.

Figure 5.9B (upper panel) depicts the signals obtained after incubating the membrane with the anti-MPR300 antiserum. Here, strong signals at approx. 300 kDa were detected. As these signals match to the expected mass of the MPR300, they were assigned to this receptor. Comparing both cell types, the MPR300 signals observed in the HEK samples were more focused. Especially in the HeLa SNAPIN KO cells, the MPR300 bands were less sharp. α-Tubulin was detected at approx. 50 kDa with similar intensities among all samples (Figure 5.9A, lower panel). Only for the HeLa SNAPIN KO sample of the first replicate and the HEK 293 SNAPIN KO samples of the second replicate, slightly stronger α-Tubulin signals were observed.

The relative MRP300 intensities calculated based on the signals obtained after immune detection are shown in figure 5.9C. Here, the MPR300 signal of each sample was normalized to the corresponding α-Tubulin intensity. In comparison to the wt samples, a lower relative MPR300 signal intensity was detected in the SNAPIN KO cells for both cell lines. This observation was consistent among all replicates. However, when comparing the abundances of the receptor within the wt and KO cells, a higher variability in the MPR300 levels was detected among the two replicates of the SNAPIN KO cell lysates. As a result of this, the MPR300 KO/wt-fold change varied between 0.44 and 0.63 in the HEK 293 samples and between 0.54 and 0.69 in the HeLa cell lysates. Nevertheless, the results described in this section support the previously detected downregulation of MPR300 in SNAPIN KO cells compared to their wt counterpart observed in the MS-based proteome comparison approach (Figure 5.8, table 5.7).

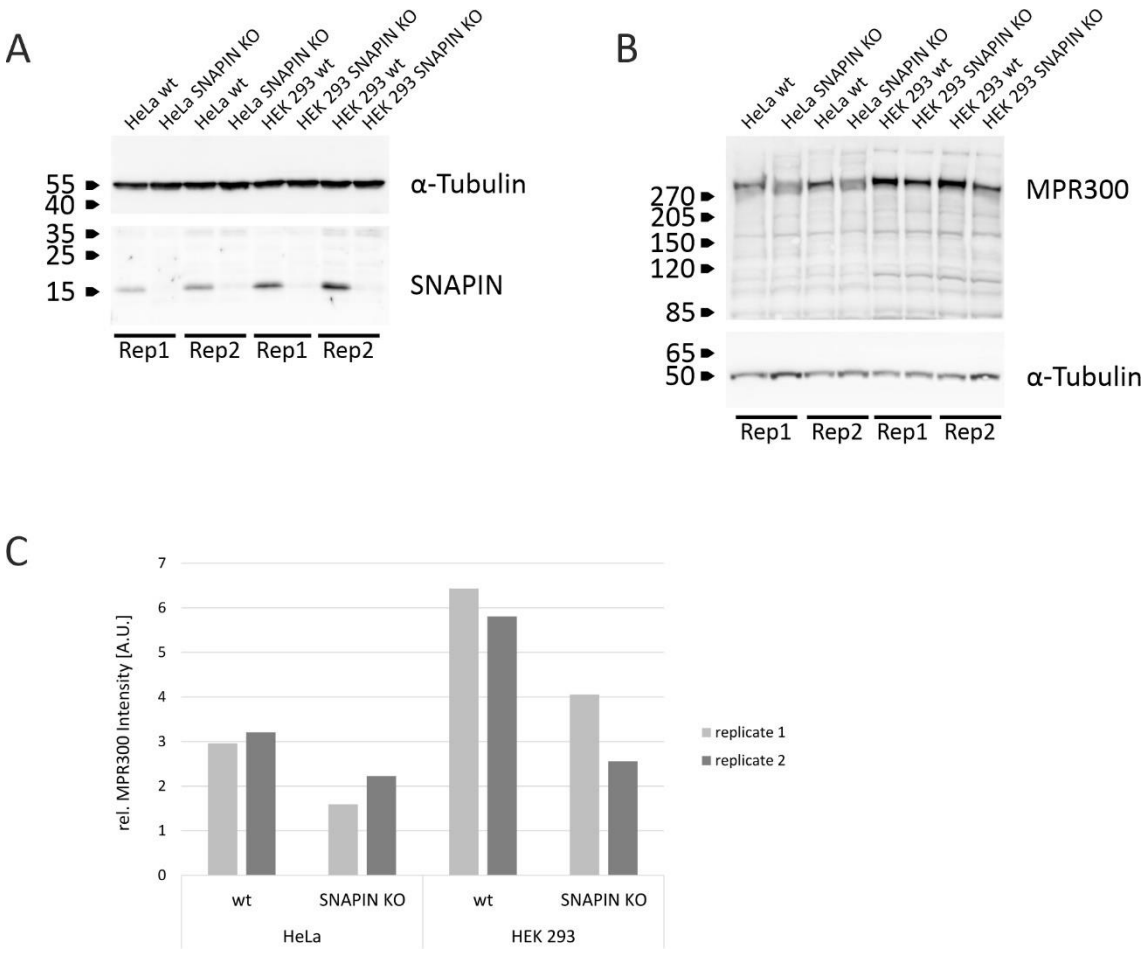


**Figure 5.9: Immune detection-based investigations of the MPR300 level in wt and SNAPIN KO cells.**
Proteins derived from HeLa and HEK 293 wt and SNAPIN KO cells were separated by SDS-PAGE and transferred onto a nitrocellulose membrane. SNAPIN levels of the different samples were investigated by immune detection using a protein specific antibody (A) (α-Tubulin: 1 s exposure; SNAPIN: 10 s exposure). MPR300 signals were visualized by using an antiserum directed against the third domain of this receptor (B) (α-Tubulin + MPR300: 1 s exposure). α-Tubulin detection was used as a loading control (A+B). The relative MPR300 intensities of the different samples were calculated by normalizing the MPR300 signal to the corresponding α-Tubulin intensity (C).

### 5.1.7. Investigating the effect of elevated intracellular cAMP levels on endocytosis in HEK 293 wt and SNAPIN KO cells

The MPR300 has been described as an important receptor for the transport of lysosomal enzymes from the trans-Golgi network (TGN) to endosomes as well as for the internalization of mannose-6-phosphate containing and non-glycosylated proteins from the extracellular space (reviewed by Braulke and Bonifacino 2009). In order to investigate whether the MPR300 downregulation detected in the SNAPIN KO cells influences endocytosis, an internalization experiment with the lysosomal enzyme ASA was performed. Additionally, the effect of elevated intracellular cAMP levels on ASA endocytosis was analyzed. For this purpose, HEK 293 wt and SNAPIN KO cells were incubated with biotinylated ASA in the presence or in the absence of

FSK/db-cAMP. Here, biotinylated ASA was used in order to be distinguishable from its endogenous counterpart. After cell lysis, the amount of internalized biotinylated ASA was quantified by an ELISA and normalized to the protein concentration of the corresponding lysate.

Figure 5.10 shows the relative amounts of internalized, biotinylated ASA (in ng/µg) identified within the single replicates of the different sample groups (indicated as dots). The corresponding mean values (+/- standard deviation) are depicted as bar charts.
For both cell types, no differences in the endocytosis of biotinylated ASA was detected when comparing the FSK/db-cAMP treated samples with the non-stimulated controls. Analysis of the cell lysates by Western Blotting and pCREB immune detection indicates a successful FSK/db-cAMP-dependent activation of PKA in the wt cells (data not shown). Compared to that, inconclusive results regarding the stimulation-induced activation of PKA were obtained for the SNAPIN KO cells (data not shown).
However, comparison of the HEK 293 wt and the SNAPIN KO cells indicate a treatment-independent reduction of ASA internalization in the KO samples. Statistical analysis was performed by using a one-way ANOVA (p-value 0.0055) followed by a Tukey honest significant difference (HSD) post hoc test (homoscedastic, homogeneity of variance was tested by a Brown-Forsythe test (p-value 0.5633)). By comparing the mean values of the non-stimulated HEK 293 wt and SNAPIN KO cells, a p-value of 0.014 was obtained. A similar p-value was calculated for the comparison of the means of the two cell types after FSK/db-cAMP-treatment (p-value 0.046).

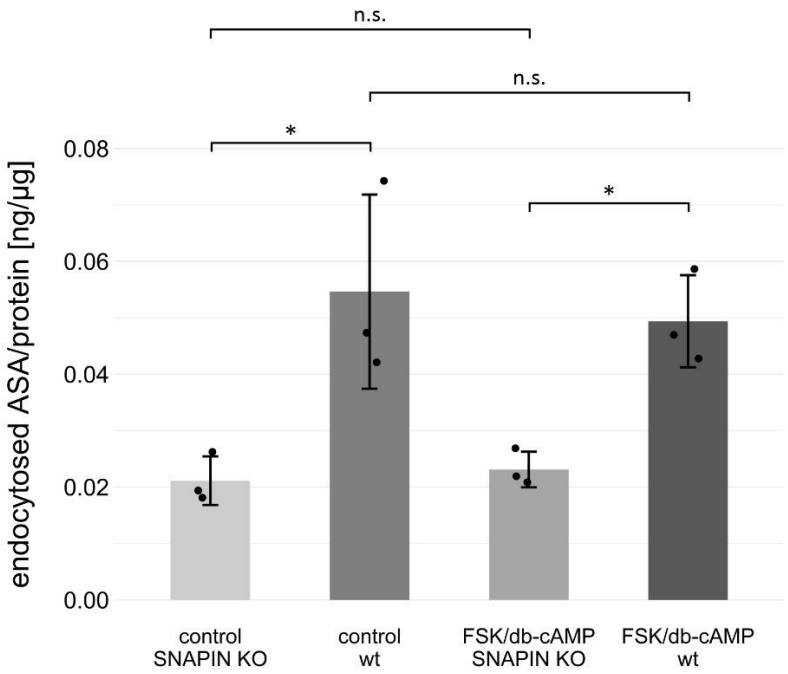


**Figure 5.10: Investigation of the internalization of biotinylated ASA in HEK 293 wt and SNAPIN KO cells upon elevated intracellular cAMP levels.**
Endocytosis of a lysosomal hydrolase was investigated by incubating HEK 293 wt and SNAPIN KO cells with biotinylated ASA and FSK/db-cAMP. DMSO treated cells served as a control. The amount of internalized, biotinylated ASA was analyzed by an ELISA and subsequently normalized to the protein concentration of the lysate. For each sample group, the relative biotinylated ASA amounts detected in the single replicates are indicated as dots. The corresponding mean values are depicted as bar charts (+/- standard deviation). Statistical analysis was performed by a one-way ANOVA (p-value 0.0055) followed by Tukey HSD post hoc test (p-value$_{\text{wt control-KO control}}$ 0.014; p- value$_{\text{wt FSK/db-cAMP-KO FSK/db-cAMP}}$ 0.046). (n.s.: not significant (p-value > 0.05), * p-value < 0.05).

### 5.1.8. Investigating the spatial distribution of LAMP-2 in HeLa wt and SNAPIN KO cells after FSK/db-cAMP treatment

SNAPIN is part of BORC, a complex known to be involved in lysosome positioning (Pu et al. 2015). In order to investigate changes in the subcellular distribution of lysosome/LE upon elevating the intracellular cAMP levels, the spatial distribution of lysosome-associated membrane glycoprotein 2 (LAMP-2) in HeLa wt and SNAPIN KO cells treated with FSK/db-cAMP or DMSO was analyzed. After stimulation, cells were fixed and stained with an antibody directed against LAMP-2. The DAPI containing ProLong™ Diamond was used for mounting the cover slips to the glass slides. Images were acquired as Z-stacks by using an LSM 980 confocal microscope equipped with an Airyscan 2 detector (Zeiss). In order to obtain comparable signal intensities among the different samples, the laser gain was kept constant during image acquisition. For each sample, the same adjustments of the black and white values were made in the histogram of the LAMP-2 channel in order to obtain an optimal contrast. Afterwards, the single images of one Z-stack were combined by a maximum intensity projection.

Figure 5.11 depicts the signals obtained by incubating the different samples with an anti-LAMP-2 antibody. Although LAMP-2 was detected within the whole cell, a slight accumulation of the signal in the perinuclear region was observed for the HEK wt cells. However, by comparing the FSK/db-cAMP-treated wt sample and the corresponding control, no difference in the signal distribution was identified. In DMSO treated HeLa SNAPIN KO cells, punctate LAMP-2 signals were distributed homogenously. Compared to that, a slight LAMP-2 accumulation adjacent to the nucleus was observed in case of the FSK/db-cAMP treated KO cells.

The strongest difference in the LAMP-2 signal pattern was identified between the two cell types. Whereas relatively large structures were detected by the LAMP-2 antibody in the HeLa wt cells, the signals observed in the SNAPIN KO samples were smaller and more dispersed across the cells. Reliable conclusions about differences in the summed LAMP-2 intensity between these two cell types cannot be drawn, as such an analysis requires a bigger sample size.

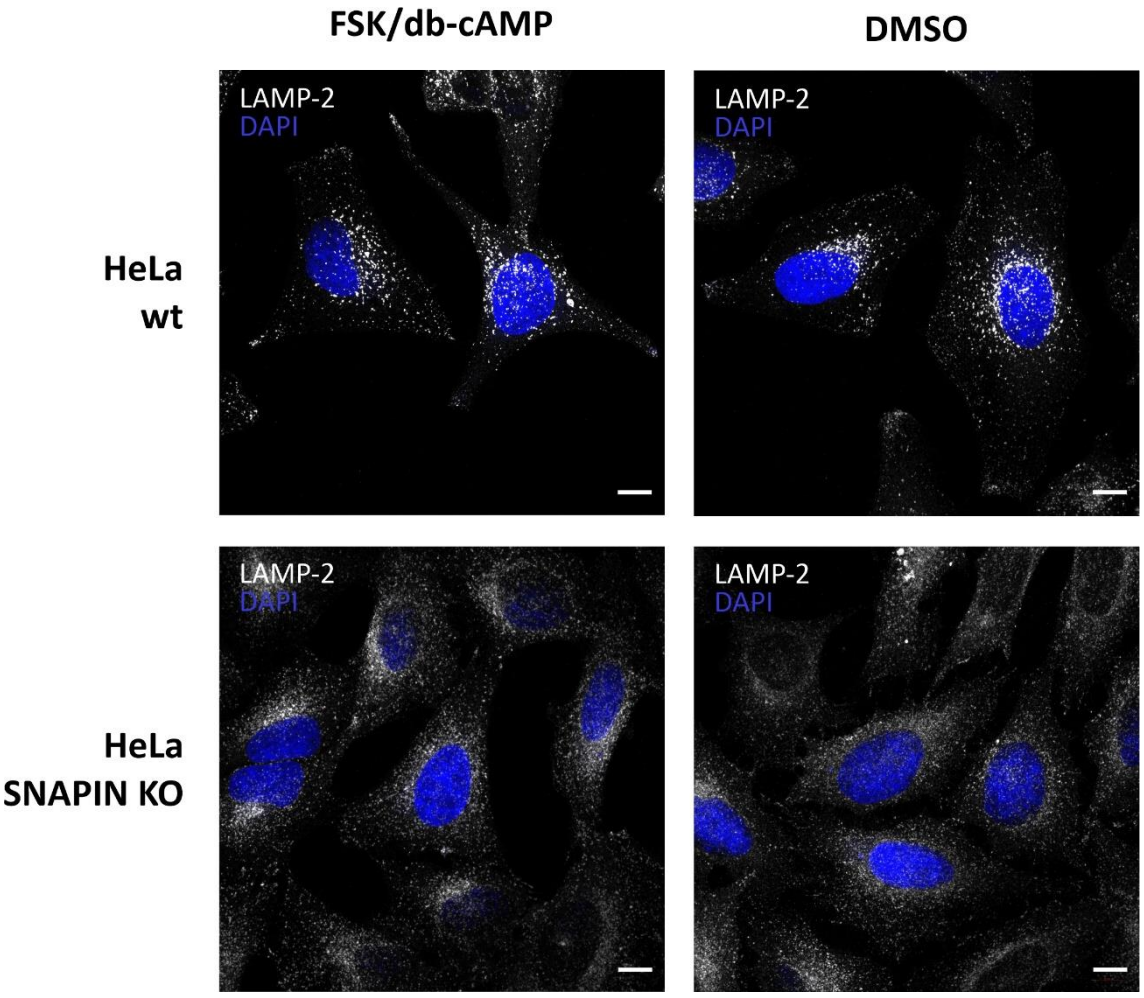


**Figure 5.11: Investigation of the LAMP-2 signal distribution in FSK/db-cAMP treated HEK 293 wt and SNAPIN KO cells as well as in the corresponding controls.**
HEK 293 wt and SNAPIN KO cells, either incubated with FSK/db-cAMP or DMSO, were stained with an antibody directed against LAMP-2. Images were acquired as Z-stacks by using the same laser gain for the different samples. After image acquisition, the single images of one Z-stack were combined by maximum intensity projection. Scale bar = 10 µm.

### 5.1.9. Investigation of cAMP-dependent changes in the exocytosis of lysosomal enzymes in HeLa wt and SNAPIN KO cells

SNAPIN has been demonstrated to be involved in tethering insulin granules to the plasma membrane in pancreatic beta cells (Somanath et al. 2016). HeLa wt and SNAPIN KO cells were used in order to investigate the impact of SNAPIN and elevated intracellular cAMP levels on the exocytosis of lysosomal enzymes (three biological replicates). For this purpose, the cells were treated with FSK/db-cAMP for 20 min. HeLa cells incubated with DMSO served as a control. Exocytosis was triggered by replacing the stimulating medium with an isosmotic buffer containing either FSK/db-cAMP or DMSO as well as $CaCl_2$ and ionomycin as an ionophore. Buffers without ionomycin, $CaCl_2$ or both supplements were used as controls in the exocytosis experiments. After 10 minutes of incubation, the release of lysosomal proteins was analyzed by measuring the activity of β-hexosaminidase (β-Hex) in the supernatant. In addition to that, the β-Hex activity assay was also performed for the different cell lysates. The total β-Hex activity of a sample was calculated as the sum of the activity determined in the lysates and the supernatant. For comparison of the different samples, the β-Hex activities were normalized to the protein amounts measured in the corresponding cell lysates.

The bar charts depicted in figure 5.12 show the mean β-Hex activities (+/- standard deviation) determined in the supernatants (A) and the total fractions (B). Additionally, the activities of the single replicates of each sample are indicated as dots. Single sample types were compared statistically by a t-test.

When evaluating the release of β-Hex in the different FSK/db-cAMP treated HeLa wt samples, the highest mean activity was measured after incubating the cells with ionomycin and $CaCl_2$ (Figure 5.12A). Nevertheless, as a high variability among the single replicates of the non-ionomycin and non-$CaCl_2$ containing sample was observed, reliable conclusions about the effect of these two supplements on β-Hex exocytosis cannot be drawn for this sample group. In case of the DMSO treated HeLa wt cells, similar average β-Hex activities were measured in the different media, thus indicating that exocytosis was not triggered by adding ionomycin and $CaCl_2$ to the cultivation medium. Compared to that, an ionomycin/$CaCl_2$-dependent increase in the release of β-Hex was observed for the HeLa SNAPIN KO cells. Here, no difference in the β-Hex activity was detected in the supernatant of the FSK/db-cAMP treated samples and the control. However, when comparing the β-Hex release of the two cell types, higher mean activities were detected in all sample groups of the HeLa SNAPIN KO cells. A significant difference was detected between the FSK/db-cAMP, ionomycin and $CaCl_2$ treated samples of these two cell types (homoscedastic, p-value 0.0047, significant threshold 0.05). Furthermore, comparison of the β-

Hex secretion between the wt and SNAPIN KO cells of the DMSO stimulation control without ionomycin and $CaCl_2$ treatment revealed a significant difference (homoscedastic, p-value 0.022, significant threshold 0.05). In addition to that, the difference in the β-Hex release observed by comparison of the DMSO treated HeLa wt and SNAPIN KO cells, incubated with ionomycin and $CaCl_2$, were also significant (homoscedastic, p-value 0.0113, significant threshold 0.05).

Figure 5.12B depicts the sum of the β-Hex activity detected in the supernatant and the lysate. Similar total β-Hex activities were observed for the different HeLa wt samples. In case of the KO cell line, a high variability in the β-Hex activity was detected between the single replicates of some conditions. Nevertheless, similar mean β-Hex activities were observed between the different samples of the HeLa SNAPIN KO cells. Comparison of the two cell lines indicates a lower total β-Hex activity within the HeLa wt cells. A significant difference (two sample t-test) was observed when comparing the β-Hex activities of the two cell lines detected for the FSK/db-cAMP, ionomycin and $CaCl_2$ treated samples (homoscedastic, p-value 0.0034, significance threshold 0.05). Similarly, the differences in the total β-Hex activities detected for the wt and SNAPIN KO cells in the DMSO (homoscedastic, p-value 0.0137, significance threshold 0.05) as well as in the FSK/db-cAMP (homoscedastic, p-value 0.0431, significance threshold 0.05) controls without ionomycin and $CaCl_2$ were statistically significant (two sample t-test).

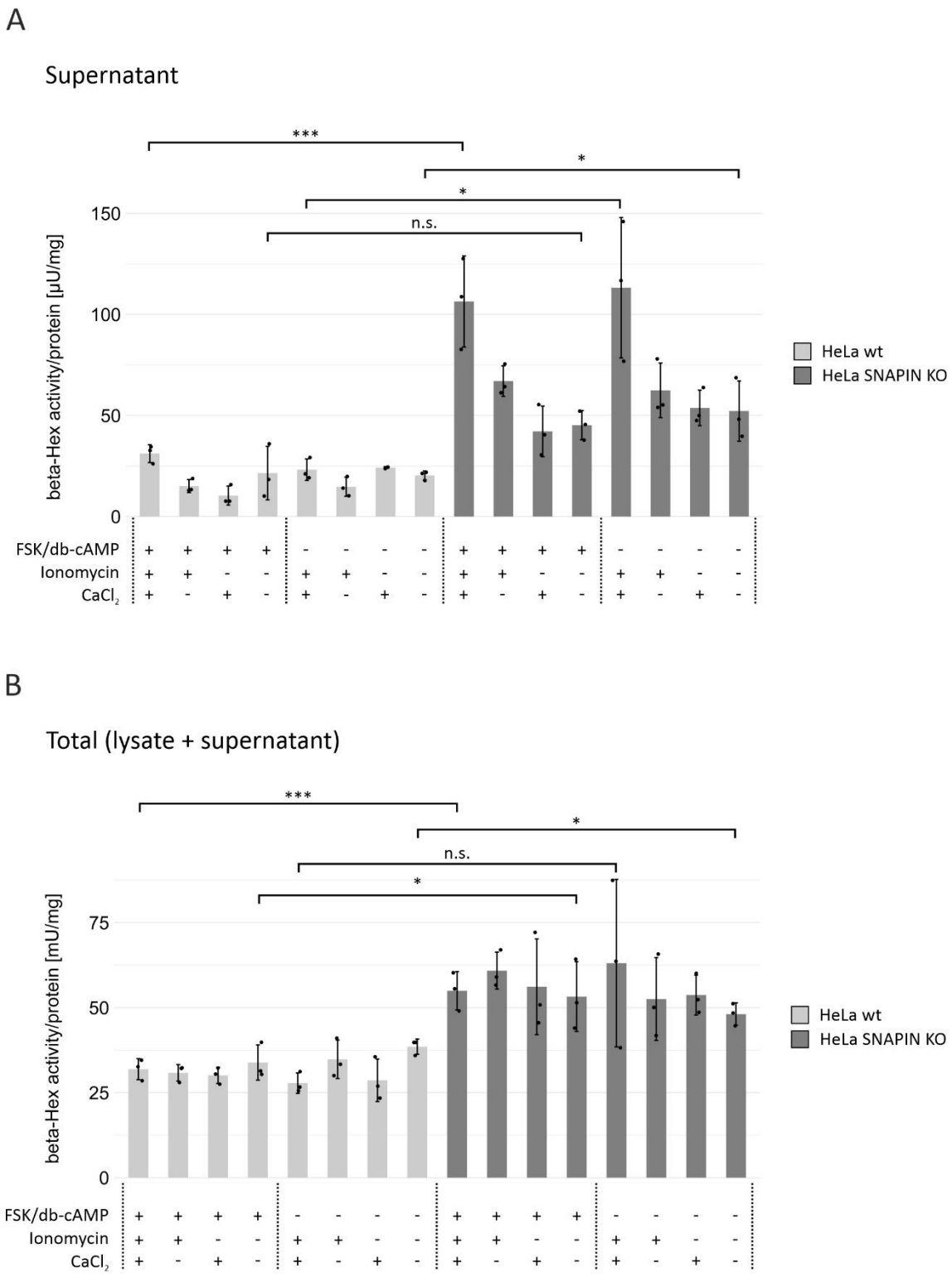


**Figure 5.12: Investigation of cAMP-mediated exocytosis of a lysosomal protein in HeLa wt and SNAPIN KO cells.** The experiment was performed in three biological replicates. cAMP levels were elevated by adding FSK/db-cAMP to the medium. Cells treated with DMSO served as a control. Exocytosis was triggered by replacing the medium with a buffer containing $CaCl_2$ and ionomycin. Buffers without $CaCl_2$, ionomycin or both supplements were used as controls of the exocytosis experiment. The release of lysosomal enzymes was investigated by measuring the β-Hex activity in the supernatant (A). The total β-Hex activities of the different samples were calculated as the sum of the activity determined in the supernatant and the cell lysate (B). For data comparison, β-Hex activities were normalized to the protein amount determined for the corresponding lysates (A+B). Mean normalized β-Hex activities are shown as bar charts (+/- standard deviation). The activities measured for the single replicates are indicated as dots. Statistical analysis was performed by a t-test. (* p-value < 0.05; *** p-value <0.005, n.s.: not significant)

### 5.1.10. Co-immunoprecipitation with phosphomimetic SNAPIN variants

The replacement of an amino acid residue at a potential phospho-site by an acidic amino acid such as glutamate is intended to mimic a permanent phosphorylation whereas its substitution by alanine imitates the non-phosphorylated isoform. These phosphomimetic substitutions are often used in order to investigate the biological function of a certain phosphorylation site.

Compared to the control, the SNAPIN peptide containing the S133 phospho-site has been identified to be less abundant in the lysosomal membrane fraction when treating the cells with FSK/db-cAMP (section 5.1.2.2). Potential interaction partners of the S133 phosphorylated and non-phosphorylated SNAPIN isoform were investigated by a phosphomimetic study. For this purpose, co-immunoprecipitation was performed with isotopically labeled HEK 293 SNAPIN KO cells stably transfected with a plasmid encoding for a Myc-tagged SNAPIN variant either containing a serine to alanine (S133A) or a serine to glutamate (S133E) substitution at position 133. Precipitation of the SNAPIN variants was achieved by using Myc-Trap-beads. Non-transfected HEK 293 SNAPIN KO cells served as a control for unspecific protein binding to the beads. The experiment was performed in three biological replicates.

The protein lysate (input) used for the IP as well as the supernatant after the pull-down assay were investigated by SDS-PAGE, Western Blotting and immune detection.
Figure 5.13 shows signals detected after incubating the nitrocellulose membrane with antibodies directed against SNAPIN and α-Tubulin. α-Tubulin was detected as a 55 kDa signal. Except for the SNAPIN S133A Rep1 and the SNAPIN S133E Rep2 samples, the α-Tubulin signal intensities were similar between the lysates (Input IP). Signals at approx. 20 kDa were detected in case of all SNAPIN S133A and S133E input samples when incubating the corresponding membrane with the anti-SNAPIN antibody. These signals match with the expected molecular mass of the Myc-tagged SNAPIN variants. A slightly higher signal intensity was detected for the SNAPIN S133E samples compared to SNAPIN S133A lysate. However, no signals were observed for the HEK 293 SNAPIN KO samples further substantiating the KO genotype of these cells.
Compared to the input, lower amounts of α-Tubulin were detected in the supernatant after IP which was a consequence of diluting the cell lysate prior to the pull-down assay. Additionally, varying α-Tubulin signals were observed in the supernatants with the lowest amount detected in the SNAPIN KO samples. This suggests an increased unspecific binding of this protein to the beads when the antigen is not present. However, SNAPIN was also detected in the supernatant after IP indicating an incomplete pull-down. Normalization of the SNAPIN signals was not possible as the α-Tubulin signals were inconsistent. In addition to the 20 kDa SNAPIN polypeptide, one or two signals with a smaller molecular mass were detected in the

supernatants by the anti SNAPIN antibody. These might correspond to SNAPIN versions expressed from a small proportion of plasmids containing the genetic information of a truncated SNAPIN proteoform. Some of these signals were also observed for higher exposure times of the membrane containing the input samples (data not shown).

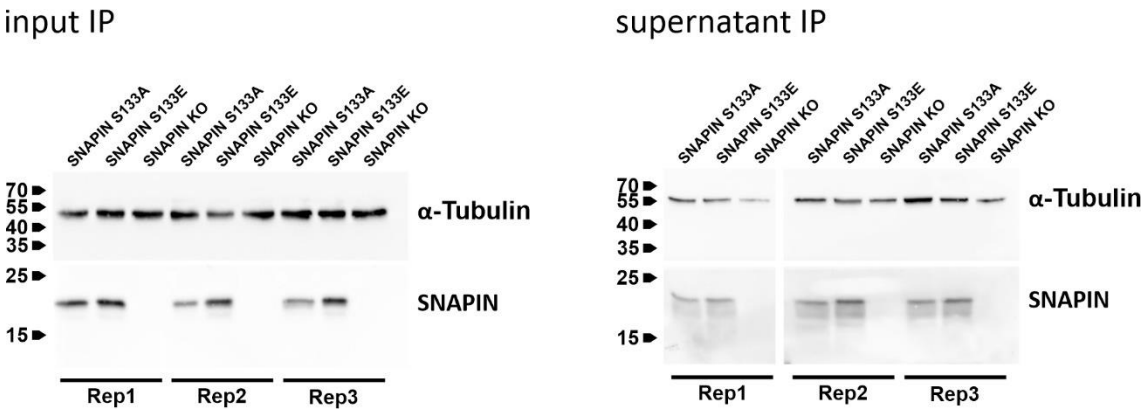


**Figure 5.13: Immune detection of SNAPIN and α-Tubulin in the IP input and the IP supernatant samples.**
HEK 293 SNAPIN KO cells were stably transfected with a plasmid carrying a gene either encoding for the phosphomimetic SNAPIN S133E or the non-phophorylatable SNAPIN S133A isoform. After isotopic labeling of the cells, immunoprecipitation was performed by using Myc-Trap beads directed against the Myc-tag of the SNAPIN proteoforms. Untransfected SNAPIN KO cells served as a control. The experiment was performed in triplicates. Proteins were separated according to their molecular mass by SDS-PAGE and subsequently transferred onto a nitrocellulose membrane. Immune detection of the SNAPIN variants and α-Tubulin was performed by using anti-SNAPIN and anti- α-Tubulin antibodies (α-Tubulin + SNAPIN input IP: 2 s exposure; α-Tubulin supernatant IP: 5 s exposure; SNAPIN supernatant IP: 20 s exposure).

After immunoprecipitation, eluted proteins from the SNAPIN S133A, S133E and KO samples belonging to the same replicate were mixed and loaded to an SDS gel. Proteins from gel slices were digested and analyzed by LC-MS2. MS raw data were searched against a database containing the SNAPIN sequences of the wt, S133A and S133E isoforms (without Myc-tag) as well as against a database comprising human reference protein sequences. This search was implemented in a Proteome Discoverer workflow.

Calculation of the SNAPIN S133A/KO and the SNAPIN S133E/KO ratio was performed with non-normalized protein abundances. First, the mean abundance of the three replicates for the SNAPIN KO, SNAPIN S133A and SNAPIN S133E sample group was calculated for each protein. Afterwards, these mean abundances were used for determining the SNAPIN S133A/KO and the SNAPIN S133E/KO ratio for the single proteins. In case the ratio could not be calculated because of a missing value in the KO sample group, a value of 200 was set. Furthermore, the coefficient of variation (CV) was calculated for the non-normalized abundances. For this purpose, the standard deviation of the abundances was divided by their mean values. This calculation was

performed for each protein and allowed a conclusion about the variance of the abundances among the replicates of one sample group. For both SNAPIN proteoforms (S133A and S133E), proteins found in at least two out of three replicates were used for data visualization.

Figure 5.14 shows the scatter plots generated for the SNAPIN S133A (A) and S133E (B) sample group. Here, the CV (in percent) of a single protein is plotted against its $log_2$ abundance ratio of the S133A or S133E sample group and the SNAPIN KO control ($log_2$ ratio (SNAPIN proteoform-KO)). For both SNAPIN proteoforms (S133A and S133E), most of the proteins had a higher mean abundance in the SNAPIN KO sample group thus representing unspecific pull-downs. However, proteins with a $log_2$ abundance ratio (S133A or S133E sample group – KO sample group) higher than 3.3 (10-fold enrichment in the specific IP sample) were assumed as potential interaction partners. Within the scatter plots, this threshold is indicated by the green, dashed line.
SNAPIN S133A was identified with a $log_2$ abundance ratio of 5.7 in the S133A sample group indicating its identification in the SNAPIN KO control (Figure 5.14, blue point). However, these identifications were only based on feature mapping of precursor ions probably corresponding to certain SNAPIN S133A peptides but without evidence on MS2 level. Similar observations were made in the SNAPIN S133E sample group (Figure 5.14B, blue point). Here, SNAPIN S133E peptides were also found in the SNAPIN KO samples without any PSM assigned to its features. As a result of the missing MS2 evidence, the identification of both SNAPIN proteoforms in the control could also be due to a false feature alignment on MS1 level. This becomes more apparent when considering that the SNAPIN isoforms were not found by immune detection in the KO IP input and the KO IP supernatant samples (Figure 5.13).
The peptide comprising the S133E substitution was found in the S133A samples and *vice versa*. Comparable to the MS-based SNAPIN detection in the KO cells, these identifications were only based on MS1 feature mapping without evidence on PSM level. Therefore, it is reasonable to assume that this identification might have been also caused by false MS1 precursor alignment, similar to the findings mentioned above.
According to the criteria applied in this study, nine proteins were identified as potential interaction partners of the SNAPIN S133A proteoform (Figure 5.14A). Among those, two proteins were uniquely found in this sample group whereas seven proteins were also identified to be at least 10 times more abundant in the S133E sample group compared to the KO control. Additionally, five proteins were found as possible interaction partners specific to the SNAPIN S133E proteoform (Figure 5.14B). For both SNAPIN proteoforms (S133A and S133E), unique potential interaction partners are indicated as red points together with their UniProt accession number in the scatter plots of figure 5.14. The corresponding protein names and the MS identification levels are listed in table 5.8. In this context, a MS1 identification level indicates

that no MS2 spectra was assigned to any peptide found for the particular protein in this sample group. Here, the assignments are solely based on matching of the precursor mass and retention time to an otherwise identified peptide. In contrast, protein identifications based on peptides with at least one PSM are annotated with an MS2 identification level.

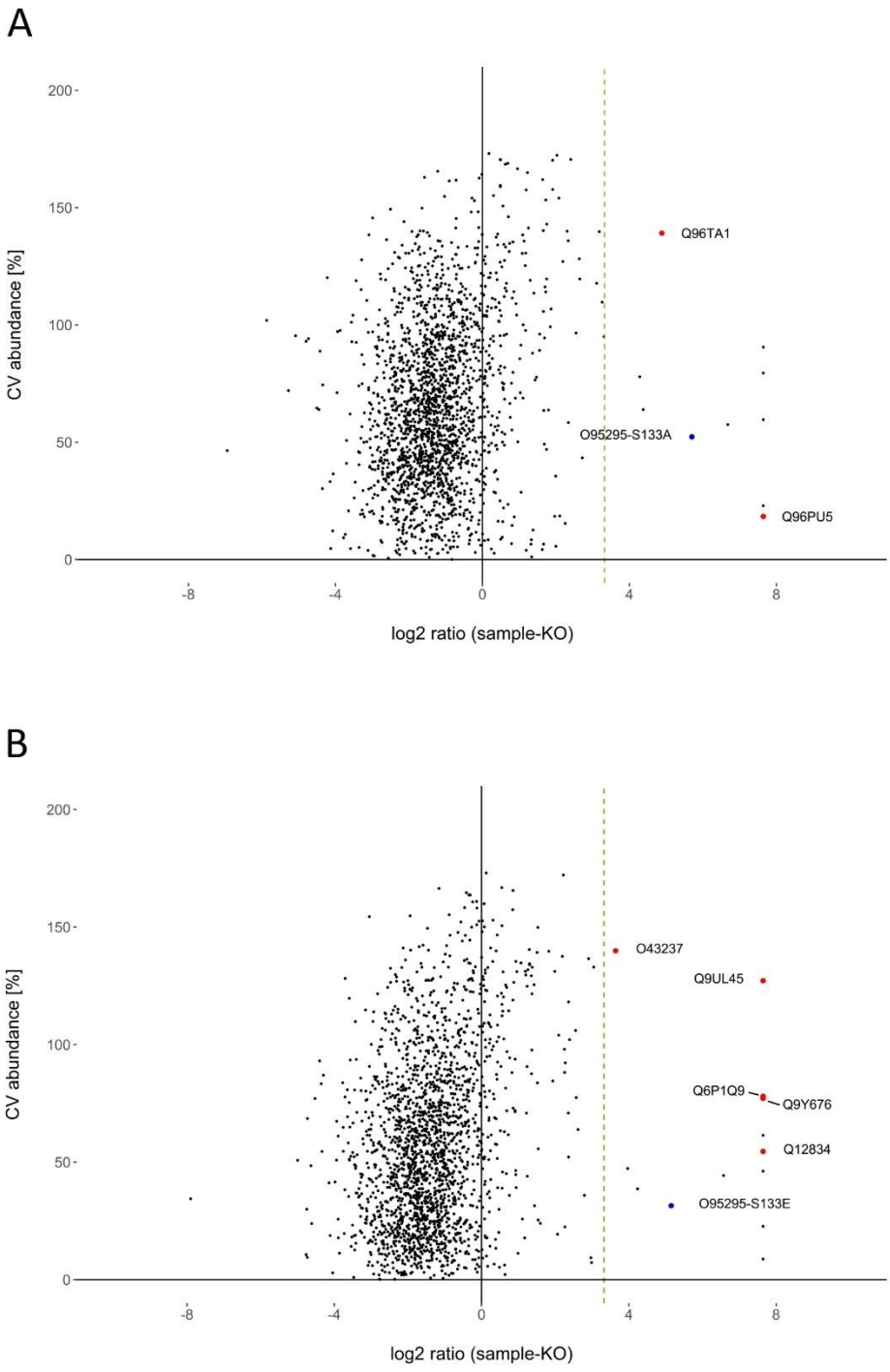


**Figure 5.14: Data analysis of the proteins identified in the IP eluate by LC-MS2.**
Calculations were based on non-normalized abundance values. For each protein identified in at least two out of three SNAPIN S133A (A) or S133E (B) pull-down experiments, the CV is plotted against the $\log_2$ abundance ratio of the samples and the KO control. Proteins with a sample/KO ratio higher than 10 ($\log_2 > 3.3$, green dashed line) were considered as potential interaction partners. Proteins uniquely identified in the SNAPIN S133A or S133E co-IP are shown as red dots. The blue point represents the bait of the particular pull-down experiment.

**Table 5.8: Description and MS identification levels corresponding to the proteins identified as potential unique interaction partners of the SNAPIN S133A or the SNPAIN S133E proteoform (red dots in figure 5.14).**

| | Uniprot accession | Protein name | MS identification level |
|---|---|---|---|
| Identified SNAPIN S133A interaction | Q96PU5 | E3 ubiquitin-protein ligase NEDD4-like | MS1 (2/3 Rep) |
| | Q96TA1 | Protein Niban 2 | MS1 (2/3 Rep) |
| Identified SNAPIN S133E interaction | Q6P1Q9 | Methyltransferase-like protein 2B | MS1 + MS2 (2/3 Rep) |
| | O43237 | Cytoplasmic dynein 1 light intermediate chain 2 | MS1 (2/3 Rep) |
| | Q12834 | Cell division cycle protein 20 homolog | MS1 + MS2 (2/3 Rep) |
| | Q9UL45 | Biogenesis of lysosome-related organelles complex 1 subunit 6 | MS2 (2/3 Rep) |
| | Q9Y676 | 28S ribosomal protein S18b, mitochondrial | MS1 (2/3 Rep) |

Direct comparison between the protein abundances of the SNAPIN S133A and the SNAPIN S133E sample group is difficult as the quantity of the recombinantly produced protein might vary after stable transfection with different constructs. When using transfected cells for pull-down experiments, such variations in the bait concentration might influence the quantity of co-immunoprecipitated interaction partners. In order to overcome this variability, the protein abundances of each channel and sample group have been normalized on the according SNAPIN quantities.

Figure 5.15 shows the abundance ratios of the seven proteins found as potential interaction partners in the SNAPIN S133A and the SNAPIN S133E sample group (based on normalized abundances). The corresponding protein names as well as the MS identification levels are listed in table 5.9. In figure 5.15, abundance ratios of single replicates are indicated as dots. The bars depict the ratios of the mean abundances determined from all relevant replicates. Here, the mean protein abundance of one sample group was calculated prior to the ratio determination. Compared to the calculation of the mean ratio based on the single replicate ratios, this considers a higher number of quantification values as one protein found in two out of three replicates might not have been always identified in the same replicate among the S133E and S133A sample groups. In this case, only one single replicate ratio would be calculated whereas the second quantification value identified for each sample group would be lost (see figure 5.15, Protein Q8IY63 and Q96FH0).

By comparing the normalized abundance ratios of the proteins found in the SNAPIN S133A and S133E sample group, no mutation induced differences in the interaction of the SNAPIN proteoforms and the co-immunoprecipitated proteins were detected (Figure 5.15). Except for the biogenesis of lysosome-related organelles complex 1 (BORC) subunit 2 (Accession Q6QNY1),

a high variability of the single replicate ratios was detected, thus indicating high variations in the protein abundances between the replicates.

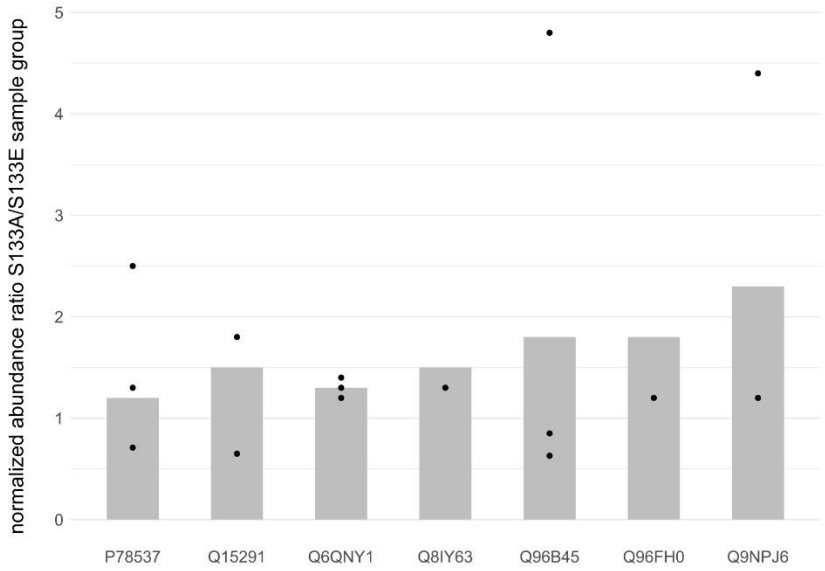


**Figure 5.15: Comparison of the normalized abundance ratios of proteins identified as potential interaction partners in the SNAPIN S133A and S133E pull down experiments (min. found in 2/3 replicates).**
The dots represent the ratios determined for the single replicate. The bars indicate the ratios of the mean abundances determined from all relevant replicates. Here, the mean protein abundance of one sample group was calculated prior to the ratio determination.

**Table 5.9: Description and MS identification levels corresponding to the proteins identified as potential interaction partners of both SNAPIN proteoforms (Figure 5.15).**

| Uniprot accession | Protein name | MS identification level S133A sample group | MS identification level S133E sample group |
|---|---|---|---|
| P78537 | Biogenesis of lysosome-related organelles complex 1 subunit 1 | MS2 (3/3 Rep) | MS2 (3/3 Rep) |
| Q15291 | Retinoblastoma-binding protein 5 | MS1 (3/3 Rep) | MS1 (2/3 Rep) |
| Q6QNY1 | Biogenesis of lysosome-related organelles complex 1 subunit 2 | MS2 (3/3 Rep) | MS2 (3/3 Rep) |
| Q8IY63 | Angiomotin-like protein 1 | MS1 + MS2 (2/3 Rep) | MS1 + MS2 (2/3 Rep) |
| Q96B45 | BLOC-1-related complex subunit 7 | MS1 + MS2 (3/3 Rep) | MS2 (3/3 Rep) |
| Q96FH0 | BLOC-1-related complex subunit 8 | MS1 + MS2 (2/3 Rep) | MS1 + MS2 (2/3 Rep) |
| Q9NPJ6 | Mediator of RNA polymerase II transcription subunit 4 | MS1 + MS2 (3/3 Rep) | MS2 (3/3 Rep) |

SNAPIN is a known subunit of the BORC and the BLOC-1 complex (Starcevic and Dell'Angelica 2004; Pu et al. 2015). Among the proteins precipitated by the SNAPIN S133A and S133E proteoforms, four other subunits either belonging to BORC or the BLOC-1 complex were found

(P78537, Q6QNY1, Q96B45, Q96FH0) (Starcevic and Dell'Angelica 2004; Pu et al. 2015). However, as the abundance ratios of these proteins were not consistently changed between the replicates, the precipitation between these subunits and the two SNAPIN isoforms seems to be independent from the substitution of serine at position 133. Interestingly, BLOC-1 subunit 6 (BLOC1S6), another member of BLOC-1, has been identified as a possible unique interaction partner of the SNAPIN S133E proteoform (Figure 5.14B). This might suggest a charge dependent interaction between these two proteins which might also occur when the serine 133 is phosphorylated. Nevertheless, as the CV of this protein was rather high, the unique interaction of BLOC1S6 with SNAPIN S133E needs to be further analyzed in order to draw reliable conclusions.

## 5.2. Method development for the detection of different lysine PTMs in a single MS experiment

Protein lysine modifications are prominent PTMs in eukaryotic cells responsible for the regulation of protein degradation, gene expression, signaling pathways and other cellular processes (Ciechanover et al. 1980; Hershko et al. 1980; Hebbes et al. 1988; Gu and Roeder 1997; Strahl et al. 1999; Chen et al. 2001; Huang et al. 2006; Wang et al. 2008; Kaimori et al. 2016; Elkouris et al. 2016; Fischer et al. 2017). Peptide centric bottom up mass spectrometry is a common tool used for identifying these PTMs. Prior to the MS analysis, lysine modification containing peptides are often enriched by immunoprecipitation using PTM-specific antibodies (Choudhary et al. 2009; Guo et al. 2014). Based on the specificity of the antibody, studies aiming at identifying the diversity of lysine modifications within the cells require the utilization of several of these immunoaffinity-based approaches thus making the investigations expensive and laborious. Additionally, the ability to investigate lysine modification containing peptides by this method depends on the quality and availability of a proper antibody which might hinder investigations of rare or novel lysine modifications. Another drawback of the antibody-based enrichment techniques is the requirement of a high amount of sample which might be a problem when dealing with limited amounts of starting material such as enriched organelles.

The present studies aimed at developing a non-antibody-based technique for enhancing the identification of multiple different lysine PTM containing peptides from low abundant complex samples. As depicted in figure 5.16, two different methods were tested. Based on the procedure, the methods are called the serial digestion technique and the selective derivatization-based method. The common starting point of both techniques is the tryptic digestion of the protein mixture (Figure 5.16, step 1). Here, the protease trypsin cleaves proteolytically after lysine and arginine residues (Olsen et al. 2004). As trypsin is assumed to be sensitive towards lysine modifications such as acetylation, a missed cleavage site might be introduced next to these modified amino acid residues (Smith et al. 2003; Peters et al. 2003; Freitas et al. 2004; Burlingame et al. 2005).

In case of the serial digestion technique, tryptic peptides are first biotinylated with NHS-biotin, a primary amine reactive reagent leading to biotinylation of peptide N-termini and the side chain of lysines (Figure 5.16, step 2.1). Lysines already modified by PTMs remain unbiotinylated. The next step within the workflow requires the ability of a protease to cleave adjacent to different endogenous PTM-containing lysine residues. LysN, a protease cleaving N-terminal to lysine residues, has already been described to cleave next to mono- and dimethylated lysines (Nonaka

et al. 1995; Taouatas et al. 2010). Similar properties have been published for the proteinase LysArginase which cleaves N-terminal to lysine and arginine residues (Tallant et al. 2006; Tallant et al. 2007; Huesgen et al. 2015). It is assumed that these enzymes might have an expanded cleavage capability which is why they are used for the digestion of PTM containing peptides within the serial digestion-based workflow (Figure 5.16, step 3.1). Here, the capability of the enzymes to cleave adjacent to PTM containing lysine residues would result in the removal of the biotinylated, N-terminal amino acid groups from the modified peptide. This cleavage is crucial as the last step of the serial digestion workflow comprises the incubation of the double digested samples with streptavidin (Figure 5.16, step 4.1). In this step, the strong affinity of biotin to streptavidin is used to remove any biotinylated peptide from the supernatant, thus leaving the PTM-containing peptides in the supernatant (Figure 5.16, step 4.1). Nevertheless, due to the specificity of trypsin, peptides with both, an internal PTM-containing as well as a C-terminal unmodified lysine residue might be generated during the first digestion of the protein sample (see figure 5.16, step 1, succinylated peptide). After incubation with NHS-biotin, this C-terminal lysine residue is biotinylated and needs to be separated from the PTM containing part of the peptide in order to prevent the loss of this PTM site during streptavidin incubation (see figure 5.16, step 2.1, succinylated peptide). Therefore, a cleavage capability of LysN and LysArginase next to biotinylated lysine residues would further enhance the efficiency of this method, as biotin-containing lysine residues could be removed from the C-terminus of post translationally modified tryptic peptides (see figure 5.16, step 3.1, succinylated peptide).

The second technique starts with the selective derivatization of the α-amino group present at the N-terminus of the tryptic peptides in order to block these groups from NHS-based modifications (Figure 5.16, step 2.2). Afterwards, NHS-biotin is used for biotinylation of unmodified lysine residues (Figure 5.16, step 3.2). Incubation with streptavidin leads to a depletion of biotinylated peptides, thus leaving only peptides comprising a C-terminal arginine in the supernatant (Figure 5.16, step 4.2). As non-lysine PTM containing peptides are depleted during this workflow, the reduced complexity could also be associated with an improved identification of arginine modifications.

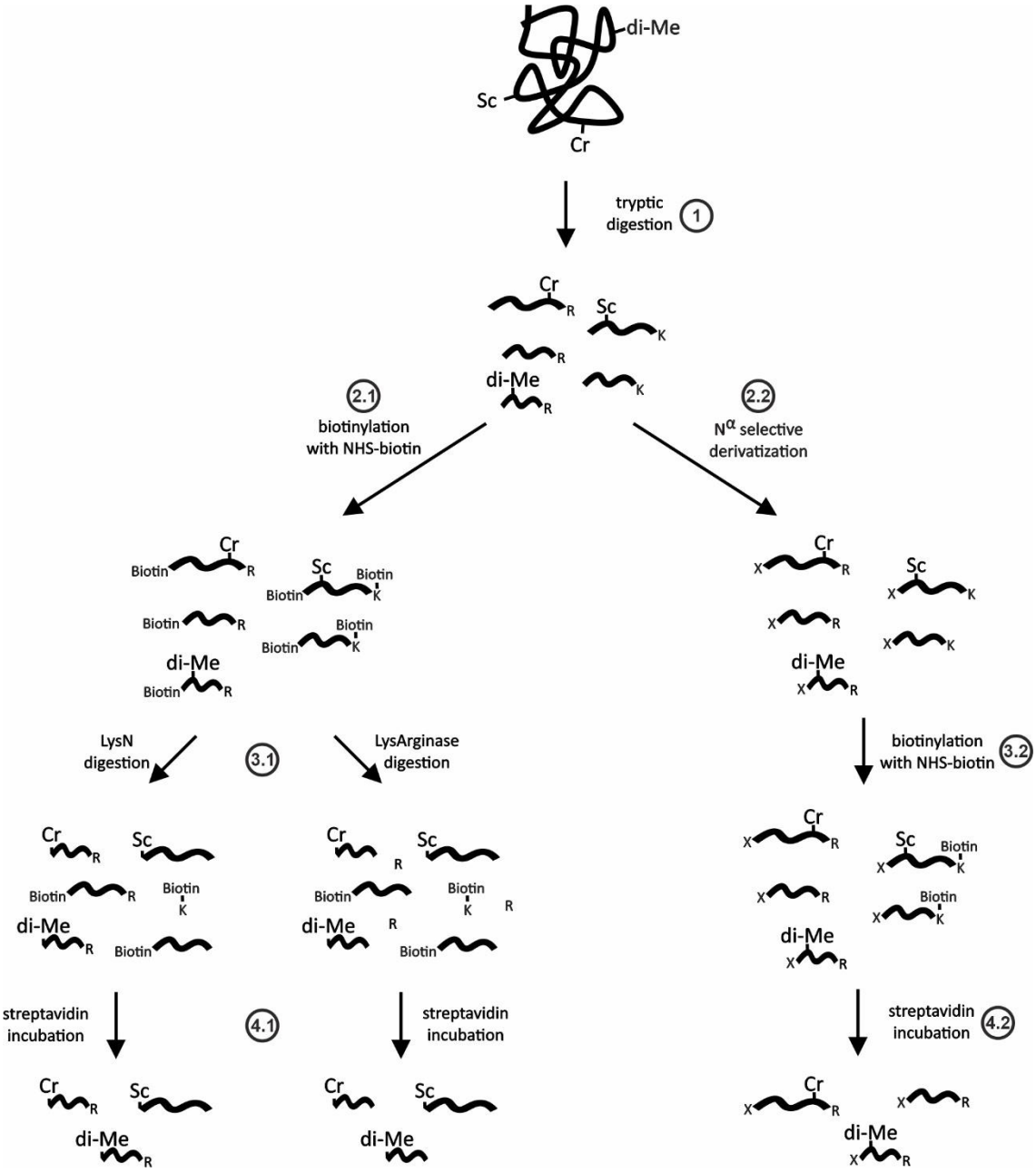


**Figure 5.16: Schematic overview of the two different workflows tested for enhancing the identification of lysine PTM containing peptides.**

In both techniques, proteins are digested with trypsin. For the serial digestion workflow (branch 2.1), tryptic peptides are biotinylated and subsequently incubated with LysN or LysArginase. Biotinylated peptides are removed by incubating the mixture with streptavidin. In case of the derivatization-based method (branch 2.2), α-amino groups at the N-terminus of the tryptic peptides are modified (indicated by X). Afterwards, the derivatized peptides are biotinylated and incubated with streptavidin. Abbreviations: Sc = succinylation; di-Me = di-methylation; Cr = crotonylation

### 5.2.1. Serial digestion workflow

#### 5.2.1.1. Single peptide-based evaluation of LysN's cleavage property next to biotinylated lysines

The ability of LysN in cleaving adjacent to mono- and dimethylated lysine residues has already been described (Taouatas et al. 2010). As mentioned earlier, the efficiency of the serial digestion-based workflow would be enhanced if LysN is also able to cleave next to biotinylated lysine residues. In order to evaluate this capability, a synthetic peptide was biotinylated with sulfo-NHS-biotin, digested with LysN and subsequently analyzed by MALDI-TOF MS (Figure 5.17A). In these MS-based approaches, biotinylation events via NHS-biotin can be identified by a mass shift of 226 m/z.

The MALDI-TOF spectra acquired by the analysis of the reaction products are shown in figure 5.17B. NHS-biotin incubation was associated with biotinylation of the synthetic precursor peptide (1531.7 m/z) at two to three positions (1983.9 m/z & 2210.0 m/z). The digestion of the non-biotinylated peptide with LysN yielded a peak at 1039.5 m/z, corresponding to the peptide C-terminus after N-terminal cleavage of the precursor at position K5. When incubating the biotinylated peptide with LysN, a peak at 1265.6 m/z was detected. This signal was not observed in any other sample. The 1265.6 m/z peak matches the expected mass of the biotinylated KHLEDLER peptide. However, in two similar experiments, the 1265.6 m/z peak was also observed in the biotinylated, non-digested sample (data not shown).

The biotinylation of the precursor peptide at three positions indicates at least one unspecific biotinylation event. Reliable conclusions about the ability of LysN to cleave adjacent to biotinylated lysine residues is not possible, as the 1265.6 m/z peak was also observed in the NHS-biotin treated, non-digested sample in two similar, independent experiments. Assuming that the peak detected at 1265.6 m/z corresponds to the biotinylated KHLEDLER peptide, the weak intensity of this signal compared to its non-biotinylated counterpart (1039.5 m/z) could either be assigned to an impaired LysN digestion at the modified lysine residue or to changes in the ionization behavior during MALDI. However, the incompleteness of the LysN digestion as indicated by the prominent 1531.7 m/z peak of the non-biotinylated sample suggests the necessity of optimizing the digestion conditions irrespective of lysine's biotinylation status.

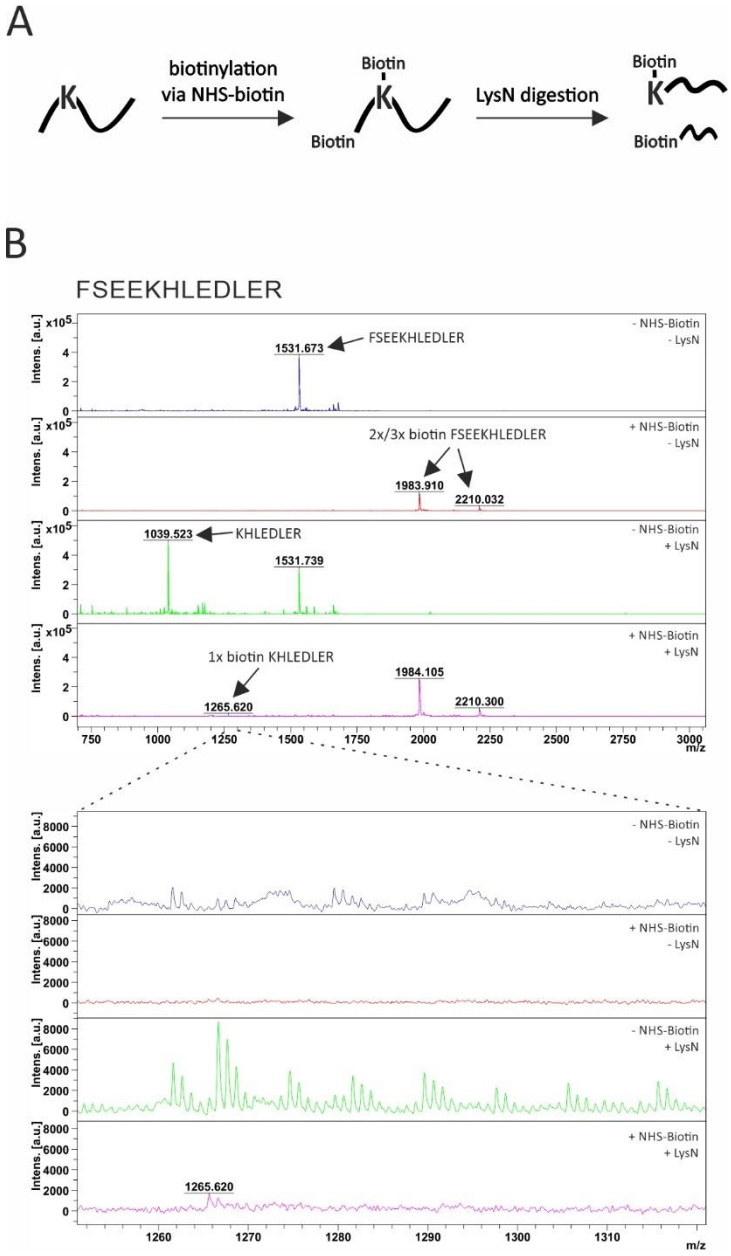


**Figure 5.17: LysN digestion of a biotinylated, synthetic peptide.**
A synthetic peptide was biotinylated and subsequently incubated with LysN (A). Non-biotinylated and/or non-digested peptides served as controls. Reaction products were analyzed by MALDI-TOF MS (B).

### 5.2.1.2. Optimization of LysN digestion with a non-biotinylated synthetic peptide

As the LysN digestion of the non-biotinylated sample was incomplete (see figure 5.17B), the conditions for the enzymatic reaction should be optimized. The improvement of the digestion conditions was assumed to also enhance the cleavage of the biotinylated peptides. The characteristics of LysN have been investigated by Nonaka et al. in 1995. Within that study, the authors highlighted the importance of divalent cations such as $Mn^{2+}$, $Zn^{2+}$ and $Mg^{2+}$ for the enzyme activity (Nonaka et al. 1995). Thus, the synthetic peptide MHTGHANAKHIAGLSR was

incubated in the presence of different divalent cations. This peptide has been designed with the intention to yield a high LysN cleavage efficiency. The sequence was chosen based on the predicted influence of lysine-adjacent amino acids on the frequency of LysN cleavages published by Gershon (2014). In addition to testing the influence of cations, the effect of different peptide:LysN mass ratios on the cleavage efficiency was investigated. Analysis of the reaction products was performed by LC-MS2 measurements using a Dionex LC-system coupled to a LTQ Orbitrap Velos mass spectrometer. Database searches were performed by using the Mascot search engine implemented in the Proteome Discoverer software. The relative cleavage efficiency was calculated as the ratio of chromatographic peak areas of the cleaved and the non-cleaved precursor peptide multiplied by a factor of 1000 to yield a reasonable number.

Figure 5.18A shows the influence of different peptide:LysN ratios on the relative cleavage efficiency of the protease (without cations). The highest number of cleavage events was observed when using a peptide:LysN mass ratio of 25:1. Further reduction of the peptide:LysN ratio led to a tremendous reduction in the cleavage efficiency.

Within the present study, two different concentrations of $ZnCl_2$, $MnCl_2$ and $MgCl_2$ were tested (Figure 5.18B). Among those, the samples containing 0.1 mM $MgCl_2$ and those without additional cations featured the highest LysN cleavage efficiency but also the biggest variance between the two technical replicates (tr). Compared to that, the addition of 0.1 mM $ZnCl_2$ and 0.1 mM $MnCl_2$ seemed to reduce LysN activity. No cleavage was observed for the sample containing 1 mM $ZnCl_2$ in the digestion buffer. The effects of the addition of 1 mM $MgCl_2$ and 1 mM $MnCl_2$ to the reaction seemed to be comparable to those detected for the 0.1 mM $MgCl_2$ sample.

LysN digestion can be optimized by adjusting the peptide:LysN ratio to 25:1. Compared to that, the effect of the different cations investigated within the study is inconclusive. Incubation of NHS-biotin treated peptides with LysN in presence of 0.1 mM $MgCl_2$ (peptide:LysN ratio 25:1) was not associated with the detection of the biotinylated, C-terminal cleavage product in MALDI-TOF MS (data not shown). Nevertheless, as the data presented here might suggest an increase in LysN's cleavage efficiency of the non-biotinylated peptide in presence of 0.1 mM $MgCl_2$, this condition was used together with a peptide:protease ratio of 25:1 in further LysN digestion experiments.

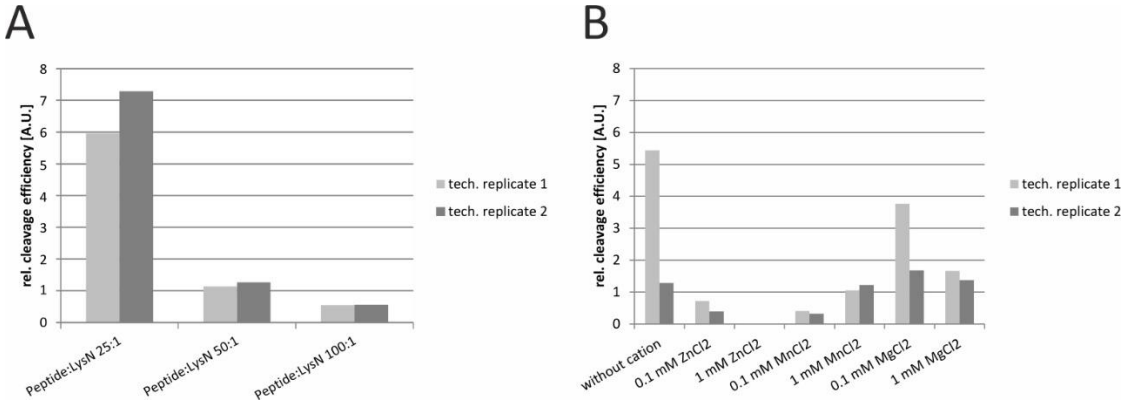


**Figure 5.18: Optimizing the LysN cleavage of non-biotinylated peptides.**
The relative protease cleavage efficiencies (in arbitrary units) were calculated as the ratio of the chromatographic peak area of the C-terminal product and the precursor peptide (x1000) (A+B). Different peptide:LysN mass ratios (A) as well as the influence of the addition of divalent cations to the digestion buffer (B) were tested regarding their effect on the cleavage efficiency.

### 5.2.1.3. Protein-based evaluation of LysN's and LysArginase's cleavage property next to biotinylated lysines

LysArginase, a protease cleaving N-terminal of lysine and arginine residues, might be useful as a substitute of LysN in the serial digestion workflow (Tallant et al. 2006; Tallant et al. 2007; Huesgen et al. 2015). Comparable to LysN, its cleavage ability adjacent to methylated lysines has already been described (Huesgen et al. 2015).

Detailed investigations of LysN's and LysArginase's cleavage capability next to biotin-modified lysine residues was performed by using biotinylated BSA and cell lysate as substrates. Although the serial digestion workflow described in figure 5.16 comprises the LysN digestion of tryptic, biotin-containing peptides, utilization of denatured, biotinylated proteins was assumed in being sufficient for evaluating enzyme's cleavage capability at biotin-modified lysine residues. This assumption was made in order to simplify data analysis. Successful LysN and LysArginase cleavage of a biotinylated, tryptic peptide would lead to a loss of the biotin-containing lysine and could therefore only be determined indirectly. Compared to that, enzymatic cleavage at a biotin containing lysine residue on protein level leads to the formation of peptides containing a biotinylation at the N-terminal side chain which can easily be assessed by LC-MS2.

#### *5.2.1.3.1. Proteolytic cleavage of biotinylated BSA by LysN and LysArginase*

BSA was biotinylated with NHS-biotin und subsequently digested by LysN or LysArginase (Figure 5.19A). As depicted in the previous section, a protein:LysN ratio of 25:1 and a concentration of 0.1 mM $MgCl_2$ might lead to an increase of cleavage efficiency. Therefore, these conditions were used for the LysN digestion of the biotinylated BSA. LysArginase digestion was performed with

the same protein:protease ratio but with 10mM $CaCl_2$ present in the digestion buffer. The experiment was performed in three technical replicates (tr1-tr3). Digestion products were investigated by LC-MS2 measurements (LTQ Orbitrap Velos mass spectrometer). Raw data analysis was performed by using the MaxQuant software.

Figure 5.19B depicts the number of biotinylated and non-biotinylated peptides identified for both enzymes. Approx. 80 peptides were identified when digesting the non-biotinylated BSA with LysN or LysArginase. Roughly the same number of biotinylated peptides were detected when incubating the NHS-Biotin treated samples with LysN. Compared to that, digestion of the biotinylated BSA with LysArginase yielded approx. 20 biotin-containing peptides.
The reproducibility of the enzymatic digestion of biotinylated BSA across the three replicates is shown in figure 5.19C. Out of the approx. 80 biotinylated peptides detected after LysN digestion of the NHS-biotin treated sample, 62 peptides were found in all three replicates. LysArginase digestion of the biotinylated BSA only yielded an overlap of 11 biotin-containing peptides across the replicates.
The biotinylated peptides identified after LysN and LysArginase digestion were used for investigating the position of the biotin-containing lysine residue within the amino acid sequence. In this case, peptides containing the biotinylated lysine at the N-terminus indicate a successful enzymatic cleavage adjacent to the modified lysine residue. Figure 5.19D shows the proportion of the different modification sites among the biotinylated peptides. Almost 100 % of the peptides identified after LysArginase digestion of the NHS-Biotin treated BSA featured their biotinylation site at an internal lysine residue. In case of the LysN digestion, approx. 58 % of the biotin-containing peptides comprised its modification at the N-terminal lysine side chain. Besides that, 40 % of the peptides in this sample group featured the biotin modification at an internal lysine residue and in 2 % of the cases, the biotinylation site could not be clearly assigned.
Figure 5.19E depicts the mean percentages of the numbers of missed cleavage sites (MCS) identified among the three technical replicates. Compared to the control (-NHS-Biotin), biotinylation of BSA was associated with an increased proportion of MCS after LysN digestion. In case of LysArginase, only a slight increase in the percentage of peptides featuring a missed cleavage site was observed when comparing the NHS-Biotin treated and non-biotinylated sample.
Summarizing the results described in this section, LysN seems to be able to cleave adjacent to biotinylated lysine residues but its cleavage capability is impaired. This leads to an increased proportion of peptides with missed cleavages. Compared to that, biotinylation is only associated with a slight increase in the percentage of MCS in the LysArginase digested samples. This might be a combinatory effect of LysArginase's ability to also cleave N-terminal of arginine residues

and the fact, that this enzyme already featured a higher proportion of MCS in the control sample. Additionally, cleavage of LysArginase next to biotinylated lysine residues might lead to peptides with a reduced charge state after electrospray ionization as these hydrolysis products would only feature one primary amine group at the N-terminus. Singly charged peptides were not fragmented with the MS settings used in this study which would explain the low number of identifications with an N-terminal biotinylated lysine residue in the LysArginase sample group. However, in order to further investigate the cleavage capability of these two enzymes, similar investigations were performed with a complex biotinylated protein mixture.

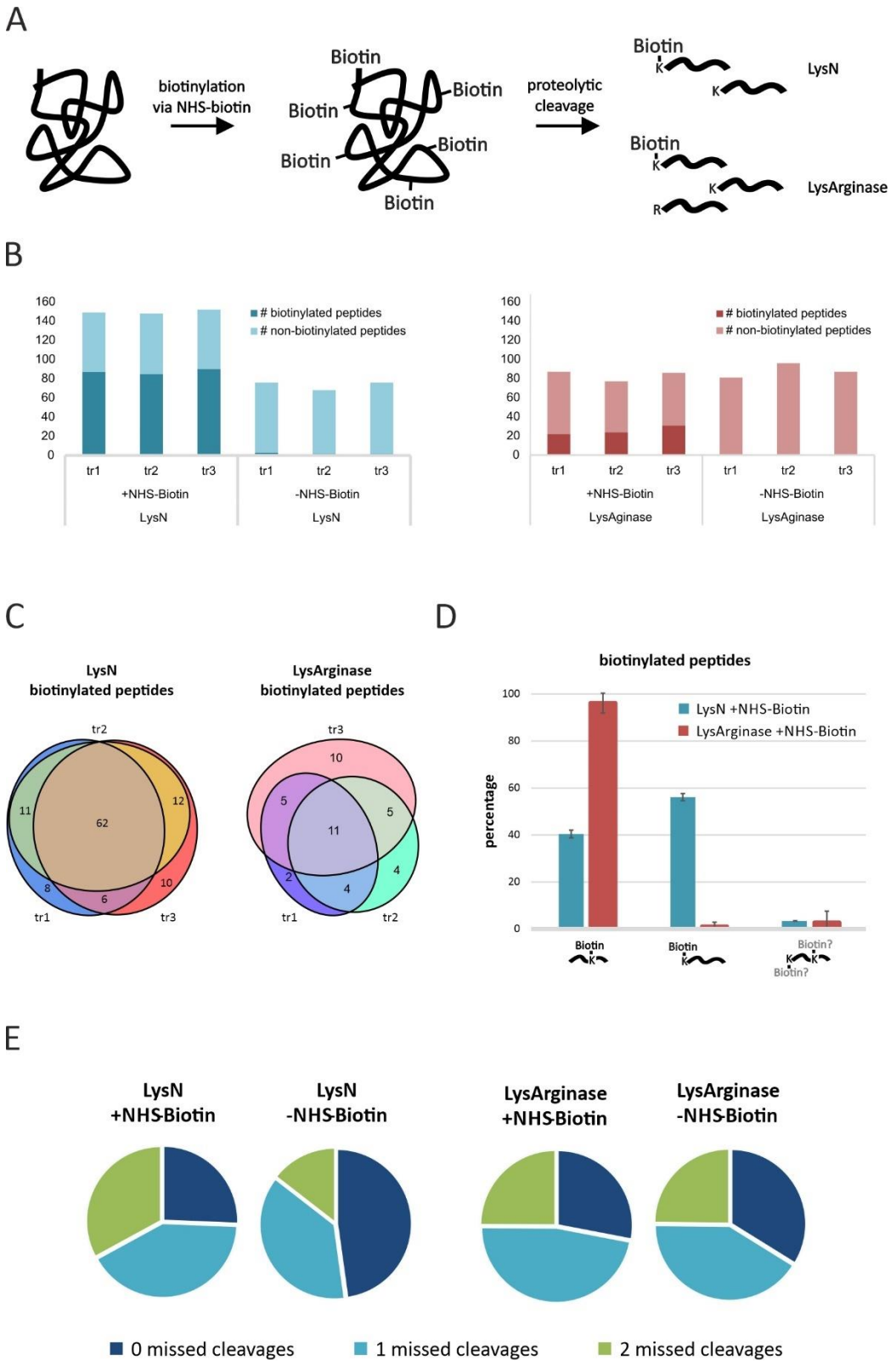


**Figure 5.19: Proteolytic cleavage of biotinylated BSA by LysN and LysArginase.**
BSA was biotinylated with NHS-biotin, digested with LysN or LysArginase and subsequently analyzed by LC-MS2 (A). Non-biotinylated samples served as controls. The experiment was performed in three technical replicates (tr1-tr3). The number of biotinylated and non-biotinylated peptides identified in the different sample groups and replicates are depicted as a bar graph (B). The Venn diagrams indicate the overlap of the biotinylated peptides detected across the single replicates (C). For both sample groups, the mean percentages (+/- standard deviation) of peptides either with an N-terminal, internal or ambiguous biotinylation sites are shown in D. The pie charts represent the mean proportion of the numbers of missed cleavage sites detected for the peptides of the different samples (standard deviation less than 4%) (E).

#### *5.2.1.3.2. Proteolytic cleavage of biotinylated proteins from HEK lysates by LysN and LysArginase*

In order to investigate the cleavage capability of LysN and LysArginase adjacent to biotinylated lysines, isotopically labeled proteins from HEK cell lysate (light, medium and heavy labeled) were incubated with NHS-biotin and subsequently digested. The experiment was performed in biological triplicates. Prior to the LC-MS2 measurement (LTQ Orbitrap Velos mass spectrometer), isotopically labeled peptides of the three replicates belonging to one sample group were combined. Raw data were processed by using the MaxQuant software. Only peptides found in all three replicates and featuring a posterior error probability (PEP) smaller than 0.01 were used for data analysis.

Figure 5.20A shows the number of biotinylated and non-biotinylated peptides identified within the different sample groups. Biotinylation of the protein mixtures prior to LysN and LysArginase digestion was associated with a reduced number of identified peptides in case of both enzymes. Unlike the observations made in the experiment using biotinylated BSA as a substrate (Figure 5.19B), similar proportions of biotin-containing peptides were detected after digesting the NHS-Biotin treated protein mixture with LysN or LysArginase, respectively (approx. 35-36 %).

More than 80 % of the biotinylated peptides identified after LysN digestion featured their modification at an internal lysine (Figure 5.20B). In contrast to the LysN results obtained in the BSA experiments (Figure 5.19D), a biotin-containing N-terminal lysine residue was only detected for 7 % of the modified peptides. For this enzyme, roughly the same proportions of non-assignable modification sites and biotinylated protein N-termini were observed. Compared to that, only 2 % of the LysArginase derived biotinylated peptides featured an N-terminal biotinylated lysine residue whereas the majority (90 %) comprised an internal modification site.

The dependency between protein biotinylation and the proportion of the different number of MCS is depicted in figure 5.20C. In case of both enzymes, the proportion of missed cleavages was increased when proteins are biotinylated prior to the digestion. However, like the results obtained in the BSA experiment (Figure 5.19E), only a slight increase in the proportion of MCS was observed in the biotinylated and non-biotinylated LysArginase sample groups.

The effect of the digestion of biotinylated samples on the protein sequence coverage was investigated. Figure 5.20D shows the boxplots of the sequence coverage (in percent) for the different sample groups. Protein biotinylation followed by digestion with LysN or LysArginase was associated with a lower median sequence coverage compared to the non-biotinylated samples.

The results obtained in this section indicate an impaired ability of LysN to cleave adjacent to biotinylated lysine residues in the complex protein mixture. However, the observation made for

the LysArginase digested biotinylated HEK samples are comparable to those described in section 5.2.1.3.1. Therefore, a reduced charge state of LysArginase-derived biotinylated peptides cannot be excluded as a reason for the low identification rate of peptides featuring a biotinylation at the N-terminal lysine residue in this sample group.

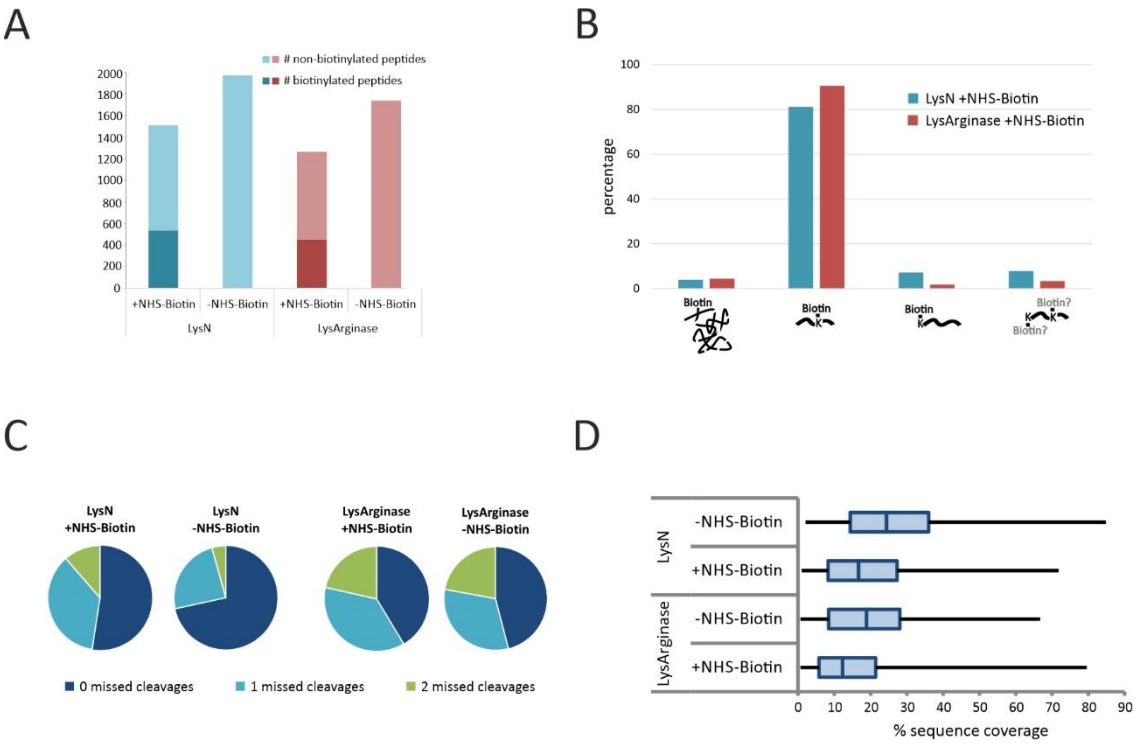


**Figure 5.20: Proteolytic cleavage of biotinylated proteins from HEK 293 cell lysate with LysN and LysArginase.** Isotopically labeled proteins were modified with NHS-biotin, digested with LysN or LysArginase and analyzed by LC-MS2. Non-biotinylated protein samples served as controls. The experiment was performed in triplicates. Only peptides identified in all three replicates of one sample group and those featuring a PEP smaller than 0.01 were used for data analysis. The number of biotinylated and non-biotinylated peptides in the different sample groups are shown in a bar graph (A). For both sample groups, the percentages of peptides either with a protein N-terminal, peptide N-terminal, internal or ambiguous biotinylation sites are depicted in B. The pie charts represent the proportion of the numbers of missed cleavage sites detected for the peptides of the different samples (C). The median sequence coverages for proteins are depicted as boxplots (blue line within the box: median; box: 25/75% quartile; end of black lines: min/max values)

### 5.2.1.4. Investigating the capability of the serial digestion workflow for enhancing the identification of lysine modified peptides

HEK protein lysate was used as a starting material for investigating the capability of the serial digestion workflow to enhance the identification of lysine modified peptides (see figure 5.16). Proteins were digested with trypsin before peptides were biotinylated with NHS-biotin. Non-biotinylated samples served as controls. Remaining NHS-biotin was quenched and subsequently removed by an SCX chromatography-based peptide clean-up step. For the second digestion, biotinylated peptides were either incubated with LysN or LysArginase. Afterwards, biotinylated

amino acids and peptides were precipitated by incubating the mixtures with streptavidin beads, potentially leaving the lysine PTM containing peptides in the supernatant. The experiment was performed in three technical replicates. After each step of the workflow, a sample was taken as a control. Each sample was analyzed in a single LC-MS2 run using a Dionex LC-system coupled to an LTQ Orbitrap Velos mass spectrometer.

In classical MS data analysis approaches, peptide modifications must be specified prior to the database search, thus hindering the identification of non-defined PTMs. However, several non-restrictive search algorithms have been reported, allowing the detection of non-specified modifications. Within the present study, the PeaksPTM algorithm, implemented in the PEAKS software, was used in order to identify such unspecified modifications present in the supernatants of the different samples after streptavidin incubation (Han et al. 2011). The five most abundant peptide modifications (based on their proportions on total peptide identifications) reported by the PeakPTM software for the NHS-biotin treated samples are listed in table 5.10. Pyroglutamate formation from glutamine was found as a frequent modification in the biotinylated, LysN digested sample group (approx. 12 % of peptides). Compared to that, less pyroglutamate formation was detected in the NHS-biotin treated, LysArginase digested samples (approx. 6 %). Here, oxidation at methionine was identified as the most abundant modification (approx. 13-14 %). Besides that, methylmalonylation at serine, acetylation at the protein N-terminus as well as deamination at asparagine and glutamine were reported in both sample groups after biotinylation. Methylation at lysine and arginine residues were annotated as one modification entry by the PeaksPTM algorithm. These PTMs were only detected in minor proportions in the samples incubated with streptavidin (0.3-0.5%). Here, all lysine methylation sites were found in the non-biotinylated samples. Nevertheless, no other lysine modification was found to be more abundant when considering all streptavidin incubated samples analyzed by PeaksPTM at once. Compared to the lysine methylated peptides, a similar number of methylarginine containing peptides was identified in these samples. Therefore, methylation at lysine and arginine were set as dynamic modifications in the Proteome Discoverer software when re-analyzing the samples with a classical database search.

**Table 5.10: PeaksPTM analysis of peptide samples after streptavidin incubation (serial digestion workflow).** Percentage of different peptide modifications identified by analyzing the streptavidin incubated samples with the PeaksPTM algorithm implemented in the PEAKS X software (only NHS-biotin treated samples are shown). Besides the expected variable modifications, the PeaksPTM search also allows the identification of unspecified PTM present in the Unimod database and added manually prior to data processing.

| | +NHS-biotin +LysN digestion | | | +NHS-biotin +LysArginase digestion | | |
|---|---|---|---|---|---|---|
| | ***tr1*** | ***tr2*** | ***tr3*** | ***tr1*** | ***tr2*** | ***tr3*** |
| **Pyro-glu from Q** | 12.1 % | 13.8 % | 9.9 % | 5.3 % | 7.0 % | 6.4 % |
| **Acetylation (Protein N-term)** | 15.3 % | 10.4 % | 7.2 % | 5.0 % | 6.6 % | 6.4 % |
| **Methylmalonylation (S)** | 12.6 % | 10.1 % | 10.2 % | 5.3 % | 7.5 % | 5.8 % |
| **Oxidation (M)** | 9.3 % | 14.1 % | 9.9 % | 13.9 % | 14.5 % | 13.0 % |
| **Deamidation (NQ)** | 3.3 % | 2.1 % | 2.0 % | 1.8 % | 2.2 % | 2.4 % |

PTM profiling by algorithms such as PeaksPTM might be prone to false discoveries as the increase in search space also increases the frequency of false data assignments. Therefore, the data of the streptavidin incubated samples were reprocessed in a classical database search using the Mascot algorithm accessed from the Proteome Discoverer software. Acetylation at protein N-termini, oxidation at methionine, biotinylation at peptide N-termini and lysine as well as methylation at lysine and arginine were set as dynamic modifications. The same settings were used for analyzing the samples taken after each step of the serial digestion workflow. For data processing, raw files belonging to the same step within the workflow (e.g. +NHS-biotin & -NHS-biotin) were processed together. The false-discovery rate (FDR) was controlled with the help of the Percolator algorithm (Käll et al. 2007). In order to analyze the data on peptide level, information about methylation sites were fused to the amino acid sequence. Afterwards, redundant sequence entries were removed for each replicate and sample group.

Table 5.11 comprises the average number (+/- standard deviation) of peptides and PSMs identified in the different sample groups. Additionally, the percentages of methylated peptides and PSMs are shown. On average, approx. 14,000 peptides and 21,000 PSMs were detected in the trypsin digested samples. Here, less than 0.1 % of the peptides were methylated. Compared to that, biotinylation of tryptic peptides followed by SCX chromatography peptide purification led to a strong decrease in peptide and PSM identifications. A similar tendency was observed for the non-biotinylated (-NHS-biotin control (ctrl.)), SCX chromatography purified peptides, although the decrease is lower compared to the NHS-biotin treated samples. However, in comparison to the tryptically digested samples without any further treatment, peptide biotinylation combined with SCX chromatography-based sample clean-up was associated with a strong increase in the detection of arginine methylated peptides (1.8 %) whereas only a slightly

higher proportion of lysine methylation was observed (0.14 %). The highest percentage of peptide lysine methylation was detected in the non-biotinylated, SCX chromatography purified sample group (3 %). Incubation of the biotinylated peptides with LysN was associated with a slight decrease in peptide and PSM identifications accompanied with a reduced detection of methylation sites (0.5 % methylated arginines). This effect was even higher for the non-biotinylated, LysN digested samples. Here, the proportion of lysine methylated peptides amounted only to 0.2 %. Similar tendencies were observed when incubating the biotinylated and non-biotinylated peptides with LysArginase. In case of the NHS-biotin treated, LysArginase digested sample group, 0.42 % of the peptides featured a methylated arginine residue. Compared to that, the percentages of peptide arginine and lysine methylation amount to 0.48 % and 0.58 % respectively in the non-biotinylated, LysArginase digested samples. Incubation of the non-biotinylated, LysN/LysArginase digested samples with streptavidin was associated with a further reduction of the average number of peptides and PSMs identified during data analysis. The lowest peptide identification rate was observed for the NHS-biotin treated, LysN/LysArginase digested and streptavidin incubated samples. Here, the average number of PSMs was lower compared to the number of identified peptides. This indicates that the identification of several peptides in this sample group was based on MS1 feature mapping to PSMs found in other raw files processed together with the biotinylated, LysN/LysArginase digested and streptavidin incubated samples. However, by comparing the biotinylated and non-biotinylated streptavidin incubated samples, almost no difference in the proportion of methylated peptides was detected. Therefore, complete sample processing by the serial digestion workflow was not associated with an increased identification of methylation sites.

**Table 5.11: Average number and standard deviation of peptides and PSMs found in the different sample groups of the serial digestion workflow (n=3) (first part of table).**
The percentage of methylated peptides/PSMs compared to the total number of peptides/PSMs is given in parenthesis. * biotinylated and non-biotinylated peptides before second digestion with the particular enzyme. Table continues on the next page.

| | | | # total pep. | # meth. pep. [K] | # meth. pep. [R] | # meth. pep. [K+R] | # total PSMs | # meth. PSMs [K] | # meth. PSMs [R] | # meth. PSMs [K+R] |
|---|---|---|---|---|---|---|---|---|---|---|
| Tryptic peptides | | | 13935 ± 66 | 7 ± 1 (0.05 %) | 9 ± 1 (0.07 %) | 2 ± 1 (0.02 %) | 21046 ± 352 | 26 ± 2 (0.13 %) | 42 ± 1 (0.20 %) | 6 ± 1 (0.03 %) |
| Biotinylated peptides | *before LysN** | *+NHS-Biotin* | 4223 ± 207 | 6 ± 1 (0.14 %) | 76 ± 9 (1.80 %) | 1 ± 1 (0.03 %) | 5397 ± 372 | 2 ± 1 (0.04 %) | 94 ± 15 (1.73 %) | 1 ± 1 (0.02 %) |
| | | *-NHS-Biotin ctrl* | 7127 ± 270 | 212 ± 3 (2.97 %) | 101 ± 4 (1.42 %) | 2 ± 1 (0.02 %) | 9946± 424 | 375 ± 24 (3.77 %) | 176 ± 4 (1.77 %) | 2 ± 1 (0.02 %) |
| | *before LysArg** | *+NHS-Biotin* | 4181 ± 277 | 6 ± 1 (0.15 %) | 73 ± 12 (1.74 %) | 2 ± 1 (0.04 %) | 5442 ± 539 | 2 ± 1 (0.04 %) | 98 ± 30 (1.77 %) | 1 ± 1 (0.01 %) |
| | | *-NHS-Biotin ctrl* | 7005 ± 303 | 206 ± 9 (2.95 %) | 97 ± 10 (1.38 %) | 1 ± 1 (0.02 %) | 9731 ± 573 | 341 ± 44 (3.50 %) | 171 ± 34 (1.75 %) | 2 ± 2 (0.02 %) |
| Double digested peptides | *LysN* | *+NHS-Biotin* | 3191 ± 89 | 4 ± 1 (0.11 %) | 15 ± 2 (0.47 %) | 1 ± 0 (0.03 %) | 3271 ± 351 | 1 ± 1 (0.02 %) | 19 ± 2 (0.59 %) | 1 ± 2 (0.01 %) |
| | | *-NHS-Biotin ctrl* | 3782 ± 14 | 8 ± 1 (0.20 %) | 26 ± 3 (0.68 %) | 1 ± 1 (0.02 %) | 4798 ± 533 | 15 ± 3 (0.32 %) | 56 ± 7 (1.18 %) | 0 (0.00 %) |
| | *LysArg* | *+NHS-Biotin* | 2696 ± 233 | 2 ± 1 (0.06 %) | 11 ± 2 (0.42 %) | 1 ± 0 (0.04 %) | 2767 ± 337 | 1 ± 1 (0.05 %) | 16 ± 3 (0.59 %) | 1 ± 0 (0.04 %) |
| | | *-NHS-Biotin ctrl* | 3575 ± 209 | 21 ± 1 (0.58 %) | 17 ± 3 (0.48 %) | 0 ± 0 (0.00 %) | 4297 ± 468 | 38 ± 5 (0.89 %) | 26 ± 4 (0.62 %) | 0 (0.00 %) |

**Table 5.11 (second part): Average number and standard deviation of peptides and PSMs found in the different sample groups of the serial digestion workflow (n=3).**
The percentage of methylated peptides/PSMs compared to the total number of peptides/PSMs is given in parenthesis. * biotinylated and non-biotinylated peptides before second digestion with the particular enzyme.

| | | | # total pep. | # meth. pep. [K] | # meth. pep. [R] | # meth. pep. [K+R] | # total PSMs | # meth. PSMs [K] | # meth. PSMs [R] | # meth. PSMs [K+R] |
|---|---|---|---|---|---|---|---|---|---|---|
| Streptavidin incubated peptides | *LysN* | *+NHS-Biotin* | 623 ± 214 | 2 ± 2 (0.28 %) | 4 ± 1 (0.60 %) | 0 ± 0 (0.00 %) | 122 ± 28 | 0 (0.00 %) | 1 ± 2 (0.95 %) | 0 (0.00 %) |
| | | *-NHS-Biotin ctrl* | 2588 ± 855 | 6 ± 1 (0.23 %) | 12 ± 4 (0.48 %) | 0 ± 0 (0.00 %) | 3750 ± 503 | 7 ± 3 (0.18 %) | 40 ± 3 (1.07 %) | 0 (0.00 %) |
| | *LysArg* | *+NHS-Biotin* | 557 ± 103 | 1 ± 0 (0.18 %) | 3 ± 2 (0.60 %) | 0 ± 0 (0.00 %) | 230 ± 65 | 0 (0.00 %) | 3 ± 2 (1.43 %) | 0 (0.00 %) |
| | | *-NHS-Biotin ctrl* | 2819 ± 270 | 11 ± 2 (0.40 %) | 10 ± 1 (0.35 %) | 0 ± 0 (0.00 %) | 3419 ± 462 | 21 ± 4 (0.62 %) | 23 ± 1 (0.69 %) | 0 (0.00 %) |

Insufficient peptide biotinylation could be a reason for the low amount of peptide methylation identified in the streptavidin incubated samples. Although the reduced number of peptides and PSMs detected in the NHS-biotin treated samples indicate a successful biotinylation, incomplete peptide modification after treatment with the NHS-ester could lower the effectiveness of the workflow. In order to evaluate the efficiency of peptide biotinylation prior to the second digestion, the percentage of biotinylated PSMs as well as of PSMs with unmodified primary amines was investigated (Figure 5.21). Approx. 95 % of the PSMs detected in the NHS-biotin treated samples were biotinylated whereas approx. 5 % featured at least one unmodified primary amine within their sequence. Compared to that, such unmodified primary amines were observed within 99 % of the PSMs identified in the non-biotinylated control. In this sample group, less than 1 % of the PSMs were biotinylated.

The results indicate a nearly complete biotinylation of the primary amines present within the peptides after incubation with the NHS-biotin.

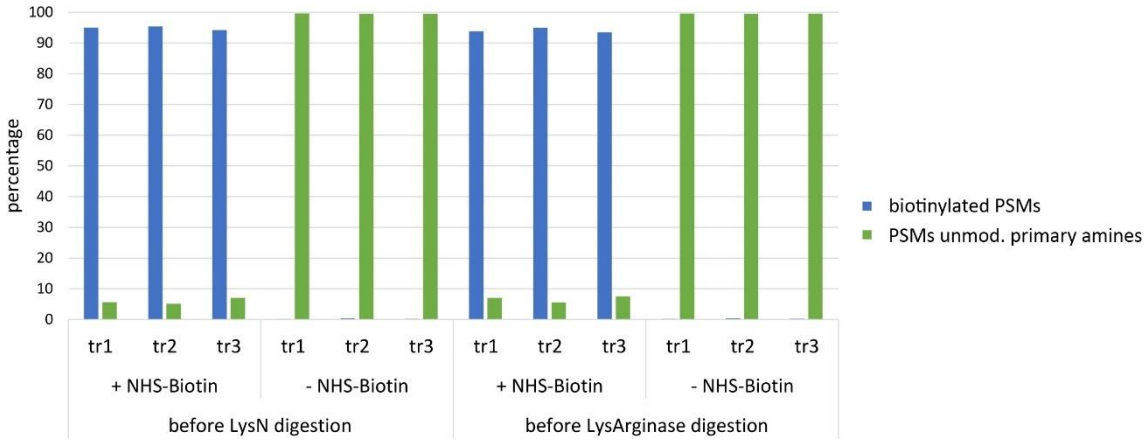


**Figure 5.21: Investigation of the percentage of biotinylated PSMs in different sample groups of the serial digestion workflow.**
Percentage of biotinylated PSMs as well as of PSMs with unmodified primary amines after incubation of tryptic peptides with NHS-biotin. Non-biotinylated samples served as a control. The samples were taken prior to the second digestion with LysN or LysArginase, respectively.

As the number of detected methylated peptides and PSMs decreased after the second digestion (Table 5.11), the methylation position within the sequence before incubation with LysN and LysArginase was investigated. The capability of both enzymes to cleave N-terminal of methylated lysine residues has already been described (Taouatas et al. 2010; Huesgen et al. 2015). Additionally, LysArginases' cleavage property adjacent to methylated arginines has been published (Huesgen et al. 2015). Therefore, if the methylation site is located at the C-terminus of the peptides after tryptic digestion, incubation with LysN or LysArginase might remove the methylated amino acid, thus lowering the number of detected methylated peptides.

Table 5.12 comprises the average numbers and percentages of peptides with C-terminal and non-C-terminal methylation sites. Prior to the LysN and LysArginase digestion, the total number of methylated peptides detected in the non-biotinylated control was more than four times higher compared to the NHS-biotin treated samples. 74-78 % of the methylated peptides identified in the +NHS-biotin sample group featured their methylation site at the C-terminal amino acid before incubation with the second proteolytic enzyme. This proportion was lower in the corresponding non-biotinylated controls (59-60 %).

The high proportion of methylation at the C-terminal amino acid prior to the second digestion indicates that trypsin was able to cleave adjacent to methylated lysine and arginine residues. Therefore, the reduction of methylated peptides detected in the double digested samples might have been caused by the removal of the modified amino acid after incubation with LysN and LysArginase.

**Table 5.12: Average numbers (+/- standard deviation) and percentages of peptides with a C-terminal and non-C-terminal methylation site.**

| | | | # total meth. pep. | # pep. meth. C-terminus | # pep. meth. not C-terminus |
|---|---|---|---|---|---|
| Biotinylated peptides | *before LysN* | *+NHS-Biotin* | 85 ± 9 | 63 ± 5 (74 %) | 22 ± 4 (26 %) |
| | | *-NHS-Biotin ctrl* | 354 ± 10 | 214 ± 9 (60 %) | 141 ± 16 (40 %) |
| | *before LysArg* | *+NHS-Biotin* | 82 ± 12 | 64 ± 10 (78 %) | 18 ± 4 (22 %) |
| | | *-NHS-Biotin ctrl* | 343 ± 25 | 203 ± 6 (59 %) | 140 ± 19 (41 %) |

### 5.2.2. Derivatization-based method – Investigations of $N^{\alpha}$-selective peptide derivatization

The second workflow tested for enhancing the identification of lysine PTM containing peptides, is based on the selective derivatization of the alpha amino group present at peptides' N-termini after tryptic digestion. Figure 5.22 shows an overview of the four different derivatization techniques used in the initial experiment within the present study. N-terminal selective transamination was performed according to the procedure published by Sonomura et al. (2011). Here, the N-terminal amino group of the peptide was substituted by a carbonyl group derived from glyoxylic acid. For $N^{\alpha}$-selective acetylation, peptides were incubated with acetic acid anhydride like described by Mikami et al. (2012). N-terminal propionylation was performed similarly. According to the method published by Chen et al. (2017), selective reductive alkylation of the N-terminal amino group was performed by incubating the peptides with benzaldehyde at pH 6.1 in the presence of cyanoborohydride as a reducing agent.

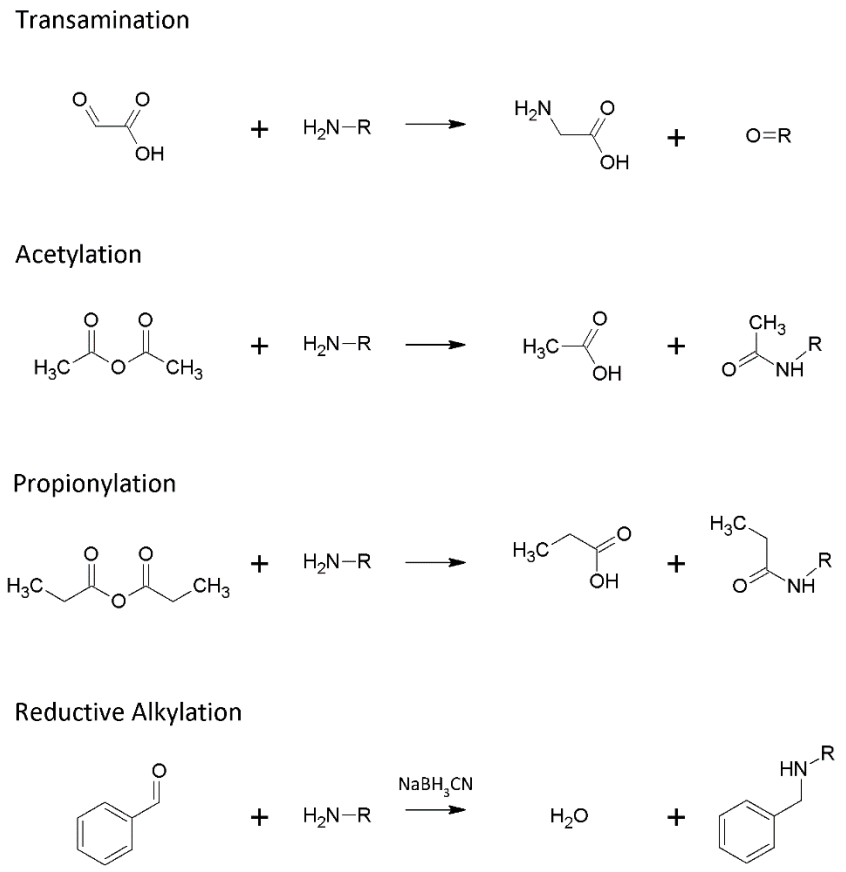


**Figure 5.22: Overview of the chemical reactions used for $N^{\alpha}$-selective derivatization of peptide N-termini.**

#### 5.2.2.1. Single peptide-based evaluation of different $N^{\alpha}$-selective derivatization techniques

In order to evaluate the mass shifts obtained by the $N^{\alpha}$-selective derivatization methods, a synthetic peptide containing an internal lysine residue was modified by the different techniques. After its modification, the peptide was incubated with NHS-LC-biotin or NHS-biotin in order to detect remaining free primary amine groups within the sequence (Figure 5.23A). Here, biotinylation with NHS-LC-biotin led to a mass shift of 339 m/z whereas utilization of NHS-biotin was associated with a mass shift of 226 m/z. Peptide analysis on MS1 level was performed by MALDI-TOF MS.

Figure 5.23B shows the peaks detected for the transaminated sample group. Single (1870.9 m/z) and double biotinylation (2209.9 m/z) was observed when incubating the precursor peptide (1531.7 m/z) with NHS-LC-Biotin. Transamination of the non-biotinylated peptide was associated with the expected mass shift of -1 m/z (1530.7 m/z). However, a second, unexpected peak at 1604 m/z was detected within this sample, thus indicating the occurrence of a side reaction. Like the transaminated peptide, this side product was singly biotinylated after incubation with NHS-LC-Biotin (1869.6 m/z and 1943.8 m/z).

In case of the acetic acid anhydride treated sample, mass shifts of 42 m/z and 84 m/z, corresponding to the singly (1573.7 m/z) and doubly acetylated (1615.7 m/z) precursor peptide, were detected (Figure 5.23C). Biotinylation of this sample was associated with the detection of a singly acetylated, biotin-containing peptide at 1912.8 m/z.

Comparable to the acetic acid anhydride treated sample, single (1587.7 m/z) and double propionylation (1643.7 m/z) was observed when incubating the precursor peptide with propionic acid anhydride (mass shifts of 56 m/z and 112 m/z) (Figure 5.23D). After NHS-LC-Biotin based biotinylation of the anhydride treated sample, a peptide, featuring a single propionylation and biotinylation site was detected (1926.9 m/z).

Single (1757.8 m/z) and double biotinylation (1983.9 m/z) was observed when incubating the precursor peptide with NHS-Biotin (Figure 5.23E). Reductive alkylation of the precursor peptide was associated with the expected mass shift of 90 m/z (1621.6 m/z). However, a second peak detected at 1711.8 m/z within this sample indicates a double alkylation of the precursor peptide. Incubation of the alkylation-modified sample with NHS-biotin was associated with the detection of a singly alkylated, biotin-containing peptide at 1847.8 m/z.

The detection of doubly acetylated, propionylated and alkylated peptides indicates a non-selective modification of the peptide N-terminus and the lysine side chain by the different derivatization techniques. Although the possibility of a double alkylation at the peptide N-terminus has been described by Chen et al. (2017), such a peptide would be biotinylatable by NHS-biotin at the internal lysine residue. A peak corresponding to a double alkylated and

biotinylated peptide was not observed thus further highlighting peptide alkylation at the N-terminus and the lysine side chain.

Even though the derivatization techniques might not be 100 % selective, reliable conclusion about the reaction stoichiometry cannot be drawn based on the mass spectrometry data as differences in the ionization behavior between the peptide species influence the signal intensity. Additionally, the findings described here for the synthetic model peptide might not be easily transferrable to other peptides. Therefore, the acetylation-, propionylation- and alkylation-based $N^{\alpha}$-selective derivatization techniques were also tested on complex peptide mixtures. Combined with LC-MS2 measurements, these investigations were assumed to yield a more detailed perspective regarding the reaction selectivity and in allowing a more representative evaluation of the different methods. The transamination technique was not further investigated as formation of unknown reaction side products would interfere with proper peptide identification during analysis of the MS data.

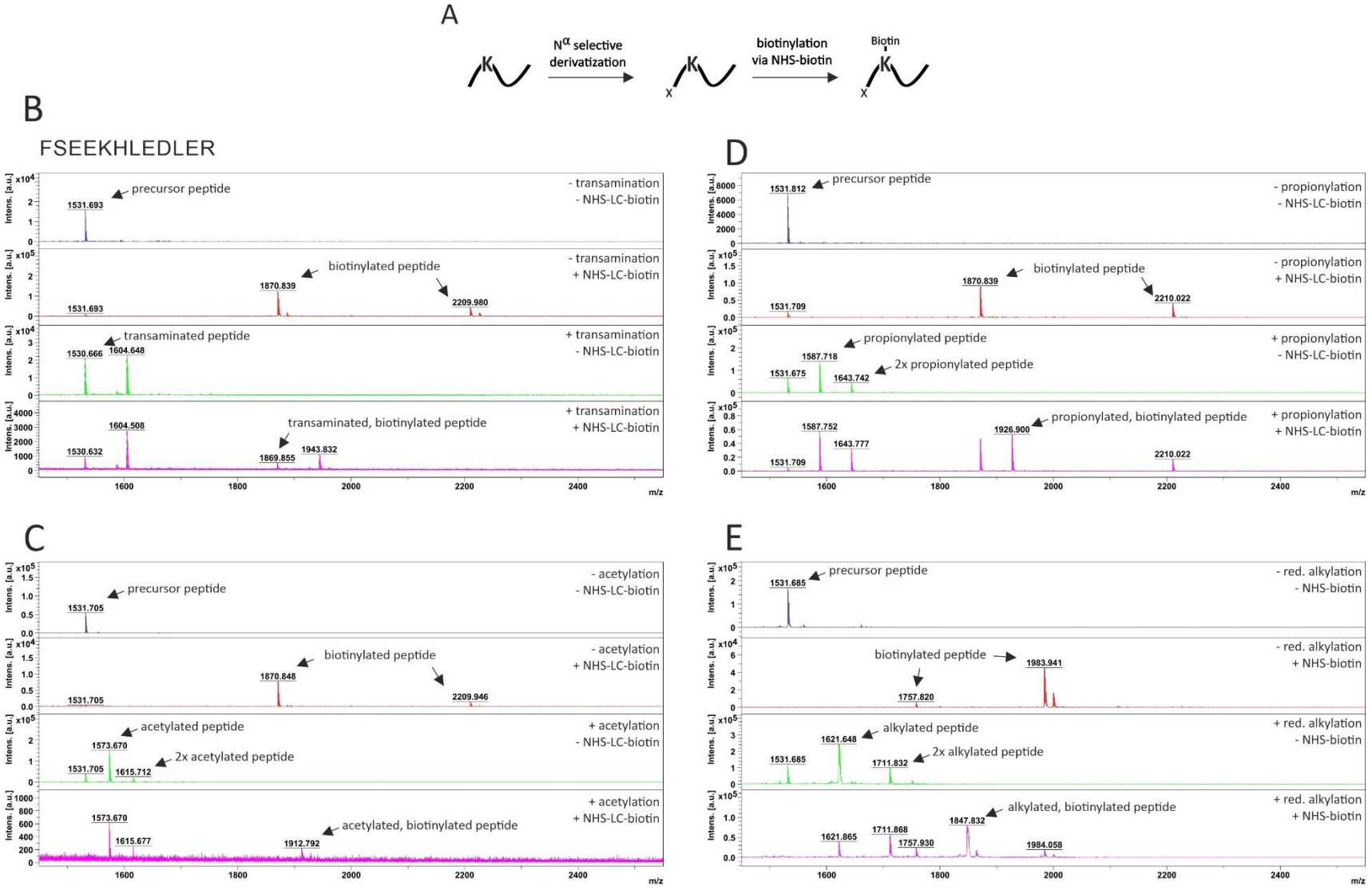


**Figure 5.23: Investigation of different Nα-selective derivatization techniques at single peptide level.**
The synthetic peptide was derivatized and subsequently biotinylated by NHS-LC-biotin or NHS-Biotin in order to identify remaining primary amine groups present within the sequence (A). The X indicates the derivatized amino group. The transamination- (B), acetylation- (C), propionylation- (D) and reductive alkylation derivatization method (E) were tested regarding their selectivity towards peptides' alpha amino group. MS1 data acquisition was performed by MALDI-TOF MS.

#### 5.2.2.2. $N^{\alpha}$-selective derivatization of a complex protein mixture

For investigating the different derivatization techniques regarding their selectivity towards the peptide N-terminus in a complex sample, HEK proteins were digested with trypsin. Afterwards, the tryptic peptides were derivatized by $N^{\alpha}$-selective acetylation, propionylation and reductive alkylation (Figure 5.24A). The experiment was performed in technical triplicates (tr1-3). Peptide analysis was performed by LC-MS2 using a Dionex LC-system coupled to an LTQ Orbitrap Velos mass spectrometer. The Mascot search engine implemented in the Proteome Discoverer software was used to search raw data against a human reference database with the single derivatizations set as variable modifications according to the sample.

In LC-MS2 data analysis, only mass shifts defined as variable modifications will appear in the final output of the processing results. This hinders the identification of side products occurring during the chemical derivatization processes of peptides, as any undefined mass shift will not be identified as a PSM by the search algorithm. Nevertheless, the occurrence of such side products with a high frequency/abundance increases the probability that these peptides will be fragmented in the data-dependent MS data acquisition mode. Therefore, the number of MS2 spectra increases but as these fragment ions do not match to any expected peptide feature, the number of PSMs will not rise. As a result of that, the percentage of matched MS2 spectra can be used as indication for the occurrence of highly abundant side products during the derivatization process. Table 5.13 shows the number of MS2 spectra and PSMs identified by a combined analysis of the three replicates for each sample group. For all derivatization techniques, 59 to 60 % of the MS2 spectra were assigned to a certain peptide feature. This indicates that unexpected side reactions were not highly abundant, as the same percentage of identifications was observed for the non-derivatized sample (input).

**Table 5.13: Number of MS2 spectra and PSMs identified for the different derivatization techniques as well as for the input.**
HEK 293 proteins were digested and subsequently derivatized by acetylation, propionylation or reductive alkylation. A non-derivatized samples served as a control (input). The experiment was performed in three technical replicates. The peptide mixtures were analyzed by LC-MS2. Raw data were searched against a human reference database with the different derivatizations set as variable modifications

| | # MS2 spectra | # PSMs | % matched spectra |
|---|---|---|---|
| **input (w/o derivatization)** | 122,645 | 72,702 | 59 |
| **acetylation** | 121,951 | 73,546 | 60 |
| **propionylation** | 121,566 | 73,057 | 60 |
| **red. alkylation** | 125,268 | 73,881 | 59 |

For data analysis on peptide group level, information about the derivatization sites were fused to the amino acid sequence. Afterwards, redundant sequence entries were removed in the single replicates.

Figure 5.24B shows the number of derivatized and underivatized peptides identified in each replicate of the different sample groups. No distinction was made between modifications occurring at the N-terminus or the lysine residue. Approx. 16,000 peptides were detected in the different replicates of the non-derivatized peptide sample (input). Compared to that, roughly 18,000 peptides were obtained in the acetylated sample group. Among those, 44 % (approx. 8,000 peptides) were identified as being acetylated. These 44 % also comprise endogenous protein N-terminal acetylation sites as this modification cannot be distinguished from peptide derivatization caused by the incubation with the acetic anhydride. Nevertheless, as only 76-80 acetylated peptides derived from protein N-termini were identified in the acetic anhydride treated samples, their contribution to the total number of acetylation sites is rather low. In the propionylated sample group, a total number of approx. 18,000 peptides were detected in the single replicates. Here, approx. 33 % of the peptides were propionylated. A slightly lower number of total peptides were identified in the reductive alkylation sample group (approx. 17,400 peptides). However, this sample group contained the highest proportion of derivatized peptides (88 %).

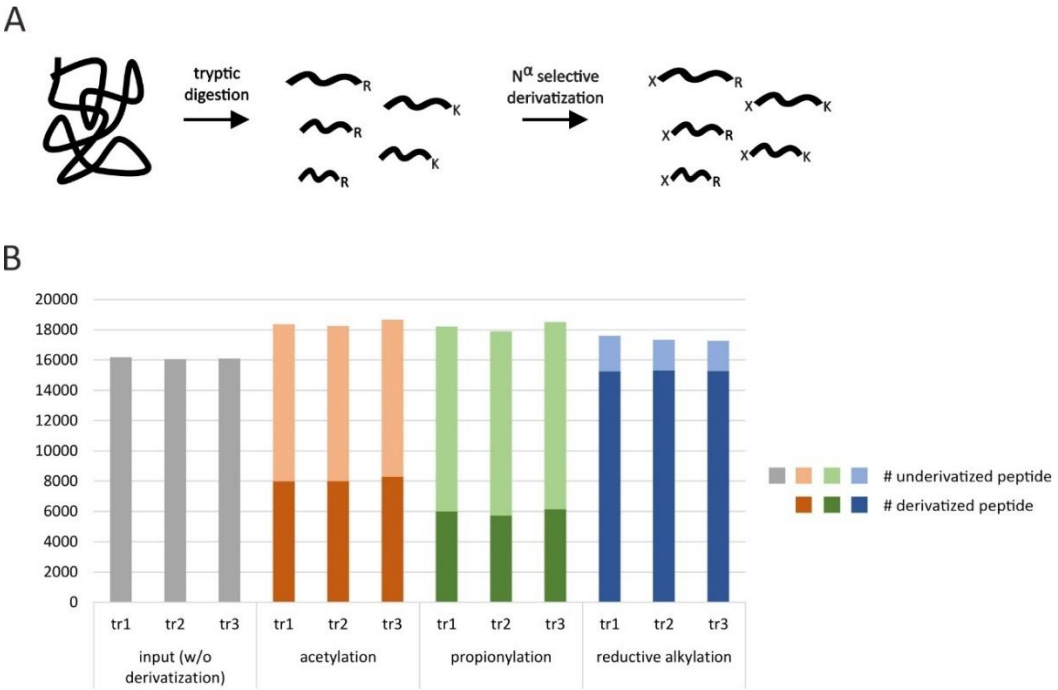


**Figure 5.24: Number of derivatized and underivatized peptides in the different sample groups.**
Proteins were digested and subsequently derivatized (A). The X indicates the derivatized amino group. The different numbers of derivatized and underivatized peptides identified in the replicates of the different sample groups are shown in B.

In order to investigate the reproducibility of the derivatization techniques, the overlap of derivatized peptides identified in the single replicates of the different sample groups are shown in a Venn diagram (Figure 5.25). The size of the Venn diagrams reflects the total number of derivatized peptides detected for the different sample groups. In case of peptide acetylation by acetic anhydride, 71 % of the acetylated peptides were found in all three replicates (6,676 peptides). Compared to that, 4,688 derivatized peptides were identified in all replicates of the propionylated sample group (67 %). The highest number of derivatized peptides were detected after reductive alkylation. Here, 68 % of the alkylated peptides were found in all replicates (12,199).

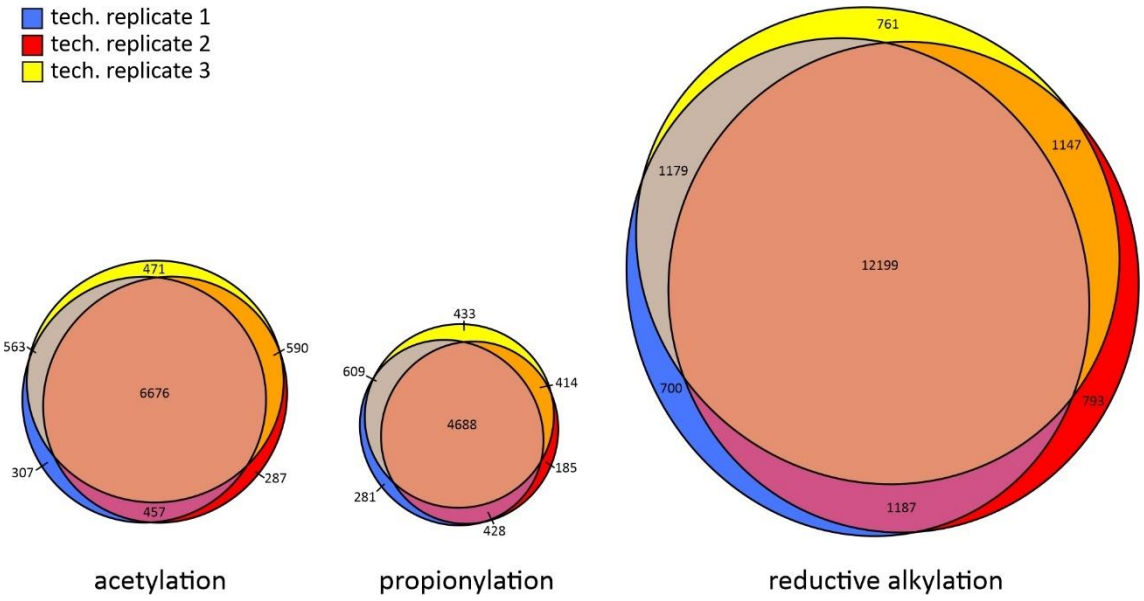


**Figure 5.25: Overlap of the derivatized peptides identified in the single replicates of the different sample groups.** The size of the Venn diagram reflects the total number of derivatized peptides found for the different derivatization techniques.

$N^{\alpha}$-selectivity of the different techniques was investigated by analyzing the derivatization site of peptides identified in all three replicates (Figure 5.26). The highest proportion of N-terminal peptide derivatization was detected for the reductive alkylation sample group (92 %). However, comparable $N^{\alpha}$-selectivity was observed for the acetylation- and propionylation-based techniques (88 % and 85 %). In case of these two derivatization methods, approx. 10 % of the peptides featured their modification in the side chain of lysine. Compared to that, a derivatization of the lysine residue was only detected for 3 % of the alkylated peptides. A modification of both, the peptide N-terminus and the lysine side chain, was identified for 5 % of the derivatized peptides of the reductive alkylation and propionylation sample group. Among the acetylated peptides, such a double modification was only detected for 2 % of the peptides.

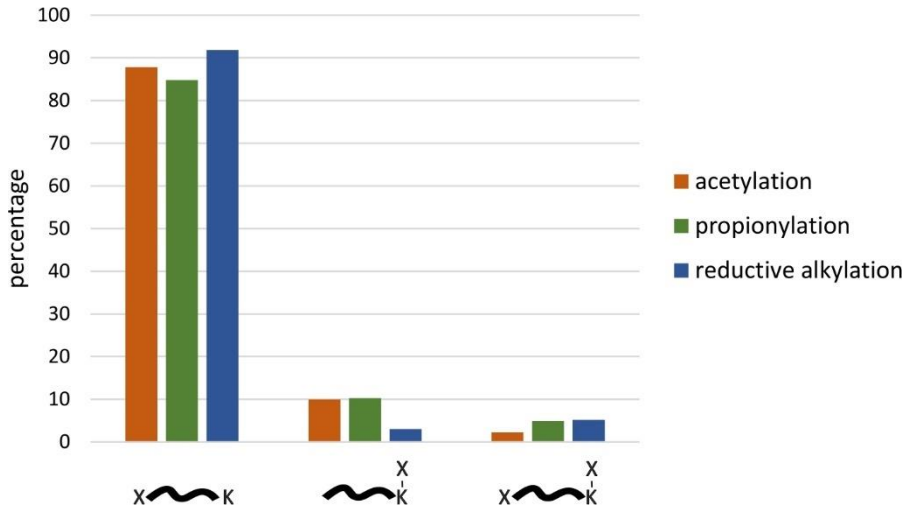


**Figure 5.26: Proportion of derivatization sites detected for peptides found in all three replicates of the different sample groups.**
The X indicates the position of the derivatized amino group.

A high $N^{\alpha}$-selectivity was observed for all derivatization techniques tested within this study. Nevertheless, the results indicate that utilization of the reductive alkylation-based technique in the $N^{\alpha}$-selective derivatization workflow might be advantageous as this method yields the highest number of derivatized peptides combined with a good derivatization reproducibility. Therefore, this technique was used for investigating the capability of the derivatization-based workflow to enhance the identification of lysine PTM-containing peptides.

### 5.2.2.3. Validating the $N^{\alpha}$-selective derivatization workflow for enhancing the identification of lysine modified peptides

The usability of the $N^{\alpha}$-selective derivatization workflow for increasing the identification of lysine modified peptides was investigated by using HEK protein lysate as a starting material. After tryptic digestion, peptide's N-termini were selectively derivatized by reductive alkylation. Subsequently, remaining primary amines were biotinylated with NHS-biotin. The last step of the workflow comprised the streptavidin-based depletion of biotinylated peptides. After each step of the workflow, a sample was taken as a control. The experiment was performed in three technical replicates. Samples were analyzed by LC-MS2 using a Dionex-LC system coupled to an LTQ Orbitrap Velos mass spectrometer. Note that the reductive alkylated samples investigated in section 5.2.2.2 were used as a starting material in this experiment.

The MS data of the derivatized peptide samples incubated with streptavidin were processed with the PeaksPTM algorithm implemented in the PEAKS X software. As mentioned in the section 5.2.1.4, this algorithm enables the identification of unspecified modifications. Table 5.14

comprises modifications in NHS-biotin treated samples identified for more than 1 % of the peptides. More than 80 % of the peptides identified in the biotinylated samples featured an alkylation at the peptide N-terminus or the side chain of lysine. Double alkylation either at the lysine residue or the peptide N-terminus was observed for approx. 12 % of the peptides detected in the biotinylated samples. Additionally, more than 9 % of the peptides were modified by oxidation at methionine or propionamide at cysteine due to alkylation of thiol groups with acrylamide in these sample groups. Methylation at lysine and arginine was annotated as one modification entry by the PeaksPTM algorithm. In the NHS-biotin treated samples, 1.3-1.5 % of the peptides were reported as being methylated at lysine or arginine residues. The vast majority of these methylation sites were found at arginine side chains. Compared to that, lysine methylations were almost exclusively identified in the non-biotinylated samples.

**Table 5.14: PeaksPTM analysis of peptide samples after streptavidin incubation ($N^{\alpha}$-selective derivatization workflow).**
Percentage of different peptide modifications identified by analyzing the derivatized and streptavidin incubated samples with the PeaksPTM search implemented in the PEAKS software (only NHS-biotin treated samples are shown). Besides the expected variable modifications, the PeaksPTM search also allows the identification of unspecified PTM present in the Unimod database and added manually prior to the data processing.

| | Technical replicate 1 | Technical replicate 2 | Technical replicate 3 |
|---|---|---|---|
| **Alkylation (K/N-term))** | 83.2 % | 81.3 % | 80.8 % |
| **Oxidation (M)** | 19.4 % | 20.2 % | 19.2 % |
| **2x Alkylation (K/N-term)** | 12.0 % | 13.4 % | 14.0 % |
| **Propionamide (C)** | 10.6 % | 9.7 % | 11.0 % |
| **Deamidation (NQ)** | 1.5 % | 1.4 % | 1.5 % |
| **Methylation (KR)** | 1.3 % | 1.5 % | 1.5 % |

Non-restrictive search algorithms such as PeaksPTM might be prone to false discoveries due to the increased search space. Therefore, based on the modifications identified by the PeaksPTM software, the raw data of the streptavidin incubated samples were reprocessed using the Mascot search engine. Here, alkylation (at K/N-term), double alkylation (at K/N-term), acetylation (at protein N-term), oxidation (at methionine), biotinylation (at K/N-term) as well as methylation (at R/K) were set as variable modifications. Samples taken during the different steps of the workflow were analyzed accordingly. For data processing, raw files belonging to the same step within the workflow (e.g. +NHS-biotin & -NHS-biotin) were processed together. The Percolator algorithm was used in order to control the FDR (<0.01) (Käll et al. 2007).

Figure 5.27 depicts the percentage of reductive alkylated and biotinylated PSMs as well as of PSMs with unmodified primary amines detected in the biotinylated and non-biotinylated

samples prior to streptavidin incubation. More than 90 % of the PSMs identified in the NHS-biotin treated sample and the non-biotinylated control featured a reductive alkylation site. Nevertheless, approx. 65 % of the PSMs in the non-biotinylated control featured at least one unmodified primary amine within their sequence. Compared to that, the proportion of unmodified primary amines detected in the NHS-biotin treated samples was strongly reduced (less than 3 %). In contrast, approx. 40 % of the PSMs identified in this sample group comprised at least one biotinylated amino acid thus suggesting a successful peptide biotinylation after NHS-biotin treatment.

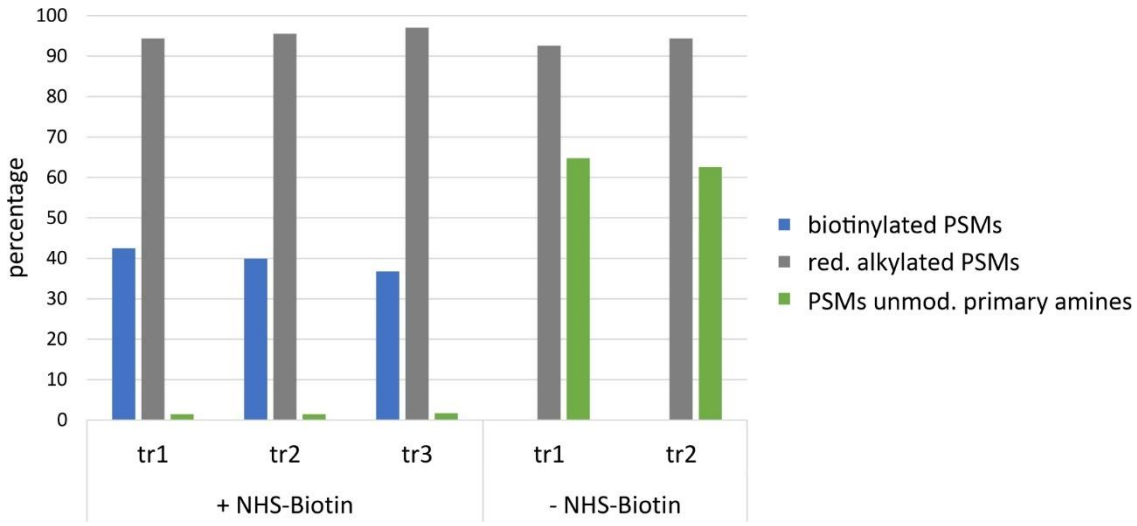


**Figure 5.27: Investigation of the percentage of biotinylated and reductive alkylated PSMs in different sample groups of the N$^{\alpha}$-selective derivatization workflow.**
Percentages of biotinylated and reductive alkylated PSMs as well as of PSMs with unmodified primary amine detected in NHS-biotin treated sample and the non-biotinylated control prior to streptavidin incubation are depicted.

Data analysis on peptide group level was performed by fusing information about methylation sites to the amino acid sequence. Afterwards, redundant sequence entries were removed for each replicate and sample group.

Figure 5.28 shows the average number (+/- standard deviation) of arginine and lysine containing peptides detected in the single steps of the N$^{\alpha}$-selective derivatization workflow. The highest number of peptide identifications was detected after tryptic digestion of the HEK protein lysate. Compared to that, less peptides were found in the samples derivatized by reductive alkylation (second bar, without SCX chromatography-based sample clean-up). Each additional step of the workflow was associated with a further loss of identifications. Interestingly, the identification loss is not uniform throughout the different peptide species. Whereas the number of arginine containing peptides stayed nearly constant among the first three steps of the workflow, the percentage of lysine containing peptides decreased in the NHS-biotin treated samples compared

to the peptide population detected after reductive alkylation. After streptavidin incubation of the biotinylated samples, an increase in the proportion of arginine containing peptides was observed. In this sample group, only 10 % lysine containing peptides were detected. Therefore, the results indicate a shift in the peptide population towards arginine containing features after NHS-biotin treatment.

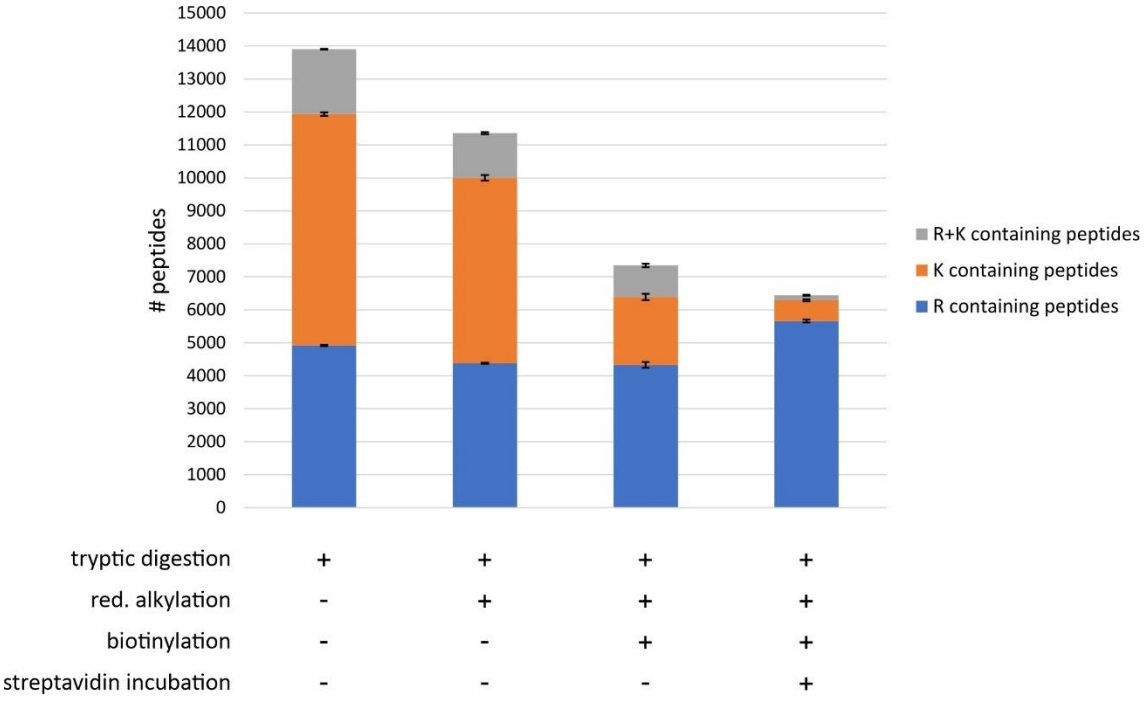


**Figure 5.28: Number of lysine and arginine containing peptides in the different sample groups of the Nα-selective derivatization workflow.**
Average number of lysine and arginine containing peptides (+/- standard deviation) detected in the single steps of Nα-selective derivatization workflow. Note that the reductive alkylated, non-biotinylated samples (second bar) were not purified by SCX chromatography.

The average number of methylated peptides and PSMs (+/- standard deviation) detected in the different sample groups of the Nα-selective derivatization workflow are listed in table 5.15. Here, the tryptic digested sample group is the same as the one analyzed in the serial digestion workflow (see section 5.2.1.4). Less than 0.1 % of the peptides detected after tryptic digestion were methylated. Similar proportions were observed after reductive alkylation, although the total number of peptides identified in this group was reduced compared to the tryptic digested samples. SCX chromatography-based sample clean-up of the biotinylated and non-biotinylated peptides was associated with a further reduction in the number of peptide identifications. Here, the peptide loss was higher in the NHS-biotin treated samples compared to the non-biotinylated controls. In contrast to the tryptic digested and alkylated sample groups, NHS-biotin treatment followed by SCX chromatography-based sample clean-up was associated with an increased

identification of PSMs featuring a methylated arginine residue (191 ± 10). Here, also higher numbers of arginine methylated peptides (118 ± 5) were detected. In comparison, a slightly lower amount of methylarginine containing peptides was observed in case of the non-biotinylated, SCX chromatography purified samples. However, this group featured the highest number of lysine methylated peptides (155) and PSMs (299) among all samples taken during the derivatization workflow. Compared to the corresponding non-depleted sample group, incubation of the biotinylated peptides with streptavidin was associated with a slight reduction in the total amount of PSMs and peptides detected during LC-MS2 analysis. Whereas the number of identified methylated peptides remained nearly unaltered in the biotinylated and streptavidin incubated samples, an increase in the proportion of peptides featuring an arginine methylation was observed. A slight decrease in the total number of peptides and PSMs was detected when incubating the non-biotinylated samples with streptavidin. Here, streptavidin incubation was also associated with a loss of lysine methylated peptides (109).

**Table 5.15: Average number and standard deviation of peptides and PSMs found in the different sample groups of the $N^{\alpha}$-selective derivatization workflow (n=3).**
The percentage of methylated peptides/PSMs compared to the total number of peptides/PSMs is given in parenthesis. * indicates mean values of samples groups comprising only two technical replicates. For these sample groups, the standard deviation was not calculated.

| | | # total pep. | # meth. pep. [K] | # meth. pep. [R] | # meth. pep. [K+R] | # total PSMs | # meth. PSMs [K] | # meth. PSMs [R] | # meth. PSMs [K+R] |
|---|---|---|---|---|---|---|---|---|---|
| Tryptic peptides | | 13935 ± 66 | 7 ± 1 (0.05 %) | 9 ± 1 (0.07 %) | 2 ± 1 (0.02 %) | 21046 ± 352 | 26 ± 2 (0.13 %) | 42 ± 1 (0.20 %) | 6 ± 1 (0.03 %) |
| Red. alk. Peptides | | 11381 ± 112 | 11 ± 1 (0.09 %) | 11 ± 1 (0.10 %) | 3 ± 0 (0.03 %) | 21729 ± 328 | 29 ± 6 (0.13 %) | 38 ± 4 (0.17 %) | 8 ± 1 (0.04 %) |
| Biotinylated peptides | *+NHS-Biotin* | 7348 ± 220 | 15 ± 2 (0.20 %) | 118 ± 5 (1.60 %) | 1 ± 0 (0.01 %) | 11113 ± 623 | 4 ± 1 (0.04 %) | 191 ± 10 (1.72 %) | 2 ± 1 (0.02 %) |
| | *-NHS-Biotin ctrl* | 8666* | 155* (1.78 %) | 99* (1.14 %) | 1* (0.01 %) | 14017* | 299* (2.13 %) | 184* (1.31 %) | 1* (0.01 %) |
| Streptavidin incubated peptides | *+NHS-Biotin* | 6475 ± 66 | 11 ± 4 (0.17 %) | 117 ± 7 (1.80 %) | 1 ± 0 (0.02 %) | 8883 ± 174 | 3 ± 1 (0.03 %) | 201 ± 22 (2.26 %) | 4 ± 0 (0.05 %) |
| | *-NHS-Biotin ctrl* | 8469* | 109* (1.28 %) | 111* (1.31 %) | 3* (0.04 %) | 12704* | 196* (1.55 %) | 135* (1.06 %) | 3* (0.02 %) |

Data analysis of the $N^{\alpha}$-selective derivatized, biotinylated samples indicate an increased identification of arginine methylated peptides independent of streptavidin incubation. Similar observations were made for methylation at lysine residues in the SCX chromatography purified, non-biotinylated sample groups. The population of lysine and arginine methylated peptides identified in the single groups were compared in two Venn diagrams (Figure 5.29). Here, amino acid specific methylations found in two out of two replicates (-NHS-Biotin ctrl) or in at least two out of three replicates (+NHS-Biotin) were used for the comparison.

The highest number of unique lysine methylations was observed in the non-biotinylated and non-streptavidin incubated sample group. Compared to that, 43 methylated lysine residues were detected after incubating the non-biotinylated peptides with streptavidin. Additionally, an overlap of 39 lysine methylated peptides was identified between these two sample groups. In contrast, no unique lysine methylation was observed for the NHS-biotin treated samples. However, peptide biotinylation was associated with an increased identification of arginine methylations. Here, incubation of the NHS-biotin treated sample with streptavidin was linked to an unique identification of 34 methylations at arginine residues. In comparison, 43 unique arginine methylated peptides were detected in the non-streptavidin incubated samples. 11 and 13 unique arginine methylated peptides were observed in the two non-biotinylated sample groups, respectively. In total, 32 arginine methylation sites were shared between all samples.

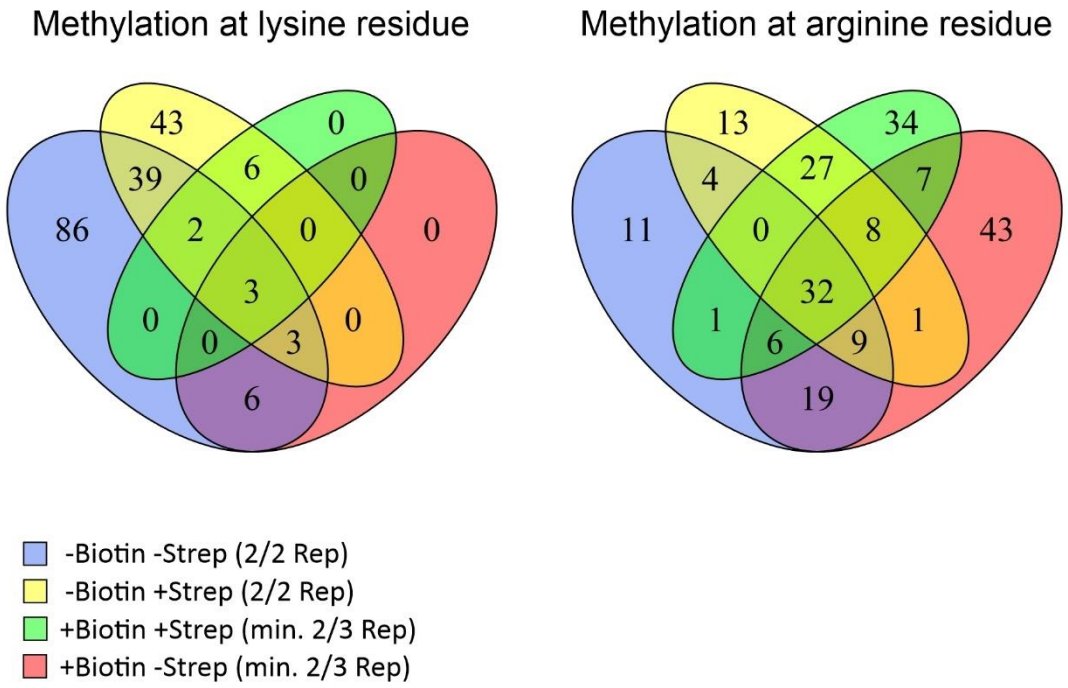


**Figure 5.29: Comparison of methylated peptides detected in different samples groups of the $N^{\alpha}$-selective derivatization workflow.**
Methylated peptides found in two out of two replicates (-NHS-biotin ctrl) or in at least two out of three replicates (+NHS-biotin) were used for generating the Venn diagrams.

In order to evaluate the reproducibility of PTM-identifications with the $N^{\alpha}$-selective derivatization workflow, the methylated peptide populations detected in the three biotinylated and streptavidin incubated replicates were compared (Figure 5.30). Here, 65 % (105 peptides) of the methylated peptides were found in all replicates thus indicating the reproducibility of the identification of peptide methylations by this workflow.

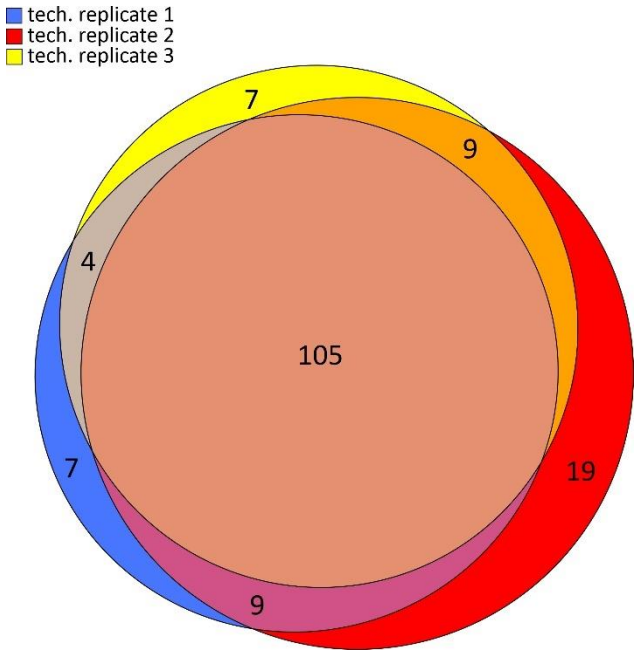


**Figure 5.30: Comparison of the methylated peptides identified in the three replicates after biotinylation and streptavidin-based depletion.**

### 5.2.3. Comparison of methylated peptides identified after SCX chromatography-based sample clean-up in both workflows

The data obtained during the investigations of the two workflows suggest an SCX chromatography-based increase of methylated peptides. However, as the N-termini of the peptides are alkylated prior to biotinylation and SCX chromatography-based sample clean-up within the $N^{\alpha}$-selective derivatization workflow, the populations of methylated peptides might differ compared to those detected after SCX chromatography-based peptide purification during the serial digestion workflow. The overlaps within the populations of methylated peptides identified in the different samples are depicted by two Venn diagrams (Figure 5.31). For both, the LysN- and the LysArginase-based serial digestion workflow, three NHS-biotin treated and three non-biotinylated samples were prepared. The data of these six samples were combined prior to the comparison. Here, methylated peptides detected in at least four out of six replicates were used. In case of the SCX chromatography purified samples obtained during the $N^{\alpha}$-selective

derivatization workflow, the comparison was based on methylated peptides found in two out of two (-NHS-Biotin ctrl) or in at least two out of three replicates (+NHS-Biotin).

The highest number of unique lysine methylation was detected for the non-derivatized and non-biotinylated samples (157 peptides). Within the derivatized, non-biotinylated sample group, 88 unique methyllysines were identified. Compared to that, unique lysine methylated peptides were not detected in the two NHS-biotin treated sample groups. In contrast, peptide biotinylation was associated with an increased number of uniquely identified methylated arginine residues compared to the non-biotinylated samples. Therefore, the results indicate a complimentary identification of methylated peptides among the different sample groups.

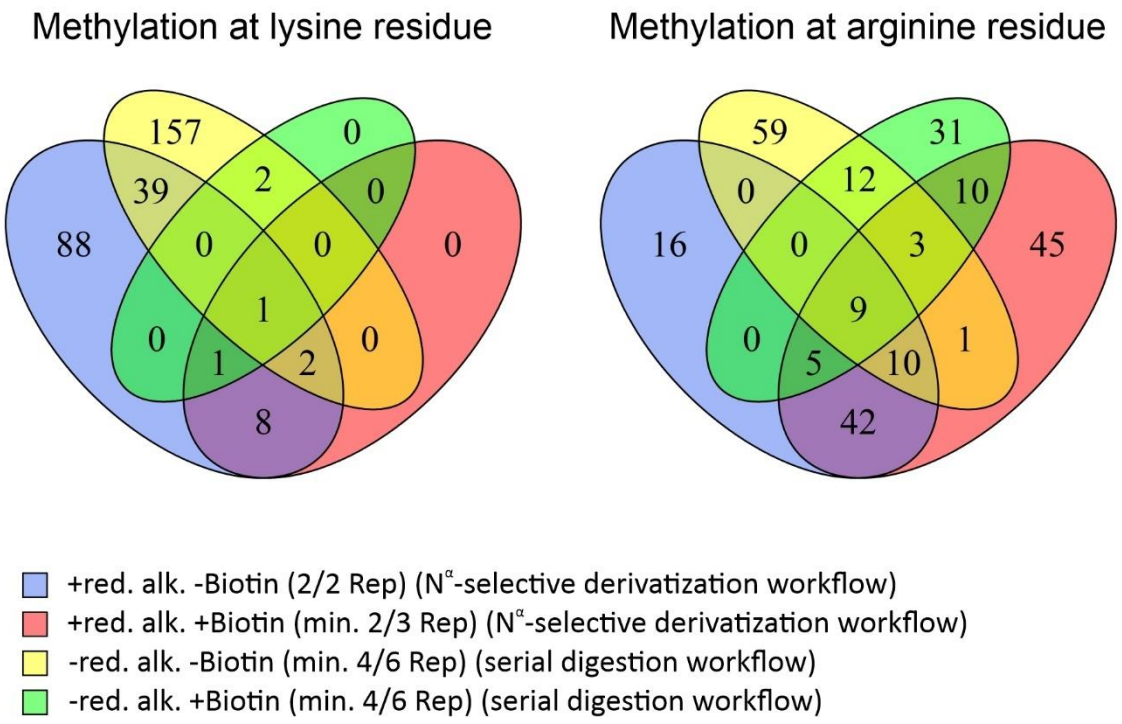


**Figure 5.31: Comparison of methylated peptides detected after SCX chromatography-based sample clean-up in the serial digestion and the Nα-selective derivatization workflow.**
In case of sample groups derived from the serial digestion workflow, methylated peptides found in at least four out of six replicates were used for the comparison. For the Nα-selective derivatized sample groups, methylated peptides found in two out of two (-NHS-biotin ctrl) or in at least two out of three replicates (+NHS-biotin) were used for generating the Venn diagrams.

# 6. Discussion

## 6.1. SNAPIN, a multifunctional protein with altered phosphorylation pattern upon elevation of cAMP levels

Inside the cell, cAMP is generated by Acs in response to the activation of stimulatory GPCR. Glucagon, a peptide hormone secreted by pancreatic cells at low plasma glucose levels, is a known ligand mediating the activation of this pathway (Jelinek et al. 1993; reviewed by Habegger et al. 2010). The elevation of intracellular cAMP levels leads to an activation of protein kinase A (Walsh et al. 1968; Tao et al. 1970). In turn, PKA triggers the production of free glucose inside the cells by stimulating processes such as glycogenolysis, thus playing a key role in the cellular response machinery after sensing deprivation of this monosaccharide (reviewed by Unger 1985).

The expression of genes encoding for lysosomal proteins is another process triggered under nutrient deprivation which correlates with an increase in macromolecule degradation (Sardiello et al. 2009; Settembre et al. 2011). Based on their contribution in starvation-induced catabolic processes, one could hypothesize a functional relationship between PKA and lysosomes. So far, Mucolipin 1 is the only known lysosomal membrane protein getting phosphorylated upon PKA activation (Vergarajauregui et al. 2008). In order to further investigate the influence of elevated intracellular cAMP levels on lysosomal processes, the initial part of the present study aimed at identifying cAMP-mediated changes in the phosphorylation status of lysosomal membrane and lysosome associated proteins.

### 6.1.1. FSK/db-cAMP treatment triggers PKA activation

FSK/db-cAMP mediated PKA activation was monitored by detecting the phosphorylation status at S133 of CREB. This amino acid residue of CREB has been shown to be a direct target of PKA (Montminy and Bilezikjian 1987; Gonzalez and Montminy 1989). Its phosphorylation is associated with the activation of this transcription factor thus mediating transcription of cAMP responsive genes (Montminy and Bilezikjian 1987; Gonzalez and Montminy 1989).

Within the present study, FSK/db-cAMP stimulation was associated with a strong increase in the p-CREB (S133) signal intensity compared to the non-treated control (Figure 5.1). As the CREB

protein level was not significantly affected by the treatment, the p-CREB signal observed after cell stimulation with FSK/db-cAMP was caused by phosphorylation of CREB at S133.

Besides PKA, several kinases such as PKB and the calcium/calmodulin-dependent protein kinase (CaMK) I & II have been demonstrated to mediate CREB phosphorylation at S133 (Sheng et al. 1991; Du and Montminy 1998). However, in order to mediate CREB phosphorylation upon FSK/db-cAMP treatment, kinase activity must be regulated by cAMP. In 2005, Delghandi et al. investigated the ability of several kinases directly or indirectly regulated by cAMP and $Ca^{2+}$ (PKA, PKB, mitogen-activated protein kinase p38 (MAPK p38), CaMKII) to phosphorylate CREB at S133 upon FSK treatment in NIH 3T3 cells. Among those, PKA was the only kinase directly catalyzing CREB phosphorylation whereas p38 triggered CREB-induced transcription in a PKA-dependent manner (Delghandi et al. 2005). Although these results suggest a rather specific activation of PKA upon increased intracellular cAMP levels, one has to keep in mind that kinase signaling networks are highly interlaced, thus potentially hampering the assignment of a modification site to a specific pathway. In addition to the crosstalk of different kinase signaling pathways, the discovery of EPACs as intracellular cAMP sensors further demonstrates the complexity of the networks affected by this second messenger (Kawasaki et al. 1998; Rooij et al. 1998). Although Delghandi et al. (2005) demonstrated that CREB phosphorylation is not affected by EPAC activation, other proteins and processes might also be regulated by synergistic or antagonistic action of cAMP sensors. Therefore, the assignment of one phospho-site as a PKA target also requires investigations of changes in the phosphorylation pattern upon PKA-specific inhibition when using elevated intracellular cAMP levels as a stimulus.

### 6.1.2. Elevation of intracellular cAMP levels leads to the identification of regulated phospho-sites

After demonstrating the successful activation of PKA upon FSK/db-cAMP treatment, cAMP-dependent changes in protein phosphorylation patterns were investigated. When analyzing whole cell lysates, the detection of an altered phospho-site abundance can either result from the activation of kinases and phosphatases or from changes in the protein degradation and expression. Here, a shift in protein homeostasis after cell treatment implies the activation of important regulatory processes. If the increase of the protein abundance correlates with an upregulation of one of its phospho-sites, kinase activation needs to mediate both, the elevation of the protein level as well as the phosphorylation of the raised number of the particular modification-site compared. Similarly, downregulation of phospho-sites caused by a treatment-induced reduction of protein expression or increased degradation might also require further modulation of kinase and phosphatase activity. Whether this modulation is needed depends on

the turnover rate of the affected protein. A short treatment-independent cellular half-life time or a stimulation-induced degradation of phosphoproteins diminish the abundance of phosphopeptides without modulating phosphatase activity.

Within the present study, PKA/EPAC were stimulated by increasing the intracellular cAMP level during a 30 min treatment of the cells with FSK/db-cAMP. Although the turnover rates are highly variable, a half-life of less than 5 hours in cell cycle arrested HeLa cells was only reported for a minority of proteins (Cambridge et al. 2011). This suggests that only few proteins will undergo significant turnover during the 30 min treatment applied in this study. Nevertheless, PKA as one of the major intracellular cAMP sensors has already been demonstrated to stimulate gene expression by phosphorylating the CREB transcription factor (Montminy and Bilezikjian 1987; Gonzalez and Montminy 1989). A detailed study about PKA induced changes in gene expression was performed by Zambon et al. (2005). Here, RNA analysis identified more than 700 genes as being at least 1.5 fold up- and downregulated upon treatment of murine lymphoma cells with a cAMP analog for two hours compared to the 0 hour control group (Zambon et al. 2005). Besides influencing the protein level by regulating gene expression, elevations of cAMP levels have also been shown to induce degradation of short-lived proteins via the ubiquitin-proteasome pathway (Lokireddy et al. 2015). Considering these effects of cAMP on modulating protein levels, the necessity of monitoring protein abundances when investigating cAMP-dependent changes in phosphorylation events in a long-term treatment becomes apparent. However, protein levels were not assumed to be altered during the 30 minute FSK/db-cAMP treatment applied within this study.

Known PKA target sites of CaMKK1, PFKFB2 and CAD were identified as being upregulated in phosphopeptides from the whole cell lysate upon FSK/db-cAMP treatment (PhosphoSitePlus online repository; phosphosite.org, retrieved 24.10.2019) (Carrey et al. 1985; Okuno et al. 2001; Pozuelo Rubio et al. 2003) (Table 5.2). This indicates the successful activation of PKA by the stimulus applied in this experiment.

Besides these known PKA target sites, several phosphopeptides, so far unknown to be regulated upon PKA activation, were identified (according to PhosphoSitePlus, retrieved 24.10.2019) (Figure 5.2, table 5.1, table 5.2, table 5.3). For example, the phosphatidylinositol 3-phosphate 5-kinase (PIKFYVE) phospho-site detected as being upregulated after FSK/db-cAMP treatment has been previously identified as an AMP-activated protein kinase and PKB target (Berwick et al. 2004; Liu et al. 2013). In these two studies, contradictory results regarding the impact of the phosphorylation on PIKFYVE activity were obtained. Whereas Liu et al. (2013) demonstrated that phosphorylation at S307 did not affect the activity of the enzyme, Berwick et al. (2004) observed

an increase level of the PIKFYVE enzymatic product phosphatidylinositol 3,5-bisphosphate ($PI(3,5)P_2$) after phosphorylating this amino acid *in vitro*. Nevertheless, substitution of this serine residue in the PKB consensus motif to alanine has been shown to be associated with impaired epidermal growth factor receptor (EGFR) degradation (Er et al. 2013). Supported by other experiments in that study, the authors concluded a correlation between the EGFR breakdown and the $PI(3,5)P_2$ level, thus indicating PIKFYVE and its phospho-site as a regulator in receptor trafficking (Er et al. 2013). The FSK/db-cAMP-dependent regulation of the S307 phospho-site identified in the present study might suggest the intracellular cAMP level as a regulator of PIKFYVE activation.

In contrast to the upregulated phopsho-site found for PIKFYVE, FSK/db-cAMP treatment was also associated with a downregulation of phosphorylation events at certain amino acid residues (Figure 5.2, table 5.1, table 5.3). For example, such a downregulation was identified for the Ras-related protein Rab-12 (Table 5.3). Rab-12 belongs to the family of Ras GTPases and has been demonstrated to mediate lysosome-dependent degradation of the transferrin receptor in mouse embryonic fibroblasts (MEF) cells (Matsui et al. 2011). Considering the potential role of the PIKFYVE phospho-site identified within the present study, the significant downregulation of Rab-12 might suggest a role of cAMP in receptor degradation. This hypothesis is further supported by the study of Salazar and González (2002) which demonstrated that PKA inhibition results in a diminished ligand-activated EGFR degradation independent from alterations in receptor-ligand internalization.

Two phospho-sites of the CREB-regulated transcription coactivator 3 (CRTC3) have been identified as being highly downregulated after FSK/db-cAMP treatment (Table 5.3). CRTC3 belongs to the transducers of regulated CREB (TORC) family which act as CREB1 coactivators (Iourgenko et al. 2003; Conkright et al. 2003). The regulation of TORC activity has been well studied for CRTC2. Here, the salt-inducible kinase 2 (SIK2) phosphorylates CRTC2, thus mediating its binding to 14-3-3 proteins and promotes its translocation from the nucleus to the cytoplasm (Screaton et al. 2004). Similarly, SIK1 has been demonstrated to be able to phosphorylate and deactivate all three members of the TORC family suggesting the SIKs as important modulator of these transcriptional coactivators (Katoh et al. 2006). In turn, phosphorylation of SIK by PKA is associated with a downregulation of their kinase activity which directly affects the TORC phospho-pattern and TORC-mediated gene expression (Screaton et al. 2004; Sonntag et al. 2018). The two CRTC3 phospho-sites identified within the present study (S329 and S370) are known SIK targets (Clark et al. 2012). Together with S62 and S162, these phospho-sites are important for the regulation of CRTC3's function as a transcriptional coactivator (Clark et al. 2012). CRTC3 in vitro phosphorylation at S162, S329 and S370 with SIK1-3 was associated with

an increased binding to 14-3-3 (Clark et al. 2012). Therefore, the data presented here are in line with the current literature which suggests SIK inactivation upon PKA stimulation as being associated with a phosphorylation decrease of CRTC3 thus inducing the expression of its target genes (Sonntag et al. 2018).

### 6.1.3. FSK/db-cAMP treatment alters the phosphorylation pattern of lysosomal and lysosome-associated proteins

cAMP-dependent changes in the phosphorylation pattern of lysosomal and lysosome-associated proteins were investigated by enriching these organelles followed by their separation into a soluble and membrane fraction. The effect of changes in protein expression and degradation on the detection of regulated phospho-sites has been described in detail in the previous section. However, dealing with enriched organelles further complicates the interpretation of phospho-data sets as lysosome-associated proteins might dissociate after stimulation, thus being identified with a downregulated phospho-site although the phosphorylation pattern might not necessarily change. Similarly, treatment induced membrane remodeling might also be associated with changes in the composition of posttranslationally modified proteins potentially being reflected in the data set as a regulated PTM-site. Therefore, investigating the non-phospho-enriched lysosomal fractions plays an important role in order to distinguish between proteins with regulated phosphorylation sites and those with changed subcellular localization after cell stimulation.

No significantly regulated phosphopeptides were identified in the soluble lysosomal fraction. Among the highly regulated phosphopeptides in this fraction, the two non-lysosomal proteins Golgin subfamily member 1 and PRRCA2 were found. In contrast, 238 proteins found in at least two out of three PKA and DMSO treated replicates featured “lysosome” as a gene ontology (GO) annotation in the non-phospho-enriched proteomic data set of the soluble lysosomal fraction. Therefore, the absence of phosphopeptides derived from lysosomal enzymes in the soluble fraction after phospho-enrichment might have been rather caused by the low stoichiometry of these phospho-sites present within these samples than by the loss of the lysosomal proteins during the organelle enrichment and fractionation. To my knowledge, nothing is known about kinases phosphorylating proteins inside the lumen of lysosomes. In contrast, the lysosomal tartrate-resistant acid phosphatase type 5 has been demonstrated to be involved in protein dephosphorylation (Ek-Rylander et al. 1994; Suter et al. 2001). Therefore, it seems to be unlikely that this PTM persists over a longer period once the phosphoprotein has reached this degradative organelle. Arylsulfatase B and β-glucuronidase are examples for two lysosomal

hydrolases detected as being phosphorylated directly at the amino acid residue in human lung tumors (Gasa and Makita 1983; Fujita et al. 1985). However, these phosphoproteins were identified in homogenates without any lysosomal enrichment, thus lacking the evidence that these phosphorylations occur in mature lysosomes (Gasa and Makita 1983; Fujita et al. 1985). Most lysosomal enzymes feature a phosphorylation at the mannose carbohydrate moiety. Here, the mannose-6-phosphoate group is posttranslationally attached to the hydrolases during transport through the Golgi apparatus and has an important role in delivering these enzymes to the endosomes (Tabas and Kornfeld 1980; Varki and Kornfeld 1980; Waheed et al. 1981; reviewed by Braulke and Bonifacino 2009). Similarly to the phosphopeptide enrichment, metal based affinity chromatography such as $TiO_2$ or $Fe^{3+}$-immobilized metal affinity chromatography (IMAC) can also be used for enriching M6P containing peptides (Kang et al. 2018; Čaval et al. 2019). Compared to IMAC-based techniques, Čaval et al. (2019) demonstrated that the $TiO_2$ method used in this study to enrich for phosphopeptides only yielded low amounts M6P-containing peptides during MS analysis using HCD for peptide fragmentation. Although it remains elusive how many M6P-containing peptides after $TiO_2$ enrichment were not identified due to suboptimal peptide fragmentation in the study of Čaval et al. (2019), the results indicate that a competition among the phospho- and M6P-peptides was probably not the reason for the missing detection of phosphopeptides derived from lysosomal hydrolases in the soluble fraction. This finding further supports the hypothesis mentioned earlier, that lysosomal enzymes are not excessively phosphorylated directly at the protein moiety in mature lysosomes.

FSK/db-cAMP treatment followed by preparation of the lysosomal membrane fraction and phosphopeptide enrichment was associated with the detection of upregulation of known PKA targeted phospho-sites of the CD44 antigen and the CAD protein (PhosphoSitePlus online repository; phosphosite.org, retrieved 09.05.2019) (Carrey et al. 1985; Tzircotis et al. 2006) (Table 5.5). The same CAD phospho-site identified here has also been found as being highly upregulated after FSK/db-cAMP treatment in the whole cell phospho-data set described in the previous section. This supports the reproducibility of the stimuli applied in the two independent experiments. Furthermore, the CD44 antigen as well as the CAD protein were not regulated in the non-phospho-enriched proteomic data set upon FSK/db-cAMP treatment, thus indicating a cAMP-mediated phosphorylation of the detected amino acid residues. Significantly or highly regulated phosphopeptides after FSK/db-cAMP treatment have been identified for the lysosomal proteins Mucolipin 1, RPTOR, mTOR, RUBCN as well as for the lysosome-associated protein SNAPIN. None of these phospho-sites have previously been listed as direct PKA targets in the PhosphoSitePlus online repository (retrieved 09.05.2019) (Figure 5.3, table 5.4, table 5.5, table 5.6).

Together with mLST8 (mammalian lethal with SEC13 protein 8) and the two inhibitory subunits PRAS40 (Proline-rich AKT1 substrate 1) and DEPTOR (DEP domain-containing mTOR-interacting protein), the serine/threonine kinase mTOR and its regulatory associated protein RPTOR are components of the mechanistic target of rapamycin complex 1 (mTORC1) (Kim et al. 2002; Kim et al. 2003; Sancak et al. 2007; Vander Haar et al. 2007; Peterson et al. 2009). The importance of mTORC1 signaling in different cellular processes has been reviewed in detail by Saxton and Sabatini (2017). Upon activation of the mTOR signaling pathway, RPTOR binds substrates to the mTORC1 complex, thus enabling their phosphorylation by the mTOR kinase (Nojima et al. 2003; Schalm et al. 2003). The highly upregulated RPTPOR phospho-site (S877) identified within the present study has recently been assigned as a TANK-binding kinase 1 target (Antonia et al. 2019). Here, RPTOR phosphorylation at S877 has been demonstrated to inhibit mTOR activity (Antonia et al. 2019). The S877 containing RPTOR phosphopeptide detected as being exclusively present in the lysosomal membrane fraction of the FSK/db-cAMP treated samples featured one tryptic missed cleavage site (MCS). In addition to this, the same phospho-site was identified in a peptide without MCS in the present data set. This peptide was found in all three replicates of the FSK/db-cAMP stimulated samples and the DMSO controls without a treatment-induced regulation. Therefore, it is reasonable to assume that the upregulation identified for the RPTOR phospho-site at S877 was rather caused by a slightly different tryptic cleavage efficiency of this peptide within the different sample groups than by cAMP-mediated regulation. However, the mTOR S2448 phospho-site was found to be upregulated after FSK/db-cAMP treatment in the lysosomal membrane fraction. A cAMP-dependent regulation of the mTOR protein level was not detected in the non-phospho-enriched proteomic data set, thus suggesting its presence in the lysosomal membrane fraction independent from the treatment. The mTOR S2448 phospho-site has been previously assigned as a PKB target whereas more recent studies indicate a p70S6 kinase (S6K) dependent phosphorylation at this position (Navé et al. 1999; Sekulić et al. 2000; Chiang and Abraham 2005; Holz and Blenis 2005). As the p70S6 kinase is located downstream of mTOR in the mTOR signaling pathway, its phosphorylation at S2448 was hypothesized as being part of feedback loop (Chiang and Abraham 2005; Holz and Blenis 2005). In 2010, Rosner et al. demonstrated a correlation between a diminished mTOR activity and a downregulation of mTOR phosphorylation at S2448. Here, mTOR activity was monitored indirectly by quantifying the two S6K target sites S235 and S236 of 40S ribosomal protein S6 (S6) upon inhibition of mTOR itself or phosphoinoside-3-kinase, an upstream kinase in the mTOR signaling pathway (Rosner et al. 2010). Both S6 phospho-sites were also found in the present study as being upregulated in the lysosomal membrane fraction after FSK/db-cAMP treatment. Together with the phosphorylation of mTOR at S2448, these findings indicate the activation of S6K upon FSK/db-cAMP treatment,

thus potentially reflecting the stimulation of the mTOR signaling pathway under the conditions applied in this study. However, recent studies suggest a PKA dependent phosphorylation of the S6 phospho-sites S235 and S236 in medium-sized spiny neurons which is independent of the mTOR signaling pathway (Biever et al. 2015). Based on these findings, further experiments are required in order to elucidate whether the S6 phosphorylation found in the present study was caused by the activation of an mTORC1 dependent or independent pathway (or both). Nevertheless, the role of PKA in regulating mTORC1 activity is controversially discussed in literature. Whereas activation of PKA was shown to inhibit phosphorylation of S6K in different cell types; thus indicating a decrease in mTOR activity, the lab of Martinez and co-workers suggested a PKA dependent stimulation of mTOR in human adrenocortical cells (Joussineau et al. 2014; Jewell et al. 2019). Besides the potential involvement of PKA in mTOR activation, cAMP itself was hypothesized to regulate the mTORC1 pathway in a PKA independent manner by releasing the mTOR activator Rheb from a complex with the cAMP-specific 3',5'-cyclic phosphodiesterase 4D (Kim et al. 2010). Taking together these findings, further experiments are necessary in order to evaluate the role of PKA in mTOR signaling.

Mucolipin 1 is a lysosomal cation channel which is phosphorylated by PKA at S557 and S559, thus regulating the channel activity (Vergarajauregui et al. 2008). Within the present study, an additional phospho-site at the cytosolic S10 position of this transmembrane protein has been identified as being upregulated upon FSK/db-cAMP treatment. The Mucolipin 1 protein level in the lysosomal membrane fraction was not affected by the stimulation which indicates a cAMP dependent regulation of the S10 phospho-site. The function of which is unknown.

### 6.1.4. Elevated intracellular cAMP level leads to a downregulation of SNAPIN S133 phosphorylation in the lysosomal membrane fraction

Originally identified in neurons as a protein involved in docking and release of synaptic vesicles via its interaction with SNAP-25, SNAPIN has been demonstrated to play important roles in retrograde vesicle transport, lysosome maturation and late endocytic vesicle trafficking (Ilardi et al. 1999; Lu et al. 2009; Cai et al. 2010; Ye and Cai 2014; Di Giovanni and Sheng 2015). Additionally, SNAPIN was identified as a subunit of the two complexes BLOC-1 and BORC (Starcevic and Dell'Angelica 2004; Pu et al. 2015). Similar to Mucolipin 1, SNAPIN has already been described as a PKA target (Chheda et al. 2001). Here, PKA-dependent phosphorylation of S50 has been demonstrated to enhance the binding of SNAPIN to SNAP-25 (Chheda et al. 2001; Song et al. 2011).

Neither the phospho nor the non-phospho S50 containing peptides were found in the present phospho-data set of the lysosomal membrane fraction after FSK/db-cAMP treatment. This might

have been caused by the intrinsic properties of the tryptic peptide that contains this side which might have hampered its detection via mass spectrometry. The fact that the S50 phospho-site is not listed in the PhosphoSitePlus repository in data from large-scale high-throughput experiments further supports this hypothesis (according to phosphosite.org, retrieved 08.11.2019). In contrast, other SNAPIN phosphopeptides were found in the lysosomal membrane fraction, thus indicating the association of this protein with the lysosomes. Among those, the phosphopeptide containing the S133 phospho-site was downregulated in the lysosomal membrane fraction after FSK/db-cAMP treatment (Figure 5.3, table 5.4). SNAPIN was not detected in the non-phospho enriched proteomic data set. This hampers conclusions about changes in its lysosome association upon elevated intracellular cAMP levels. The properties of SNAPIN described above as well as its presence in the two complexes BLOC-1 and BORC suggest an important role of this protein in proper lysosome function, which might also be linked with its phosphorylation pattern. Further biochemical assays were performed in order to validate the changes in SNAPIN phosphorylation detected by mass spectrometry in FSK/db-cAMP treated cells.

### 6.1.5. Investigating the effect of elevated intracellular cAMP levels on SNAPIN's protein level, lysosomal association as well as phosphorylation

As described earlier, the downregulation observed for SNAPIN's S133 phospho-site after FSK/db-cAMP treatment could either be caused by stimulus-induced dephosphorylation, changes in protein expression and degradation, or dissociation from the lysosomes. SNAPIN was not identified in the non-phospho enriched proteomic data set, thus requiring additional methods in order to evaluate the influence of the FSK/db-cAMP treatment on SNAPIN itself and its phosphorylation status. The influence of elevated cAMP levels on whole cell SNAPIN level and its association to the lysosomes was investigated by Western Blot and immune detection.

#### 6.1.5.1. FSK/db-cAMP treatment does not affect SNAPIN's protein level but might lead to its dissociation from lysosomes

When analyzing whole cell lysates, no changes in the intracellular SNAPIN level were identified upon FSK/db-cAMP treatment, thus indicating that its balance of expression and degradation was not altered due to the stimulus (Figure 5.4). Compared to that, investigating the SNAPIN amount present in the enriched lysosomal fraction suggested a FSK/db-cAMP-dependent dissociation of SNAPIN from these organelles, although its relative intensity did not significantly change between the treated and non-treated samples (Figure 5.5). Here, the failure to reach significance was probably caused by one measurement outlier in the control group which lowers

the mean abundance and increases the standard deviation. Therefore, repetition of the experiment is required to increase the robustness of this assay. If the dissociation is verified, it would be one explanation for the downregulation of the S133 phospho-site observed in the phosphoproteomic data set of the lysosomal membrane fraction. However, protein translocation can be associated with changes in the PTM pattern of the membrane anchoring binding partner or of the transposed polypeptide itself (Zwang et al. 2009; Huang et al. 2015). Hence, changes of the phosphorylation status of SNAPIN S133 as well as at other PTM-sites could also be associated with its translocation.

#### 6.1.5.2. FSK/db-cAMP treatment alters the phosphorylation pattern of SNAPIN

In order to investigate alterations in SNAPIN's phosphorylation profile upon FSK/db-cAMP treatment, 2D-gelelectrophoresis was performed with whole cell lysate. As the isoelectric point (PI) is also influenced by other acidic protein modifications such as acetylation and glycosylation with sialic acid, a phosphatase treated sample was also analyzed by 2D-gelelectrophoresis in order to map different SNAPIN proteoforms to phosphorylated isoform (Gruener and Ismond 1997; Barrabés et al. 2010). FSK/db-cAMP treatment was associated with an increase and decrease of the PI of SNAPIN, thus probably representing phosphorylation and dephosphorylation events (Figure 5.6). This was in line with the observations made in the phosphoproteomic data set of the lysosomal membrane fraction as well as with the PKA-dependent phosphorylation of SNAPIN at S50 described in literature (Chheda et al. 2001). Considering the number of proteoforms found in the phosphatase treated sample as well as in the DMSO control of the first replicate, three different SNAPIN phosphorylation sites have been detected in this experiment. Although the tendency seemed to be similar, precise determination of the number of SNAPIN isoforms identified in the FSK/db-cAMP treated sample and non-treated samples of the second replicate was difficult, as the relatively high background signal might have hindered the detection of faint proteoform pattern.

The results obtained after 2D-gelelectrophoresis suggests SNAPIN as a highly phosphorylated protein. In addition to the PKA mediated S50 phosphorylation, the leucine-rich repeat kinase 2 has been reported to phosphorylate SNAPIN at T117 (Chheda et al. 2001; Yun et al. 2013). The SNAPIN S133 phospho-site identified within the present study as being downregulated upon FSK-db-cAMP treatment in the lysosomal membrane fraction has been previously detected in a proteome wide screen for possible cyclin-dependent kinase (CDK) 2 substrates (Chi et al. 2008). In order to further elucidate potential kinases involved in the phosphorylation of SNAPIN at S133, the NetPhos 3.1 web tool was used (cbs.dtu.dk/services/NetPhos, 09.11.2019) (Blom et al. 1999; Blom et al. 2004). This algorithms makes predictions about possible targets for 17

different kinases based on phospho-sites assigned to these enzymes in literature (Blom et al. 2004). Although a bioinformatic investigation using the NetPhos 3.1 web tool supports the phosphorylation potential of this phosphopeptide at this position, the algorithm was not able to predict a kinase involved in modifying the serine 133 with high confidence. Among the kinases above the 0.5 score-threshold (CDK5, Glycogen synthase kinase-3, MAPK p38), CDK5 was predicted with the highest probability as being responsible for SNAPIN phosphorylation at S133 (score 0.593). Together with the identification of the S133 phospho-site in the large scale CDK2 substrate screen, the results of the bioinformatics analysis indicate the involvement of cyclin dependent kinases in phosphorylating SNAPIN at this position. Comparison of the amino acid composition adjacent to serine 133 with the CDK consensus sequence (S/T-P-X-R/K) further supports this hypothesis (reviewed by Malumbres 2014). However, additional experiments are necessary in order to unravel the potential role of CDKs in SNAPIN phosphorylation.

Within the present study, two to three SNAPIN proteoforms were identified after incubating the cell lysate with an alkaline phosphatase. This indicates the presence of at least one phosphorylation independent isoform with a different PI compared to the unmodified protein (Figure 5.6). It is reasonable to assume that this second isoform neither features highly complex PTMs such as branched glycans nor results of proteolytic cleavage of the original protein or consists of an alternative splicing variant as its molecular weight was similar to the unmodified SNAPIN proteofom. Besides phosphorylation, the only SNAPIN PTM validated in classical biochemical approaches is O-GlcNAcylation (Song et al. 2011). However, as this PTM is not known to change the PI of a protein, SNAPIN O-GlcNAcylation does probably not cause the occurrence of the additional proteoform in the 2D-gel (reviewed by Hart et al. 2011). Therefore, further studies are required in order to characterize the different non-phosphorylated SNAPIN isoforms.

In summary, the results of the biochemical approaches described in this section strongly demonstrate alterations in SNAPIN's phosphorylation pattern upon elevated intracellular cAMP levels. These changes might be caused by the activation of PKA but in order to further elucidate the role of this kinase on SNAPIN phosphorylation, additional experiments with PKA-specific inhibitors are required. In addition to its passive fate as being affected by intracellular cAMP levels, SNAPIN might also be involved in modulating the amounts of this second messenger inside the cell. This hypothesis is based on the interaction of SNAPIN with proteins involved in GPCR signaling such as the adenylyl cyclase type VI and the regulator of G protein signaling 7 (Hunt et al. 2003; Chou et al. 2004).

### 6.1.6. SNAPIN KO is associated with a decrease in the MPR300 level

After identification of SNAPIN as a lysosome-associated protein with regulated phosphorylation sites upon elevation of cAMP levels, the role of this protein in different cellular processes was investigated. For this purpose, the CRISPR-Cas9 method was used in order to generate a functional SNAPIN gene knock-out in HEK 293 and HeLa cells (Figure 5.7). Once generated, the proteomes of the HEK 293 SNAPIN KO and wt cells were compared by a mass spectrometry-based approach (Figure 5.8, table 5.7). Although no significant changes in the protein levels were observed according to the standard thresholds, manual comparison of the abundance values of the single replicates indicated a SNAPIN KO-dependent decrease in the MPR300 abundance. In order to validate this finding, the MPR300 levels in HEK 293 and HeLa SNAPIN KO cells were investigated by Western Blot quantification and compared to those detected in the corresponding wt cells. Here, SNAPIN KO was associated with a decrease in the MPR300 level, thus supporting the findings of the MS-based proteome comparison (Figure 5.9). Furthermore, the cell type independent reduction of the MPR300 abundance after knocking out SNAPIN indicates that the observations originally made in the MS-based analysis of HEK 293 cells were not caused by secondary effects of the CRISPR-Cas9 method. For example, such an effect could have been caused by the insertion of the Cas9-plasmid DNA next to regulatory genomic regions under the selection pressure of the antibiotic.

The transmembrane protein MPR300 plays an important role in binding newly synthesized lysosomal hydrolases at the Golgi apparatus and in delivering these enzymes to the endosomal compartment (reviewed by van Meel and Klumperman 2008). Once the cargo is delivered, the MPR300 is sorted back to the Golgi apparatus to start another round of this transport cycle (Duncan and Kornfeld 1988). In addition to that, the MPR300 has been described as being located at the plasma membrane (Kaplan et al. 1977). Here, the receptor is able to bind M6P containing enzymes and mediate their internalization and transport to endosomes (Kaplan et al. 1977).

The decreased MPR300 level detected in the SNAPIN KO cells could be explained by a dysregulation of its degradation. As the MPR300 continuously cycles between the TGN and the endosomal compartment, a precise sorting machinery is required in order to prevent the receptor from reaching the lysosomes which might induce its degradation. The role of the “Retromer” complex in retrograde protein transport from endosomes to the Golgi apparatus has been reviewed in detail within the past years (Lucas and Hierro 2017; Vagnozzi and Praticò 2019). However, different studies indicate the involvement of additional proteins in MPR300 recycling although the exact mechanism is still debated in literature. Whereas the Pfeffer group

suggested a combinatory contribution of Rab9 and Tip47 (Perilipin-3) in MPR retrieval to the TGN, more recent results from Bulankina et al. (2009) indicate that Tip47 is not involved in this process (Riederer et al. 1994; Díaz and Pfeffer 1998; Carroll et al. 2001). However, Díaz and Pfeffer (1998) demonstrated a decrease in the MPR300 level upon Tip47 knock down which is similar to the observations made within the present study in the SNAPIN KO cells. The authors assigned this phenomenon to a reduced MPR300 half-life, caused by a Tip47-dependent missorting of this receptor and its degradation in the lysosomal compartment (Díaz and Pfeffer 1998). Based on this, one could hypothesize a similar role of SNAPIN in MPR300 endosome/TGN sorting. Such an impact would explain the decreased MPR300 levels detected in the SNAPIN KO cells. However, this explanation would only be valid if the retrograde transport of late endosomes (LE), the LE-lysosome fusion and the lysosomal function is not affected by the SNAPIN KO itself. In 2010, Cai et al. identified SNAPIN as a regulator in late endosomal retrograde transport. Furthermore, characterization of SNAPIN KO neurons demonstrated an increased LAMP-1 level as well as a decrease in the abundance of mature Cathepsin D, a proteoform often used as an indicator for lysosome maturation as its precursor isoform is cleaved in the acidic environment of these organelles (Lu et al. 2009; Cai et al. 2010). The authors predicted SNAPIN as a protein involved in endosome-lysosome fusion and lysosome maturation (Lu et al. 2009; Cai et al. 2010). Based on these findings, it remains elusive whether the SNAPIN KO might lead to an increase in lysosome-based degradation of missorted MPR300 and further experiments are required in order to answer this question.

A diminished biosynthesis rate might be another explanation for the decrease in the MPR300 level detected in the SNAPIN KO cells. So far, little is known about the influence of SNAPIN on gene transcription and protein translation. In 2009, Ginter-Matuszewska et al. described the interaction of SNAPIN with Pumilio homolog 2 (Pumilio2) and Nanos homolog 1 (NANOS1). In *Drosophila*, Pumilio and NANOS have been demonstrated to form a complex which inhibits translation of mRNA by removing the poly-A-tail (Wreden et al. 1997). This suggests a similar function in humans. Although originally described as being predominantly expressed in human germ cells (plus Pumilio2 in embryonic stem cells), database analysis of Pumilio2 and NANOS1 indicates a high protein expression in different tissues such as colon and kidney (proteinatlas.org, retrieved 12.11.2019) (Moore et al. 2003; Jaruzelska et al. 2003; Uhlén et al. 2015). Based on the SNAPIN interaction, one could hypothesize a regulatory function of SNAPIN upon binding to these proteins. In this case, SNAPIN KO could be associated with the release Pumilo2 and NANOS1 from a regulatory complex thus promoting posttranscriptional inhibition of protein biosynthesis. This might then be associated with the reduced MPR300 level detected in the SNAPIN KO cells. Nevertheless, this function of SNAPIN is highly speculative as not only

the involvement of Pumilio2 and NANOS1 in regulation of mRNA translation needs to be further validated in humans. In fact, SNAPIN interaction would also need to inhibit Pumilio2 and NANOS1 function. Additionally, the impact of both proteins on MPR300 mRNA translation would need to be demonstrated.

### 6.1.7. MPR-mediated endocytosis is decreased in SNAPIN KO cells

The proteome comparison of SNAPIN KO cells revealed a decrease in the MPR300 compared to their wt counterparts. The reason for the downregulation in the SNAPIN KO cells remains elusive. As the MPR300 has important functions in the endocytosis of M6P containing acidic hydrolases, the internalization of ASA was investigated in HEK 293 wt and SNAPIN KO cells. Both cell types were also incubated with FSK/db-cAMP or DMSO in order to determine the influence of elevated intracellular cAMP levels on the internalization process. Such a cAMP-dependent effect would justify further investigations of the potential role of the altered SNAPIN phosphorylation pattern detected after FSK/db-cAMP treatment on MPR mediated endocytosis.

In both cell types, FSK/db-cAMP treatment was not associated with alterations in ASA internalization (Figure 5.10). Analysis of the cell lysates by Western Blotting and pCREB immune detection suggested a successful activation of PKA upon elevated cAMP levels in the wt cells (data not shown). Together, these results indicate that the FSK/cb-cAMP dependent changes in the SNAPIN phosphorylation status have no effect on the endocytosis kinetics of ligand-MPR complex. Investigations of the pCREB level in SNAPIN KO cell lysates yielded inconclusive results regarding the PKA activation after FSK/db-cAMP treatment (data not shown). As a stimulus-induced activation of PKA was demonstrated for the wt cells, further investigations are required in order to determine whether the SNAPIN KO influences parts of the intracellular cAMP signaling pathway.

However, when comparing the two different genotypes, significant, treatment-independent differences in the MPR mediated internalization of ASA were observed (Figure 5.10). Here, SNAPIN KO cells showed a strong decrease in the endocytosis rate compared to their wt counterparts. The easiest explanation for this observation would be the downregulation of MPR300 identified in the SNAPIN KO cells in previous experiments. Nevertheless, this would require that the levels of this receptor at the plasma membrane are diminished upon SNAPIN KO. If the MPR300 levels displayed at the cell surface are not altered, the reduced ASA endocytosis rate observed after SNAPIN KO would rather be caused by a dysfunction of the internalization machinery after ligand binding than by the decreased amounts of surface exposed receptor itself. So far, little is known about a potential role of SNAPIN in modulating the

endocytosis kinetics after formation of ligand-receptor complex. In 2010, Cai et al. demonstrated an impaired degradation of EGFR in murine SNAPIN KO cells. As the EGF/EGFR internalization rate was not altered between the wt and SNAPIN KO cells, the authors concluded that at least part of this observation was caused by defects in cargo delivery to the lysosomes (Cai et al. 2010). The EGFR can be internalized via adaptor protein 2 containing, clathrin-coated plasma membrane fissions (Beguinot et al. 1984; Hanover et al. 1984; Sorkin et al. 1996). Similarly, the cytosolic domain of the MPR300 contains the YXXϕ (ϕ = bulky hydrophobic residue) motif enabling the binding to the clathrin adaptors AP1 and AP2 (Jadot et al. 1992; Doray et al. 2007). These similarities might indicate a common internalization mechanism of these receptors. However, an alternative, clathrin-independent route for EGFR endocytosis has been described, thus further complicating the comparison to the MPR300 based internalization process (Sigismund et al. 2005; Henriksen et al. 2013). Therefore, the findings of Cai et al. (2010) regarding the EGFR endocytosis rate in SNAPIN KO cells might only be transferable with certain limitations to the uptake of MPR300-ligand complexes as the exact mechanism involved in EGFR internalization was not investigated. Hence, independent experiments need to be performed in order to identify the potential role of SNAPIN in MPR300 endocytosis. Additionally, further studies investigating the influence of SNAPIN in MPR300 cell surface localization are required.

### 6.1.8. SNAPIN KO is associated with a reduced size of LE/lysosomes

SNAPIN KO has been demonstrated to alter late endosome trafficking in neurons due to alterations in dynein-driven transport (Cai et al. 2010). In 2015, Pu et al. reported a SNAPIN knock down mediated perinuclear clustering of LE/lysosomes in HeLa cells by influencing the kinesin mediated anterograde transport. In order to further investigate SNAPIN-dependent LE/lysosome positioning, HeLa wt and SNAPIN KO cells were stained with an anti-LAMP-2 antibody and analyzed by confocal microscopy. Here, the influence of elevated intracellular cAMP levels in both genotypes were investigated by treating the cells with FSK/db-cAMP or DMSO (control).

In HeLa wt cells, the LAMP-2 signal was distributed throughout the whole cell with slight accumulation at the perinuclear region (Figure 5.11). For this cell type, no difference in the signal pattern was observed for the treated and non-treated cells (Figure 5.11). The missing effect of elevated intracellular cAMP levels on LAMP-2 signal distribution indicate that the alterations of the SNAPIN phosphorylation status detected upon FSK/db-cAMP treatment in the previous experiments were not associated with changes of LE/lysosomes subcellular localization. Recently, Tapia et al. (2019) demonstrated a PKA-induced translocation of lysosomes to the

Golgi region, triggered by the activation of the KDEL-receptor (KDELR), a GPCR located at the Golgi apparatus and involved in the regulation of membrane trafficking at this organelle (Giannotta et al. 2012; Cancino et al. 2014). In order to demonstrate the impact of protein kinase A on this process, the authors activated the KDELR with an artificial ligand in the presence or absence of an cAMP analog and/or PKA inhibitors in HeLa cells in which the adenylyl cyclase 9, a protein involved in PKA activation at the Golgi apparatus, was knocked down (Cancino et al. 2014; Tapia et al. 2019). However, these findings of Tapia et al. (2019) appear contradictory to the results obtained within the present study. The reasons for these different outcomes remain unclear. One possible explanation might be the activation of additional pathways due the simultaneous stimulation of the KDELR and cell treatment with cAMP analogs or PKA inhibitors which contributed to lysosome repositioning in the studies of Tapia et al. (2019).

Compared to the wt cells, SNAPIN KO was associated with smaller LAMP-2 positive puncta and a more homogeneous LE/lysosome distribution throughout the whole cell (Figure 5.11). This observation was independent of the treatment, although the FSK/db-cAMP stimulated SNAPIN KO cells might have featured a slight shift of the LAMP-2 positive structures towards the perinuclear region compared to the DMSO treated control (Figure 5.11). In order to further investigate the potential changes in LE/lysosome positions after FSK/db-cAMP treatment of the SNAPIN KO cells, additional experiments with statistical analysis of treatment-dependent LAMP-2 signal redistribution are needed. Such a LE/lysosome re-localization might require dynein-driven retrograde transport mechanism of at least one of these organelles. So far, different effectors are known to mediate dynein-dependent movement of LE/lysosome from the cell periphery towards the perinuclear region (for review see Pu et al. 2016). In 2010, Cai et al. identified SNAPIN as an interaction partner of the dynein intermediate chain. Within the same study, overexpression of a SNAPIN version carrying the L99K substitution which abolishes the binding to dynein was demonstrated to strongly affect LE retrograde transport (Cai et al. 2010). A similar tendency was observed for SNAPIN KO in cortical neurons (Cai et al. 2010). At first sight, these findings might be in contradiction with the potential FSK/db-cAMP treatment dependent changes in the distribution of LE/lysosomes described within the present study for the SNAPIN KO cells. Nevertheless, the results published by Cai et al. (2010) indicate that the LE movement towards the perinuclear region was not totally abolished upon SNAPIN KO and overexpression of the L99K proteoform. This might suggest the presence of at least partial compensatory mechanisms mediating LE/lysosome movement within the cells if SNAPIN is absent.

Recently, SNAPIN was identified as a subunit of BORC (Pu et al. 2015). BORC mediates the binding of ADP-ribosylation factor-like protein 8 to LE/lysosomes which facilitates the

recruitment of kinesin-1 to those organelles thus promoting their anterograde transport (Pu et al. 2015). Here, SNAPIN knock down (KD) was correlated with a perinuclear clustering of LAMP-1 positive structures (lysosomes) (Pu et al. 2015). Such a juxtanuclear accumulation of LE/lysosomes was not observed in cells lacking SNAPIN within the present study. Similar to the LE/lysosome distribution in SNAPIN KO cells shown in Figure 5.11, Cai et al. (2010) detected LAMP-1 positive structures throughout the whole cytoplasm of MEF cells lacking SNAPIN. Compared to the wt cells, an increase in the colocalization of LAMP-1 and MPR300 was observed after SNAPIN KO (Cai et al. 2010). As the MPR300 is not located to mature lysosomes, the results indicate an accumulation of late endosomes/immature lysosomes in the SNAPIN KO cells (Sahagian and Neufeld 1983; Griffiths et al. 1988; Cai et al. 2010). This phenomenon might also be associated with impaired LE-lysosome fusion after SNAPIN KO. In 2009, Lu et al. identified SNAPIN as an interaction partner of Syntaxin-8, a late endosome SNARE component, potentially indicating its role in LE fusion events (Antonin et al. 2002). Therefore, impairments in the LE fusion machinery after SNAPIN KO might be another explanation for the reduced size of LAMP-2 positive structures compared to the wt cells.

Very recently, the regulatory function of the two BORC subunits Diaskedin and Myrlysin on LE/lysosomal size was published (Yordanov et al. 2019). The authors demonstrated an increased $PI(3,5)P_2$ level (PIKFYVE activity) in Diaskedin KO cells which was associated with a reduced LE/lysosome size (Yordanov et al. 2019). As SNAPIN is also a BORC subunit, this finding might suggest a similar function of SNAPIN in LE/lysosome size regulation which would explain the LAMP-2 staining pattern observed after knocking down this protein within the present study. However, Yordanov et al. (2019) showed that the knock out of the BORC subunit 6 (Lyspersin) did not affect the size of LE/lysosomes. Therefore, the effect might have rather been caused by individual subunits than by the whole BORC, thus hampering conclusion about the role of SNAPIN in regulating LE/lysosome size via modulating the $PI(3,5)P_2$ levels.

### 6.1.9. The exocytosis of the lysosomal hydrolase β-hexosaminidase is upregulated in SNAPIN KO cells

SNAPIN might play a key role in the secretion of synaptic vesicles (SV) by interacting with SNAP-25 and potentially modulating the recruitment of synaptotagmin-1 to the SNARE complex (Ilardi et al. 1999; Tian et al. 2005). A similar SNAPIN function has been demonstrated in the secretion of insulin in pancreatic cells (Song et al. 2011; Somanath et al. 2016). Based on the involvement in these secretory events, the role of SNPAIN in lysosome exocytosis was investigated in HeLa wt and SNAPIN KO cells. In addition, the effect of cAMP on the exocytosis of lysosomes was analyzed by treating the cells with FSK/db-cAMP or DMSO (control).

Elevation of the intracellular cAMP and $Ca^{2+}$ levels was not associated with an increase in the exocytosis of β-hexosaminidase (β-Hex) in HeLa wt cells (Figure 5.12A). This finding was surprising as both compounds have already been described in potentiating each other to promote exocytosis of lysosomes in rat fibroblasts (Rodríguez et al. 1999). However, the exocytosis behavior might differ among cell types which might explain the discrepancy between the lysosome secretion of HeLa wt cells and rat fibroblast. Nevertheless, the β-Hex exocytosis was increased in HeLa cells upon SNAPIN knock-out. Here, the exocytosis was triggered in the presence of $Ca^{2+}$ and ionomycin in a cAMP independent manner, yielding a maximum β-Hex activity of approx. 110 µU/mg protein in the supernatant. In comparison to the wt samples, a 1.2-2.3-fold higher total β-Hex activity was measured for the SNAPIN KO cells (Figure 5.12B). It is reasonable to assume that this difference contributed to the increased β-Hex activity detected in the supernatant of $Ca^{2+}$ stimulated cells after SNAPIN knock-out. However, as for these samples a 3.4-4.9-fold increase in the β-Hex activity was observed, the different basal β-Hex levels do not fully explain the discrepancy between the exocytosis rates detected for the two cell types. Hence, these findings indicate an effect of SNAPIN on lysosome exocytosis.

In non-professional secretory cells, the exocytosis of lysosomal hydrolases can be ascribed to different cellular processes. For example, these enzymes can enter the secretory pathway when missing the binding to MPR at the Golgi apparatus (reviewed by Braulke and Bonifacino 2009). Additionally, conventional lysosomes have been described to be able to fuse with the plasma membrane in a $Ca^{2+}$-regulated way (Rodríguez et al. 1997). Here, the SNARE machinery involved in $Ca^{2+}$-dependent secretion of conventional lysosomes comprises SNAP-23, Syntaxin-4 as well as synaptotagmin-7 and the lysosomal TI-VAMP/VAMP7 (Martinez et al. 2000; Rao et al. 2004). SNAPIN is a known regulator of SV and insulin secretion in neurons and pancreatic cells (Ilardi et al. 1999; Song et al. 2011; Somanath et al. 2016). In these processes, SNAPIN's function is modulated by PKA-dependent phosphorylation at S50 (Chheda et al. 2001; Song et al. 2011). Based on its lysosome-association, one could hypothesize a similar function of SNAPIN in exocytosis of these organelles. In addition, SNAPIN has been demonstrated to interact with SNAP-23, a component of the SNARE complex involved in exocytosis of lysosomal enzymes, thus further suggesting its involvement in the secretion of conventional lysosomes (Buxton et al. 2003; Rao et al. 2004). However, the results mentioned above clearly demonstrates that neither SNAPIN nor cAMP were directly involved in the secretion of β-Hex in HeLa cells. In contrast, the data might suggest an inhibitory effect of SNAPIN in lysosome exocytosis as the β-Hex release was significantly increased in SNAPIN KO compared to the wt cells.

Considering the smaller size and higher number of LAMP-2 positive structures in the microscopic analysis of SNAPIN KO cells (Figure 5.11), the increase in β-Hex secretion might have also been

associated with changes in the subcellular localization of LE/lysosomes. In this case, SNAPIN itself would not act as a negative regulator of lysosome secretion but its knock out would cause a redistribution of LE/lysosomes which favors the fusion of these organelles with the plasma membrane.

As mentioned earlier, lysosomal hydrolases might escape the endosomal transport route when missing the binding to MPR, thus entering the secretory pathway departing from the Golgi apparatus and being released into the extracellular space (reviewed by Braulke and Bonifacino 2009). The MPRs are crucial for delivering lysosomal hydrolases to the endosomal system as cells lacking the MPR300 have been shown to feature an increased proportion of secreted lysosomal hydrolases, a process which can be reversed by (re-)introducing this receptor (Kyle et al. 1988). Based on the observed downregulation of the MPR300 in SNAPIN KO compared to wt cells (Figure 5.8 and figure 5.9), the diminished receptor level might have additionally contributed to the increased β-Hex release via the secretory pathway in this cell line. Nevertheless, the exocytosis of post-Golgi vesicles has been demonstrated to be $Ca^{2+}$-independent (Jaiswal et al. 2009). Therefore, this pathway would rather continuously contribute to an increased secretion of lysosomal hydrolases whereas it would not be affected by the $Ca^{2+}$ stimulus. Hence, it is reasonable to assume that the increased extracellular β-Hex activity observed after $Ca^{2+}$ stimulation of the SNAPIN KO cells has been mostly caused by the exocytosis of conventional lysosomes or another yet unknown mechanism.

In addition to the possibilities described above, one has to mention that the increased β-Hex activity detected in supernatant of the HeLa SNAPIN KO cells could have also been caused by an increase in cellular apoptosis. A lactate dehydrogenase (LDH) assay, performed with the supernatants and the cell lysates, failed to deliver clear results (data not shown). Although the LDH activity values of the SNAPIN KO and wt supernatants were close to the blanks and no genotype specific differences were observed, only very weak activities were measured for random lysates samples of both cell types. In case of the cell lysates, a slightly higher LDH activity was determined compared to the supernatants but the values were still close to the blanks. Therefore, one cannot exclude that the low LDH activity measured in the supernatants was simply caused by the small proportion of active LDH in the cell lysates. Hence, further experiments are required in order to investigate potential differences in the apoptosis behavior of Hela wt and SNAPIN KO cells under the conditions used for examining lysosomal secretion. However, tests by Rodríguez et al. (1997) revealed only a minor amount of LDH release when treating rat fibroblasts with PBS containing 1 mM $Ca^{2+}$ and 10 µM ionomycin for 10 min. Although this finding might not be easily transferable to the HeLa cells investigated within the

present study, it suggests that the treatment itself is not necessarily associated with a tremendous induction of apoptosis.

### 6.1.10. BLOC1S6 potentially interacts with SNAPIN S133E but not with the S133A isoform

SNAPIN was found to be phosphorylated at S133. In order to identify possible interaction partners of this SNAPIN isoform, pull-down assays with HEK 293 SNAPIN KO cells expressing the phosphomimetic S133E or the non-phosphorylatable S133A SNAPIN proteoform were performed. HEK 293 SNAPIN KO cells were used as a control.

As expected, the different SNAPIN proteoforms were detected in the lysates of the stably transfected HEK cells used for the IP (Figure 5.13). In contrast, no SNAPIN signal was observed for the untransfected HEK 293 SNAPIN KO cells thus highlighting the functional gene knock out present within this cell line and its suitability as a control in the immunoprecipitation assay. After incubation with the Myc-Trap beads, SNAPIN was detected in the supernatant which indicates an incomplete pull-down (Figure 5.13). Additionally, a non-distinct signal pattern below the SNAPIN signal was observed when incubating the membrane containing the supernatant samples with the SNAPIN antibody. This pattern might be attributed to smaller SNAPIN polypeptides caused by minor amounts of plasmids with nonsense mutations. Nevertheless, the presence of these SNAPIN versions in the supernatant after the immunoprecipitation indicates that they have not bound to the Myc-Trap beads and therefore probably not interfered with the pull-down assay itself.

In the MS data set of the eluted proteins from the Myc-Trap beads, SNAPIN was found in the untransfected SNAPIN KO cells (Figure 5.14). However, these identifications were solely based on feature mapping of precursor ions between different runs but without evidence on MS2 level. As SNAPIN was not detected in the IP input samples after Western Blot analysis of the untransfected SNAPIN KO cells, it is reasonable to assume that the detection of this protein in the control samples might have been caused by false feature alignment on MS1 level and can be disregarded. Similarly, the peptide comprising the S133E substitution was found by MS1 feature mapping in the S133A samples and *vice versa*. Comparable to the detection of SNAPIN in the KO sample, this finding is probably also caused by false data alignments between the different raw files as the evidence for the identification on MS2 level is missing.

In total, seven proteins were shared as potential interaction partners of the SNAPIN S133A and S133E proteoforms (Figure 5.15, table 5.9). Among those, BORCS7 and BORCS8 are known subunits of BORC whereas BLOC1S1 and BLOC1S2 can be associated with BORC and the BLOC-1 complex (Starcevic and Dell'Angelica 2004; Pu et al. 2015). As SNAPIN has also been identified

as a subunit of these complexes, these data indicated a successful precipitation of known SNAPIN-associated proteins thus indicating the reliability of this immunoprecipitation assay as well as of the data analysis pipeline for identifying SNAPIN interaction partners (Starcevic and Dell'Angelica 2004; Pu et al. 2015). However, when comparing the normalized abundance ratios determined for these proteins in the S133A and S133E based pull down, a high variability between the single replicates was observed. This hinders conclusions about the proteoform-based regulation of SNAPIN's interaction with these proteins although BLOC1S1, BLOC1S2 and BORCS7 were found in all three replicates with MS2 based identifications (Table 5.9). A high ratio variability among independent replicates is a well-known issue in affinity purification assays. Another problem in MS-based pull-down approaches might be derived from false positive identifications like those obtained for the SNAPIN detection in the knock-out cells. Therefore, the MS data presented here can only be used as a starting point for the identification of S133A and S133A specific SNAPIN binding proteins but needs to be validated before deducing further working hypothesizes.

Data analysis revealed a potential SNAPIN S133A isoform specific interaction with the E3 ubiquitin-protein ligase NEDD4-like and Niban 2 (Figure 5.14, table 5.8). In case of the S133E-proteoform, five proteins have been identified as isoform-specific potential binding partners (Figure 5.14, table 5.8). The BLOC1 subunit 6 was one of the proteins uniquely identified in this group. As mentioned earlier, other BLOC-1 subunits (BLOC1S1 and BLOC1S2) were also found to co-immunoprecipitate but binding of these proteins to SNAPIN might not have been favored by one of the proteoforms. This finding is interesting as it might suggest the selective interaction of SNAPIN S133E to a specific subunit of BLOC-1 without promoting the co-precipitation of other components of this complex. However, when interpreting these data, one has to keep in mind that BLOC1S1 and BLOC1S2 are also subunits of BORC (Pu et al. 2015). Therefore, it might be possible that SNAPIN's interaction with the BORC is independent from the substitution whereas its binding to BLOC1S6 is enhanced by a negatively charged residue at position 133.

BLOC-1 is a complex involved in the biogenesis of lysosome related organelles (Falcón-Pérez et al. 2002). Recently, a regulatory role of BLOC-1 in the formation of recycling endosome (RE) tubules in HeLa cells has been suggested (Delevoye et al. 2016). Here, the authors hypothesized that the recruitment of BLOC-1 to budding RE facilitates the binding of motor protein kinesin-like protein KIF13A to these structures, thus linking RE to microtubules and promoting their elongation (Delevoye et al. 2016). Based on the identification of the S133E proteoform as a potential interaction partner of BLOC1S6, one could hypothesize a contribution of the S133 phosphorylated SNAPIN isoform in this process.

## 6.2. Development of non-antibody-based methods for enhancing the identification of specific PTM

A major challenge in bottom-up MS-based PTM analysis is the low abundance of posttranslationally modified peptides within a complex mixture. In order to solve this problem, PTM enrichment strategies are used. Within the present study, two novel methods aiming at enhancing the identification of different amino-acid specific modifications were developed and tested regarding their functionality.

### 6.2.1. Serial digestion workflow

Trypsin is a protease, that cleaves C-terminal of lysine and arginine residues (Olsen et al. 2004). This proteolytic enzyme has an impaired cleavage efficiency when lysine residues are modified by PTMs such as di- and trimethylation as well as acetylation (Peters et al. 2003; Smith et al. 2003; reviewed by Burlingame et al. 2005). In the serial digestion workflow, proteins are first digested with trypsin (Figure 5.16, step 1). Afterwards, primary amines are modified with a biotin-derivative (NHS-biotin) and incubated with a second protease assumed to cleave N-terminal of lysine residues regardless of their modification status (Figure 5.16, step 2.1 + step 3.1). Therefore, the second proteolytic enzyme releases biotin-containing peptide fragments formerly located N-terminal of the modification site (Figure 5.16, peptide mixture after step 3.1). Efficient removal of biotinylated amino acid residues from PTM containing peptides is crucial, before incubating the double digested mixture with streptavidin-beads (Figure 5.16, step 4.1). Here, biotinylated peptides are depleted, thus leaving non-biotin containing, posttranslationally modified peptide species in the supernatant (Figure 5.16, peptide mixture after step 4.1).
Based on the specificity of trypsin, the proteolytic cleavage with this enzyme in the beginning of the workflow might lead to peptides featuring both, an internal PTM-containing as well as a C-terminal unmodified lysine residue (Figure 5.16, see succinylated peptide after step 1). In the course of the biotinylation procedure, this C-terminal lysine residue is biotinylated and needs to be separated from the PTM containing amino acid sequence in order to prevent the loss of this PTM site during streptavidin incubation (Figure 5.16, see succinylated peptide after step 2.1). Therefore, the efficiency of the workflow would be enhanced if the second protease would also cleave adjacent to biotinylated lysine residues in order to remove this C-terminal biotin-containing amino acid (Figure 5.16, see succinylated peptide after step 3.1). For tryptic peptides featuring a C-terminal arginine, such a cleavage is not required as all biotinylated amino acid stretches are removed when the second enzyme cleaves adjacent to the PTM containing lysine

residue (Figure 5.16, see di-methylated peptide after step 3.1). Therefore, peptides containing a lysine PTM site would be present in the supernatant after streptavidin incubation even if the second enzyme does not cleave next to biotinylated lysine residues but here, the yield would be restricted to peptides featuring a C-terminal arginine residue after tryptic digestion.

In this study, the proteases LysN and LysArginase were used for the second digestion. LysN cleaves N-terminal of lysine residues, whereas LysArginase is able to hydrolyze the peptide bonds N-terminal of arginine and lysine side chains (Nonaka et al. 1995; Tallant et al. 2006; Tallant et al. 2007; Huesgen et al. 2015). Both enzymes have already been described in cleaving adjacent to methylated lysine residues (Taouatas et al. 2010; Huesgen et al. 2015). Based on these properties, it was assumed that these proteases might have an expanded cleavage capability which enables them to cleave also next to biotinylated lysines. Therefore, both enzymes were tested regarding their ability to cleave adjacent to biotinylated lysine residues.

#### 6.2.1.1. LysN digestion of a synthetic peptide is incomplete irrespective of lysine biotinylation

Incubation of the synthetic peptide with sulfo-NHS-biotin was associated with up to three biotinylation events (Figure 5.17B). As the peptide featured only two primary amines, biotinylation at three positions indicates an unspecific reaction of the NHS-biotin with another amino acid. The reactivity of NHS-esters towards non-amine groups have been known for decades (Miller et al. 1992). For example, Miller and colleagues demonstrated an O-biotinylation of serine's hydroxyl group with different NHS-biotin derivatives under mild conditions influenced on the presence of a histidine residue in a close-by position (Miller and Kurosky 1993; Miller et al. 1997). Here, histidine was hypothesized to affect the nucleophilicity of serines' hydroxyl group in presence of an additional amino acid located between these residues (Miller and Kurosky 1993). Both amino acids were also present within the sequence of the synthetic peptide used in this study, but probably their distance was too large for the histidine to influence the reactivity of the serine side chain. The unspecific biotinylation event cannot be mapped to a specific site based on the MS1 data. Nevertheless, its finding is of importance for the interpretation of MS2-based large scale studies in general. The primary amine reactive property of the NHS group is commonly used in different biochemical approaches such as in protein cross-linking based interaction studies or in peptide labeling for MS-based quantifications (Ross et al. 2004; Fasci et al. 2018). In these approaches, peptides with products of unknown side reactions will not be found during classical database searches thus lowering the identification.

The detection of the peak corresponding to the C-terminal, biotinylated cleavage product after LysN digestion indicates the capability of this enzyme to hydrolyze the peptide bond adjacent to biotin-containing lysine residues. However, as this peak was also detected in the non-digested,

NHS-biotin treated sample in two similar, independent experiments (data not shown), the ability of LysN to cleave N-terminal of biotinylated lysines needs to be further investigated.
The non-biotinylated peptides were not digested completely by LysN. Reliable conclusions about the cleavage efficiency are not possible based on the signal intensities of the different species, as the ionization behavior is an intrinsic property of each peptide and might be influenced by its amino acid composition and modification status. Nevertheless, the incomplete digestion indicated suboptimal cleavage conditions. Therefore, the next step aimed at optimizing LysN's digestion behavior by varying the peptide to protease ratio as well as by adding different divalent cations to the digestion buffer.

#### 6.2.1.2. Adjustments of the peptide:LysN ratio influence the cleavage efficiency of LysN

Different peptide:LysN mass ratios were tested regarding their influence on the relative cleavage efficiency of a synthetic precursor peptide. Here, a peptide:LysN mass ratio of 25:1 yielded the highest abundance ratio of cleaved *versus* non-cleaved peptides (Figure 5.18A). Compared to that, a tremendous reduction in the cleavage efficiency was observed when reducing the peptide:LysN ratio to 50:1 and 100:1, respectively. Similar investigations were performed by Taouatas et al. (2010). Here, the authors used BSA as a substrate for investigating LysN's cleavage efficiency at eight different ratios ranging from 50:1 to 1000:1 (Taouatas et al. 2010). In that study, BSA cleavage was most efficient at ratios 50:1, 85:1 and 100:1. A BSA:LysN ratio of 25:1 was not tested by the authors, thus hindering conclusion whether a further increase in the protease proportion would have led to an even higher efficiency.
LysN is a metalloendopeptidase requiring divalent cations as co-factors (Nonaka et al. 1995). Therefore, the effect of different cations on LysN's hydrolytic activity was investigated. Among the different conditions tested, the highest cleavage efficiency was observed for samples containing 0.1 mM $MgCl_2$ or no additional cations in the digestion buffer (Figure 5.18B). However, as these samples also featured the biggest variance, reliable conclusions whether these conditions might be more beneficial than adding 1 mM $MnCl_2$ or 1 mM $MgCl_2$ to the digestion buffer cannot be drawn. Interestingly, the cleavage efficiency might have been reduced in presence of 0.1 mM $ZnCl_2$ and even totally abolished at a 10-fold higher concentration of this salt. This is surprising as LysN was originally identified as a zinc-metalloendopeptidase (Nonaka et al. 1995). In 1995, the same authors investigated the activity of the metal-deprived LysN apoenzyme upon (re-)addition of different divalent cations (Nonaka et al. 1995). Here, the presence of $Zn(CH_3COO)_2$ restores LysN's activity whereas its catalytic function was even increased after adding $MnCl_2$ to the digestion buffer (Nonaka et al. 1995).

Such a correlation was not observed within the present study. The reasons for these divergent observations remain elusive.

Based on the findings described in this section, a protein:LysN ratio of 25:1 as well as a $MgCl_2$ concentration of 0.1 mM in the digestion buffer were used in further LysN digestion experiments.

#### 6.2.1.3. LysN and LysArginase digestion of NHS-biotin treated complex samples is associated with a low identification rate of biotinylated peptides

In order to avoid a bias by one specific peptide sequence on the evaluation of the digestion efficiency, LysN's and LysArginase's cleavage capabilities at biotinylated BSA and proteins from HEK 293 cell lysates were investigated.

By comparing the numbers of biotin-containing BSA peptides detected after proteolysis with these proteases, a strong reduction in the identification of biotinylated species was identified in the LysArginase treated sample (Figure 5.19B). One possible explanation for this observation might be a higher number of missed cleavages compared to the LysN digest. This could lead to peptide masses incompatible with the MS acquisition settings or to amino acid sequences with more MCS than those searched during database analysis. Such an increase in the proportion of MCS was observed for LysN but not for LysArginase (Figure 5.19E). Therefore, it is reasonable to assume that the reduced number of biotinylated peptides observed in the LysArginase digested samples was at least partially caused by other effects such as a charge state reduction of the biotin-containing peptides. Here, derivatization of the basic ε-amino group of lysine followed by LysArginase digestion might yield peptides containing only one primary amine at the N-terminus. Although this peptide will be protonated in the acidic chromatography conditions, it might only be singly charged after electrospray ionization. Compared to that, LysN digestions might yield higher charge states as the phenomenon described above might be partially compensated by the increased peptide length and by the potential presence of internal arginine residues within the sequence. As singly charged precursor ions are not fragmented during proteomic MS data acquisition, reliable conclusions about a charge reduction in the biotinylated, LysArginase-derived peptides cannot be drawn. Therefore, additional experiments with fragmentation of singly charged precursor ions are required in order to investigate this hypothesis. Nevertheless, peptides comprising an N-terminal biotinylation were found after LysN digestion of biotinylated BSA, thus indicating the capability of this protease to cleave adjacent to this modification although the biotinylation-dependent increase in the proportion of MCS suggests a reduced cleavage efficiency (Figure 5.19D+E). Compared to that, approx. 95 % of the biotinylated peptides found after LysArginase digestion featured their modification at an internal lysine residue. The bias towards these peptides might also be explainable by the

hypothesized charge state reduction mentioned before. Here, peptides containing an internal biotinylated lysine feature two basic residues, one at the side chain of the N-terminal residue and the other at its α-amino group. Based on this, the precursor ion might be multiply charged after ESI, thus explaining its preferential detection compared to peptides featuring the modification at the N-terminus.

Comparable to the observations made for BSA digestion, only slight biotinylation-dependent differences in proportion of MCS were detected for the LysArginase digested proteins from HEK 293 lysate (Figure 5.20C). This finding indicates that the observations made for the digested BSA samples where not caused by a protein specific sequence effect but rather applies to a wide range of proteins, thus further supporting the hypothesis of a biotinylation-dependent charge state reduction of LysArginase derived peptides. In contrast, an increase in the number of missed cleavages as well as a reduced median protein sequence coverage was observed when comparing the biotinylated to non-biotinylated LysN digested samples (Figure 5.20C+D). This indicates a less efficient LysN cleavage adjacent to biotin-containing lysine residues similar to the observations made in the BSA biotinylation experiment (Figure 5.19E + Figure 5.20C). However, when comparing the BSA and the HEK protein samples digested with LysN, an increase in the mixture complexity was associated with a reduced proportion of identified, biotin-containing peptides (Figure 5.19B + Figure 5.20A). Among those, approx. 80% featured their biotinylation site at an internal lysine thus indicating a stronger impairment of LysN's cleavage adjacent to biotinylated residues in the complex peptide mixture compared to the BSA sample (Figure 5.19D + Figure 5.20B).

In summary, LysN is able to cleave adjacent to biotinylated lysine residues but its cleavage is strongly impaired. Reliable conclusions about LysArginase's cleavage ability at these modified residues cannot be drawn based on the potential charge state reduction of N-terminal biotinylated peptides. Nevertheless, both enzymes were used in the serial digestion workflow, as their primary task was to cleave N-terminal to PTM containing lysine residues. Any additional cleavage event adjacent to biotinylated lysines was assumed to increase the efficiency of the workflow. Lysine PTM containing peptides which featured a C-terminal arginine residue after tryptic digestion are assumed to be present in the supernatant after streptavidin incubation irrespective of LysN's and LysArginase's capability to cleave next to biotinylated lysine residues (see section 6.2.1 and Figure 5.16).

#### 6.2.1.4. Applying the complete serial digestion workflow does not lead to an enhanced identification of peptides containing methylated lysine residues

As the serial digestion workflow was intended to enhance the identification of multiple different lysine modifications, the supernatant after streptavidin incubation was analyzed by a non-

restrictive search algorithm in order to identify a range of unknown PTMs within the sample. Considering the biotinylated and non-biotinylated samples of the LysN and LysArginase groups at once, methylation was the most frequently reported lysine/arginine modification.

In order to monitor the proportion of this PTM among the different samples taken at each step of the workflow, the corresponding raw data were analyzed by setting methylation at lysine and arginine as a dynamic modification in a classical database search (Table 5.11). The highest number of peptide identification was obtained after tryptic digestion of the protein mixture. Considering the sequential arrangement of the workflow, the next step comprised the biotinylation of the tryptic peptides. Here, an efficient removal of excess quenched NHS-biotin is crucial in order to prevent binding of free biotin to the streptavidin beads. Using the classical C18 reversed phase sample clean-up procedure after NHS-biotin treatment yielded a low binding efficiency of biotinylated peptides to the streptavidin beads (data not shown). This was probably caused by the inefficient removal of excess, free biotin during the C18 reversed phase sample clean-up. Size exclusion chromatography (SEC) also failed to deliver a good separation of peptides and compounds with a low molecular mass (data not shown). Among the different methods tested, SCX chromatography was identified as the most feasible sample clean-up procedure after NHS-based peptide biotinylation. However, SCX chromatography of the non-biotinylated sample was associated with a tremendous reduction in the number of identified peptides. In case of the NHS-biotin treated samples, the loss after SCX chromatography was even higher. This indicates that the biotinylation of peptides' α- and ε-amino groups influences the ability of the resulting secondary amine to get protonated in an acidic environment, thus altering the retention at the SCX stationary phase. In addition, the biotinylation independent identification loss observed after SCX chromatography-based sample clean-up demonstrates the limitation of this method in terms of the peptide recovery. Interestingly, the reduced number of peptide identifications after SCX chromatography was associated with an increased proportion of methylated peptides, indicating a weak increase in the number of identifications of this PTM by the chromatographic procedure. After SCX-chromatography of the non-biotinylated samples, an increased number of methylations were found at lysine and arginine residues. Compared to that, methylations were almost exclusively identified at arginine side chains among the biotinylated peptides after SCX chromatography-based sample clean-up. This suggests an interference of the NHS-biotin treatment and the detectability of lysine methylation. The usability of SCX chromatography for enhancing the identification of methylated peptides is already known. In 2012, the Acuto group performed a large scale analysis to identify arginine methylation sites by a cation exchange-based method (Uhlmann et al. 2012). Under acidic chromatography conditions, the authors aimed at separating modified from unmodified

peptides by using the higher positive charge state of arginine methylated peptides caused by the inefficiency of trypsin to cleave adjacent to this PTM containing residue (Uhlmann et al. 2012). With this technique, they were able to detect 39 arginine methylation sites out of 4-6 mg starting material in four independent experiments (Uhlmann et al. 2012). Compared to that, 73-101 methylarginine containing peptides were detected after SCX chromatography-based sample clean-up of the biotinylation and non-biotinylated mixtures within the present study by using only 1/80 of the amount of starting material. Here, the identification of peptide methylation was not restricted to the presence of a missed tryptic cleavage adjacent to the modified residue, as more than 60 % of all methylated peptides featured their modification at the C-terminus (Table 5.12). Therefore, the SCX chromatography method applied in this study appears to be useful for enhancing the identification of methylated peptides irrespective of the presence of a missed cleavage site C-terminal of the PTM containing amino acid. Furthermore, the enhanced identification was not restricted to arginine methylations as also an increased number of methyllysines were detected in the non-biotinylated sample group after SCX chromatography-based sample clean-up.

The second digestion of the biotinylated and non-biotinylated peptides with LysN or LysArginase was associated with a reduction in peptide identifications compared to the singly digested samples (Table 5.11). This might have been caused by the protease-specific removal of C-terminal basic amino acids thus potentially lowering the charge state of these peptides during ESI and influencing their detection during MS analysis compared to tryptic peptides. In addition to the reduced identification of total peptides after double digestion, a tremendous decline of detected peptide methylation was observed. One possible explanation for this observation might be the capability of trypsin to cleave C-terminal of monomethylated residues (Table 5.12). As the cleavage ability of LysN and LysArginase next to monomethylated residues has already been demonstrated, the second digestion step might remove the methylated amino acids located at the C-terminus of the peptide thus explaining the decline in the detection of peptide methylation in the double digested samples (Taouatas et al. 2010; Huesgen et al. 2015).

Incubation of the biotinylated and non-biotinylated samples with streptavidin correlated with a reduced number of peptide identifications (Table 5.11). In case of the unbiotinylated sample, this might indicate an unspecific binding of non-biotin containing peptides to the streptavidin beads. Compared to the non-biotinylated samples, a tremendous reduction in the identification rate was observed when incubating the biotinylated peptides with streptavidin. This indicates a successful precipitation of biotinylated peptides by the streptavidin beads, although reliable conclusions about the completeness of the pull-down cannot be drawn based on these numbers. Additionally, this reduction indicates a successful biotinylation of the peptides by the NHS-ester

which was further verified by the detection of a high proportion of biotin-modified peptides in the complex samples (Figure 5.21). However, the reduced peptide complexity in the supernatant after depletion did not yield an enhanced identification of methylated peptides.
In summary, the serial digestion workflow was not associated with an enhanced identification of lysine PTM containing peptides. However, the SCX chromatography conditions applied for sample clean-up yielded an increased number and proportion of detected lysine and arginine methylation (Table 5.11). Here, a reduction of the sample complexity is assumed to further improve the identification of these PTM-containing peptides. Therefore, peptide fractionation after or during SCX chromatography should be investigated as a strategy for improved methylation detection in proteomics.

### 6.2.2. $N^{\alpha}$-selective derivatization workflow

As the application of the complete serial-digestion workflow was not associated with an increased identification of lysine modifications, a second method was tested. The $N^{\alpha}$-selective derivatization workflow is based on the selective *in vitro* modification of peptides' α-amino group, followed by NHS-based biotinylation of primary amines in the side chain of lysine and their subsequent pull-down by streptavidin beads. Here, an efficient selective derivatization of the α-amino group was assumed to be the bottleneck reaction during this workflow. Transamination, acetylation and reductive alkylation have already been described as $N^{\alpha}$-selective derivatization methods in different proteomic or peptide-based approaches (Sonomura et al. 2011; Mikami et al. 2012; Chen et al. 2017). Therefore, these techniques were selected and tested regarding their selectivity and efficiency under the experimental conditions used within the present study. In addition to the methods mentioned above, peptides were also propionylated by using propionic anhydride according to the procedure originally described for $N^{\alpha}$-selective acetylation (Mikami et al. 2012). This method was used as *in vitro* acetylation by acetic acid anhydride might be indistinguishable from endogenous protein acetylation.

#### 6.2.2.1. Reductive alkylation is a highly selective and efficient method for derivatization of α-amino groups

The different derivatization methods were tested regarding their reactivity by using a synthetic peptide containing an internal lysine residue as a reactant (Figure 5.23). The expected mass shifts were observed after applying the different methods to the peptide. In addition to that, the peptide transamination experiment yielded an additional mass shift of 74 m/z probably caused by an unspecific side reaction. This side reaction might reflect the high reactivity of the N-terminal carbonyl group generated by this derivatization method (Dixon and Fields 1972).

Based on this observation, *in vitro* transamination is not feasible for a derivatization of peptides in MS approaches as unknown side products impair peptide detection in large scale MS experiments. Therefore, this method was not further investigated within the present study. In contrast, peptide derivatization with the other methods was associated with the detection of one to two potential modification sites. After incubation with NHS-biotin, the doubly derivatized peptides were not found to be biotinylated, thus indicating the derivatization of both, the α- and the ε-amino group. In addition to that, NHS-biotin treatment of the derivatized samples yielded peptides featuring one derivatization and one biotinylation site. This suggest the presence of one primary amine group after applying the different derivatization methods and prior to the biotinylation process. However, mapping of the different modification sites to specific amino acids was not possible based on the MS1 data acquired with MALDI-TOF MS. Additionally, the findings obtained by analyzing the synthetic peptide might not be transferable to the plethora of peptides generated in a bottom-up MS experiment. Hence, the acetylation, propionylation and reductive alkylation method were applied to peptides of HEK proteins digested with trypsin. Selectivity, efficiency and reproducibility were investigated by LC-MS2 measurements.

The percentage of MS2 spectra successfully matched to a peptide sequence (PSMs) were almost identical between the different derivatization techniques and the input (Table 5.13). This indicates that unexpected side reactions were not highly abundant after applying the derivatization technique to the HEK peptides.

Compared to the non-derivatized input, a higher number of peptides were identified in the derivatized sample groups (Figure 5.24). This might be attributed to multiple reasons. For example, reductive alkylation, propionylation and acetylation might alter the chromatographic behavior of peptides during LC thus rectifying the elution pattern throughout the gradient leading to a less complex peptide mixture entering the spectrometer at a given time point. Especially the addition of the phenyl-group during reductive alkylation with benzaldehyde is expected to increase the hydrophobicity of the peptides which then leads to a delayed elution in reversed-phase chromatography. Another possibility might be the occurrence of varying numbers of modifications at one specific amino acid residue. Peptides found as being singly and doubly modified at the N-terminus will be listed twice in the output table. At least for reductive alkylation, such a double modification of the N-terminus has already been described (Chen et al. 2017). A third reason for the increased number of identifications might be an incomplete derivatization of peptides. In this case, the peptide sequence will be identified as unmodified and modified during database analysis, thus yielding two entries in the output table.

Among the three derivatization methods tested, reductive alkylation yielded the highest proportion of derivatized peptides (Figure 5.24). So far, little is known about the efficiency of

anhydride based $N^{\alpha}$-selective derivatization of complex peptide mixtures. In the original paper in which the acidic anhydride-based derivatization method was described, the authors tested the efficiency on Cytochrome C derived peptides (Mikami et al. 2012). Although they reported an efficient modification of peptides, this observation might be difficult to extrapolate to more complex samples (Mikami et al. 2012). In peptides derived from one single, low molecular mass protein, only a limited number of different amino acids are present at the N-termini. Compared to that, proteolytic digestion of a complex sample yields a more representative peptide mixture thus allowing more reliable conclusions about the reactivity of a derivatization method. This might explain the difference in the acetylation efficiency detected by Mikami et al. (2012) and in the present study. Additionally, one has to keep in mind that a distinction between *in vitro* and endogenous acetylation sites is not possible when using acetic acid anhydride for the derivatization procedure. Therefore, endogenous acetylation sites might have increased the number of acetylated peptides detected in this experiment. However, their contribution to the total number of detected acetylated peptides is expected to be rather low as these endogenous modifications are usually only found in minor amounts without prior enrichment in shotgun proteomics. Nevertheless, in order to prevent this bias, the propionylated data set might yield more comprehensive results regarding the derivatization efficiency. Here, the proportion of derivatized peptides was lower compared to the acetylated sample group. This was probably not only caused by the endogenous acetylation sites raising the proportion of acetylated peptides but also by derivatization-based differences in behavior during LC and ESI.

Sequence comparison of the derivatized peptides identified among the three technical replicates indicates a high reproducibility of each individual method (Figure 5.25). Importantly, the three derivatization techniques featured a high selectivity towards modification of the α-amino group (Figure 5.26).

Among the different methods tested, reductive alkylation was the only derivatization technique yielding a high reproducibility, efficiency and $N^{\alpha}$-selectivity. Therefore, this method was used in order to investigate the derivatization-based workflow for enhancing PTM identification.

#### 6.2.2.2. Applying the complete $N^{\alpha}$-selective derivatization workflow enhances the identification of arginine but not of lysine methylated peptides

Similar to the procedure described for the serial digestion method, the MS data of the derivatized and streptavidin incubated samples were used for database analysis using an unrestricted PTM search in order to get an overview about the different potential modifications present after applying the complete workflow. Among the different modifications reported by the algorithm in the NHS-biotin treated samples, 1.3-1.5 % of the peptides featured a methylation site either at lysine or arginine residues (Table 5.14). In case of these samples,

methylation was almost exclusively detected at arginine side chains. Compared to that, methyllysine containing peptides were more abundant than methylation at arginine residues in the non-biotinylated samples. For monitoring the proportion of these PTMs at the different steps of the workflow, each sample taken during the validation study of the method was analyzed in a classical database search by setting lysine and arginine methylations as dynamic modifications.

Starting with the highest number of identifications directly after tryptic digestion of proteins from HEK 293 cell lysate, each additional step in the workflow was associated with a decline in the number of peptide detections (Figure 5.28, table 5.15). Interestingly, this reduction was not uniform throughout the different peptide species. Compared to the non-biotinylated sample (without SCX chromatography-based sample clean-up), the peptide mixture modified with NHS-biotin and desalted via SCX chromatography featured a tremendous loss of lysine containing species (Figure 5.28). As the number of arginine containing peptides was nearly identical between these samples, this finding indicates alterations in the retention of biotinylated peptides during SCX chromatography. Direct comparison of the number of peptide identifications after SCX chromatography of biotinylated and non-biotinylated samples further supports this biotinylation effect (Table 5.15). As already discussed in sections of the serial digestion workflow, this phenomenon might be ascribed to the influence of the biotinylation on the ability of the amine group to get protonated under the acidic conditions used in this study.
Similar to the observations made in the serial digestion workflow, SCX chromatography was associated with an increased detection of methylated peptides (Table 5.15). Whereas the NHS-biotin treated samples featured only an increase in methylarginine containing peptides, a higher number of methylated peptides was identified at lysine and arginine residues in case of the non-biotinylated samples. Incubation with streptavidin was not associated with huge changes in the proportions of peptide methylations identified for the single sample groups. The missing improvement of methyllysine identification in the NHS-biotin treated, streptavidin incubated samples was surprising as peptides featuring this PTM were found in the non-biotinylated samples, thus indicating their potential detectability. It is reasonable to assume that the missing identification of these peptides was probably not caused by the introduction of missed cleavage sites next to methylated lysine residues. Such an MCS would have resulted in the formation of peptides with an internal methylated and a C-terminal, unmodified lysine residue. Although this peptide would have been biotinylated by the NHS-biotin treatment, it should have been detectable in the non-streptavidin incubated sample group but here, methyllysine containing peptides were only found in minor proportions. Therefore, this observation might rather indicate a side reaction occurring at monomethylated lysine residues after incubation with NHS-

biotin. If the NHS-ester were able to react with the secondary amine present at the monomethylated lysine residue, such a peptide would not have been identified during database analysis as this mass shift was not set as a variable modification. Besides that, biotinylation at monomethylated lysine residues would also lead to a depletion of these peptides during streptavidin incubation. This would dramatically affect the usability of the present workflow for enhancing the identification of this PTM. A preliminary database analysis of the biotinylated and non-biotinylated samples after SCX chromatography with a mass shift of 240 m/z (biotinylation + methylation) set as a variable modification at lysine residues was associated with the identification of up to 105 high confident peptide groups featuring this modification (data not shown). Here, the modification was predominantly found in biotinylated samples suggesting that at least some of these peptides are true identifications. However, as this modification is not commonly searched in MS data analyses, further verification of the identifications is required in order to validate the reactivity of the NHS-ester with monomethylated lysine side chains.

Applying the complete derivatization workflow to a peptide mixture was associated with an increase in the detection of methylarginines which were identified with a high reproducibility among the different replicates (Figure 5.30). An improvement in the identification of arginine modifications was expected as the sample complexity was reduced by the biotinylation and depletion of unmodified lysine containing peptides. However, a similar effect was achieved by SCX chromatography of the biotinylated and non-biotinylated sample which also resulted in an increased identification of monomethylated peptides. This demonstrates the applicability of the SCX chromatography-based sample clean up procedure for enhancing the identification of these peptides. Possible steps for further improving the SCX chromatography-associated increase in the number of identifications of methylated peptide have already been described in section 6.2.1.4. In addition to that, utilization of SCX columns with a higher capacity might further enhance the identification rate as additional peptides were detected when applying a second round of sample clean-up with the flow through of the first chromatographic step (data not shown).

The methylated peptides found in the different steps during the workflow (applied to a complex peptide mixture) were compared in order to investigate their redundancy. This comparison revealed only a partial overlap among the methylated peptides found at the different steps of the workflow (Figure 5.29). In case of methylarginines, it might therefore be beneficial to investigate the biotinylated samples before and after streptavidin incubation to get the most comprehensive methylation data set. Due to the potential interference of the NHS-biotin treatment with monomethylated lysine residues, the highest yield of unique identifications of

methyllysine containing peptides might be achieved by SCX-chromatography without biotinylation.

### 6.2.3. SCX chromatography increases the identification of unique methylated peptides in a large-scale analysis

The utilization of SCX chromatography for enhancing the identification of methylated peptides has been described in the previous sections dealing with the serial digestion and the derivatization-based workflows. However, the starting material desalted by the SCX chromatography-based method differed between these two techniques, as the derivatization workflow comprised an $N^{\alpha}$-selective reductive alkylation of the peptides prior to the NHS-treatment. Therefore, SCX chromatography of these samples was assumed to yield different peptide populations as the physicochemical properties might be altered depending on the derivatization/biotinylation/modification status. Therefore, methylated peptide species identified in the single samples were compared regarding their redundancy (Figure 5.31). For lysine methylations, the highest number of modified peptides is obtainable by analyzing non-biotinylated samples with and without reductive alkylation of the α-amino group. Here, many of the identified methylated peptides were non-redundant between the workflows even after stringent filtering of peptides that only occurred in single replicates. In case of methylarginine, all samples featured a unique set of modified peptides. Taken together, this would justify the utilization of all four strategies to obtain the most comprehensive result. Additionally, one has to consider the unique methylarginine containing peptides identified after applying the complete $N^{\alpha}$-derivatization workflow, thus adding an additional layer of analysis for the achievement of detailed methylation data sets.

Among the samples featuring an increased identification of methyllysines, 109-212 peptides with lysine monomethylation sites were identified within the present study by using only 50 µg of derivatized or non-derivatized peptides as starting material. In 2013, Cao et al. detected 323 monomethylated sites (at lysine) in an antibody-based large scale approach. However, the authors used 20 mg protein as starting material and did an SCX chromatography-based fractionation of the peptide samples after the enrichment (Cao et al. 2013). In a similar approach, Guo et al. (2014) identified 234 monomethylated peptides (at lysine) by immunoaffinity purification (10 mg protein starting material). Compared to these studies, the afore-mentioned number of methylated peptides detected in the study presented here without method optimization and with the low amount of starting material is remarkable. Fine tuning of the single steps is assumed to improve the identification even further.

In samples with an increased methylarginine detection, 73-118 peptides have been identified to contain a methylated arginine residue. These numbers are comparable to those obtained by Uhlmann et al. (2012) in a large-scale arginine methylation analysis performed on T-cells. Here, the authors identified 39, 66 and 215 arginine methylation sites by SCX-, IEF- and HILIC-based enrichment/fractionation methods, respectively. In an antibody based approach, Guo et al. (2014) identified 2053 monomethylarginine containing peptides. However, the authors used 10 mg of proteins as a starting material which is 200 times more than the amount of derivatized or non-derivatized peptides used in this study. Considering the potential increase in detection of methylarginine containing peptides after method improvement, the procedures presented here might be a valuable alternative for large-scale methylation studies with limited amount of starting material.

### 6.2.4. A potential workflow for comprehensive analysis of protein lysine and arginine methylation

Considering all aspects mentioned in the previous sections, a potential workflow for the comprehensive analysis of protein methylation would start with trypsin digestion of the protein mixture (Figure 6.1). A subfraction of this tryptic digest is directly used for SCX chromatography followed by LC-MS2 analysis. The remaining peptide mixture is split into two groups. Here, one group is treated with NHS-biotin prior to SCX-based sample clean-up and MS analysis. Compared to that, the second group of the tryptic peptides is derivatized at their α-amino groups by reductive alkylation. Afterwards, these peptides are split again into two parts, one of which is biotinylated and the other one remaining unbiotinylated. After SCX chromatography of both of these parts, the non-biotinylated peptides and a small fraction of the NHS-biotinylated sample are analyzed by LC-MS2. Additionally, the remaining biotinylated peptides are incubated with streptavidin before they are also used for MS-based analysis of peptide methylation. After the database search, the methylation sites identified by the different samples can be integrated and are assumed to yield a comprehensive overview of the occurrence of this PTM at lysine and arginine side chains within different proteins. Besides its standalone application, this workflow could also be used in combination with enrichment strategies for other PTMs thus potentially contributing to the identification of PTM-crosstalk.

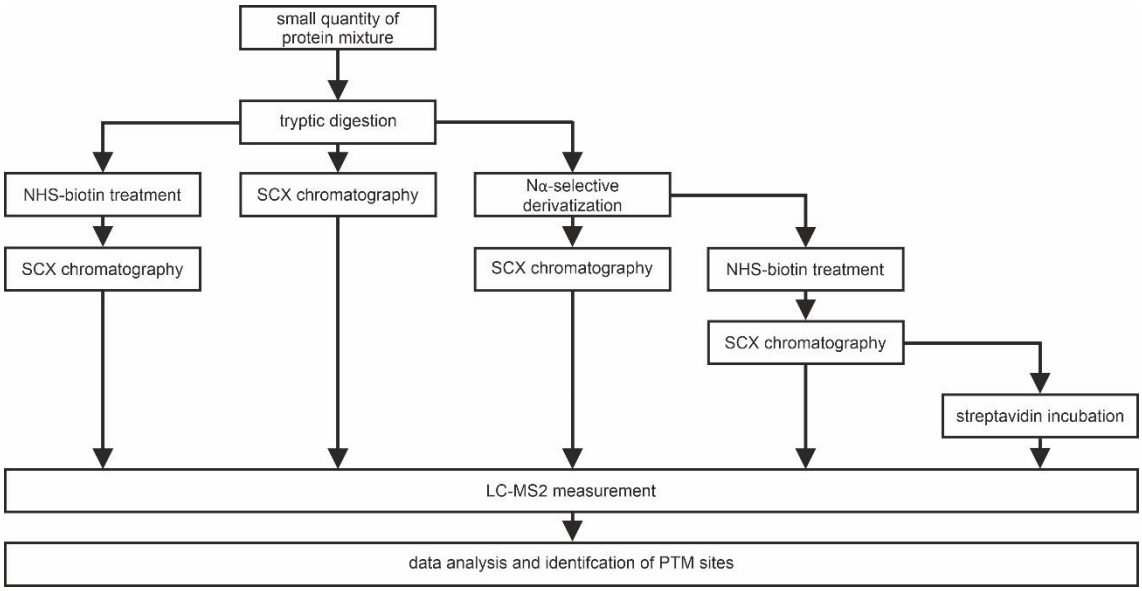


**Figure 6.1: Overview of a workflow suggested for the comprehensive analysis of protein methylation sites.**

# 7. Appendix

## 7.1 Phosphoproteomic data

### 7.1.1. Phosphoproteomic analysis of samples from whole cell lysate after Torin1 treatment

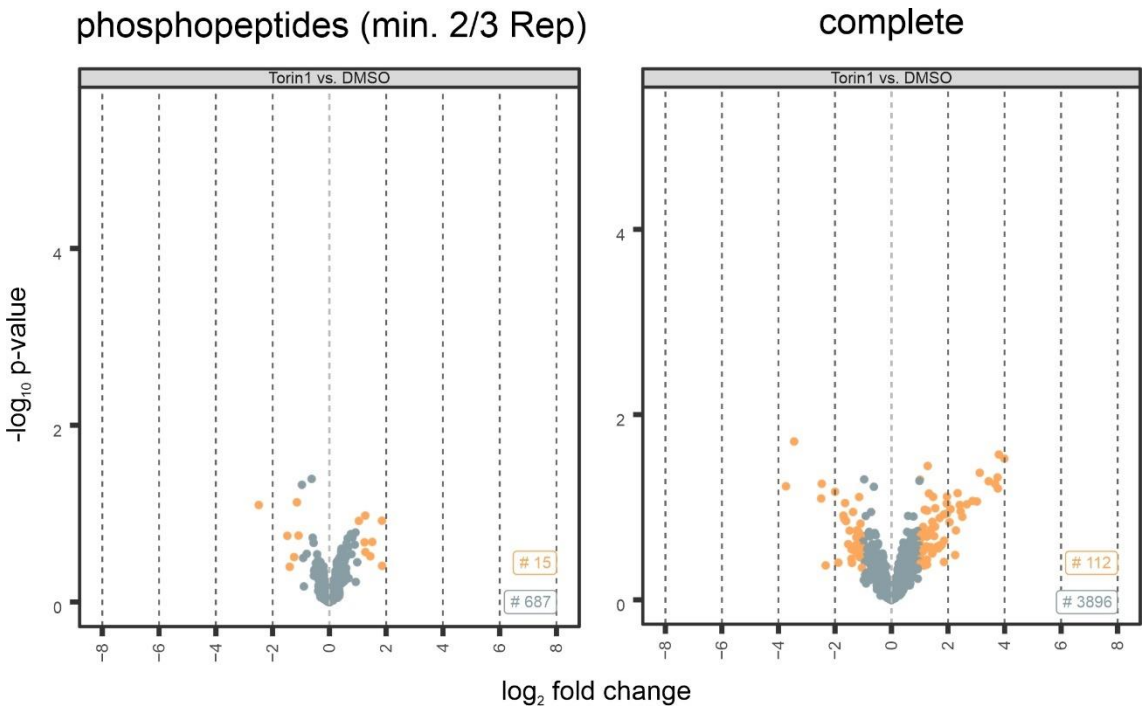


**Figure 7.1: Phosphopeptide enrichment from whole cell lysate digest (Torin1 vs. DMSO).**
$TiO_2$-based phosphopeptide enrichment was performed with peptides derived from tryptic digestion of whole cell lysate. Phosphopeptides were fractionated via SCX chromatography prior to LC-MS2 measurement. The experiment was performed in three biological replicates. Raw data were analyzed using the MaxQuant software. Statistical analysis (Torin1 vs DMSO) was either performed on phosphopeptides found in at least two out of three replicates (left, adjusted p-value threshold 0.05) or on the complete peptide data set (right, adjusted p-value threshold 0.15) by using the limma package implemented in an R-script.

### 7.1.2. Phosphoproteomic analysis of samples from whole cell lysate after FSK/db-cAMP treatment by using the complete peptide data set

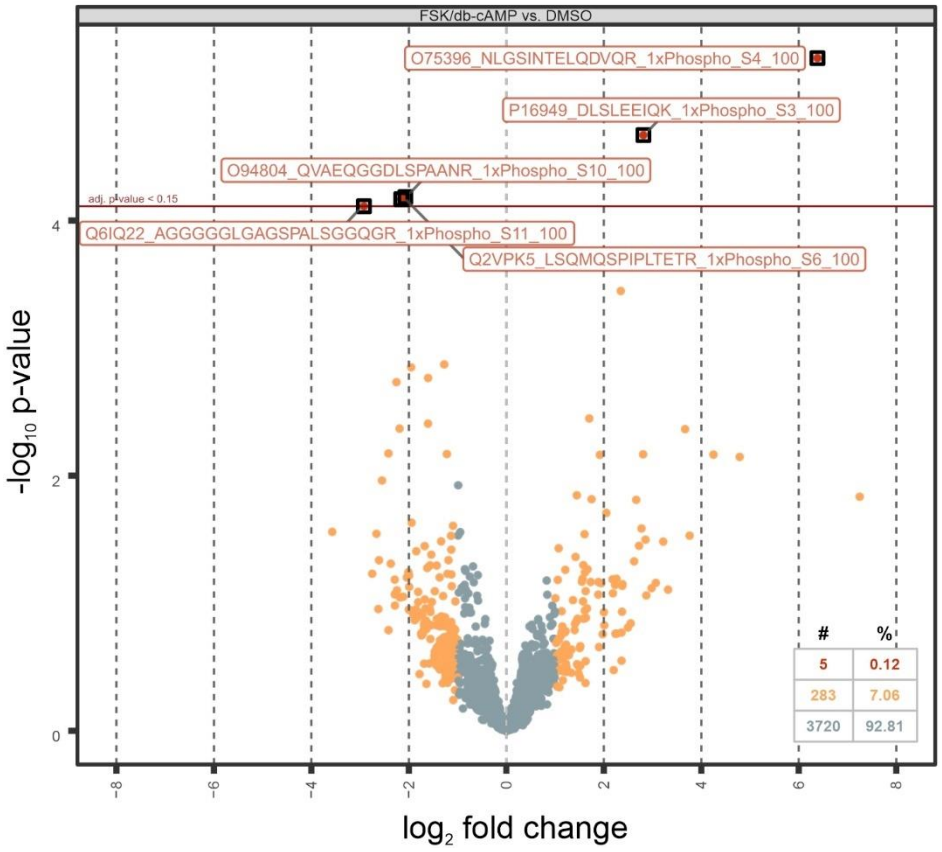


**Figure 7.2: Phosphopeptide enrichment from whole cell lysate digest (FSK/db-cAMP vs. DMSO, complete data set).** $TiO_2$-based phosphopeptide enrichment was performed with peptides derived from tryptic digestion of whole cell lysate. Phosphopeptides were fractionated via SCX chromatography prior to LC-MS2 measurements. The experiment was performed in three biological replicates. Raw data were analyzed using the MaxQuant software. Statistical analysis (FSK/db-cAMP vs DMSO) was performed on the complete peptide data set (adjusted p-value threshold 0.15) by using the limma package implemented in an R-script.

### 7.1.3. Phosphoproteomic analysis of samples from the lysosomal soluble fraction after Torin1 treatment

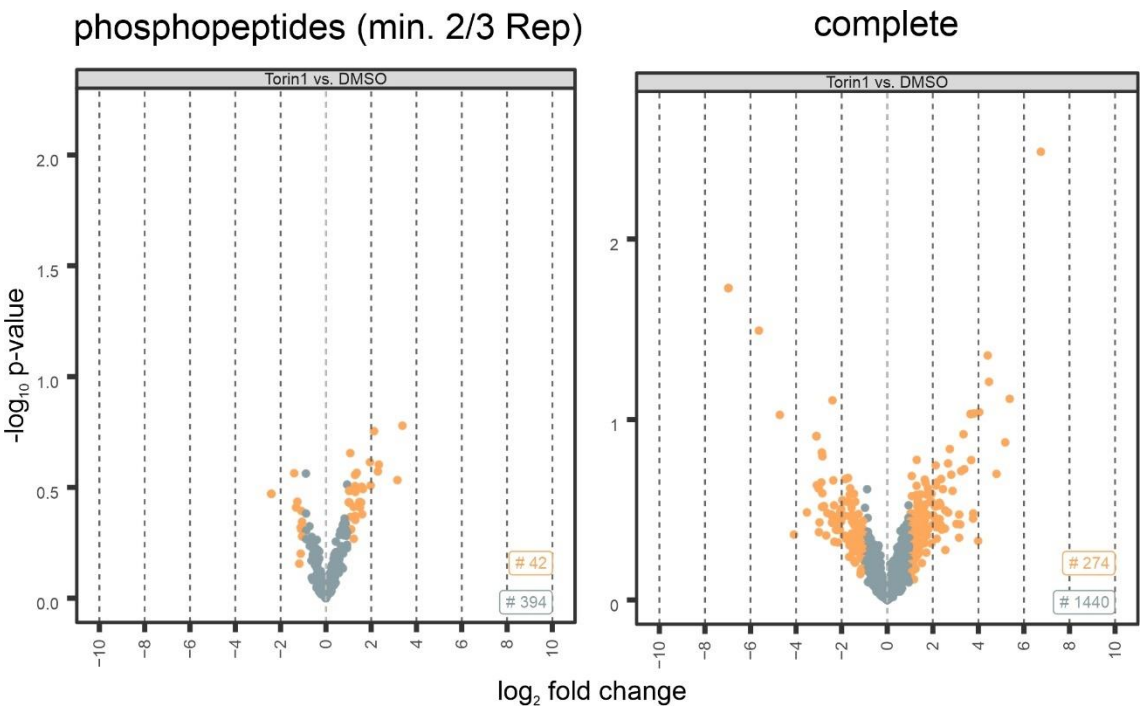


**Figure 7.3: Phosphopeptide enrichment from lysosomal soluble fraction (Torin1 vs. DMSO).**
Lysosomes from isotopically labeled cells were enriched and subsequently separated into a water soluble and membrane fraction. After tryptic digestion, phosphopeptide enrichment was performed by $TiO_2$. The experiment was performed in three biological replicates. Phosphopeptides derived from the soluble fractions were analyzed with an LTO Orbitrap Velos mass spectrometer. Raw data were searched against a human reference database by using the Mascot search engine. Statistical analysis (Torin1 vs DMSO) was either performed on phosphopeptides found in at least two out of three replicates (left, adjusted p-value threshold 0.05) or on the complete peptide data set (right, adjusted p-value threshold 0.15) by using the limma package implemented in an R-script.

### 7.1.4. Phosphoproteomic analysis of samples from the lysosomal soluble fraction after FSK/db-cAMP treatment

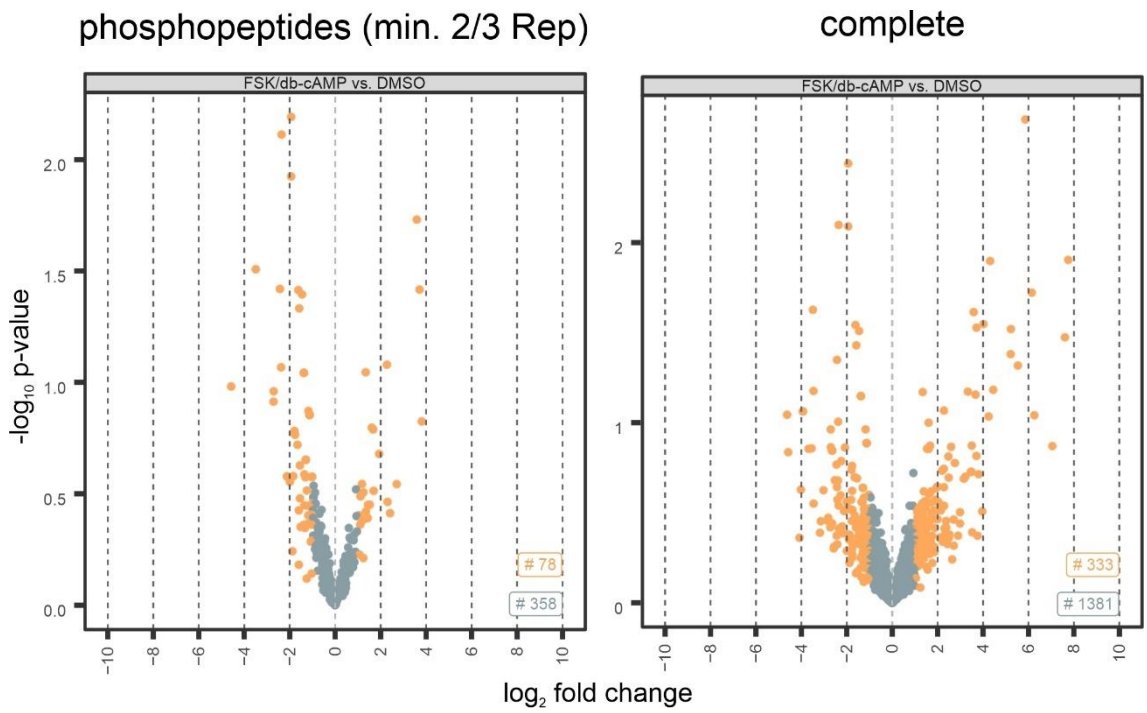


**Figure 7.4: Phosphopeptide enrichment from lysosomal soluble fraction (FSK/db-cAMP vs. DMSO).**
Lysosomes from isotopically labeled cells were enriched and subsequently separated into a water soluble and membrane fraction. After tryptic digestion, phosphopeptide enrichment was performed by $TiO_2$. The experiment was performed in three biological replicates. Phosphopeptides derived from the soluble fractions were analyzed with an LTO Orbitrap Velos mass spectrometer. Raw data were searched against a human reference database by using the Mascot search engine. Statistical analysis (FSK/db-cAMP vs DMSO) was either performed on phosphopeptides found in at least two out of three replicates (left, adjusted p-value threshold 0.05) or on the complete peptide data set (right, adjusted p-value threshold 0.15) by using the limma package implemented in an R-script.

### 7.1.5. Phosphoproteomic analysis of samples from the lysosomal membrane fraction after Torin1 treatment

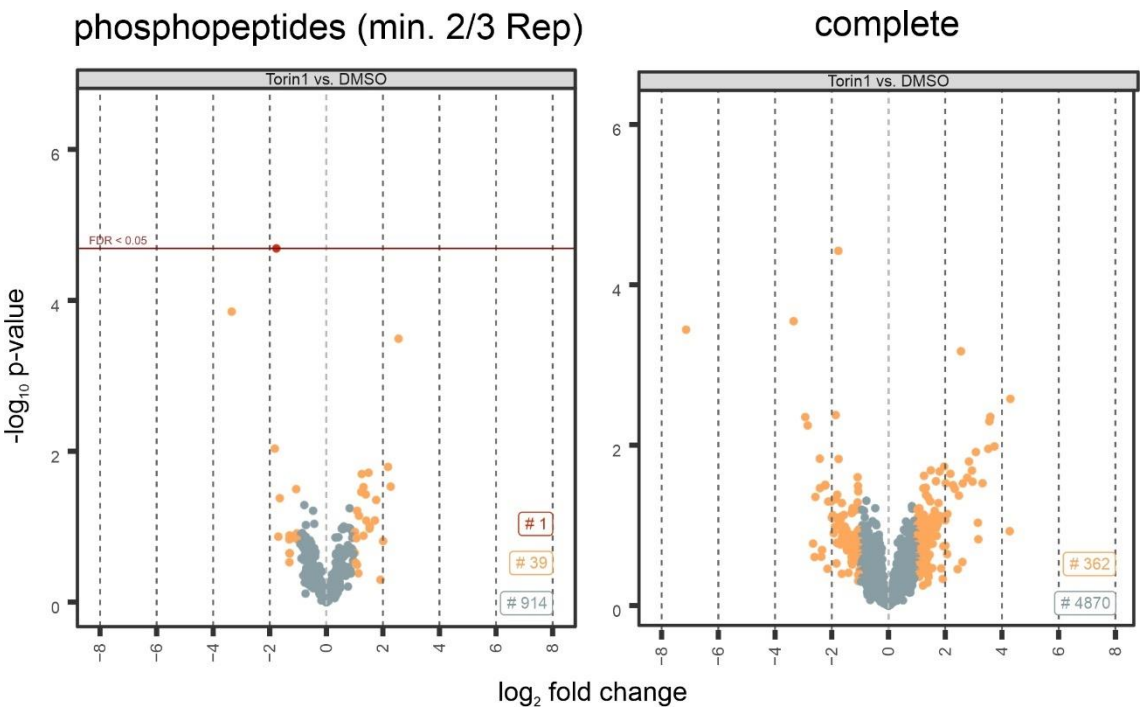


**Figure 7.5: Phosphopeptide enrichment from lysosomal membrane fraction (Torin1 vs. DMSO).**
Lysosomes from isotopically labeled cells were enriched and subsequently separated into a water soluble and membrane fraction. After tryptic digestion, phosphopeptide enrichment was performed by $TiO_2$. The experiment was performed in three biological replicates. Phosphopeptides derived from the membrane fractions were analyzed with an Orbitrap Fusion Lumos mass spectrometer. Raw data were searched against a human reference database by using the Mascot search engine. Statistical analysis (Torin1 vs DMSO) was either performed on phosphopeptides found in at least two out of three replicates (left, adjusted p-value threshold 0.05) or on the complete peptide data set (right, adjusted p-value threshold 0.15) by using the limma package implemented in an R-script.

### 7.1.6. Phosphoproteomic analysis of samples from the lysosomal membrane fraction after FSK/db-cAMP treatment by using the complete peptide data set

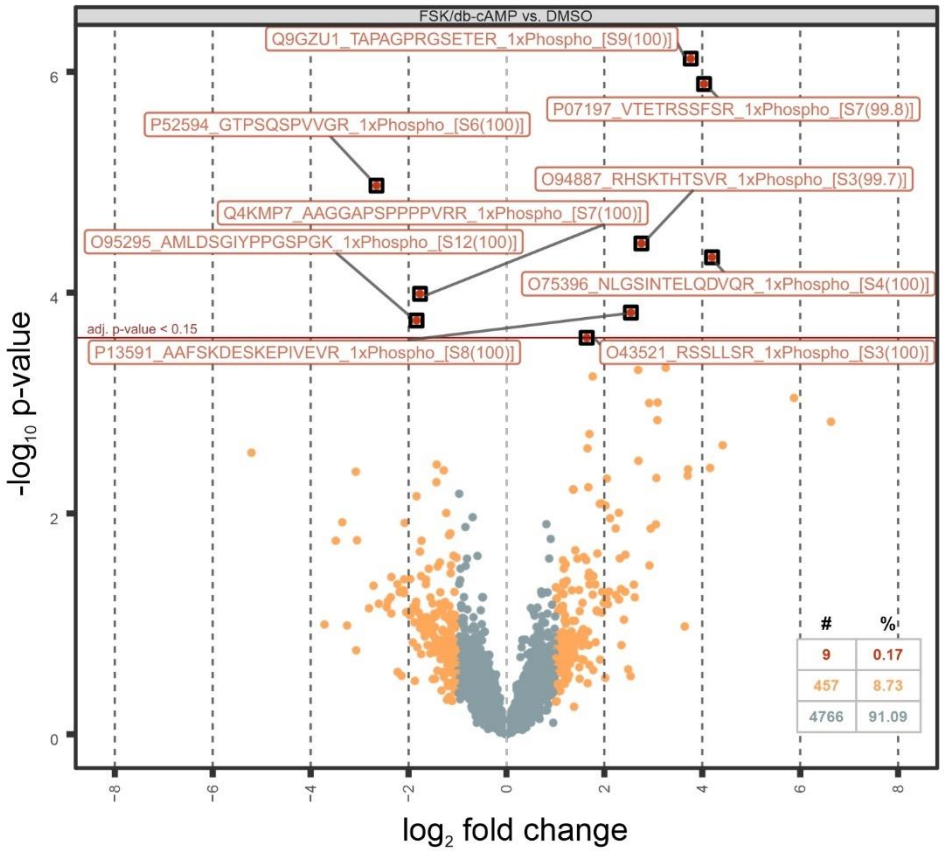


**Figure 7.6: Phosphopeptide enrichment from lysosomal membrane (FSK/db-cAMP vs. DMSO, complete data set).** Lysosomes from isotopically labeled cells were enriched and subsequently separated into a water soluble and membrane fraction. After tryptic digestion, phosphopeptide enrichment was performed by $TiO_2$. The experiment was performed in three biological replicates. Phosphopeptides derived from the membrane fractions were analyzed with an Orbitrap Fusion Lumos mass spectrometer. Raw data were searched against a human reference database by using the Mascot search engine. Statistical analysis (FSK/db-cAMP vs DMSO) was performed on the complete peptide data set (adjusted p-value threshold 0.15) by using the limma package implemented in an R-script.

## 7.2 2D-gel electrophoresis of FSK/db-cAMP and DMSO treated sample

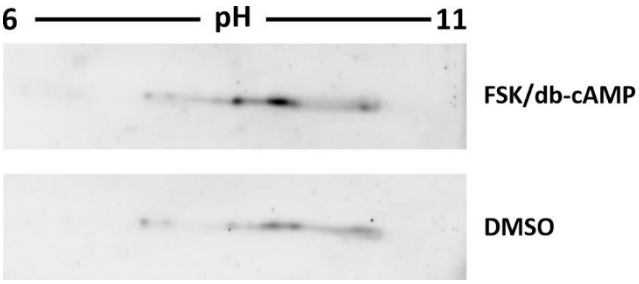


**Figure 7.7: Immune detection of SNAPIN after 2D-gelelectrophoresis and Western Blot in FSK/db-cAMP and DMSO treated samples.**
The SNAPIN signals depicted here are derived from the same analysis as the one shown in section 5.1.3.3 (first replicate, FSK/db-cAMP and DMSO samples). The only difference between figure 7.7 and figure 5.6A is that the signals of both samples shown in figure 7.7 were detected with the same exposure time (Exposure time FSK/db-cAMP sample and DMSO control: 3 min).

## 7.3 SNAPIN KO via CRISPR-Cas9

### 7.3.1. Alignment of the sequencing reads to the reference sequence for HEK 293 SNAPIN KO clone A7

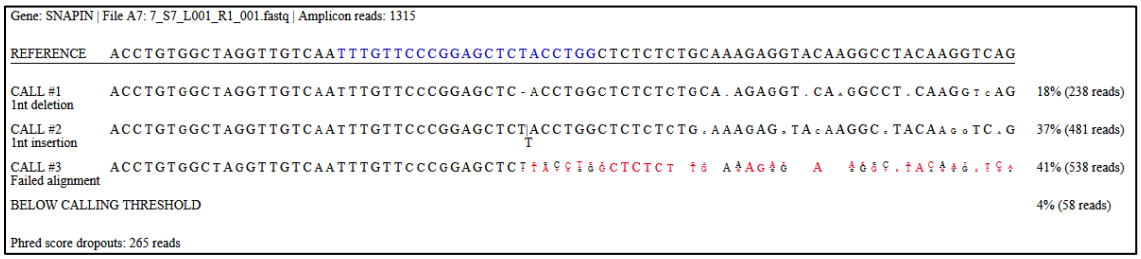


**Figure 7.8: Detailed analysis of HEK 293 SNAPIN KO clone A7.**
KO cells were generated with the CRISPR-Cas9 method. Monoclonal cell populations were prepared, and the KO was validated by NGS. Sequencing data were analyzed with the "outknocker" web-tool (Schmid-Burgk et al. 2014). Here, the alignment of the sequencing reads to the reference sequence is shown for HEK 293 SNAPIN KO clone A7.

### 7.3.2. Alignment of the sequencing reads to the reference sequence for HeLa SNAPIN KO clon A12

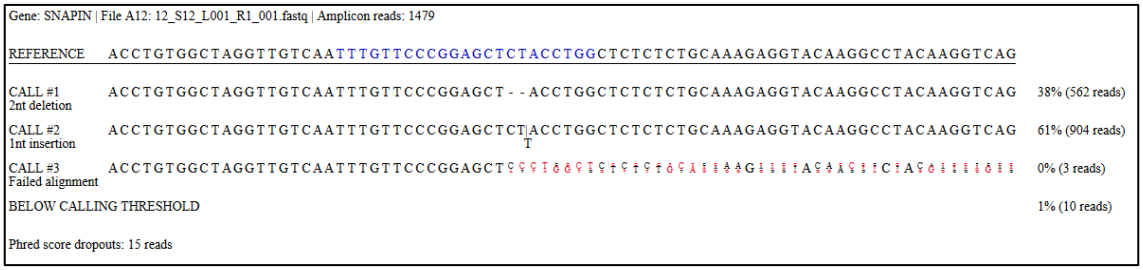


**Figure 7.9: Detailed analysis of HeLa SNAPIN KO clone A12.**
KO cells were generated with the CRISPR-Cas9 method. Monoclonal cell populations were prepared, and the KO was validated by NGS. Sequencing data were analyzed with the "outknocker" web-tool (Schmid-Burgk et al. 2014). Here, the alignment of the sequencing reads to the reference sequence is shown for HeLa SNAPIN KO clone A12.

## 7.4 PCA plot proteome comparison

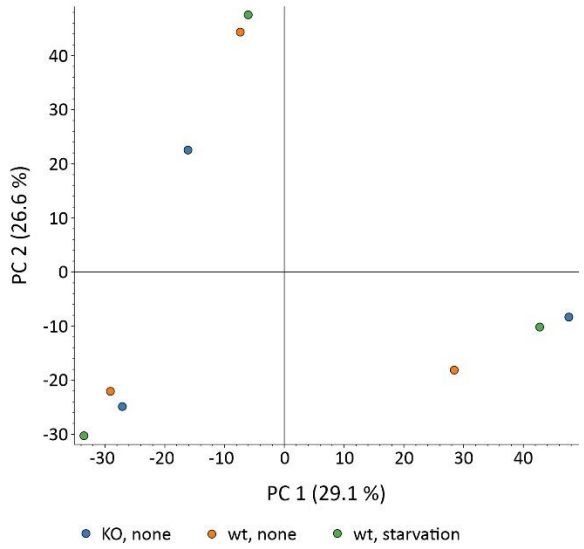


**Figure 7.10: PCA plot of proteome comparison samples.**
The colors represent the different treatments and genotypes investigated in the present study. Isotopically labeled whole cell protein samples were digested and analyzed by LC-MS2. Data processing was performed with PD.

## 7.5 pCMV6_SNAPIN vector map

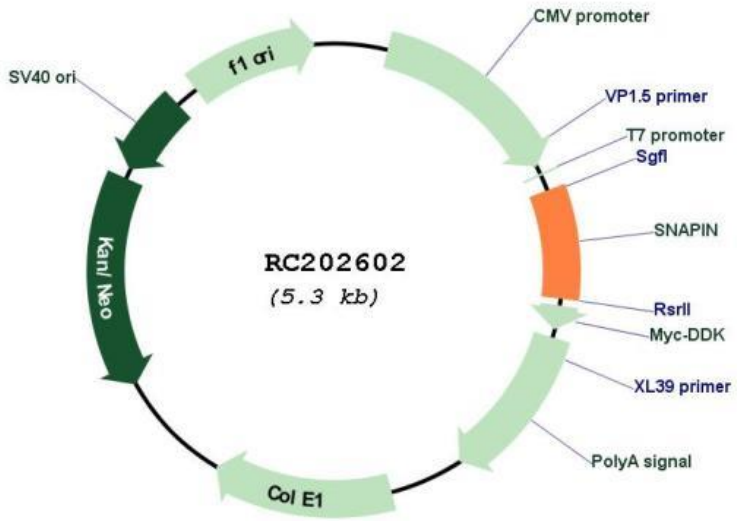


**Figure 7.11: Vector map of the pCMV6_SNAPIN plasmid obtained from Origene (Rockville, USA).**
Image source: https://www.origene.com/drawmapbysku?SKU=RC202602

# References


Acosta-Jaquez, H. A.; Keller, J. A.; Foster, K. G.; Ekim, B.; Soliman, G. A.; Feener, E. P.; Ballif, B. A.; Fingar, D. C. (2009): Site-specific mTOR phosphorylation promotes mTORC1-mediated signaling and cell growth. In *Molecular and cellular biology* 29 (15), pp. 4308–4324. DOI: 10.1128/MCB.01665-08.

Aebersold, R.; Mann, M. (2003): Mass spectrometry-based proteomics. In *Nature* 422 (6928), pp. 198–207. DOI: 10.1038/nature01511.

Agilent Technologies SDM Manual: QuikChange II Site-Directed Mutagenesis Kit. https://www.agilent.com/cs/library/usermanuals/Public/200523.pdf. Instruction Manual.

Ambrosio, A. L.; Di Pietro, S. M. (2016): Storage pool diseases illuminate platelet dense granule biogenesis. In *Platelets* 28 (2), pp. 138–146. DOI: 10.1080/09537104.2016.1243789.

Antonia, R. J.; Castillo, J.; Herring, L. E.; Serafin, D. S.; Liu, P.; Graves, L. M.; Baldwin, A. S.; Hagan, R. S. (2019): TBK1 limits mTORC1 by promoting phosphorylation of Raptor Ser877. In *Scientific reports* 9 (1), p. 13470. DOI: 10.1038/s41598-019-49707-8.

Antonin, W.; Fasshauer, D.; Becker, S.; Jahn, R.; Schneider, T. R. (2002): Crystal structure of the endosomal SNARE complex reveals common structural principles of all SNAREs. In *Nature structural biology* 9 (2), pp. 107–111. DOI: 10.1038/nsb746.

Aronson, N. N.; de Duve, C. (1968): Digestive activity of lysosomes. II. The digestion of macromolecular carbohydrates by extracts of rat liver lysosomes. In *The Journal of biological chemistry* 243 (17), pp. 4564–4573.

Barrabés, S.; Sarrats, A.; Fort, E.; Llorens, R. de; Rudd, P. M.; Peracaula, R. (2010): Effect of sialic acid content on glycoprotein pI analyzed by two-dimensional electrophoresis. In *Electrophoresis* 31 (17), pp. 2903–2912. DOI: 10.1002/elps.200900764.

Barriocanal, J. G.; Bonifacino, J. S.; Yuan, L.; Sandoval, I. V. (1986): Biosynthesis, glycosylation, movement through the Golgi system, and transport to lysosomes by an N-linked carbohydrate-independent mechanism of three lysosomal integral membrane proteins. In *The Journal of biological chemistry* 261 (35), pp. 16755–16763.

Bedford, M. T.; Frankel, A.; Yaffe, M. B.; Clarke, S.; Leder, P.; Richard, S. (2000): Arginine methylation inhibits the binding of proline-rich ligands to Src homology 3, but not WW, domains. In *The Journal of biological chemistry* 275 (21), pp. 16030–16036. DOI: 10.1074/jbc.M909368199.

Beguinot, L.; Lyall, R. M.; Willingham, M. C.; Pastan, I. (1984): Down-regulation of the epidermal growth factor receptor in KB cells is due to receptor internalization and subsequent degradation in lysosomes. In *Proceedings of the National Academy of Sciences of the United States of America* 81 (8), pp. 2384–2388. DOI: 10.1073/pnas.81.8.2384.

Berthet, J.; Rall, T. W.; Sutherland, E. W. (1957): The relationship of epinephrine and glucagon to liver phosphorylase. IV. Effect of epinephrine and glucagon on the reactivation of phosphorylase in liver homogenates. In *The Journal of biological chemistry* 224 (1), pp. 463–475.

Berwick, D. C.; Dell, G. C.; Welsh, G. I.; Heesom, K. J.; Hers, I.; Fletcher, L. M.; Cooke, F. T.; Tavaré, J. M. (2004): Protein kinase B phosphorylation of PIKfyve regulates the trafficking of GLUT4 vesicles. In *Journal of cell science* 117 (Pt 25), pp. 5985–5993. DOI: 10.1242/jcs.01517.

Biever, A.; Puighermanal, E.; Nishi, A.; David, A.; Panciatici, C.; Longueville, S.; Xirodimas, D.; Gangarossa, G.; Meyuhas, O.; Hervé, D.; Girault, J.-A.; Valjent, E. (2015): PKA-dependent phosphorylation of ribosomal protein S6 does not correlate with translation efficiency in striatonigral and striatopallidal medium-sized spiny neurons. In *The Journal of neuroscience : the official journal of the Society for Neuroscience* 35 (10), pp. 4113–4130. DOI: 10.1523/JNEUROSCI.3288-14.2015.

Birkeli, K. A.; Llorente, A.; Torgersen, M. L.; Keryer, G.; Taskén, K.; Sandvig, K. (2003): Endosome-to-Golgi transport is regulated by protein kinase A type II alpha. In *The Journal of biological chemistry* 278 (3), pp. 1991–1997. DOI: 10.1074/jbc.M209982200.

Blom, N.; Gammeltoft, S.; Brunak, S. (1999): Sequence and structure-based prediction of eukaryotic protein phosphorylation sites. In *Journal of molecular biology* 294 (5), pp. 1351–1362. DOI: 10.1006/jmbi.1999.3310.

Blom, N.; Sicheritz-Pontén, T.; Gupta, R.; Gammeltoft, S.; Brunak, S. (2004): Prediction of post-translational glycosylation and phosphorylation of proteins from the amino acid sequence. In *Proteomics* 4 (6), pp. 1633–1649. DOI: 10.1002/pmic.200300771.

Boisvert, F.-M.; Cote, J.; Boulanger, M.-C.; Cleroux, P.; Bachand, F.; Autexier, C.; Richard, S. (2002): Symmetrical dimethylarginine methylation is required for the localization of SMN in Cajal bodies and pre-mRNA splicing. In *The Journal of cell biology* 159 (6), pp. 957–969. DOI: 10.1083/jcb.200207028.

Borodinova, A. A.; Kuznetsova, M. A.; Alekseeva, V. S.; Balaban, P. M. (2019): Histone acetylation determines transcription of atypical protein kinases in rat neurons. In *Scientific reports* 9 (1), p. 4332. DOI: 10.1038/s41598-019-40823-z.

Bowman, S. L.; Bi-Karchin, J.; Le, L.; Marks, M. S. (2019): The road to lysosome-related organelles: Insights from Hermansky-Pudlak syndrome and other rare diseases. In *Traffic (Copenhagen, Denmark)* 20 (6), pp. 404–435. DOI: 10.1111/tra.12646.

Braulke, T.; Bonifacino, J. S. (2009): Sorting of lysosomal proteins. In *Biochimica et biophysica acta* 1793 (4), pp. 605–614. DOI: 10.1016/j.bbamcr.2008.10.016.

Braun, M.; Waheed, A.; Figura, K. von (1989): Lysosomal acid phosphatase is transported to lysosomes via the cell surface. In *The EMBO journal* 8 (12), pp. 3633–3640.

Bright, N. A.; Davis, L. J.; Luzio, J. P. (2016): Endolysosomes are the principal intracellular sites of acid hydrolase activity. In *Current biology : CB* 26 (17), pp. 2233–2245. DOI: 10.1016/j.cub.2016.06.046.

Bryson, B. D.; White, F. M. (2015): Quantitative profiling of lysine acetylation reveals dynamic crosstalk between receptor tyrosine kinases and lysine acetylation. In *PloS one* 10 (5), e0126242. DOI: 10.1371/journal.pone.0126242.

Bulankina, A. V.; Deggerich, A.; Wenzel, D.; Mutenda, K.; Wittmann, J. G.; Rudolph, M. G.; Burger, K. N. J.; Höning, S. (2009): TIP47 functions in the biogenesis of lipid droplets. In *The Journal of cell biology* 185 (4), pp. 641–655. DOI: 10.1083/jcb.200812042.

Burlingame, A. L.; Zhang, X.; Chalkley, R. J. (2005): Mass spectrometric analysis of histone posttranslational modifications. In *Methods (San Diego, Calif.)* 36 (4), pp. 383–394. DOI: 10.1016/j.ymeth.2005.03.009.

Burnett, G.; Kennedy, E. P. (1954): The enzymatic phosphorylation of proteins. In *The Journal of biological chemistry* 211 (2), pp. 969–980.

Butcher, R. W.; Sutherland, E. W. (1962): Adenosine 3',5'-phosphate in biological materials. I. Purification and properties of cyclic 3',5'-nucleotide phosphodiesterase and use of this enzyme to characterize adenosine 3',5'-phosphate in human urine. In *The Journal of biological chemistry* 237, pp. 1244–1250.

Buxton, P.; Zhang, X.-M.; Walsh, B.; Sriratana, A.; Schenberg, I.; Manickam, E.; Rowe, T. (2003): Identification and characterization of Snapin as a ubiquitously expressed SNARE-binding protein that interacts with SNAP23 in non-neuronal cells. In *The Biochemical journal* 375 (Pt 2), pp. 433–440. DOI: 10.1042/BJ20030427.

Cai, Q.; Lu, L.; Tian, J.-H.; Zhu, Y.-B.; Qiao, H.; Sheng, Z.-H. (2010): Snapin-regulated late endosomal transport is critical for efficient autophagy-lysosomal function in neurons. In *Neuron* 68 (1), pp. 73–86. DOI: 10.1016/j.neuron.2010.09.022.

Cambridge, S. B.; Gnad, F.; Nguyen, C.; Bermejo, J. L.; Krüger, M.; Mann, M. (2011): Systems-wide proteomic analysis in mammalian cells reveals conserved, functional protein turnover. In *Journal of proteome research* 10 (12), pp. 5275–5284. DOI: 10.1021/pr101183k.

Cancino, J.; Capalbo, A.; Di Campli, A.; Giannotta, M.; Rizzo, R.; Jung, J. E.; Di Martino, R.; Persico, M.; Heinklein, P.; Sallese, M.; Luini, A. (2014): Control systems of membrane transport at the interface between the endoplasmic reticulum and the Golgi. In *Developmental cell* 30 (3), pp. 280–294. DOI: 10.1016/j.devcel.2014.06.018.

Cao, X.-J.; Arnaudo, A. M.; Garcia, B. A. (2013): Large-scale global identification of protein lysine methylation in vivo. In *Epigenetics* 8 (5), pp. 477–485. DOI: 10.4161/epi.24547.

Carlson, D. M. (1966): Oligosaccharides isolated from pig submaxillary mucin. In *The Journal of biological chemistry* 241 (12), pp. 2984–2986.

Carrey, E. A.; Campbell, D. G.; Hardie, D. G. (1985): Phosphorylation and activation of hamster carbamyl phosphate synthetase II by cAMP-dependent protein kinase. A novel mechanism for regulation of pyrimidine nucleotide biosynthesis. In *The EMBO journal* 4 (13B), pp. 3735–3742.

Carroll, K. S.; Hanna, J.; Simon, I.; Krise, J.; Barbero, P.; Pfeffer, S. R. (2001): Role of Rab9 GTPase in facilitating receptor recruitment by TIP47. In *Science (New York, N.Y.)* 292 (5520), pp. 1373–1376. DOI: 10.1126/science.1056791.

Čaval, T.; Zhu, J.; Tian, W.; Remmelzwaal, S.; Yang, Z.; Clausen, H.; Heck, A. J. R. (2019): Targeted analysis of lysosomal directed proteins and their sites of mannose-6-phosphate modification. In *Molecular & cellular proteomics : MCP* 18 (1), pp. 16–27. DOI: 10.1074/mcp.RA118.000967.

Chatterjee, S.; Velicer, L. F.; Sweeley, C. C. (1975): Glycosphingolipid glycosyl hydrolases and glycosidases of synchronized human KB cells. In *The Journal of biological chemistry* 250 (13), pp. 4972–4979.

Chen, D.; Disotuar, M. M.; Xiong, X.; Wang, Y.; Chou, D. H.-C. (2017): Selective N-terminal functionalization of native peptides and proteins. In *Chemical science* 8 (4), pp. 2717–2722. DOI: 10.1039/c6sc04744k.

Chen, L.; Fischle, W.; Verdin, E.; Greene, W. C. (2001): Duration of nuclear NF-kappaB action regulated by reversible acetylation. In *Science (New York, N.Y.)* 293 (5535), pp. 1653–1657. DOI: 10.1126/science.1062374.

Chen, Y.; Yuan, Y.; Li, W. (2018): Sorting machineries: how platelet-dense granules differ from α-granules. In *Bioscience reports* 38 (5). DOI: 10.1042/BSR20180458.

Chheda, M. G.; Ashery, U.; Thakur, P.; Rettig, J.; Sheng, Z. H. (2001): Phosphorylation of Snapin by PKA modulates its interaction with the SNARE complex. In *Nature cell biology* 3 (4), pp. 331–338. DOI: 10.1038/35070000.

Chiang, G. G.; Abraham, R. T. (2005): Phosphorylation of mammalian target of rapamycin (mTOR) at Ser-2448 is mediated by p70S6 kinase. In *The Journal of biological chemistry* 280 (27), pp. 25485–25490. DOI: 10.1074/jbc.M501707200.

Chiruvella, K. K.; Liang, Z.; Wilson, T. E. (2013): Repair of double-strand breaks by end joining. In *Cold Spring Harbor perspectives in biology* 5 (5), a012757. DOI: 10.1101/cshperspect.a012757.

Chi, Y.; Welcker, M.; Hizli, A. A.; Posakony, J. J.; Aebersold, R.; Clurman, B. E. (2008): Identification of CDK2 substrates in human cell lysates. In *Genome biology* 9 (10), R149. DOI: 10.1186/gb-2008-9-10-r149.

Choudhary, C.; Kumar, C.; Gnad, F.; Nielsen, M. L.; Rehman, M.; Walther, T. C.; Olsen, J. V.; Mann, M. (2009): Lysine acetylation targets protein complexes and co-regulates major cellular functions. In *Science (New York, N.Y.)* 325 (5942), pp. 834–840. DOI: 10.1126/science.1175371.

Chou, J.-L.; Huang, C.-L.; Lai, H.-L.; Hung, A. C.; Chien, C.-L.; Kao, Y.-Y.; Chern, Y. (2004): Regulation of type VI adenylyl cyclase by Snapin, a SNAP25-binding protein. In *The Journal of biological chemistry* 279 (44), pp. 46271–46279. DOI: 10.1074/jbc.M407206200.

Ciciotte, S. L.; Gwynn, B.; Moriyama, K.; Huizing, M.; Gahl, W. A.; Bonifacino, J. S.; Peters, L. L. (2003): Cappuccino, a mouse model of Hermansky-Pudlak syndrome, encodes a novel protein that is part of the pallidin-muted complex (BLOC-1). In *Blood* 101 (11), pp. 4402–4407. DOI: 10.1182/blood-2003-01-0020.

Ciechanover, A.; Heller, H.; Elias, S.; Haas, A. L.; Hershko, A. (1980): ATP-dependent conjugation of reticulocyte proteins with the polypeptide required for protein degradation. In *Proceedings of the National Academy of Sciences of the United States of America* 77 (3), pp. 1365–1368. DOI: 10.1073/pnas.77.3.1365.

Clark, K.; MacKenzie, K. F.; Petkevicius, K.; Kristariyanto, Y.; Zhang, J.; Choi, H. G.; Peggie, M.; Plater, L.; Pedrioli, P. G. A.; McIver, E.; Gray, N. S.; Arthur, J. S. C.; Cohen, P. (2012): Phosphorylation of CRTC3 by the salt-inducible kinases controls the interconversion of classically activated and regulatory macrophages. In *Proceedings of the National Academy of Sciences of the United States of America* 109 (42), pp. 16986–16991. DOI: 10.1073/pnas.1215450109.

Coffey, J. W.; de Duve, C. (1968): Digestive activity of lysosomes. I. The digestion of proteins by extracts of rat liver lysosomes. In *The Journal of biological chemistry* 243 (12), pp. 3255–3263.

Cohen, S. N.; Chang, A. C.; Hsu, L. (1972): Nonchromosomal antibiotic resistance in bacteria: genetic transformation of Escherichia coli by R-factor DNA. In *Proceedings of the National Academy of Sciences of the United States of America* 69 (8), pp. 2110–2114.

Conkright, M. D.; Canettieri, G.; Screaton, R.; Guzman, E.; Miraglia, L.; Hogenesch, J. B.; Montminy, M. (2003): TORCs: transducers of regulated CREB activity. In *Molecular cell* 12 (2), pp. 413–423. DOI: 10.1016/j.molcel.2003.08.013.

Corbin, J. D.; Keely, S. L.; Park, C. R. (1975): The distribution and dissociation of cyclic adenosine 3':5'-monophosphate-dependent protein kinases in adipose, cardiac, and other tissues. In *The Journal of biological chemistry* 250 (1), pp. 218–225.

Cox, J.; Mann, M. (2008): MaxQuant enables high peptide identification rates, individualized p.p.b.-range mass accuracies and proteome-wide protein quantification. In *Nature biotechnology* 26 (12), pp. 1367–1372. DOI: 10.1038/nbt.1511.

Cox, J.; Neuhauser, N.; Michalski, A.; Scheltema, R. A.; Olsen, J. V.; Mann, M. (2011): Andromeda: a peptide search engine integrated into the MaxQuant environment. In *Journal of proteome research* 10 (4), pp. 1794–1805. DOI: 10.1021/pr101065j.

Cullinane, A. R.; Curry, J. A.; Golas, G.; Pan, J.; Carmona-Rivera, C.; Hess, R. A.; White, J. G.; Huizing, M.; Gahl, W. A. (2012): A BLOC-1 mutation screen reveals a novel BLOC1S3 mutation in Hermansky-Pudlak Syndrome type 8. In *Pigment cell & melanoma research* 25 (5), pp. 584–591. DOI: 10.1111/j.1755-148X.2012.01029.x.

de Duve, C.; Pressman, B. C.; Gianetto, R.; Wattiaux, R.; Applemans, F. (1955): Tissue fractionation studies. 6. Intracellular distribution patterns of enzymes in rat-liver tissue. In *The Biochemical journal* 60 (4), pp. 604–617. DOI: 10.1042/bj0600604.

Delevoye, C.; Heiligenstein, X.; Ripoll, L.; Gilles-Marsens, F.; Dennis, M. K.; Linares, R. A.; Derman, L.; Gokhale, A.; Morel, E.; Faundez, V.; Marks, M. S.; Raposo, G. (2016): BLOC-1 brings together the actin and microtubule cytoskeletons to generate recycling endosomes. In *Current biology : CB* 26 (1), pp. 1–13. DOI: 10.1016/j.cub.2015.11.020.

Delghandi, M. P.; Johannessen, M.; Moens, U. (2005): The cAMP signalling pathway activates CREB through PKA, p38 and MSK1 in NIH 3T3 cells. In *Cellular signalling* 17 (11), pp. 1343–1351. DOI: 10.1016/j.cellsig.2005.02.003.

Deribe, Y. L.; Pawson, T.; Dikic, I. (2010): Post-translational modifications in signal integration. In *Nature structural & molecular biology* 17 (6), pp. 666–672. DOI: 10.1038/nsmb.1842.

Di Giovanni, J.; Sheng, Z.-H. (2015): Regulation of synaptic activity by snapin-mediated endolysosomal transport and sorting. In *The EMBO journal* 34 (15), pp. 2059–2077. DOI: 10.15252/embj.201591125.

Di Pietro, S. M.; Dell'Angelica, E. C. (2005): The cell biology of Hermansky-Pudlak syndrome: recent advances. In *Traffic (Copenhagen, Denmark)* 6 (7), pp. 525–533. DOI: 10.1111/j.1600-0854.2005.00299.x.

Díaz, E.; Pfeffer, S. R. (1998): TIP47: A cargo selection device for mannose 6-phosphate receptor trafficking. In *Cell* 93 (3), pp. 433–443. DOI: 10.1016/S0092-8674(00)81171-X.

Dittmer, F.; Ulbrich, E. J.; Hafner, A.; Schmahl, W.; Meister, T.; Pohlmann, R.; Figura, K. von (1999): Alternative mechanisms for trafficking of lysosomal enzymes in mannose 6-phosphate receptor-deficient mice are cell type-specific. In *Journal of cell science* 112 (Pt 10), pp. 1591–1597.

Dixon, H. B.F.; Fields, R. (1972): [33] Specific modification of NH2-terminal residues by transamination. In : Enzyme Structure, Part B, vol. 25: Elsevier (Methods in Enzymology), pp. 409–419.

Doll, S.; Dreßen, M.; Geyer, P. E.; Itzhak, D. N.; Braun, C.; Doppler, S. A.; Meier, F.; Deutsch, M.-A.; Lahm, H.; Lange, R.; Krane, M.; Mann, M. (2017): Region and cell-type resolved quantitative proteomic map of the human heart. In *Nature communications* 8 (1), p. 1469. DOI: 10.1038/s41467-017-01747-2.

Doray, B.; Lee, I.; Knisely, J.; Bu, G.; Kornfeld, S. (2007): The gamma/sigma1 and alpha/sigma2 hemicomplexes of clathrin adaptors AP-1 and AP-2 harbor the dileucine recognition site. In *Molecular biology of the cell* 18 (5), pp. 1887–1896. DOI: 10.1091/mbc.e07-01-0012.

Dowle, M.; Srinivasan, A. (2019): data.table: Extension of `data.frame`. https://CRAN.R-project.org/package=data.table.

Du, K.; Montminy, M. (1998): CREB is a regulatory target for the protein kinase Akt/PKB. In *The Journal of biological chemistry* 273 (49), pp. 32377–32379. DOI: 10.1074/jbc.273.49.32377.

Duncan, J. R.; Kornfeld, S. (1988): Intracellular movement of two mannose 6-phosphate receptors: return to the Golgi apparatus. In *The Journal of cell biology* 106 (3), pp. 617–628. DOI: 10.1083/jcb.106.3.617.

Ebhardt, H. A.; Root, A.; Liu, Y.; Gauthier, N. P.; Sander, C.; Aebersold, R. (2018): Systems pharmacology using mass spectrometry identifies critical response nodes in prostate cancer. In *NPJ systems biology and applications* 4, p. 26. DOI: 10.1038/s41540-018-0064-1.

Ek-Rylander, B.; Flores, M.; Wendel, M.; Heinegård, D.; Andersson, G. (1994): Dephosphorylation of osteopontin and bone sialoprotein by osteoclastic tartrate-resistant acid phosphatase. Modulation of osteoclast adhesion in vitro. In *The Journal of biological chemistry* 269 (21), pp. 14853–14856.

Elkouris, M.; Kontaki, H.; Stavropoulos, A.; Antonoglou, A.; Nikolaou, K. C.; Samiotaki, M.; Szantai, E.; Saviolaki, D.; Brown, P. J.; Sideras, P.; Panayotou, G.; Talianidis, I. (2016): SET9-mediated regulation of TGF-β signaling links protein methylation to pulmonary fibrosis. In *Cell reports* 15 (12), pp. 2733–2744. DOI: 10.1016/j.celrep.2016.05.051.

Eng, J. K.; McCormack, A. L.; Yates, J. R. (1994): An approach to correlate tandem mass spectral data of peptides with amino acid sequences in a protein database. In *J Am Soc Mass Spectrom* 5 (11), pp. 976–989. DOI: 10.1016/1044-0305(94)80016-2.

Engvall, E.; Perlmann, P. (1972): Enzyme-linked immunosorbent assay, Elisa. 3. Quantitation of specific antibodies by enzyme-labeled anti-immunoglobulin in antigen-coated tubes. In *Journal of immunology (Baltimore, Md. : 1950)* 109 (1), pp. 129–135.

Er, E. E.; Mendoza, M. C.; Mackey, A. M.; Rameh, L. E.; Blenis, J. (2013): AKT facilitates EGFR trafficking and degradation by phosphorylating and activating PIKfyve. In *Science signaling* 6 (279), ra45. DOI: 10.1126/scisignal.2004015.

Erickson, A. H.; Blobel, G. (1979): Early events in the biosynthesis of the lysosomal enzyme cathepsin D. In *The Journal of biological chemistry* 254 (23), pp. 11771–11774.

Erickson, A. H.; Conner, G. E.; Blobel, G. (1981): Biosynthesis of a lysosomal enzyme. Partial structure of two transient and functionally distinct NH2-terminal sequences in cathepsin D. In *The Journal of biological chemistry* 256 (21), pp. 11224–11231.

Falcón-Pérez, J. M.; Starcevic, M.; Gautam, R.; Dell'Angelica, E. C. (2002): BLOC-1, a novel complex containing the pallidin and muted proteins involved in the biogenesis of melanosomes and platelet-dense granules. In *The Journal of biological chemistry* 277 (31), pp. 28191–28199. DOI: 10.1074/jbc.M204011200.

Fasci, D.; van Ingen, H.; Scheltema, R. A.; Heck, A. J. R. (2018): Histone interaction landscapes visualized by crosslinking mass spectrometry in intact cell nuclei. In *Molecular & cellular proteomics : MCP* 17 (10), pp. 2018–2033. DOI: 10.1074/mcp.RA118.000924.

Fenn, J. B.; Mann, M.; Meng, C. K.; Wong, S. F.; Whitehouse, C. M. (1989): Electrospray ionization for mass spectrometry of large biomolecules. In *Science (New York, N.Y.)* 246 (4926), pp. 64–71. DOI: 10.1126/science.2675315.

Filipek, P. A.; Araujo, M. E. G. de; Vogel, G. F.; Smet, C. H. de; Eberharter, D.; Rebsamen, M.; Rudashevskaya, E. L.; Kremser, L.; Yordanov, T.; Tschaikner, P.; Fürnrohr, B. G.; Lechner, S.; Dunzendorfer-Matt, T.; Scheffzek, K.; Bennett, K. L.; Superti-Furga, G.; Lindner, H. H.; Stasyk, T.; Huber, L. A. (2017): LAMTOR/Ragulator is a negative regulator of Arl8b- and BORC-dependent late endosomal positioning. In *The Journal of cell biology* 216 (12), pp. 4199–4215. DOI: 10.1083/jcb.201703061.

Fischer, A.; Mühlhäuser, W. W. D.; Warscheid, B.; Radziwill, G. (2017): Membrane localization of acetylated CNK1 mediates a positive feedback on RAF/ERK signaling. In *Science advances* 3 (8), e1700475. DOI: 10.1126/sciadv.1700475.

Fowler, S.; de Duve, C. (1969): Digestive activity of lysosomes. 3. The digestion of lipids by extracts of rat liver lysosomes. In *The Journal of biological chemistry* 244 (2), pp. 471–481.

Fox, J.; Weisberg, S. (2019): An {R} companion to applied regression. https://socialsciences.mcmaster.ca/jfox/Books/Companion/. In *Sage*.

Freissmuth, M.; Casey, P. J.; Gilman, A. G. (1989): G proteins control diverse pathways of transmembrane signaling. In *FASEB journal : official publication of the Federation of American Societies for Experimental Biology* 3 (10), pp. 2125–2131.

Freitas, M. A.; Sklenar, A. R.; Parthun, M. R. (2004): Application of mass spectrometry to the identification and quantification of histone post-translational modifications. In *Journal of cellular biochemistry* 92 (4), pp. 691–700. DOI: 10.1002/jcb.20106.

Fujita, M.; Taniguchi, N.; Makita, A.; Ono, M.; Oikawa, K. (1985): Protein phosphorylation of β-glucuronidase in human lung cancer—Identification of serine- and threonine-phosphates. In *Biochemical and biophysical research communications* 126 (2), pp. 818–824. DOI: 10.1016/0006-291X(85)90258-X.

Gasa, S.; Makita, A. (1983): Phosphorylation on protein and carbohydrate moieties of a lysosomal arylsulfatase B variant in human lung cancer transplanted into athymic mice. In *The Journal of biological chemistry* 258 (8), pp. 5034–5039.

Geoghegan, V.; Guo, A.; Trudgian, D.; Thomas, B.; Acuto, O. (2015): Comprehensive identification of arginine methylation in primary T cells reveals regulatory roles in cell signalling. In *Nature communications* 6, p. 6758. DOI: 10.1038/ncomms7758.

Gershon, P. D. (2014): Cleaved and missed sites for trypsin, lys-C, and lys-N can be predicted with high confidence on the basis of sequence context. In *Journal of proteome research* 13 (2), pp. 702–709. DOI: 10.1021/pr400802z.

Giannotta, M.; Ruggiero, C.; Grossi, M.; Cancino, J.; Capitani, M.; Pulvirenti, T.; Consoli, G. M. L.; Geraci, C.; Fanelli, F.; Luini, A.; Sallese, M. (2012): The KDEL receptor couples to Gαq/11 to activate Src kinases and regulate transport through the Golgi. In *The EMBO journal* 31 (13), pp. 2869–2881. DOI: 10.1038/emboj.2012.134.

Gillet, L. C.; Leitner, A.; Aebersold, R. (2016): Mass spectrometry applied to bottom-up proteomics: Entering the high-throughput era for hypothesis testing. In *Annual review of analytical chemistry (Palo Alto, Calif.)* 9 (1), pp. 449–472. DOI: 10.1146/annurev-anchem-071015-041535.

Ginter-Matuszewska, B.; Spik, A.; Rembiszewska, A.; Koyias, C.; Kupryjanczyk, J.; Jaruzelska, J. (2009): The SNARE-associated component SNAPIN binds PUMILIO2 and NANOS1 proteins in human male germ cells. In *Molecular human reproduction* 15 (3), pp. 173–179. DOI: 10.1093/molehr/gap004.

Gonzalez, G. A.; Montminy, M. R. (1989): Cyclic AMP stimulates somatostatin gene transcription by phosphorylation of CREB at serine 133. In *Cell* 59 (4), pp. 675–680. DOI: 10.1016/0092-8674(89)90013-5.

Griffiths, G.; Hoflack, B.; Simons, K.; Mellman, I.; Kornfeld, S. (1988): The mannose 6-phosphate receptor and the biogenesis of lysosomes. In *Cell* 52 (3), pp. 329–341. DOI: 10.1016/s0092-8674(88)80026-6.

Gruener, L.; Ismond, M.A.H. (1997): Effects of acetylation and succinylation on the functional properties of the canola 12S globulin. In *Food Chemistry* 60 (4), pp. 513–520. DOI: 10.1016/S0308-8146(97)00016-2.

Guardia, C. M.; Farías, G. G.; Jia, R.; Pu, J.; Bonifacino, J. S. (2016): BORC functions upstream of kinesins 1 and 3 to coordinate regional movement of lysosomes along different microtubule tracks. In *Cell reports* 17 (8), pp. 1950–1961. DOI: 10.1016/j.celrep.2016.10.062.

Guo, A.; Gu, H.; Zhou, J.; Mulhern, D.; Wang, Y.; Lee, K. A.; Yang, V.; Aguiar, M.; Kornhauser, J.; Jia, X.; Ren, J.; Beausoleil, S. A.; Silva, J. C.; Vemulapalli, V.; Bedford, M. T.; Comb, M. J. (2014): Immunoaffinity enrichment and mass spectrometry analysis of protein methylation. In *Molecular & cellular proteomics : MCP* 13 (1), pp. 372–387. DOI: 10.1074/mcp.O113.027870.

Gu, W.; Roeder, R. G. (1997): Activation of p53 sequence-specific DNA binding by acetylation of the p53 C-terminal domain. In *Cell* 90 (4), pp. 595–606.

Habegger, K. M.; Heppner, K. M.; Geary, N.; Bartness, T. J.; DiMarchi, R.; Tschöp, M. H. (2010): The metabolic actions of glucagon revisited. In *Nature reviews. Endocrinology* 6 (12), pp. 689–697. DOI: 10.1038/nrendo.2010.187.

Hadley, W.; Romain, F.; Lionel, H.; Kirill, M. (2019): dplyr: A grammar of data manipulation. https://CRAN.R-project.org/package=dplyr.

Hadley, W. (2019): stringr: Simple, consistent wrappers for common string operations. https://CRAN.R-project.org/package=stringr.

Hanbo, C. (2018): VennDiagram: generate high-resolution Venn and euler plots. https://CRAN.R-project.org/package=VennDiagram.

Hanover, J. A.; Willingham, M. C.; Pastan, I. (1984): Kinetics of transit of transferrin and epidermal growth factor through clathrin-coated membranes. In *Cell* 39 (2), pp. 283–293. DOI: 10.1016/0092-8674(84)90006-0.

Han, X.; He, L.; Xin, L.; Shan, B.; Ma, B. (2011): PeaksPTM: Mass spectrometry-based identification of peptides with unspecified modifications. In *Journal of proteome research* 10 (7), pp. 2930–2936. DOI: 10.1021/pr200153k.

Hardman, G.; Perkins, S.; Brownridge, P. J.; Clarke, C. J.; Byrne, D. P.; Campbell, A. E.; Kalyuzhnyy, A.; Myall, A.; Eyers, P. A.; Jones, A. R.; Eyers, C. E. (2019): Strong anion exchange-mediated phosphoproteomics reveals extensive human non-canonical phosphorylation. In *The EMBO journal*, e100847. DOI: 10.15252/embj.2018100847.

Harter, C.; Mellman, I. (1992): Transport of the lysosomal membrane glycoprotein lgp120 (lgp-A) to lysosomes does not require appearance on the plasma membrane. In *The Journal of cell biology* 117 (2), pp. 311–325. DOI: 10.1083/jcb.117.2.311.

Hart, G. W.; Housley, M. P.; Slawson, C. (2007): Cycling of O-linked beta-N-acetylglucosamine on nucleocytoplasmic proteins. In *Nature* 446 (7139), pp. 1017–1022. DOI: 10.1038/nature05815.

Hart, G. W.; Slawson, C.; Ramirez-Correa, G.; Lagerlof, O. (2011): Cross talk between O-GlcNAcylation and phosphorylation: roles in signaling, transcription, and chronic disease. In *Annual review of biochemistry* 80, pp. 825–858. DOI: 10.1146/annurev-biochem-060608-102511.

Hasilik, A.; Neufeld, E. F. (1980): Biosynthesis of lysosomal enzymes in fibroblasts. Synthesis as precursors of higher molecular weight. In *The Journal of biological chemistry* 255 (10), pp. 4937–4945.

Hasilik, A.; Klein, U.; Waheed, A.; Strecker, G.; Figura, K. von (1980): Phosphorylated oligosaccharides in lysosomal enzymes: identification of alpha-N-acetylglucosamine(1)phospho(6)mannose diester groups. In *Proceedings of the National Academy of Sciences of the United States of America* 77 (12), pp. 7074–7078. DOI: 10.1073/pnas.77.12.7074.

Hebbes, T. R.; Thorne, A. W.; Crane-Robinson, C. (1988): A direct link between core histone acetylation and transcriptionally active chromatin. In *The EMBO journal* 7 (5), pp. 1395–1402.

Henriksen, L.; Grandal, M. V.; Knudsen, S. L. J.; van Deurs, B.; Grøvdal, L. M. (2013): Internalization mechanisms of the epidermal growth factor receptor after activation with different ligands. In *PloS one* 8 (3), e58148. DOI: 10.1371/journal.pone.0058148.

Henzel, W. J.; Billeci, T. M.; Stults, J. T.; Wong, S. C.; Grimley, C.; Watanabe, C. (1993): Identifying proteins from two-dimensional gels by molecular mass searching of peptide fragments in protein sequence databases. In *Proceedings of the National Academy of Sciences of the United States of America* 90 (11), pp. 5011–5015. DOI: 10.1073/pnas.90.11.5011.

Hershko, A.; Ciechanover, A.; Heller, H.; Haas, A. L.; Rose, I. A. (1980): Proposed role of ATP in protein breakdown: conjugation of protein with multiple chains of the polypeptide of ATP-dependent proteolysis. In *Proceedings of the National Academy of Sciences of the United States of America* 77 (4), pp. 1783–1786. DOI: 10.1073/pnas.77.4.1783.

Hoflack, B.; Kornfeld, S. (1985): Lysosomal enzyme binding to mouse P388D1 macrophage membranes lacking the 215-kDa mannose 6-phosphate receptor: evidence for the existence of a second mannose 6-phosphate receptor. In *Proceedings of the National Academy of Sciences of the United States of America* 82 (13), pp. 4428–4432. DOI: 10.1073/pnas.82.13.4428.

Holz, M. K.; Blenis, J. (2005): Identification of S6 kinase 1 as a novel mammalian target of rapamycin (mTOR)-phosphorylating kinase. In *The Journal of biological chemistry* 280 (28), pp. 26089–26093. DOI: 10.1074/jbc.M504045200.

Holz, M. K.; Ballif, B. A.; Gygi, S. P.; Blenis, J. (2005): mTOR and S6K1 mediate assembly of the translation preinitiation complex through dynamic protein interchange and ordered phosphorylation events. In *Cell* 123 (4), pp. 569–580. DOI: 10.1016/j.cell.2005.10.024.

Höning, S.; Hunziker, W. (1995): Cytoplasmic determinants involved in direct lysosomal sorting, endocytosis, and basolateral targeting of rat lgp120 (lamp-I) in MDCK cells. In *The Journal of cell biology* 128 (3), pp. 321–332. DOI: 10.1083/jcb.128.3.321.

Höning, S.; Griffith, J.; Geuze, H. J.; Hunziker, W. (1996): The tyrosine-based lysosomal targeting signal in lamp-1 mediates sorting into Golgi-derived clathrin-coated vesicles. In *The EMBO journal* 15 (19), pp. 5230–5239. DOI: 10.1002/j.1460-2075.1996.tb00908.x.

Hornbeck, P. V.; Zhang, B.; Murray, B.; Kornhauser, J. M.; Latham, V.; Skrzypek, E. (2015): PhosphoSitePlus, 2014: mutations, PTMs and recalibrations. In *Nucleic acids research* 43 (Database issue), D512-20. DOI: 10.1093/nar/gku1267.

Huang, B. X.; Lee, R.; Akbar, M.; Kim, H.-Y. (2015): Threonine 34 phosphorylation by phosphoinositide-dependent protein kinase 1 facilitates dissociation of Akt from the plasma membrane. In *The international journal of biochemistry & cell biology* 64, pp. 195–201. DOI: 10.1016/j.biocel.2015.04.007.

Huang, E. C.; Henion, J. D. (1990): LC/MS and LC/MS/MS determination of protein tryptic digests. In *J Am Soc Mass Spectrom* 1 (2), pp. 158–165. DOI: 10.1016/1044-0305(90)85052-N.

Huang, J.; Perez-Burgos, L.; Placek, B. J.; Sengupta, R.; Richter, M.; Dorsey, J. A.; Kubicek, S.; Opravil, S.; Jenuwein, T.; Berger, S. L. (2006): Repression of p53 activity by Smyd2-mediated methylation. In *Nature* 444 (7119), pp. 629–632. DOI: 10.1038/nature05287.

Huang, J. S.; Huang, S. S.; Tang, J. (1979): Cathepsin D isozymes from porcine spleens. Large scale purification and polypeptide chain arrangements. In *The Journal of biological chemistry* 254 (22), pp. 11405–11417.

Huesgen, P. F.; Lange, P. F.; Rogers, L. D.; Solis, N.; Eckhard, U.; Kleifeld, O.; Goulas, T.; Gomis-Rüth, F. X.; Overall, C. M. (2015): LysargiNase mirrors trypsin for protein C-terminal and methylation-site identification. In *Nature methods* 12 (1), pp. 55–58. DOI: 10.1038/nmeth.3177.

Hunt, D. F.; Yates, J. R.; Shabanowitz, J.; Winston, S.; Hauer, C. R. (1986): Protein sequencing by tandem mass spectrometry. In *Proceedings of the National Academy of Sciences of the United States of America* 83 (17), pp. 6233–6237. DOI: 10.1073/pnas.83.17.6233.

Hunt, R. A.; Edris, W.; Chanda, P. K.; Nieuwenhuijsen, B.; Young, K. H. (2003): Snapin interacts with the N-terminus of regulator of G protein signaling 7. In *Biochemical and biophysical research communications* 303 (2), pp. 594–599. DOI: 10.1016/s0006-291x(03)00400-5.

Hurrell, T.; Segeritz, C.-P.; Vallier, L.; Lilley, K. S.; Cromarty, A. D. (2019): A proteomic time course through the differentiation of human induced pluripotent stem cells into hepatocyte-like cells. In *Scientific reports* 9 (1), p. 3270. DOI: 10.1038/s41598-019-39400-1.

Ilardi, J. M.; Mochida, S.; Sheng, Z. H. (1999): Snapin: a SNARE-associated protein implicated in synaptic transmission. In *Nature neuroscience* 2 (2), pp. 119–124. DOI: 10.1038/5673.

International Human Genome Sequencing Consortium (2004): Finishing the euchromatic sequence of the human genome. In *Nature* 431 (7011), pp. 931–945. DOI: 10.1038/nature03001.

Iourgenko, V.; Zhang, W.; Mickanin, C.; Daly, I.; Jiang, C.; Hexham, J. M.; Orth, A. P.; Miraglia, L.; Meltzer, J.; Garza, D.; Chirn, G.-W.; McWhinnie, E.; Cohen, D.; Skelton, J.; Terry, R.; Yu, Y.; Bodian, D.; Buxton, F. P.; Zhu, J.; Song, C.; Labow, M. A. (2003): Identification of a family of cAMP response element-binding protein coactivators by genome-scale functional analysis in mammalian cells. In *Proceedings of the National Academy of Sciences of the United States of America* 100 (21), pp. 12147–12152. DOI: 10.1073/pnas.1932773100.

Itakura, E.; Kishi-Itakura, C.; Mizushima, N. (2012): The hairpin-type tail-anchored SNARE syntaxin 17 targets to autophagosomes for fusion with endosomes/lysosomes. In *Cell* 151 (6), pp. 1256–1269. DOI: 10.1016/j.cell.2012.11.001.

Jadot, M.; Canfield, W. M.; Gregory, W.; Kornfeld, S. (1992): Characterization of the signal for rapid internalization of the bovine mannose 6-phosphate/insulin-like growth factor-II receptor. In *The Journal of biological chemistry* 267 (16), pp. 11069–11077.

Jaiswal, J. K.; Rivera, V. M.; Simon, S. M. (2009): Exocytosis of post-Golgi vesicles is regulated by components of the endocytic machinery. In *Cell* 137 (7), pp. 1308–1319. DOI: 10.1016/j.cell.2009.04.064.

Jaruzelska, J.; Kotecki, M.; Kusz, K.; Spik, A.; Firpo, M.; Reijo Pera, R. A. (2003): Conservation of a Pumilio-Nanos complex from Drosophila germ plasm to human germ cells. In *Development genes and evolution* 213 (3), pp. 120–126. DOI: 10.1007/s00427-003-0303-2.

Jelinek, L. J.; Lok, S.; Rosenberg, G. B.; Smith, R. A.; Grant, F. J.; Biggs, S.; Bensch, P. A.; Kuijper, J. L.; Sheppard, P. O.; Sprecher, C. A. (1993): Expression cloning and signaling properties of the rat glucagon receptor. In *Science (New York, N.Y.)* 259 (5101), pp. 1614–1616. DOI: 10.1126/science.8384375.

Jewell, J. L.; Fu, V.; Hong, A. W.; Yu, F.-X.; Meng, D.; Melick, C. H.; Wang, H.; Lam, W.-L. M.; Yuan, H.-X.; Taylor, S. S.; Guan, K.-L. (2019): GPCR signaling inhibits mTORC1 via PKA phosphorylation of Raptor. In *eLife* 8. DOI: 10.7554/eLife.43038.

Jiang, P.; Nishimura, T.; Sakamaki, Y.; Itakura, E.; Hatta, T.; Natsume, T.; Mizushima, N. (2014): The HOPS complex mediates autophagosome-lysosome fusion through interaction with syntaxin 17. In *Molecular biology of the cell* 25 (8), pp. 1327–1337. DOI: 10.1091/mbc.E13-08-0447.

Jia, R.; Guardia, C. M.; Pu, J.; Chen, Y.; Bonifacino, J. S. (2017): BORC coordinates encounter and fusion of lysosomes with autophagosomes. In *Autophagy* 13 (10), pp. 1648–1663. DOI: 10.1080/15548627.2017.1343768.

Jinek, M.; Chylinski, K.; Fonfara, I.; Hauer, M.; Doudna, J. A.; Charpentier, E. (2012): A programmable dual-RNA-guided DNA endonuclease in adaptive bacterial immunity. In *Science (New York, N.Y.)* 337 (6096), pp. 816–821. DOI: 10.1126/science.1225829.

Joussineau, C. de; Sahut-Barnola, I.; Tissier, F.; Dumontet, T.; Drelon, C.; Batisse-Lignier, M.; Tauveron, I.; Pointud, J.-C.; Lefrançois-Martinez, A.-M.; Stratakis, C. A.; Bertherat, J.; Val, P.; Martinez, A. (2014): mTOR pathway is activated by PKA in adrenocortical cells and participates in vivo to apoptosis resistance in primary pigmented nodular adrenocortical disease (PPNAD). In *Human molecular genetics* 23 (20), pp. 5418–5428. DOI: 10.1093/hmg/ddu265.

Kaimori, J.-Y.; Maehara, K.; Hayashi-Takanaka, Y.; Harada, A.; Fukuda, M.; Yamamoto, S.; Ichimaru, N.; Umehara, T.; Yokoyama, S.; Matsuda, R.; Ikura, T.; Nagao, K.; Obuse, C.; Nozaki, N.; Takahara, S.; Takao, T.; Ohkawa, Y.; Kimura, H.; Isaka, Y. (2016): Histone H4 lysine 20 acetylation is associated with gene repression in human cells. In *Scientific reports* 6, p. 24318. DOI: 10.1038/srep24318.

Käll, L.; Canterbury, J. D.; Weston, J.; Noble, W. S.; MacCoss, M. J. (2007): Semi-supervised learning for peptide identification from shotgun proteomics datasets. In *Nature methods* 4 (11), pp. 923–925. DOI: 10.1038/nmeth1113.

Kamemura, K.; Hayes, B. K.; Comer, F. I.; Hart, G. W. (2002): Dynamic interplay between O-glycosylation and O-phosphorylation of nucleocytoplasmic proteins: alternative glycosylation/phosphorylation of THR-58, a known mutational hot spot of c-Myc in lymphomas, is regulated by mitogens. In *The Journal of biological chemistry* 277 (21), pp. 19229–19235. DOI: 10.1074/jbc.M201729200.

Kang, J.-Y.; Shin, K. K.; Kim, H. H.; Min, J.-K.; Ji, E. S.; Kim, J. Y.; Kwon, O.; Oh, D.-B. (2018): Lysosomal targeting enhancement by conjugation of glycopeptides containing mannose-6-phosphate glycans derived from glyco-engineered yeast. In *Scientific reports* 8 (1), p. 8730. DOI: 10.1038/s41598-018-26913-4.

Kaplan, A.; Achord, D. T.; Sly, W. S. (1977): Phosphohexosyl components of a lysosomal enzyme are recognized by pinocytosis receptors on human fibroblasts. In *Proceedings of the National Academy of Sciences of the United States of America* 74 (5), pp. 2026–2030. DOI: 10.1073/pnas.74.5.2026.

Katoh, Y.; Takemori, H.; Lin, X.-Z.; Tamura, M.; Muraoka, M.; Satoh, T.; Tsuchiya, Y.; Min, L.; Doi, J.; Miyauchi, A.; Witters, L. A.; Nakamura, H.; Okamoto, M. (2006): Silencing the constitutive active transcription factor CREB by the LKB1-SIK signaling cascade. In *The FEBS journal* 273 (12), pp. 2730–2748. DOI: 10.1111/j.1742-4658.2006.05291.x.

Kawasaki, H.; Springett, G. M.; Mochizuki, N.; Toki, S.; Nakaya, M.; Matsuda, M.; Housman, D. E.; Graybiel, A. M. (1998): A family of cAMP-binding proteins that directly activate Rap1. In *Science (New York, N.Y.)* 282 (5397), pp. 2275–2279. DOI: 10.1126/science.282.5397.2275.

Kennelly, P. J.; Krebs, E. G. (1991): Consensus sequences as substrate specificity determinants for protein kinases and protein phosphatases. In *The Journal of biological chemistry* 266 (24), pp. 15555–15558.

Kent, W. J.; Sugnet, C. W.; Furey, T. S.; Roskin, K. M.; Pringle, T. H.; Zahler, A. M.; Haussler, D. (2002): The human genome browser at UCSC. In *Genome research* 12 (6), pp. 996–1006. DOI: 10.1101/gr.229102.

Kim, D.-H.; Sarbassov, D. D.; Ali, S. M.; King, J. E.; Latek, R. R.; Erdjument-Bromage, H.; Tempst, P.; Sabatini, D. M. (2002): mTOR interacts with raptor to form a nutrient-sensitive complex that signals to the cell growth machinery. In *Cell* 110 (2), pp. 163–175. DOI: 10.1016/s0092-8674(02)00808-5.

Kim, D.-H.; Sarbassov, D. D.; Ali, S. M.; Latek, R. R.; Guntur, K. V. P.; Erdjument-Bromage, H.; Tempst, P.; Sabatini, D. M. (2003): GbetaL, a positive regulator of the rapamycin-sensitive pathway required for the nutrient-sensitive interaction between raptor and mTOR. In *Molecular cell* 11 (4), pp. 895–904. DOI: 10.1016/s1097-2765(03)00114-x.

Kim, E.; Goraksha-Hicks, P.; Li, L.; Neufeld, T. P.; Guan, K.-L. (2008): Regulation of TORC1 by Rag GTPases in nutrient response. In *Nature cell biology* 10 (8), pp. 935–945. DOI: 10.1038/ncb1753.

Kim, H. W.; Ha, S. H.; Lee, M. N.; Huston, E.; Kim, D.-H.; Jang, S. K.; Suh, P.-G.; Houslay, M. D.; Ryu, S. H. (2010): Cyclic AMP controls mTOR through regulation of the dynamic interaction between Rheb and phosphodiesterase 4D. In *Molecular and cellular biology* 30 (22), pp. 5406–5420. DOI: 10.1128/MCB.00217-10.

Kim, S.; Paik, W. K. (1965): Studies on the origin of epsilon-N-methyl-L-lysine in protein. In *The Journal of biological chemistry* 240 (12), pp. 4629–4634.

Kim, S. C.; Sprung, R.; Chen, Y.; Xu, Y.; Ball, H.; Pei, J.; Cheng, T.; Kho, Y.; Xiao, H.; Xiao, L.; Grishin, N. V.; White, M.; Yang, X.-J.; Zhao, Y. (2006): Substrate and functional diversity of lysine acetylation revealed by a proteomics survey. In *Molecular cell* 23 (4), pp. 607–618. DOI: 10.1016/j.molcel.2006.06.026.

Klose, J. (1975): Protein mapping by combined isoelectric focusing and electrophoresis of mouse tissues. A novel approach to testing for induced point mutations in mammals. In *Humangenetik* 26 (3), pp. 231–243.

Kyle, J. W.; Nolan, C. M.; Oshima, A.; Sly, W. S. (1988): Expression of human cation-independent mannose 6-phosphate receptor cDNA in receptor-negative mouse P388D1 cells following gene transfer. In *The Journal of biological chemistry* 263 (31), pp. 16230–16235.

Laemmli, U. K. (1970): Cleavage of structural proteins during the assembly of the head of bacteriophage T4. In *Nature* 227 (5259), pp. 680–685.

Larsen, M. R.; Thingholm, T. E.; Jensen, O. N.; Roepstorff, P.; Jørgensen, T. J. D. (2005): Highly selective enrichment of phosphorylated peptides from peptide mixtures using titanium dioxide microcolumns. In *Molecular & cellular proteomics : MCP* 4 (7), pp. 873–886. DOI: 10.1074/mcp.T500007-MCP200.

Larsson, J. (2019): eulerr: Area-proportional euler and Venn diagrams with ellipses. URL: https://cran.r-project.org/package=eulerr.

Le Cong; Ran, F. A.; Cox, D.; Lin, S.; Barretto, R.; Habib, N.; Hsu, P. D.; Wu, X.; Jiang, W.; Marraffini, L. A.; Zhang, F. (2013): Multiplex genome engineering using CRISPR/Cas systems. In *Science (New York, N.Y.)* 339 (6121), pp. 819–823. DOI: 10.1126/science.1231143.

Lê, S.; Josse, J.; Husson, F. (2008): FactoMineR: An R package for multivariate analysis. In *J. Stat. Soft.* 25 (1). DOI: 10.18637/jss.v025.i01.

Li, J.; O'Connor, K. L.; Cheng, X.; Mei, F. C.; Uchida, T.; Townsend, C. M.; Evers, B. M. (2007): Cyclic adenosine 5'-monophosphate-stimulated neurotensin secretion is mediated through Rap1 downstream of both Epac and protein kinase A signaling pathways. In *Molecular endocrinology (Baltimore, Md.)* 21 (1), pp. 159–171. DOI: 10.1210/me.2006-0340.

Liu, Y.; Lai, Y.-C.; Hill, E. V.; Tyteca, D.; Carpentier, S.; Ingvaldsen, A.; Vertommen, D.; Lantier, L.; Foretz, M.; Dequiedt, F.; Courtoy, P. J.; Erneux, C.; Viollet, B.; Shepherd, P. R.; Tavaré, J. M.; Jensen, J.; Rider, M. H. (2013): Phosphatidylinositol 3-phosphate 5-kinase (PIKfyve) is an AMPK target participating in contraction-stimulated glucose uptake in skeletal muscle. In *The Biochemical journal* 455 (2), pp. 195–206. DOI: 10.1042/BJ20130644.

Li, W.; Zhang, Q.; Oiso, N.; Novak, E. K.; Gautam, R.; O'Brien, E. P.; Tinsley, C. L.; Blake, D. J.; Spritz, R. A.; Copeland, N. G.; Jenkins, N. A.; Amato, D.; Roe, B. A.; Starcevic, M.; Dell'Angelica, E. C.; Elliott, R. W.; Mishra, V.; Kingsmore, S. F.; Paylor, R. E.; Swank, R. T. (2003): Hermansky-Pudlak syndrome type 7 (HPS-7) results from mutant dysbindin, a member of the biogenesis of lysosome-related organelles complex 1 (BLOC-1). In *Nature genetics* 35 (1), pp. 84–89. DOI: 10.1038/ng1229.

Lohmann, S. M.; DeCamilli, P.; Einig, I.; Walter, U. (1984): High-affinity binding of the regulatory subunit (RII) of cAMP-dependent protein kinase to microtubule-associated and other cellular proteins. In *Proceedings of the National Academy of Sciences of the United States of America* 81 (21), pp. 6723–6727. DOI: 10.1073/pnas.81.21.6723.

Lokireddy, S.; Kukushkin, N. V.; Goldberg, A. L. (2015): cAMP-induced phosphorylation of 26S proteasomes on Rpn6/PSMD11 enhances their activity and the degradation of misfolded proteins. In *Proceedings of the National Academy of Sciences of the United States of America* 112 (52), E7176-85. DOI: 10.1073/pnas.1522332112.

Long, X.; Lin, Y.; Ortiz-Vega, S.; Yonezawa, K.; Avruch, J. (2005): Rheb binds and regulates the mTOR kinase. In *Current biology : CB* 15 (8), pp. 702–713. DOI: 10.1016/j.cub.2005.02.053.

Lucas, M.; Hierro, A. (2017): Retromer. In *Current biology : CB* 27 (14), R687-R689. DOI: 10.1016/j.cub.2017.05.072.

Lu, L.; Cai, Q.; Tian, J.-H.; Sheng, Z.-H. (2009): Snapin associates with late endocytic compartments and interacts with late endosomal SNAREs. In *Bioscience reports* 29 (4), pp. 261–269. DOI: 10.1042/BSR20090043.

Luzio, J. P.; Hackmann, Y.; Dieckmann, N. M. G.; Griffiths, G. M. (2014): The biogenesis of lysosomes and lysosome-related organelles. In *Cold Spring Harbor perspectives in biology* 6 (9), a016840. DOI: 10.1101/cshperspect.a016840.

MacDonald, R. G.; Pfeffer, S. R.; Coussens, L.; Tepper, M. A.; Brocklebank, C. M.; Mole, J. E.; Anderson, J. K.; Chen, E.; Czech, M. P.; Ullrich, A. (1988): A single receptor binds both insulin-like growth factor II and mannose-6-phosphate. In *Science (New York, N.Y.)* 239 (4844), pp. 1134–1137. DOI: 10.1126/science.2964083.

Magee, A. I.; Courtneidge, S. A. (1985): Two classes of fatty acid acylated proteins exist in eukaryotic cells. In *The EMBO journal* 4 (5), pp. 1137–1144.

Mali, P.; Yang, L.; Esvelt, K. M.; Aach, J.; Guell, M.; DiCarlo, J. E.; Norville, J. E.; Church, G. M. (2013): RNA-guided human genome engineering via Cas9. In *Science (New York, N.Y.)* 339 (6121), pp. 823–826. DOI: 10.1126/science.1232033.

Malumbres, M. (2014): Cyclin-dependent kinases. In *Genome biology* 15 (6), p. 122. DOI: 10.1186/gb4184.

Mann, M.; Ong, S. E.; Grønborg, M.; Steen, H.; Jensen, O. N.; Pandey, A. (2002): Analysis of protein phosphorylation using mass spectrometry: deciphering the phosphoproteome. In *Trends in biotechnology* 20 (6), pp. 261–268.

Manza, L. L.; Stamer, S. L.; Ham, A.-J. L.; Codreanu, S. G.; Liebler, D. C. (2005): Sample preparation and digestion for proteomic analyses using spin filters. In *Proteomics* 5 (7), pp. 1742–1745. DOI: 10.1002/pmic.200401063.

Marciniak, J.; Zalewska, A.; Popko, J.; Zwierz, K. (2006): Optimization of an enzymatic method for the determination of lysosomal N-acetyl-beta-D-hexosaminidase and beta-glucuronidase in synovial fluid. In *Clinical chemistry and laboratory medicine* 44 (8), pp. 933–937. DOI: 10.1515/CCLM.2006.177.

Martina, J. A.; Chen, Y.; Gucek, M.; Puertollano, R. (2012): MTORC1 functions as a transcriptional regulator of autophagy by preventing nuclear transport of TFEB. In *Autophagy* 8 (6), pp. 903–914. DOI: 10.4161/auto.19653.

Martinez, I.; Chakrabarti, S.; Hellevik, T.; Morehead, J.; Fowler, K.; Andrews, N. W. (2000): Synaptotagmin VII regulates Ca(2+)-dependent exocytosis of lysosomes in fibroblasts. In *The Journal of cell biology* 148 (6), pp. 1141–1149. DOI: 10.1083/jcb.148.6.1141.

Matsui, T.; Itoh, T.; Fukuda, M. (2011): Small GTPase Rab12 regulates constitutive degradation of transferrin receptor. In *Traffic (Copenhagen, Denmark)* 12 (10), pp. 1432–1443. DOI: 10.1111/j.1600-0854.2011.01240.x.

Mei, F. C.; Qiao, J.; Tsygankova, O. M.; Meinkoth, J. L.; Quilliam, L. A.; Cheng, X. (2002): Differential signaling of cyclic AMP: opposing effects of exchange protein directly activated by cyclic AMP and cAMP-dependent protein kinase on protein kinase B activation. In *The Journal of biological chemistry* 277 (13), pp. 11497–11504. DOI: 10.1074/jbc.M110856200.

Mellacheruvu, D.; Wright, Z.; Couzens, A. L.; Lambert, J.-P.; St-Denis, N. A.; Li, T.; Miteva, Y. V.; Hauri, S.; Sardiu, M. E.; Low, T. Y.; Halim, V. A.; Bagshaw, R. D.; Hubner, N. C.; Al-Hakim, A.; Bouchard, A.; Faubert, D.; Fermin, D.; Dunham, W. H.; Goudreault, M.; Lin, Z.-Y.; Badillo, B. G.; Pawson, T.; Durocher, D.; Coulombe, B.; Aebersold, R.; Superti-Furga, G.; Colinge, J.; Heck, A. J. R.; Choi, H.; Gstaiger, M.; Mohammed, S.; Cristea, I. M.; Bennett, K. L.; Washburn, M. P.; Raught, B.; Ewing, R. M.; Gingras, A.-C.; Nesvizhskii, A. I. (2013): The CRAPome: a contaminant repository for affinity purification-mass spectrometry data. In *Nature methods* 10 (8), pp. 730–736. DOI: 10.1038/nmeth.2557.

Meselson, M.; Yuan, R. (1968): DNA restriction enzyme from E. coli. In *Nature* 217 (5134), pp. 1110–1114.

Mikami, T.; Takao, T.; Yanagi, K.; Nakazawa, H. (2012): N (α) selective acetylation of peptides. In *Mass spectrometry (Tokyo, Japan)* 1 (2), A0010. DOI: 10.5702/massspectrometry.A0010.

Miller, B. T.; Collins, T. J.; Nagle, G. T.; Kurosky, A. (1992): The occurrence of O-acylation during biotinylation of gonadotropin-releasing hormone and analogs. Evidence for a reactive serine. In *The Journal of biological chemistry* 267 (8), pp. 5060–5069.

Miller, B. T.; Kurosky, A. (1993): Elevated intrinsic reactivity of seryl hydroxyl groups within the linear peptide triads His-Xaa-Ser or Ser-Xaa-His. In *Biochemical and biophysical research communications* 196 (1), pp. 461–467. DOI: 10.1006/bbrc.1993.2272.

Miller, B. T.; Collins, T. J.; Rogers, M. E.; Kurosky, A. (1997): Peptide biotinylation with amine-reactive esters: differential side chain reactivity. In *Peptides* 18 (10), pp. 1585–1595. DOI: 10.1016/s0196-9781(97)00225-8.

Montminy, M. R.; Bilezikjian, L. M. (1987): Binding of a nuclear protein to the cyclic-AMP response element of the somatostatin gene. In *Nature* 328 (6126), pp. 175–178. DOI: 10.1038/328175a0.

Moore, F. L.; Jaruzelska, J.; Fox, M. S.; Urano, J.; Firpo, M. T.; Turek, P. J.; Dorfman, D. M.; Pera, R. A. R. (2003): Human Pumilio-2 is expressed in embryonic stem cells and germ cells and interacts with DAZ (Deleted in AZoospermia) and DAZ-like proteins. In *Proceedings of the National Academy of Sciences of the United States of America* 100 (2), pp. 538–543. DOI: 10.1073/pnas.0234478100.

Morgan, N. V.; Pasha, S.; Johnson, C. A.; Ainsworth, J. R.; Eady, R. A. J.; Dawood, B.; McKeown, C.; Trembath, R. C.; Wilde, J.; Watson, S. P.; Maher, E. R. (2006): A germline mutation in BLOC1S3/reduced pigmentation causes a novel variant of Hermansky-Pudlak syndrome (HPS8). In *American Journal of Human Genetics* 78 (1), pp. 160–166. DOI: 10.1086/499338.

Mowen, K. A.; Tang, J.; Zhu, W.; Schurter, B. T.; Shuai, K.; Herschman, H. R.; David, M. (2001): Arginine methylation of STAT1 modulates IFNalpha/beta-induced transcription. In *Cell* 104 (5), pp. 731–741. DOI: 10.1016/s0092-8674(01)00269-0.

Müller, M. (1972): Secretion of acid hydrolases and its intracellular source in Tetrahymena pyriformis. In *The Journal of cell biology* 52 (2), pp. 478–487.

Muñiz, M.; Alonso, M.; Hidalgo, J.; Velasco, A. (1996): A regulatory role for cAMP-dependent protein kinase in protein traffic along the exocytic route. In *The Journal of biological chemistry* 271 (48), pp. 30935–30941. DOI: 10.1074/jbc.271.48.30935.

Muñiz, M.; Martín, M. E.; Hidalgo, J.; Velasco, A. (1997): Protein kinase A activity is required for the budding of constitutive transport vesicles from the trans-Golgi network. In *Proceedings of the National Academy of Sciences of the United States of America* 94 (26), pp. 14461–14466. DOI: 10.1073/pnas.94.26.14461.

Napolitano, G.; Esposito, A.; Choi, H.; Matarese, M.; Benedetti, V.; Di Malta, C.; Monfregola, J.; Medina, D. L.; Lippincott-Schwartz, J.; Ballabio, A. (2018): mTOR-dependent phosphorylation controls TFEB nuclear export. In *Nature communications* 9 (1), p. 3312. DOI: 10.1038/s41467-018-05862-6.

Navarro, A.; Encinar, J. A.; López-Méndez, B.; Aguado-Llera, D.; Prieto, J.; Gómez, J.; Martínez-Cruz, L. A.; Millet, O.; González-Ros, J. M.; Fernández-Ballester, G.; Neira, J. L.; Ferrer-Montiel, A. (2012): Mutation of Ser-50 and Cys-66 in Snapin modulates protein structure and stability. In *Biochemistry* 51 (16), pp. 3470–3484. DOI: 10.1021/bi201574t.

Navé, B. T.; Ouwens, M.; Withers, D. J.; Alessi, D. R.; Shepherd, P. R. (1999): Mammalian target of rapamycin is a direct target for protein kinase B: identification of a convergence point for opposing effects of insulin and amino-acid deficiency on protein translation. In *The Biochemical journal* 344 Pt 2, pp. 427–431.

Neurath, H.; Walsh, K. A. (1976): Role of proteolytic enzymes in biological regulation (a review). In *Proceedings of the National Academy of Sciences of the United States of America* 73 (11), pp. 3825–3832. DOI: 10.1073/pnas.73.11.3825.

Neville, D. C.; Rozanas, C. R.; Price, E. M.; Gruis, D. B.; Verkman, A. S.; Townsend, R. R. (1997): Evidence for phosphorylation of serine 753 in CFTR using a novel metal-ion affinity resin and matrix-assisted laser desorption mass spectrometry. In *Protein science : a publication of the Protein Society* 6 (11), pp. 2436–2445. DOI: 10.1002/pro.5560061117.

Nojima, H.; Tokunaga, C.; Eguchi, S.; Oshiro, N.; Hidayat, S.; Yoshino, K.-i.; Hara, K.; Tanaka, N.; Avruch, J.; Yonezawa, K. (2003): The mammalian target of rapamycin (mTOR) partner, raptor, binds the mTOR substrates p70 S6 kinase and 4E-BP1 through their TOR signaling (TOS) motif. In *The Journal of biological chemistry* 278 (18), pp. 15461–15464. DOI: 10.1074/jbc.C200665200.

Nonaka, T.; Ishikawa, H.; Tsumuraya, Y.; Hashimoto, Y.; Dohmae, N. (1995): Characterization of a thermostable lysine-specific metalloendopeptidase from the fruiting bodies of a basidiomycete, Grifola frondosa. In *Journal of biochemistry* 118 (5), pp. 1014–1020. DOI: 10.1093/jb/118.5.1014.

Northup, J. K.; Sternweis, P. C.; Smigel, M. D.; Schleifer, L. S.; Ross, E. M.; Gilman, A. G. (1980): Purification of the regulatory component of adenylate cyclase. In *Proceedings of the National Academy of Sciences of the United States of America* 77 (11), pp. 6516–6520. DOI: 10.1073/pnas.77.11.6516.

Nühse, T. S.; Stensballe, A.; Jensen, O. N.; Peck, S. C. (2003): Large-scale analysis of in vivo phosphorylated membrane proteins by immobilized metal ion affinity chromatography and mass spectrometry. In *Molecular & cellular proteomics : MCP* 2 (11), pp. 1234–1243. DOI: 10.1074/mcp.T300006-MCP200.

O'Farrell, P. H. (1975): High resolution two-dimensional electrophoresis of proteins. In *The Journal of biological chemistry* 250 (10), pp. 4007–4021.

Ohkuma, S.; Moriyama, Y.; Takano, T. (1982): Identification and characterization of a proton pump on lysosomes by fluorescein-isothiocyanate-dextran fluorescence. In *Proceedings of the National Academy of Sciences of the United States of America* 79 (9), pp. 2758–2762. DOI: 10.1073/pnas.79.9.2758.

Okuno, S.; Kitani, T.; Fujisawa, H. (2001): Regulation of Ca(2+)/calmodulin-dependent protein kinase kinase alpha by cAMP-dependent protein kinase: I. Biochemical analysis. In *Journal of biochemistry* 130 (4), pp. 503–513. DOI: 10.1093/oxfordjournals.jbchem.a003013.

Olsen, J. V.; Ong, S.-E.; Mann, M. (2004): Trypsin cleaves exclusively C-terminal to arginine and lysine residues. In *Molecular & cellular proteomics : MCP* 3 (6), pp. 608–614. DOI: 10.1074/mcp.T400003-MCP200.

Olsen, J. V.; Blagoev, B.; Gnad, F.; Macek, B.; Kumar, C.; Mortensen, P.; Mann, M. (2006): Global, in vivo, and site-specific phosphorylation dynamics in signaling networks. In *Cell* 127 (3), pp. 635–648. DOI: 10.1016/j.cell.2006.09.026.

Ong, S.-E.; Blagoev, B.; Kratchmarova, I.; Kristensen, D. B.; Steen, H.; Pandey, A.; Mann, M. (2002): Stable isotope labeling by amino acids in cell culture, SILAC, as a simple and accurate approach to expression proteomics. In *Molecular & cellular proteomics : MCP* 1 (5), pp. 376–386.

Ong, S.-E.; Kratchmarova, I.; Mann, M. (2003): Properties of 13C-substituted arginine in stable isotope labeling by amino acids in cell culture (SILAC). In *Journal of proteome research* 2 (2), pp. 173–181.

Ong, S.-E.; Mann, M. (2005): Mass spectrometry-based proteomics turns quantitative. In *Nature chemical biology* 1 (5), pp. 252–262. DOI: 10.1038/nchembio736.

Ong, S.-E.; Mann, M. (2006): A practical recipe for stable isotope labeling by amino acids in cell culture (SILAC). In *Nature protocols* 1 (6), pp. 2650–2660. DOI: 10.1038/nprot.2006.427.

Ozaki, N.; Shibasaki, T.; Kashima, Y.; Miki, T.; Takahashi, K.; Ueno, H.; Sunaga, Y.; Yano, H.; Matsuura, Y.; Iwanaga, T.; Takai, Y.; Seino, S. (2000): cAMP-GEFII is a direct target of cAMP in regulated exocytosis. In *Nature cell biology* 2 (11), pp. 805–811. DOI: 10.1038/35041046.

Pappin, D. J.; Hojrup, P.; Bleasby, A. J. (1993): Rapid identification of proteins by peptide-mass fingerprinting. In *Current biology : CB* 3 (6), pp. 327–332. DOI: 10.1016/0960-9822(93)90195-t.

Paumet, F.; Le Mao, J.; Martin, S.; Galli, T.; David, B.; Blank, U.; Roa, M. (2000): Soluble NSF attachment protein receptors (SNAREs) in RBL-2H3 mast cells: functional role of syntaxin 4 in exocytosis and identification of a vesicle-associated membrane protein 8-containing secretory compartment. In *Journal of immunology (Baltimore, Md. : 1950)* 164 (11), pp. 5850–5857. DOI: 10.4049/jimmunol.164.11.5850.

Perera, R. M.; Zoncu, R. (2016): The lysosome as a regulatory hub. In *Annual review of cell and developmental biology* 32, pp. 223–253. DOI: 10.1146/annurev-cellbio-111315-125125.

Peters, A. H. F. M.; Kubicek, S.; Mechtler, K.; O'Sullivan, R. J.; Derijck, A. A. H. A.; Perez-Burgos, L.; Kohlmaier, A.; Opravil, S.; Tachibana, M.; Shinkai, Y.; Martens, J. H. A.; Jenuwein, T. (2003): Partitioning and plasticity of repressive histone methylation states in mammalian chromatin. In *Molecular cell* 12 (6), pp. 1577–1589.

Peterson, T. R.; Laplante, M.; Thoreen, C. C.; Sancak, Y.; Kang, S. A.; Kuehl, W. M.; Gray, N. S.; Sabatini, D. M. (2009): DEPTOR is an mTOR inhibitor frequently overexpressed in multiple myeloma cells and required for their survival. In *Cell* 137 (5), pp. 873–886. DOI: 10.1016/j.cell.2009.03.046.

Pinkse, M. W. H.; Uitto, P. M.; Hilhorst, M. J.; Ooms, B.; Heck, A. J. R. (2004): Selective isolation at the femtomole level of phosphopeptides from proteolytic digests using 2D-NanoLC-ESI-MS/MS and titanium oxide precolumns. In *Analytical chemistry* 76 (14), pp. 3935–3943. DOI: 10.1021/ac0498617.

Pols, M. S.; Brink, C. ten; Gosavi, P.; Oorschot, V.; Klumperman, J. (2013): The HOPS proteins hVps41 and hVps39 are required for homotypic and heterotypic late endosome fusion. In *Traffic (Copenhagen, Denmark)* 14 (2), pp. 219–232. DOI: 10.1111/tra.12027.

Pozuelo Rubio, M.; Peggie, M.; Wong, B. H. C.; Morrice, N.; MacKintosh, C. (2003): 14-3-3s regulate fructose-2,6-bisphosphate levels by binding to PKB-phosphorylated cardiac fructose-2,6-bisphosphate kinase/phosphatase. In *The EMBO journal* 22 (14), pp. 3514–3523. DOI: 10.1093/emboj/cdg363.

Pu, J.; Schindler, C.; Jia, R.; Jarnik, M.; Backlund, P.; Bonifacino, J. S. (2015): BORC, a multisubunit complex that regulates lysosome positioning. In *Developmental cell* 33 (2), pp. 176–188. DOI: 10.1016/j.devcel.2015.02.011.

Pu, J.; Guardia, C. M.; Keren-Kaplan, T.; Bonifacino, J. S. (2016): Mechanisms and functions of lysosome positioning. In *Journal of cell science* 129 (23), pp. 4329–4339. DOI: 10.1242/jcs.196287.

R Core Team (2019): R: A language and environment for statistical computing. R Foundation for Statistical Computing, Vienna, Austria. URL https://www.R-project.org/.

Rahman, N.; Ramos-Espiritu, L.; Milner, T. A.; Buck, J.; Levin, L. R. (2016): Soluble adenylyl cyclase is essential for proper lysosomal acidification. In *The Journal of general physiology* 148 (4), pp. 325–339. DOI: 10.1085/jgp.201611606.

Rall, T. W.; Sutherland, E. W. (1958): Formation of a cyclic adenine ribonucleotide by tissue particles. In *The Journal of biological chemistry* 232 (2), pp. 1065–1076.

Ramseyer, J.; Kaslow, H. R.; Gill, G. N. (1974): Purification of the cAMP receptor protein by affinity chromatography. In *Biochemical and biophysical research communications* 59 (2), pp. 813–821. DOI: 10.1016/s0006-291x(74)80052-5.

Rangarajan, S.; Enserink, J. M.; Kuiperij, H. B.; Rooij, J. de; Price, L. S.; Schwede, F.; Bos, J. L. (2003): Cyclic AMP induces integrin-mediated cell adhesion through Epac and Rap1 upon stimulation of the beta 2-adrenergic receptor. In *The Journal of cell biology* 160 (4), pp. 487–493. DOI: 10.1083/jcb.200209105.

Rao, S. K.; Huynh, C.; Proux-Gillardeaux, V.; Galli, T.; Andrews, N. W. (2004): Identification of SNAREs involved in synaptotagmin VII-regulated lysosomal exocytosis. In *The Journal of biological chemistry* 279 (19), pp. 20471–20479. DOI: 10.1074/jbc.M400798200.

Rappsilber, J.; Mann, M.; Ishihama, Y. (2007): Protocol for micro-purification, enrichment, pre-fractionation and storage of peptides for proteomics using StageTips. In *Nature protocols* 2 (8), pp. 1896–1906. DOI: 10.1038/nprot.2007.261.

Reczek, D.; Schwake, M.; Schröder, J.; Hughes, H.; Blanz, J.; Jin, X.; Brondyk, W.; van Patten, S.; Edmunds, T.; Saftig, P. (2007): LIMP-2 is a receptor for lysosomal mannose-6-phosphate-independent targeting of beta-glucocerebrosidase. In *Cell* 131 (4), pp. 770–783. DOI: 10.1016/j.cell.2007.10.018.

Reddy, A.; Caler, E. V.; Andrews, N. W. (2001): Plasma membrane repair is mediated by Ca2+-regulated exocytosis of lysosomes. In *Cell* 106 (2), pp. 157–169. DOI: 10.1016/S0092-8674(01)00421-4.

Ribet, D.; Hamon, M.; Gouin, E.; Nahori, M.-A.; Impens, F.; Neyret-Kahn, H.; Gevaert, K.; Vandekerckhove, J.; Dejean, A.; Cossart, P. (2010): Listeria monocytogenes impairs SUMOylation for efficient infection. In *Nature* 464 (7292), pp. 1192–1195. DOI: 10.1038/nature08963.

Riederer, M. A.; Soldati, T.; Shapiro, A. D.; Lin, J.; Pfeffer, S. R. (1994): Lysosome biogenesis requires Rab9 function and receptor recycling from endosomes to the trans-Golgi network. In *The Journal of cell biology* 125 (3), pp. 573–582. DOI: 10.1083/jcb.125.3.573.

Ritchie, M. E.; Phipson, B.; Di Wu; Hu, Y.; Law, C. W.; Shi, W.; Smyth, G. K. (2015): limma powers differential expression analyses for RNA-sequencing and microarray studies. In *Nucleic acids research* 43 (7), e47. DOI: 10.1093/nar/gkv007.

Rodbell, M.; Birnbaumer, L.; Pohl, S. L.; Krans, H. M. (1971): The glucagon-sensitive adenyl cyclase system in plasma membranes of rat liver. V. An obligatory role of guanylnucleotides in glucagon action. In *The Journal of biological chemistry* 246 (6), pp. 1877–1882.

Rodríguez, A.; Webster, P.; Ortego, J.; Andrews, N. W. (1997): Lysosomes behave as Ca2+-regulated exocytic vesicles in fibroblasts and epithelial cells. In *The Journal of cell biology* 137 (1), pp. 93–104.

Rodríguez, A.; Martinez, I.; Chung, A.; Berlot, C. H.; Andrews, N. W. (1999): cAMP regulates Ca2+-dependent exocytosis of lysosomes and lysosome-mediated cell invasion by trypanosomes. In *The Journal of biological chemistry* 274 (24), pp. 16754–16759. DOI: 10.1074/jbc.274.24.16754.

Rooij, J. de; Zwartkruis, F. J.; Verheijen, M. H.; Cool, R. H.; Nijman, S. M.; Wittinghofer, A.; Bos, J. L. (1998): Epac is a Rap1 guanine-nucleotide-exchange factor directly activated by cyclic AMP. In *Nature* 396 (6710), pp. 474–477. DOI: 10.1038/24884.

Rosner, M.; Siegel, N.; Valli, A.; Fuchs, C.; Hengstschläger, M. (2010): mTOR phosphorylated at S2448 binds to raptor and rictor. In *Amino acids* 38 (1), pp. 223–228. DOI: 10.1007/s00726-008-0230-7.

Ross, P. L.; Huang, Y. N.; Marchese, J. N.; Williamson, B.; Parker, K.; Hattan, S.; Khainovski, N.; Pillai, S.; Dey, S.; Daniels, S.; Purkayastha, S.; Juhasz, P.; Martin, S.; Bartlet-Jones, M.; He, F.; Jacobson, A.; Pappin, D. J. (2004): Multiplexed protein quantitation in Saccharomyces cerevisiae using amine-reactive isobaric tagging reagents. In *Molecular & cellular proteomics : MCP* 3 (12), pp. 1154–1169. DOI: 10.1074/mcp.M400129-MCP200.

Sahagian, G. G.; Distler, J.; Jourdian, G. W. (1981): Characterization of a membrane-associated receptor from bovine liver that binds phosphomannosyl residues of bovine testicular beta-galactosidase. In *Proceedings of the National Academy of Sciences of the United States of America* 78 (7), pp. 4289–4293. DOI: 10.1073/pnas.78.7.4289.

Sahagian, G. G.; Neufeld, E. F. (1983): Biosynthesis and turnover of the mannose 6-phosphate receptor in cultured Chinese hamster ovary cells. In *The Journal of biological chemistry* 258 (11), pp. 7121–7128.

Salazar, G.; González, A. (2002): Novel mechanism for regulation of epidermal growth factor receptor endocytosis revealed by protein kinase A inhibition. In *Molecular biology of the cell* 13 (5), pp. 1677–1693. DOI: 10.1091/mbc.01-08-0403.

Sancak, Y.; Thoreen, C. C.; Peterson, T. R.; Lindquist, R. A.; Kang, S. A.; Spooner, E.; Carr, S. A.; Sabatini, D. M. (2007): PRAS40 is an insulin-regulated inhibitor of the mTORC1 protein kinase. In *Molecular cell* 25 (6), pp. 903–915. DOI: 10.1016/j.molcel.2007.03.003.

Sancak, Y.; Peterson, T. R.; Shaul, Y. d.; Lindquist, R. A.; Thoreen, C. C.; Bar-Peled, L.; Sabatini, D. M. (2008): The Rag GTPases bind raptor and mediate amino acid signaling to mTORC1. In *Science (New York, N.Y.)* 320 (5882), pp. 1496–1501. DOI: 10.1126/science.1157535.

Sancak, Y.; Bar-Peled, L.; Zoncu, R.; Markhard, A. L.; Nada, S.; Sabatini, D. M. (2010): Ragulator-Rag complex targets mTORC1 to the lysosomal surface and is necessary for its activation by amino acids. In *Cell* 141 (2), pp. 290–303. DOI: 10.1016/j.cell.2010.02.024.

Sanger, F.; Nicklen, S.; Coulson, A. R. (1977): DNA sequencing with chain-terminating inhibitors. In *Proceedings of the National Academy of Sciences of the United States of America* 74 (12), pp. 5463–5467.

Sanny, C. G.; Hartsuck, J. A.; Tang, J. (1975): Conversion of pepsinogen to pepsin. Further evidence for intramolecular and pepsin-catalyzed activation. In *The Journal of biological chemistry* 250 (7), pp. 2635–2639.

Sardiello, M.; Palmieri, M.; Di Ronza, A.; Medina, D. L.; Valenza, M.; Gennarino, V. A.; Di Malta, C.; Donaudy, F.; Embrione, V.; Polishchuk, R. S.; Banfi, S.; Parenti, G.; Cattaneo, E.; Ballabio, A. (2009): A gene network regulating lysosomal biogenesis and function. In *Science (New York, N.Y.)* 325 (5939), pp. 473–477. DOI: 10.1126/science.1174447.

Sathe, G.; Na, C. H.; Renuse, S.; Madugundu, A.; Albert, M.; Moghekar, A.; Pandey, A. (2018): Phosphotyrosine profiling of human cerebrospinal fluid. In *Clinical proteomics* 15, p. 29. DOI: 10.1186/s12014-018-9205-1.

Saxton, R. A.; Sabatini, D. M. (2017): mTOR Signaling in Growth, Metabolism, and Disease. In *Cell* 168 (6), pp. 960–976. DOI: 10.1016/j.cell.2017.02.004.

Schalm, S. S.; Fingar, D. C.; Sabatini, D. M.; Blenis, J. (2003): TOS motif-mediated raptor binding regulates 4E-BP1 multisite phosphorylation and function. In *Current biology : CB* 13 (10), pp. 797–806. DOI: 10.1016/s0960-9822(03)00329-4.

Schmid-Burgk, J. L.; Schmidt, T.; Gaidt, M. M.; Pelka, K.; Latz, E.; Ebert, T. S.; Hornung, V. (2014): OutKnocker: a web tool for rapid and simple genotyping of designer nuclease edited cell lines. In *Genome research* 24 (10), pp. 1719–1723. DOI: 10.1101/gr.176701.114.

Schneider, C. A.; Rasband, W. S.; Eliceiri, K. W. (2012): NIH Image to ImageJ: 25 years of image analysis. In *Nature methods* 9 (7), pp. 671–675. DOI: 10.1038/nmeth.2089.

Screaton, R. A.; Conkright, M. D.; Katoh, Y.; Best, J. L.; Canettieri, G.; Jeffries, S.; Guzman, E.; Niessen, S.; Yates, J. R.; Takemori, H.; Okamoto, M.; Montminy, M. (2004): The CREB coactivator TORC2 functions as a calcium- and cAMP-sensitive coincidence detector. In *Cell* 119 (1), pp. 61–74. DOI: 10.1016/j.cell.2004.09.015.

Seamon, K. B.; Padgett, W.; Daly, J. W. (1981): Forskolin: unique diterpene activator of adenylate cyclase in membranes and in intact cells. In *Proceedings of the National Academy of Sciences of the United States of America* 78 (6), pp. 3363–3367. DOI: 10.1073/pnas.78.6.3363.

Sekulić, A.; Hudson, C. C.; Homme, J. L.; Yin, P.; Otterness, D. M.; Karnitz, L. M.; Abraham, R. T. (2000): A direct linkage between the phosphoinositide 3-kinase-AKT signaling pathway and the mammalian target of rapamycin in mitogen-stimulated and transformed cells. In *Cancer research* 60 (13), pp. 3504–3513.

Sette, C.; Conti, M. (1996): Phosphorylation and activation of a cAMP-specific phosphodiesterase by the cAMP-dependent protein kinase. Involvement of serine 54 in the enzyme activation. In *The Journal of biological chemistry* 271 (28), pp. 16526–16534. DOI: 10.1074/jbc.271.28.16526.

Settembre, C.; Di Malta, C.; Polito, V. A.; Garcia Arencibia, M.; Vetrini, F.; Erdin, S.; Erdin, S. U.; Huynh, T.; Medina, D.; Colella, P.; Sardiello, M.; Rubinsztein, D. C.; Ballabio, A. (2011): TFEB links autophagy to lysosomal biogenesis. In *Science (New York, N.Y.)* 332 (6036), pp. 1429–1433. DOI: 10.1126/science.1204592.

Settembre, C.; Zoncu, R.; Medina, D. L.; Vetrini, F.; Erdin, S.; Erdin, S.; Huynh, T.; Ferron, M.; Karsenty, G.; Vellard, M. C.; Facchinetti, V.; Sabatini, D. M.; Ballabio, A. (2012): A lysosome-to-nucleus signalling mechanism senses and regulates the lysosome via mTOR and TFEB. In *The EMBO journal* 31 (5), pp. 1095–1108. DOI: 10.1038/emboj.2012.32.

Setty, S. R. G.; Tenza, D.; Truschel, S. T.; Chou, E.; Sviderskaya, E. V.; Theos, A. C.; Lamoreux, M. L.; Di Pietro, S. M.; Starcevic, M.; Bennett, D. C.; Dell'Angelica, E. C.; Raposo, G.; Marks, M. S. (2007): BLOC-1 is required for cargo-specific sorting from vacuolar early endosomes toward lysosome-related organelles. In *Molecular biology of the cell* 18 (3), pp. 768–780. DOI: 10.1091/mbc.e06-12-1066.

Sheng, M.; Thompson, M. A.; Greenberg, M. E. (1991): CREB: a Ca(2+)-regulated transcription factor phosphorylated by calmodulin-dependent kinases. In *Science (New York, N.Y.)* 252 (5011), pp. 1427–1430. DOI: 10.1126/science.1646483.

Shevchenko, A.; Wilm, M.; Vorm, O.; Mann, M. (1996): Mass spectrometric sequencing of proteins silver-stained polyacrylamide gels. In *Analytical chemistry* 68 (5), pp. 850–858.

Shibasaki, T.; Takahashi, H.; Miki, T.; Sunaga, Y.; Matsumura, K.; Yamanaka, M.; Zhang, C.; Tamamoto, A.; Satoh, T.; Miyazaki, J.-I.; Seino, S. (2007): Essential role of Epac2/Rap1 signaling in regulation of insulin granule dynamics by cAMP. In *Proceedings of the National Academy of Sciences of the United States of America* 104 (49), pp. 19333–19338. DOI: 10.1073/pnas.0707054104.

Sigismund, S.; Woelk, T.; Puri, C.; Maspero, E.; Tacchetti, C.; Transidico, P.; Di Fiore, P. P.; Polo, S. (2005): Clathrin-independent endocytosis of ubiquitinated cargos. In *Proceedings of the National Academy of Sciences of the United States of America* 102 (8), pp. 2760–2765. DOI: 10.1073/pnas.0409817102.

Smith, C. M.; Gafken, P. R.; Zhang, Z.; Gottschling, D. E.; Smith, J. B.; Smith, D. L. (2003): Mass spectrometric quantification of acetylation at specific lysines within the amino-terminal tail of histone H4. In *Analytical biochemistry* 316 (1), pp. 23–33. DOI: 10.1016/s0003-2697(03)00032-0.

Smith, F. D.; Esseltine, J. L.; Nygren, P. J.; Veesler, D.; Byrne, D. P.; Vonderach, M.; Strashnov, I.; Eyers, C. E.; Eyers, P. A.; Langeberg, L. K.; Scott, J. D. (2017): Local protein kinase A action proceeds through intact holoenzymes. In *Science (New York, N.Y.)* 356 (6344), pp. 1288–1293. DOI: 10.1126/science.aaj1669.

Smith, H. O.; Wilcox, K. W. (1970): A restriction enzyme from Hemophilus influenzae. I. Purification and general properties. In *Journal of molecular biology* 51 (2), pp. 379–391.

Somanath, S.; Partridge, C. J.; Marshall, C.; Rowe, T.; Turner, M. D. (2016): Snapin mediates insulin secretory granule docking, but not trans-SNARE complex formation. In *Biochemical and biophysical research communications* 473 (2), pp. 403–407. DOI: 10.1016/j.bbrc.2016.02.123.

Song, W.-J.; Seshadri, M.; Ashraf, U.; Mdluli, T.; Mondal, P.; Keil, M.; Azevedo, M.; Kirschner, L. S.; Stratakis, C. A.; Hussain, M. A. (2011): Snapin mediates incretin action and augments glucose-dependent insulin secretion. In *Cell metabolism* 13 (3), pp. 308–319. DOI: 10.1016/j.cmet.2011.02.002.

Sonntag, T.; Vaughan, J. M.; Montminy, M. (2018): 14-3-3 proteins mediate inhibitory effects of cAMP on salt-inducible kinases (SIKs). In *The FEBS journal* 285 (3), pp. 467–480. DOI: 10.1111/febs.14351.

Sonomura, K.; Kuyama, H.; Matsuo, E.-I.; Tsunasawa, S.; Futaki, S.; Nishimura, O. (2011): Selective isolation of N-blocked peptide by combining AspN digestion, transamination, and tosylhydrazine glass treatment. In *Analytical biochemistry* 410 (2), pp. 214–223. DOI: 10.1016/j.ab.2010.12.006.

Sorkin, A.; Mazzotti, M.; Sorkina, T.; Scotto, L.; Beguinot, L. (1996): Epidermal growth factor receptor interaction with clathrin adaptors is mediated by the Tyr974-containing internalization motif. In *The Journal of biological chemistry* 271 (23), pp. 13377–13384. DOI: 10.1074/jbc.271.23.13377.

Stahl, D. C.; Swiderek, K. M.; Davis, M. T.; Lee, T. D. (1996): Data-controlled automation of liquid chromatography/tandem mass spectrometry analysis of peptide mixtures. In *J Am Soc Mass Spectrom* 7 (6), pp. 532–540. DOI: 10.1016/1044-0305(96)00057-8.

Starcevic, M.; Dell'Angelica, E. C. (2004): Identification of snapin and three novel proteins (BLOS1, BLOS2, and BLOS3/reduced pigmentation) as subunits of biogenesis of lysosome-related organelles complex-1 (BLOC-1). In *The Journal of biological chemistry* 279 (27), pp. 28393–28401. DOI: 10.1074/jbc.M402513200.

Stinchcombe, J. C.; Bossi, G.; Booth, S.; Griffiths, G. M. (2001): The immunological synapse of CTL contains a secretory domain and membrane bridges. In *Immunity* 15 (5), pp. 751–761. DOI: 10.1016/s1074-7613(01)00234-5.

Strahl, B. D.; Ohba, R.; Cook, R. G.; Allis, C. D. (1999): Methylation of histone H3 at lysine 4 is highly conserved and correlates with transcriptionally active nuclei in Tetrahymena. In *Proceedings of the National Academy of Sciences of the United States of America* 96 (26), pp. 14967–14972. DOI: 10.1073/pnas.96.26.14967.

Suter, A.; Everts, V.; Boyde, A.; Jones, S. J.; Lüllmann-Rauch, R.; Hartmann, D.; Hayman, A. R.; Cox, T. M.; Evans, M. J.; Meister, T.; Figura, K. von; Saftig, P. (2001): Overlapping functions of lysosomal acid phosphatase (LAP) and tartrate-resistant acid phosphatase (Acp5) revealed by doubly deficient mice. In *Development (Cambridge, England)* 128 (23), pp. 4899–4910.

Sutherland, E. W.; Rall, T. W. (1958): Fractionation and characterization of a cyclic adenine ribonucleotide formed by tissue particles. In *The Journal of biological chemistry* 232 (2), pp. 1077–1091.

Tabas, I.; Kornfeld, S. (1980): Biosynthetic intermediates of beta-glucuronidase contain high mannose oligosaccharides with blocked phosphate residues. In *The Journal of biological chemistry* 255 (14), pp. 6633–6639.

Tallant, C.; García-Castellanos, R.; Seco, J.; Baumann, U.; Gomis-Rüth, F. X. (2006): Molecular analysis of ulilysin, the structural prototype of a new family of metzincin metalloproteases. In *The Journal of biological chemistry* 281 (26), pp. 17920–17928. DOI: 10.1074/jbc.M600907200.

Tallant, C.; García-Castellanos, R.; Marrero, A.; Canals, F.; Yang, Y.; Reymond, J.-L.; Solà, M.; Baumann, U.; Gomis-Rüth, F. X. (2007): Activity of ulilysin, an archaeal PAPP-A-related gelatinase and IGFBP protease. In *Biological chemistry* 388 (11), pp. 1243–1253. DOI: 10.1515/BC.2007.143.

Tanaka, K.; Waki, H.; Ido, Y.; Akita, S.; Yoshida, Y.; Yoshida, T.; Matsuo, T. (1988): Protein and polymer analyses up tom/z 100 000 by laser ionization time-of-flight mass spectrometry. In *Rapid Commun. Mass Spectrom.* 2 (8), pp. 151–153. DOI: 10.1002/rcm.1290020802.

Tao, M.; Salas, M. L.; Lipmann, F. (1970): Mechanism of activation by adenosine 3':5'-cyclic monophosphate of a protein phosphokinase from rabbit reticulocytes. In *Proceedings of the National Academy of Sciences of the United States of America* 67 (1), pp. 408–414. DOI: 10.1073/pnas.67.1.408.

Taouatas, N.; Heck, A. J. R.; Mohammed, S. (2010): Evaluation of metalloendopeptidase Lys-N protease performance under different sample handling conditions. In *Journal of proteome research* 9 (8), pp. 4282–4288. DOI: 10.1021/pr100341e.

Tapia, D.; Jiménez, T.; Zamora, C.; Espinoza, J.; Rizzo, R.; González-Cárdenas, A.; Fuentes, D.; Hernández, S.; Cavieres, V. A.; Soza, A.; Guzmán, F.; Arriagada, G.; Yuseff, M. I.; Mardones, G. A.; Burgos, P. V.; Luini, A.; González, A.; Cancino, J. (2019): KDEL receptor regulates secretion by lysosome relocation- and autophagy-dependent modulation of lipid-droplet turnover. In *Nature communications* 10 (1), p. 735. DOI: 10.1038/s41467-019-08501-w.

Thelen, M.; Winter, D.; Braulke, T.; Gieselmann, V. (2017): SILAC-based comparative proteomic analysis of lysosomes from mammalian cells using LC-MS/MS. In *Methods in molecular biology (Clifton, N.J.)* 1594, pp. 1–18. DOI: 10.1007/978-1-4939-6934-0_1.

Theurkauf, W. E.; Vallee, R. B. (1982): Molecular characterization of the cAMP-dependent protein kinase bound to microtubule-associated protein 2. In *The Journal of biological chemistry* 257 (6), pp. 3284–3290.

Thoreen, C. C.; Kang, S. A.; Chang, J. W.; Liu, Q.; Zhang, J.; Gao, Y.; Reichling, L. J.; Sim, T.; Sabatini, D. M.; Gray, N. S. (2009): An ATP-competitive mammalian target of rapamycin inhibitor reveals rapamycin-resistant functions of mTORC1. In *The Journal of biological chemistry* 284 (12), pp. 8023–8032. DOI: 10.1074/jbc.M900301200.

Tian, J.-H.; Wu, Z.-X.; Unzicker, M.; Lu, L.; Cai, Q.; Li, C.; Schirra, C.; Matti, U.; Stevens, D.; Deng, C.; Rettig, J.; Sheng, Z.-H. (2005): The role of Snapin in neurosecretion: snapin knock-out mice exhibit impaired calcium-dependent exocytosis of large dense-core vesicles in chromaffin cells. In *The Journal of neuroscience : the official journal of the Society for Neuroscience* 25 (45), pp. 10546–10555. DOI: 10.1523/JNEUROSCI.3275-05.2005.

Towbin, H.; Staehelin, T.; Gordon, J. (1979): Electrophoretic transfer of proteins from polyacrylamide gels to nitrocellulose sheets: procedure and some applications. In *Proceedings of the National Academy of Sciences of the United States of America* 76 (9), pp. 4350–4354.

Tzircotis, G.; Thorne, R. F.; Isacke, C. M. (2006): Directional sensing of a phorbol ester gradient requires CD44 and is regulated by CD44 phosphorylation. In *Oncogene* 25 (56), pp. 7401–7410. DOI: 10.1038/sj.onc.1209724.

Uhlén, M.; Fagerberg, L.; Hallström, B. M.; Lindskog, C.; Oksvold, P.; Mardinoglu, A.; Sivertsson, Å.; Kampf, C.; Sjöstedt, E.; Asplund, A.; Olsson, I.; Edlund, K.; Lundberg, E.; Navani, S.; Szigyarto, C. A.-K.; Odeberg, J.; Djureinovic, D.; Takanen, J. O.; Hober, S.; Alm, T.; Edqvist, P.-H.; Berling, H.; Tegel, H.; Mulder, J.; Rockberg, J.; Nilsson, P.; Schwenk, J. M.; Hamsten, M.; Feilitzen, K. von; Forsberg, M.; Persson, L.; Johansson, F.; Zwahlen, M.; Heijne, G. von; Nielsen, J.; Pontén, F. (2015): Proteomics. Tissue-based map of the human proteome. In *Science (New York, N.Y.)* 347 (6220), p. 1260419. DOI: 10.1126/science.1260419.

Uhlmann, T.; Geoghegan, V. L.; Thomas, B.; Ridlova, G.; Trudgian, D. C.; Acuto, O. (2012): A method for large-scale identification of protein arginine methylation. In *Molecular & cellular proteomics : MCP* 11 (11), pp. 1489–1499. DOI: 10.1074/mcp.M112.020743.

Unger, R. H. (1985): Glucagon physiology and pathophysiology in the light of new advances. In *Diabetologia* 28 (8), pp. 574–578. DOI: 10.1007/bf00281991.

Vagnozzi, A. N.; Praticò, D. (2019): Endosomal sorting and trafficking, the retromer complex and neurodegeneration. In *Molecular psychiatry* 24 (6), pp. 857–868. DOI: 10.1038/s41380-018-0221-3.

van Meel, E.; Klumperman, J. (2008): Imaging and imagination: understanding the endo-lysosomal system. In *Histochemistry and cell biology* 129 (3), pp. 253–266. DOI: 10.1007/s00418-008-0384-0.

Vander Haar, E.; Lee, S.-I.; Bandhakavi, S.; Griffin, T. J.; Kim, D.-H. (2007): Insulin signalling to mTOR mediated by the Akt/PKB substrate PRAS40. In *Nature cell biology* 9 (3), pp. 316–323. DOI: 10.1038/ncb1547.

Vandermarliere, E.; Mueller, M.; Martens, L. (2013): Getting intimate with trypsin, the leading protease in proteomics. In *Mass spectrometry reviews* 32 (6), pp. 453–465. DOI: 10.1002/mas.21376.

Varki, A.; Kornfeld, S. (1980): Identification of a rat liver alpha-N-acetylglucosaminyl phosphodiesterase capable of removing "blocking" alpha-N-acetylglucosamine residues from phosphorylated high mannose oligosaccharides of lysosomal enzymes. In *The Journal of biological chemistry* 255 (18), pp. 8398–8401.

Vergarajauregui, S.; Oberdick, R.; Kiselyov, K.; Puertollano, R. (2008): Mucolipin 1 channel activity is regulated by protein kinase A-mediated phosphorylation. In *The Biochemical journal* 410 (2), pp. 417–425. DOI: 10.1042/BJ20070713.

Vlastaridis, P.; Kyriakidou, P.; Chaliotis, A.; van de Peer, Y.; Oliver, S. G.; Amoutzias, G. D. (2017): Estimating the total number of phosphoproteins and phosphorylation sites in eukaryotic proteomes. In *GigaScience* 6 (2), pp. 1–11. DOI: 10.1093/gigascience/giw015.

Waheed, A.; Pohlmann, R.; Hasilik, A.; Figura, K. von (1981): Subcellular location of two enzymes involved in the synthesis of phosphorylated recognition markers in lysosomal enzymes. In *The Journal of biological chemistry* 256 (9), pp. 4150–4152.

Waheed, A.; Gottschalk, S.; Hille, A.; Krentler, C.; Pohlmann, R.; Braulke, T.; Hauser, H.; Geuze, H.; Figura, K. von (1988): Human lysosomal acid phosphatase is transported as a transmembrane protein to lysosomes in transfected baby hamster kidney cells. In *The EMBO journal* 7 (8), pp. 2351–2358.

Walker, M. W.; Lloyd-Evans, E. (2015): A rapid method for the preparation of ultrapure, functional lysosomes using functionalized superparamagnetic iron oxide nanoparticles. In *Methods in cell biology* 126, pp. 21–43. DOI: 10.1016/bs.mcb.2014.10.019.

Walsh, D. A.; Perkins, J. P.; Krebs, E. G. (1968): An adenosine 3',5'-monophosphate-dependant protein kinase from rabbit skeletal muscle. In *The Journal of biological chemistry* 243 (13), pp. 3763–3765.

Walther, D. M.; Kasturi, P.; Zheng, M.; Pinkert, S.; Vecchi, G.; Ciryam, P.; Morimoto, R. I.; Dobson, C. M.; Vendruscolo, M.; Mann, M.; Hartl, F. U. (2015): Widespread proteome remodeling and aggregation in aging C. elegans. In *Cell* 161 (4), pp. 919–932. DOI: 10.1016/j.cell.2015.03.032.

Wang, Z.; Zang, C.; Rosenfeld, J. A.; Schones, D. E.; Barski, A.; Cuddapah, S.; Cui, K.; Roh, T.-Y.; Peng, W.; Zhang, M. Q.; Zhao, K. (2008): Combinatorial patterns of histone acetylations and methylations in the human genome. In *Nature genetics* 40 (7), pp. 897–903. DOI: 10.1038/ng.154.

Ward, D. M.; Pevsner, J.; Scullion, M. A.; Vaughn, M.; Kaplan, J. (2000): Syntaxin 7 and VAMP-7 are soluble N-ethylmaleimide–sensitive factor attachment protein receptors required for late endosome–lysosome and homotypic lysosome fusion in alveolar macrophages. In *Molecular biology of the cell* 11 (7), pp. 2327–2333.

Welch, E. J.; Jones, B. W.; Scott, J. D. (2010): Networking with AKAPs: context-dependent regulation of anchored enzymes. In *Molecular interventions* 10 (2), pp. 86–97. DOI: 10.1124/mi.10.2.6.

Wessel, D.; Flügge, U. I. (1984): A method for the quantitative recovery of protein in dilute solution in the presence of detergents and lipids. In *Analytical biochemistry* 138 (1), pp. 141–143.

Wickham, H. (2016): ggplot2: Elegant graphics for data analysis: Springer-book New York.

Wickham, H. (2017): tidyverse: Easily install and load the 'tidyverse'. https://CRAN.R-project.org/package=tidyverse.

Williams, M. A.; Fukuda, M. (1990): Accumulation of membrane glycoproteins in lysosomes requires a tyrosine residue at a particular position in the cytoplasmic tail. In *The Journal of cell biology* 111 (3), pp. 955–966. DOI: 10.1083/jcb.111.3.955.

Wiśniewski, J. R.; Zougman, A.; Nagaraj, N.; Mann, M. (2009): Universal sample preparation method for proteome analysis. In *Nature methods* 6 (5), pp. 359–362. DOI: 10.1038/nmeth.1322.

Wolters, G.; Kuijpers, L.; Kacaki, J.; Schuurs, A. (1976): Solid-phase enzyme-immunoassay for detection of hepatitis B surface antigen. In *Journal of clinical pathology* 29 (10), pp. 873–879.

Wreden, C.; Verrotti, A. C.; Schisa, J. A.; Lieberfarb, M. E.; Strickland, S. (1997): Nanos and pumilio establish embryonic polarity in Drosophila by promoting posterior deadenylation of hunchback mRNA. In *Development (Cambridge, England)* 124 (15), pp. 3015–3023.

Xu, G.; Paige, J. S.; Jaffrey, S. R. (2010): Global analysis of lysine ubiquitination by ubiquitin remnant immunoaffinity profiling. In *Nature biotechnology* 28 (8), pp. 868–873. DOI: 10.1038/nbt.1654.

Yang, S.; Fletcher, W. H.; Johnson, D. A. (1995): Regulation of cAMP-dependent protein kinase: enzyme activation without dissociation. In *Biochemistry* 34 (19), pp. 6267–6271. DOI: 10.1021/bi00019a002.

Yang, W. H.; Kim, J. E.; Nam, H. W.; Ju, J. W.; Kim, H. S.; Kim, Y. S.; Cho, J. W. (2006): Modification of p53 with O-linked N-acetylglucosamine regulates p53 activity and stability. In *Nature cell biology* 8 (10), pp. 1074–1083. DOI: 10.1038/ncb1470.

Yannelli, J. R.; Sullivan, J. A.; Mandell, G. L.; Engelhard, V. H. (1986): Reorientation and fusion of cytotoxic T lymphocyte granules after interaction with target cells as determined by high resolution cinemicrography. In *Journal of immunology (Baltimore, Md. : 1950)* 136 (2), pp. 377–382.

Ye, X.; Cai, Q. (2014): Snapin-mediated BACE1 retrograde transport is essential for its degradation in lysosomes and regulation of APP processing in neurons. In *Cell reports* 6 (1), pp. 24–31. DOI: 10.1016/j.celrep.2013.12.008.

Yordanov, T. E.; Hipolito, V. E. B.; Liebscher, G.; Vogel, G. F.; Stasyk, T.; Herrmann, C.; Geley, S.; Teis, D.; Botelho, R. J.; Hess, M. W.; Huber, L. A. (2019): Biogenesis of lysosome-related organelles complex-1 (BORC) regulates late endosomal/lysosomal size through PIKfyve-dependent phosphatidylinositol-3,5-bisphosphate. In *Traffic (Copenhagen, Denmark)* 20 (9), pp. 674–696. DOI: 10.1111/tra.12679.

Yun, H. J.; Park, J.; Ho, D. H.; Kim, H.; Kim, C.-H.; Oh, H.; Ga, I.; Seo, H.; Chang, S.; Son, I.; Seol, W. (2013): LRRK2 phosphorylates Snapin and inhibits interaction of Snapin with SNAP-25. In *Experimental & molecular medicine* 45, e36. DOI: 10.1038/emm.2013.68.

Zambon, A. C.; Zhang, L.; Minovitsky, S.; Kanter, J. R.; Prabhakar, S.; Salomonis, N.; Vranizan, K.; Dubchak, I.; Conklin, B. R.; Insel, P. A. (2005): Gene expression patterns define key transcriptional events in cell-cycle regulation by cAMP and protein kinase A. In *Proceedings of the National Academy of Sciences of the United States of America* 102 (24), pp. 8561–8566. DOI: 10.1073/pnas.0503363102.

Zhang, Y.; Zhang, C.; Jiang, H.; Yang, P.; Lu, H. (2015): Fishing the PTM proteome with chemical approaches using functional solid phases. In *Chemical Society reviews* 44 (22), pp. 8260–8287. DOI: 10.1039/c4cs00529e.

Zhao, Q.; Rank, G.; Tan, Y. T.; Li, H.; Moritz, R. L.; Simpson, R. J.; Cerruti, L.; Curtis, D. J.; Patel, D. J.; Allis, C. D.; Cunningham, J. M.; Jane, S. M. (2009): PRMT5-mediated methylation of histone H4R3 recruits DNMT3A, coupling histone and DNA methylation in gene silencing. In *Nature structural & molecular biology* 16 (3), pp. 304–311. DOI: 10.1038/nsmb.1568.

Zhou, B.; Zhu, Y.-B.; Lin, L.; Cai, Q.; Sheng, Z.-H. (2011): Snapin deficiency is associated with developmental defects of the central nervous system. In *Bioscience reports* 31 (2), pp. 151–158. DOI: 10.1042/BSR20100110.

Zoller, M. J.; Kerlavage, A. R.; Taylor, S. S. (1979): Structural comparisons of cAMP-dependent protein kinases I and II from porcine skeletal muscle. In *The Journal of biological chemistry* 254 (7), pp. 2408–2412.

Zwang, N. A.; Hoffert, J. D.; Pisitkun, T.; Moeller, H. B.; Fenton, R. A.; Knepper, M. A. (2009): Identification of phosphorylation-dependent binding partners of aquaporin-2 using protein mass spectrometry. In *Journal of proteome research* 8 (3), pp. 1540–1554. DOI: 10.1021/pr800894p.

## Scientific poster presentations

Parts of this thesis were presented in the following scientific posters:

Peter Schein, Volkmar Gieselmann, Marc Sylvester: Investigations of LysN cleavage capability at biotinylated lysines. Human Proteome Organization World Congress 2017, Dublin. Ireland

Peter Schein, Volkmar Gieselmann, Marc Sylvester: Investigating the Cleavage Capability of the Proteases LysN and LysArginase in Biotinylated Samples. American Society for Mass Spectrometry Annual Conference 2019, Atlanta, USA

# Acknowledgements

First of all, I would like to thank Prof. Dr. Gieselmann for giving me the opportunity to do my doctoral thesis in his working group. Furthermore, I would like to thank him for the constructive discussions we have had over the past four years and for agreeing to be the first supervisor of this thesis.

Additionally, I would like to thank Prof. Dr. Fürst for agreeing to be the second reviewer and PD Dr. van Echten-Deckert and Prof Dr. Kaenders for being the „fachnahes" and the "fachfremdes" member of the committee, respectively.

Special thanks are directed to Dr. Sylvester for his unconditional support over the past four years. I really appreciate the time he spent discussing my results and experimental ideas, regardless of his busy schedule as the head of the Core Facility Mass Spectrometry. These discussions helped me to see things from a different perspective and contributed a lot to my scientific education.

In addition, I would also like to thank the whole working group for the nice working atmosphere and the professional collaboration. Here, I especially like to highlight the excellent jobs of the technical assistants. Often, scientists take the work of the assistants for granted without appreciating the effort they put into making laboratory life easier. Special thanks are directed to Jutta Mülich for her excellent support in the wet lab as well as to Claudia Yagootfam and Bernd Gehrig for sharing their immense experience with me.

My deepest gratitude shall be expressed to Claudia Domin. Her support during the past four years cannot be put into words. She was the one who tolerated me on gloomy days and supported me in any situation. I am grateful that I met her and that she has given me strength throughout the last years.

Last but not least, I would like to thank my family for the moral and financial support during my studies and their help in difficult situations. Without them, I would not have come into the position to write this thesis. Thank you!